

# NOTE TO USERS

This reproduction is the best copy available.

**UMI**<sup>®</sup>



# TESTING AND PERFORMANCE OF STEEL FRAME / WOOD PANEL SHEAR WALLS

By  
Chang Yi Chen



Department of Civil Engineering and Applied Mechanics  
McGill University  
Montreal, Canada

A thesis submitted to the Faculty of Graduate and Postdoctoral Studies in partial  
fulfillment of the requirements of the degree of Master of Engineering

August 2004

© Chang Yi Chen, 2004



Library and  
Archives Canada

Bibliothèque et  
Archives Canada

Published Heritage  
Branch

Direction du  
Patrimoine de l'édition

395 Wellington Street  
Ottawa ON K1A 0N4  
Canada

395, rue Wellington  
Ottawa ON K1A 0N4  
Canada

*Your file* *Votre référence*

*ISBN: 0-494-12591-8*

*Our file* *Notre référence*

*ISBN: 0-494-12591-8*

#### NOTICE:

The author has granted a non-exclusive license allowing Library and Archives Canada to reproduce, publish, archive, preserve, conserve, communicate to the public by telecommunication or on the Internet, loan, distribute and sell theses worldwide, for commercial or non-commercial purposes, in microform, paper, electronic and/or any other formats.

The author retains copyright ownership and moral rights in this thesis. Neither the thesis nor substantial extracts from it may be printed or otherwise reproduced without the author's permission.

#### AVIS:

L'auteur a accordé une licence non exclusive permettant à la Bibliothèque et Archives Canada de reproduire, publier, archiver, sauvegarder, conserver, transmettre au public par télécommunication ou par l'Internet, prêter, distribuer et vendre des thèses partout dans le monde, à des fins commerciales ou autres, sur support microforme, papier, électronique et/ou autres formats.

L'auteur conserve la propriété du droit d'auteur et des droits moraux qui protègent cette thèse. Ni la thèse ni des extraits substantiels de celle-ci ne doivent être imprimés ou autrement reproduits sans son autorisation.

---

In compliance with the Canadian Privacy Act some supporting forms may have been removed from this thesis.

Conformément à la loi canadienne sur la protection de la vie privée, quelques formulaires secondaires ont été enlevés de cette thèse.

While these forms may be included in the document page count, their removal does not represent any loss of content from the thesis.

Bien que ces formulaires aient inclus dans la pagination, il n'y aura aucun contenu manquant.

  
**Canada**

This thesis is dedicated to my wife 李晓洁 and daughter 陈美璇, for their great support during my two years of study at McGill University.

## ABSTRACT

Light gauge steel frame / wood panel shear walls are more commonly being used in the residential and low-rise building markets. However in Canada, no design guide for these shear walls has been published. Furthermore, although laboratory investigations that cover the performance of light gauge steel frame / wood panel shear walls with different sheathing material have been carried out, no analytical methods have been developed to predict the in-plane stiffness and strength of light gauge steel / wood panel shear walls based on member and connection properties.

This thesis has two main objectives. One is to investigate the performance characteristics of various configuration light gauge steel frame / wood panel shear walls under monotonic and reversed cyclic loading. The second is to recommend an effective analytical model, which relies on sheathing-to-framing connection test results and the mechanical properties of structural sheathing and steel frame members, to predict the resistance and deflection of shear walls subjected to lateral loads.

Based on the analysis of test data and on observations made during the testing of 109 full-scale wall specimens, 46 of which were carried out by the author, a review of the performance of light gauge steel frame / wood panel shear walls is presented. In addition, predictions of the lateral resistance and deflection of this type of shear wall using the analytical models show satisfactory agreement with the full-scale test results.

## RÉSUMÉ

Les murs de refend en revêtements de bois et en colombages d'acier formé à froid sont utilisés de plus en plus pour la construction résidentielle et pour les immeubles bas. Cependant, au Canada, aucun guide de conception n'a été publié pour ces murs. Malgré multiples expérimentations en laboratoire avec plusieurs types de revêtement, aucune méthode analytique basée sur les techniques de construction et des membrures de ces murs n'a été développée afin de prédire la rigidité et la résistance des murs dans leur plan.

Ce mémoire a deux buts principaux. Le premier est d'étudier les caractéristiques de la performance de plusieurs configurations des murs faits d'acier formé à froid et de panneaux de bois sous différents efforts incrémentaux et différents efforts cycliques. Le second est de recommander un modèle analytique efficace, basé sur les caractéristiques des connexions entre le revêtement les colombages, en plus des revêtements et des colombages eux-mêmes, dans le but de prédire la résistance aux efforts latéraux et la flèche des murs soumis à ces efforts.

Un résumé de la performance, basé sur des analyses de données et d'observations obtenues lors d'essais sur 109 murs à grande échelle, dont 46 ont été faits par l'auteur, un sera présenté. De plus, des prédictions faites avec les modèles analytiques pour résistance et la rigidité de ce type de mur concordent de façon acceptable avec les essais à échelle réelle.

## ACKNOWLEDGEMENTS

From my heart, I would like to first thank my supervisor, Professor Colin A. Rogers, for his financial support and invaluable research advice during my two years of study, as well as his great patience and hard work spirit.

Aaron E. Branston and Felix A. Boudreault are thanked for their great help during my testing and thesis. I also want to show my thanks to three undergraduate students, Katherine Hikita, Damien Soulier and Regis Lambert for helping me finish the full-scale tests successfully during the summer of 2003.

Undergraduate student Chun Kit Hui and another graduate student Ahmed Okasha are thanked for supplying the data for the connection tests.

Marek Przykorski, Ron Sheppard, John Bartczak and Damon Kiperchuk are appreciated for their kind help and instruction in the structural lab.

I would also like to acknowledge the support provided by numerous organizations, including the Natural Sciences and Engineering Research Council of Canada, the Canada Foundation for Innovation, the Canadian Sheet Steel Building Institute, Simpson Strong-Tie Co. Inc., the Structural Board Association, Grant Forest Products Inc., MTS, and the Canam Manac Group. Assistance with the procurement of steel framing was provided by Mr. John Rice of Bailey Metal Products Ltd.

Thanks also need to be sent to Mr. James F. Heidt, a civil engineer from Beloit, Wisconsin, USA, for the time he spent reviewing draft copies of my thesis. Simon Mastrogiuseppe, a graduate student, is appreciated for his translation of my abstract.

Larry Williams, President of North American Steel Framing Alliance, is thanked for his permission to freely use some material in the Prescriptive Method for Residential Cold-formed Steel Framing, Year 2000 edition.

Dr. Hugo Lemieux, Education Coordinator from Canadian Wood Council, is appreciated for his permission to use some pictures in the Wood Design Manual, 2001.

Karen A. Ryan, Business and Administrative Manager from the American Society of Civil Engineers, is also thanked for the free use of some articles from the Journal of Structural Engineering.

Paul Jaehrlich from the Canadian Plywood Association is acknowledged for his great help and feedback about the properties of wood panels.

At last, I want to show my appreciation to my wife Xiao Jie Li and my daughter Mei Xuan Chen, for their understanding and support during my studies at McGill University.

# TABLE OF CONTENTS

Abstract.....	i
Résumé .....	ii
Acknowledgements.....	iii
List of Figures.....	ix
List of Tables .....	xii
Chapter 1 Introduction.....	1
1.1 General Overview.....	1
1.2 Statement of Problem .....	8
1.3 Thesis Objectives and Scope .....	9
1.4 Overview of Thesis.....	10
Chapter 2 Literature Review.....	11
2.1 Background.....	11
2.2 Review of Past Experimental Studies.....	13
2.2.1 Current Design Procedures .....	17
2.3 General Review of Existing Analytical Approaches for Wood-framed Shear Walls.....	19
2.3.1 McCutcheon et al .....	19
2.3.2 Easley et al .....	26
2.3.3 Gupta & Kuo.....	30
2.3.4 Kallsner & Lam .....	32
2.3.5 Stewart .....	38
2.3.6 Analytical Models from Other Resources .....	39
2.4 Finite Element Analysis.....	40
2.5 Analytical Approaches for Light Gauge Steel Frame / Wood Panel Shear Walls .....	44

Chapter 3 Shear Wall Tests .....	45
3.1 Introduction.....	45
3.2 Test Matrix.....	46
3.3 Fabrication and Test Setup .....	50
3.4 Load Protocols .....	53
3.5 Instrumentation and Measurement .....	58
3.6 General Test Results .....	59
3.7 Preliminary Values for Shear Wall Design .....	63
3.8 Failure Modes Observed during Full-scale Testing.....	69
3.9 Material Testing.....	72
 Chapter 4 Performance Evaluation of Tested Shear Walls .....	 74
4.1 Introduction.....	74
4.2 Ultimate Shear Strength ( $S_u$ ) .....	76
4.2.1 Ultimate Shear Strength vs. Screw Spacing .....	76
4.2.2 Ultimate Shear Strength vs. Sheathing Type.....	79
4.2.3 Ultimate Shear Strength vs. Aspect Ratio .....	81
4.2.4 Ultimate Shear Strength vs. Load Protocol .....	82
4.3 Yield Shear Strength ( $S_y$ ).....	85
4.3.1 Yield Shear Strength vs. Screw Spacing .....	85
4.3.2 Yield Shear Strength vs. Sheathing Type.....	87
4.3.3 Yield Shear Strength vs. Aspect Ratio .....	89
4.3.4 Yield Shear Strength vs. Load Protocol .....	90
4.4 Stiffness ( $K_e$ ).....	92
4.4.1 Stiffness vs. Screw Spacing.....	92
4.4.2 Stiffness vs. Sheathing Type.....	94
4.4.3 Stiffness vs. Aspect Ratio .....	96
4.4.4 Stiffness vs. Load Protocol .....	97
4.5 Ductility ( $\mu$ ) .....	99
4.5.1 Ductility vs. Screw Spacing.....	99
4.5.2 Ductility vs. Sheathing Type .....	101

4.5.3 Ductility vs. Aspect Ratio.....	103
4.5.4 Ductility vs. Load Protocol.....	103
4.6 Energy Dissipation Ability ( $E_r$ & $E_b$ ) .....	106
4.6.1 Energy Dissipation Ability vs. Screw Spacing.....	106
4.6.2 Energy Dissipation Ability vs. Sheathing Type .....	110
4.6.3 Energy Dissipation Ability vs. Aspect Ratio.....	113
4.6.4 Energy Dissipation Ability vs. Load Protocol.....	116
4.7 Deflection .....	120
4.8 Stud Capacity.....	122
Chapter 5 Analytical Approach .....	125
5.1 General Introduction.....	125
5.2 Performance of Individual Screwed Sheathing Connections .....	127
5.3 Simplified Strength Model .....	131
5.3.1 Assumptions .....	131
5.3.2 Details of the Simplified Model .....	134
5.3.3 Comparison of Shear Wall Capacity between Test Results and Analytical Approaches.....	140
5.4 Simplified Deflection Model .....	147
5.4.1 Introduction.....	147
5.4.2 Details of the Simplified Model .....	147
5.4.3 Comparison of Shear Wall Deflection between Test Results and Analytical Approaches.....	148
5.5 Discussion.....	152
Chapter 6 Summary and Conclusions.....	155
6.1 Summary.....	155
6.2 Performance of Light Gauge Steel / Wood Panel Shear Walls .....	156
6.3 Analytical Models.....	159
6.4 Recommendations.....	160

References.....	162
Appendix I    Wall Configurations.....	172
Appendix II    Components of Test Specimens.....	178
Appendix III    Reversed Cyclic Test Protocols .....	182
Appendix IV    Pictures of Failure Modes.....	189
Appendix V    Calculation of Capacity of Stud.....	193
Appendix VI    Comparisons of Test Results and Prediction from Analytical Models.....	201
Appendix VII    Graphs of Comparisons between Tests Results and Prediction from Analytical Models.....	228
Appendix VIII    Relative Rotation between Sheathing and Framing.....	265

## LIST OF FIGURES

Figure 1.1	Shear Wall and Diaphragm Action.....	4
Figure 1.2	Elevation of Shear Wall Segment.....	5
Figure 1.3	Typical Light Gauge Steel Framed Building.....	6
Figure 1.4	Typical Light Gauge Steel Shear Wall Construction .....	7
Figure 2.1	Geometry and Distortion of a Panel .....	20
Figure 2.2	Deformation of Frame with Two Panels .....	24
Figure 2.3	Nail Force Distribution of a Shear Wall Panel .....	27
Figure 2.4	Deformation Pattern of a Typical Single Panel Wall .....	31
Figure 2.5	Linear Elastic Model Force Distribution .....	33
Figure 2.6	Lower Bound Model Force Distribution .....	35
Figure 2.7	Upper Bound Model Force Distribution.....	36
Figure 2.8	Shear Wall Deformation and Force Assumptions .....	38
Figure 3.1	Shear Wall Test Frame .....	46
Figure 3.2	Panel Markings of Alberta Plywood CSP .....	48
Figure 3.3	Panel Markings of Richply CSP.....	49
Figure 3.4	Panel Markings of OSB .....	49
Figure 3.5	Test Frame with 8' x 8' Wall Specimen.....	51
Figure 3.6	Test Frame with 2' x 8' Wall Specimen.....	53
Figure 3.7	Typical Load-Deflection Curve for Monotonic Tests (with permanent set unloading) .....	54
Figure 3.8	Modified Load-Deflection Curve for Monotonic Tests (without permanent set unloading) .....	55
Figure 3.9	Typical Reversed Cyclic Load vs. Displacement Test Hysteresis .....	57
Figure 3.10	Typical Displacement-Time History Curve for Reversed Cyclic Tests .....	57
Figure 3.11	Layout of LVDTs on 8' x 8' Wall.....	58

Figure 3.12	Energy Dissipation for a Monotonic Shear Wall Specimen.....	60
Figure 3.13	Energy Dissipation For a Reversed Cyclic Test.....	61
Figure 3.14	EEEP Mode .....	64
Figure 3.15	EEEP Analysis for a Monotonic Test.....	64
Figure 3.16	EEEP Analysis for a Reversed Cyclic Test.....	65
Figure 4.1	Ultimate Shear Strength, $S_u$ , vs. Number of Perimeter Screws Per Panel ...	78
Figure 4.2	Ultimate Shear Strength, $S_u$ , vs. Sheathing Type.....	80
Figure 4.3	Ultimate Shear Strength, $S_u$ , vs. Aspect Ratio .....	82
Figure 4.4	Ultimate Shear Strength, $S_u$ , vs. Load Protocol .....	83
Figure 4.5	Shear Yield Strength, $S_y$ , vs. Number of Perimeter Screws Per Panel .....	86
Figure 4.6	Shear Yield Strength, $S_y$ , vs. Sheathing Type.....	88
Figure 4.7	Shear Yield Strength, $S_y$ , vs. Aspect Ratio .....	89
Figure 4.8	Shear Yield Strength, $S_y$ , vs. Load Protocol .....	91
Figure 4.9	Stiffness, $K_e$ , vs. Screw Spacing.....	93
Figure 4.10	Stiffness, $K_e$ , vs. Sheathing Type.....	95
Figure 4.11	Stiffness, $K_e$ , vs. Aspect Ratio .....	96
Figure 4.12	Stiffness, $K_e$ , vs. Load Protocol .....	98
Figure 4.13	Ductility, $\mu$ , vs. Number of Perimeter Screws Per Panel .....	100
Figure 4.14	Ductility, $\mu$ , vs. Sheathing Type.....	102
Figure 4.15	Ductility, $\mu$ , vs. Aspect Ratio .....	104
Figure 4.16	Ductility, $\mu$ , vs. Load Protocol .....	105
Figure 4.17	Energy, $E_r$ , vs. Number of Perimeter Screws Per Panel .....	107
Figure 4.18	Normalized Energy, $E_r$ , vs Number of Perimeter Screws Per Panel .....	107
Figure 4.19	Energy, $E_b$ , vs. Number of Perimeter Screws Per Panel.....	108
Figure 4.20	Normalized Energy, $E_b$ , vs. Number of Perimeter Screws Per Panel.....	108
Figure 4.21	Energy, $E_r$ , vs. Sheathing Type.....	111
Figure 4.22	Energy, $E_b$ , vs. Sheathing Type .....	112

Figure 4.23	Energy, $E_r$ , vs. Aspect Ratio .....	113
Figure 4.24	Energy, $E_b$ , vs. Aspect Ratio.....	114
Figure 4.25	Normalized Energy, $E_r$ , vs. Aspect Ratio .....	115
Figure 4.26	Normalized Energy, $E_b$ , vs. Aspect Ratio.....	116
Figure 4.27	Energy, $E_r$ , vs. Load Protocol.....	117
Figure 4.28	Energy, $E_b$ , vs. Load Protocol.....	118
Figure 4.29	Deflection vs. Wall Length.....	120
Figure 5.1	Deformations and Force Distribution in Rigid Framing Members .....	125
Figure 5.2	Typical Monotonic Test Curve for Connection Tests .....	129
Figure 5.3	Typical Cyclic Test Curve for Connection Tests. ....	130
Figure 5.4	Assumed Force Distribution in Sheathing Connections.....	135

## LIST OF TABLES

Table 3.1	Description of Wall Specimens .....	47
Table 3.2	Mechanical Properties of Wood Species in CSP Panels .....	48
Table 3.3	Test Results for Monotonic Tests .....	62
Table 3.4	Test Results for Cyclic Tests .....	63
Table 3.5	Design Parameters Resulting from Monotonic Tests. ....	67
Table 3.6	Design Parameters Resulting from Reversed Cyclic Tests (positive cycles) .....	68
Table 3.6	Design Parameters Resulting from Reversed Cyclic Tests(negative cycles) .....	69
Table 3.7	Specified Strength and Rigidity Capacities for Sheathing Panels .....	72
Table 3.8	Material Properties from Coupon Tests of Steel Framing Members.....	73
Table 4.1	Light Gauge Steel Frame / Wood Panel Shear Wall Test Program Matrix.	75
Table 4.2	Comparison of Deflection at Ultimate Load, $\Delta_{net,u}$ , vs. Wall Length .....	122
Table 4.3	Ratios of Chord Stud Loads in Tests to the Capacity Determined by CSA S136 .....	124
Table 5.1	Parameters from Monotonic Connection Tests .....	129
Table 5.2	Parameters from Cyclic Connection Tests .....	130
Table 5.3	Modified Connection Parameters for Prediction of Cyclic Tests.....	131
Table 5.4	Description of Wall Specimens Used in Analytical Comparison.....	142
Table 5.5	Combined Ratios of Full-Scale Shear Wall Test to Predicted Shear Capacity .....	143
Table 5.6	Comparisons between Different Models in Predicting $S_{y,wall}$ for Tests with EEEP25.....	146
Table 5.7	Combined Ratios of Full-Scale Shear Wall Test to Predicted Deflection .....	149

Table 5.8	The Relative Ratio of the Net Lateral Deflections Using Different Models with EEEP25 (Monotonic) .....	151
Table 5.9	The Relative Ratio of the Net Lateral Deflections Using Different Models with EEEP25 (Reversed Cyclic).....	152

# CHAPTER 1 INTRODUCTION

## 1.1 GENERAL OVERVIEW

Steel frame / wood panel walls are composed of light gauge steel studs and tracks in combination with wood panels attached by means of self-drilling/tapping screws. The walls may be designed to act as in-plane structural elements that transmit forces due to gravity and lateral loads. These types of structures were first adopted in the commercial construction industry, where they were used as panel walls for resisting gravity loads or transferring lateral loads to vertical bracing structures. Nowadays, light gauge steel frame / wood panel walls can be used as an alternative to conventional wood framed walls in the residential and low rise building markets. Walls can be divided into two basic types according to their function: load bearing and non-load bearing. Load bearing walls, which typically carry gravity loads and in some cases lateral loads, are structural elements. Non-load bearing walls are usually only designed to support their self-weight and interior partitions. This thesis is limited to the testing and analysis of the performance of lateral load carrying shear walls.

Light gauge steel members, the skeletons of shear walls, are composed of sections typically formed from steel sheet in roll-forming machines at room temperature (Yu, 2000). A partial listing of the characteristics of steel framing is as follows (Waite, 2000; Bateman, 1996):

1. It will not rot or deteriorate (corrode) if appropriate protection from humidity has been provided, and is not subject to damage from termites and fungi.
2. The required fire rating can be attained with the installation of adequate insulation such as Type X gypsum board.
3. It can be formed into unusual sectional configurations with high strength to weight ratios, making efficient use of its shape. Moreover, light gauge steel structural members can be prefabricated to reduce labour requirement and material waste.
4. Light gauge steel members are dimensionally stable regardless of fluctuations in humidity level.
5. Holes can be provided in the stud webs to allow for plumbing, electrical, and mechanical lines and components to pass through.
6. A large percentage of the steel used in the manufacture of the wall studs and tracks is recycled.

At the same time, light gauge steel members have some disadvantages (Waite, 2000; Bateman, 1996), such as thermal conduction, the requirement of a coating for corrosion protection, ease of denting, and elastic local buckling of studs and tracks. Furthermore, engineers and the construction industry are not as familiar with the design procedures and specifications as they are with hot rolled steel, reinforced concrete and wood. Hence a specialized knowledge of light gauge steel is generally needed for engineers, designers and framers.

Wood panels used in the shear walls are manufactured in many types, with the most common being plywood and oriented strand board (OSB). These panels are very suitable for light frame construction given characteristics such as: their light weight, high quality, appropriate strength and stiffness, workability and ease of installation, as well as their large size (Forest Products Laboratory, 1999; Breyer et al., 1998). The naturally occurring defects inherent to wood are, for the most part, removed during the manufacturing process of these engineered wood products; in addition, drying of the plies and strands provides low and consistent moisture content. The positioning of plies or strands in the makeup of the plywood and OSB minimizes the relative movement between layers and provides the panels with dimensional stability (Forest Products Laboratory, 1999). On the other hand, wood panels share the same common disadvantages as other wood products. For example, the strength and dimensions of wood panels change with fluctuations of the moisture content, which will decrease the effectiveness of the connections; at the same time, wood panels may be subject to deterioration if appropriate details to prevent decay are not provided (CWC, 2002).

A typical wood framed wall is composed of wood studs, top plates, and a sill plate. Studs commonly have nominal sizes of 2"x4" or 2"x6" (actual size 38 x 89 mm and 38 x 140 mm) and are placed 12", 16" or 24" (300, 400 or 600 mm) on centre. Double studs are used at corners, around openings and at intersections of walls. Top plates are made up of two lumber sections having the same size as studs, whereas sill plates are constructed with one same size section. Framing members are connected together by nails, and then the entire assembly is sheathed with wood and/or gypsum panels, which are attached with nails or screws (Salenikovitch et al., 2000). Results and observations from full-scale tests

show that nail slip, the flexibilities of the sheathing and of the stud frame, and shear deformation of the sheathing are the major factors affecting racking strength and stiffness (McCutcheon, 1985).

Under lateral loads, the roof and/or floors of a building act as diaphragms to distribute forces to the vertical bracing system. This system, which is usually composed of shear walls, then transfers the applied loads to the foundations (Figure 1.1 - 1.2).

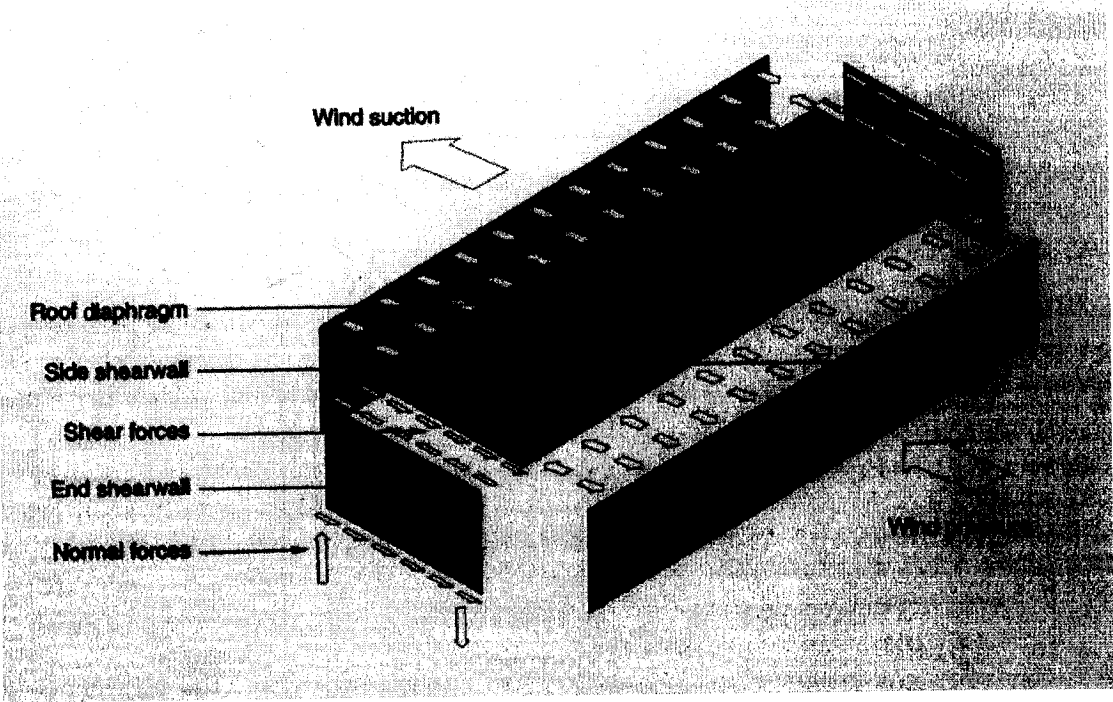


Figure 1.1 Shear Wall and Diaphragm Action (CWC, 2001)

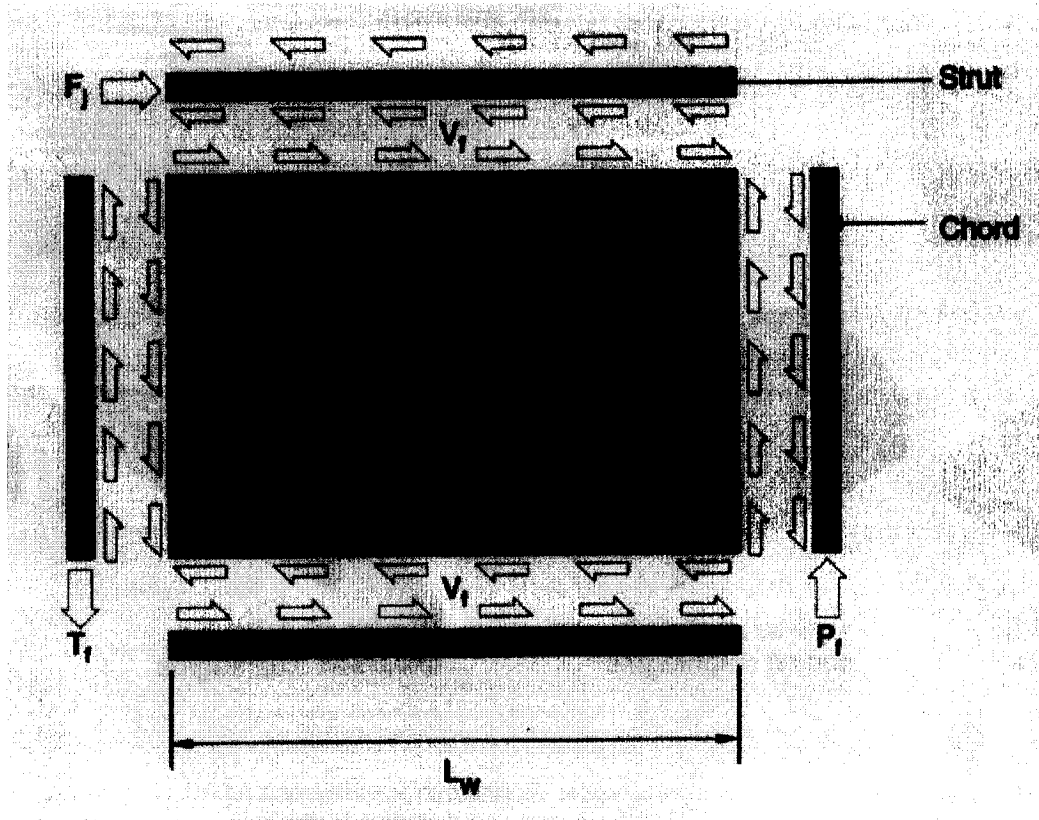


Figure 1.2 Elevation of Shear Wall Segment (CWC, 2001)

Similar to wood framed buildings, platform framing techniques can be extensively adopted in light gauge steel framing construction. Horizontal or slope sided roof and floor diaphragms are designed to resist gravity loads and transfer lateral loads to vertical bracing systems, such as light gauge steel framed shear wall system, thin steel plate bracing, diagonal X steel strap bracing, or their combinations. These vertical bracing systems then carry the loads from storey to storey and finally to the building foundation. A typical house framed in light gauge steel is illustrated in Figure 1.3.

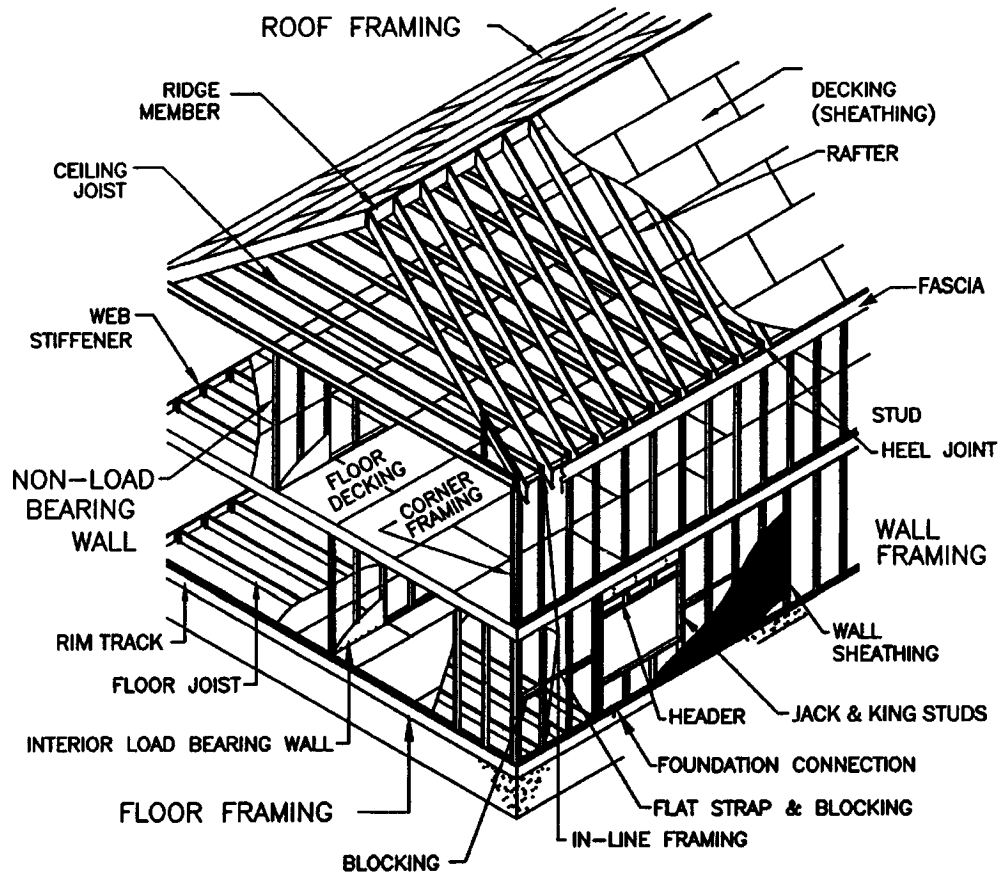


Figure 1.3: Typical Light Gauge Steel Framed Building (NASFA, 2000)

A typical light gauge steel frame / wood panel shear wall is composed of cold-formed steel studs and tracks which are connected with self-drilling/tapping screws to either plywood or OSB sheathing. Track channels without lips are used for the top and bottom members of a wall. The C-shape studs are fit into the top and bottom tracks and are typically held in place by wafer head screws. Commonly, the end chords of a shear wall are made up of two C-shape studs which are installed back-to-back and connected to one another with screws to avoid buckling under axial loads. Plywood or OSB panels are then attached to the frame using screws spaced sufficiently close to provide the necessary stiffness and strength in resisting in-plane lateral loads. Finally, the walls are fixed on the

foundation or lower storeys through hold-downs and shear anchors. A typical light gauge steel framed shear wall is illustrated in Figure 1.4.

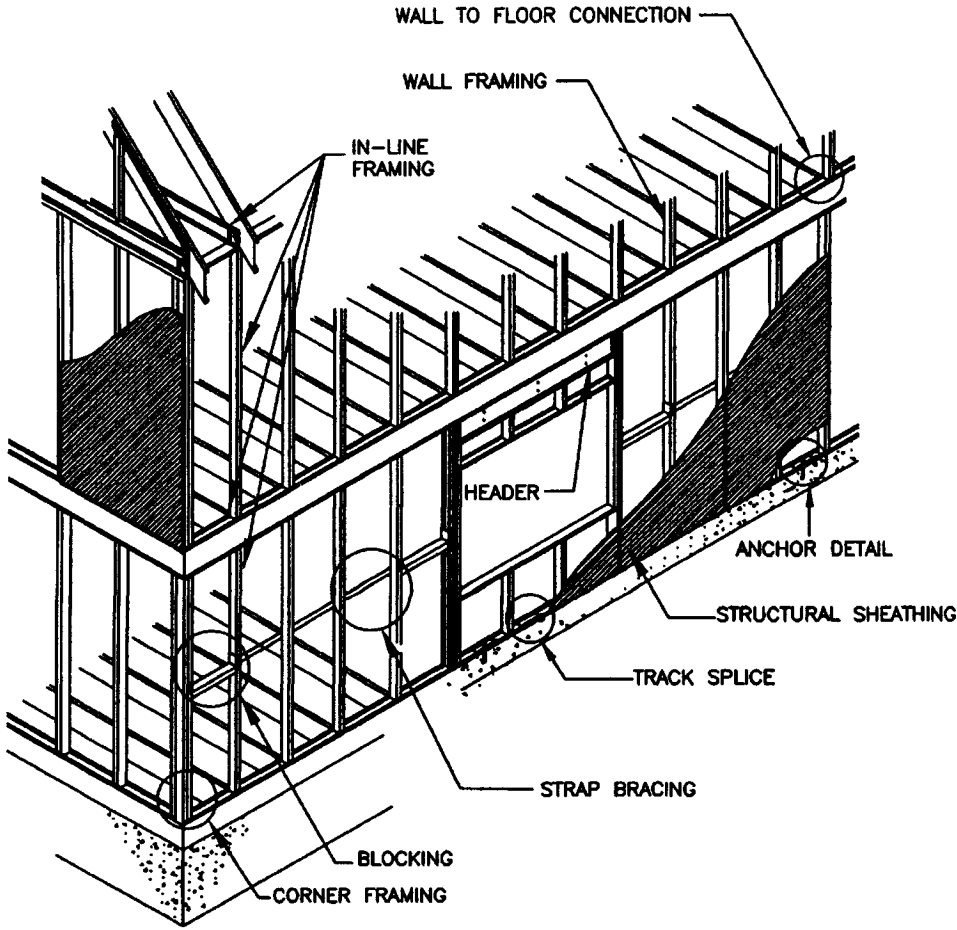


Figure 1.4: Typical Light Gauge Steel Shear Wall Construction (NASFA, 2000)

## 1.2 STATEMENT OF PROBLEM

In general, previous investigations of shear wall performance have provided information regarding the theory and use of light gauge steel / wood panel shear walls (Tarpy et al., 1978, 1980, 1982; Tissell, 1993; Serrette et al., 1996a,b, 1997a,b, 2002; Salenikovich et al., 1999; Gad et al., 1998, 1999a,b,c, 2000; Fulop & Dubina, 2002, 2003a,b; Kingsley, 1996; Branston et al., 2003; COLA-UCI, 2001; NAHB, 1997). However there remain topics to be addressed in order to extend the use of this type of structural framing, namely:

1. To the best of the author's knowledge an analytical method has not been developed to predict the in-plane stiffness and strength of light gauge steel / wood panel shear walls. An effective analytical method would allow for engineers to accurately predict the behaviour of a shear wall and provide for flexibility in terms of choices for wall configurations. An effective analytical method could also reduce the cost of research by minimizing the number of large-scale shear wall tests needed to be carried out. Eventually with the proven application of an effective analytical model, researchers could extend the results of small-scale tests to aid in the design of full size shear walls.
2. In Canada, no design guide for these shear walls has been published. In seismic areas, such as the West Coast of British Columbia and the Ottawa and St. Lawrence River valleys guidance is needed for engineers and designers. Additionally, information for use in the design of shear walls that carry lateral wind loads is required.

### **1.3 THESIS OBJECTIVES AND SCOPE**

The objectives and related scope of study for the thesis are as follows:

1. Carry out a suite of 46 light gauge steel frame / wood panel shear wall tests with varying configurations. This includes different sheathing type, wall length, screw spacing and loading protocol.

2. Investigate the performance characteristics of light gauge steel frame / wood panel shear walls. The following parameters are evaluated for a series of 109 shear wall tests, including the 46 that were carried out by the author:

- a) Maximum shear strength and yield strength;
- b) Elastic stiffness;
- c) Energy dissipating capacity and ductility;
- d) Load capacity related to relative deflection;
- e) Steel chord capacity.

3. Recommend an efficient analytical method, which is based on a mechanics approach, to predict shear wall strength and deflection. This involves the evaluation of five existing methods, developed for the analysis of wood framed shear walls, in comparison with the experimental shear wall tests.

## **1.4 OVERVIEW OF THESIS**

A literature review, presented in Chapter 2, begins with a brief review of past experimental studies and current design procedures. A general review of existing analytical approaches of wood framed shear walls is also presented.

In Chapter 3, a series of shear wall tests, carried out at McGill University in the summer of 2003, is documented. This includes a description of test procedures, load protocols, instrumentation and measurements. The results of the 46 shear wall tests completed by the author are presented. Failure modes observed during testing are discussed.

Performance evaluations of all 109 monotonic and reversed cyclic tests, carried out by Branston (2004), Boudreault (2004) and the author, are presented in detail in Chapter 4. Comparisons between specimens with different wall configurations are discussed.

Chapter 5 contains a general introduction to the force distribution in a light gauge steel frame / wood panel shear wall segment. The details of a simplified strength and deflection model are provided. In addition, a comparison between the test results and the analytical approach predictions is presented.

Conclusions and recommendations from the research are provided in Chapter 6. Other important factors in shear wall research not specifically addressed in this thesis are briefly discussed.

## CHAPTER 2 LITERATURE REVIEW

### 2.1 BACKGROUND

Low-rise wood framed buildings have existed mainly in North America and less so in Europe and other parts of the world for many years, and because of their common use an extensive amount of research has been conducted to better understand their behaviour. Structural integrity of these buildings is often obtained through the use of wood shear walls and diaphragms. Theoretical analyses and engineering practice both testify that wood framed buildings perform very well when subjected to wind or seismic loads if reasonable construction details have been incorporated into the structural system. It is anticipated that steel frame / wood panel shear walls would also possess an ability to carry the same types of loads if properly designed. On the other hand, the shortcomings with respect to wood shear walls that were identified in the aftermath of the Northridge California earthquake (January 17, 1994) can be expected to affect the performance of steel frame / wood panel shear walls. The Northridge earthquake, a major seismic event the likes of which could also occur along the west coast of BC, resulted in US \$40 billion in property damage to wood frame construction, reduced 48,000 wood frame housing units to an uninhabitable status, and was responsible for 25 fatalities, 24 of which were caused by damage to wood frame buildings (CUREE, 2001). Hence, a well thought out design approach is necessary to avoid the problems encountered during the Northridge earthquake.

Although laboratory investigations that cover the performance of light gauge steel frame / wood panel shear walls with different sheathing material have been carried out, no analytical method to predict the behaviour of this kind of structural system has been thoroughly developed. Zhao (2002), however, completed a preliminary investigation of an analytical method based on the work of Easley et al. (1982) for wood frame shear walls, which indicated that the prediction of steel frame / wood panel shear wall strength and stiffness would be feasible through the use of an analytical design method.

Based on tests, methods have been established for engineering design purposes, and many analytical methods have been developed to predict a wood frame wall's shear strength and stiffness. The methods can be divided into three main categories.

1. Empirical Equations. Simple equations are established based on extensive shear wall test data. This design approach can be only applied on walls with the same configuration and materials as were used for testing.
2. Closed form models. Models are formulated using equations of force equilibrium and the principles of energy conservation, along with simplifying assumptions, to derive the applied loads and deflections. These models are easily used for design, but can only be applied for low or moderate loads, and the assumptions also limit the possible wall configurations.
3. Finite element methods (FEM). Linear and nonlinear analyses can be performed with the help of existing computer software. These methods can be used for any wall configuration.

## 2.2 REVIEW OF PAST EXPERIMENTAL STUDIES

A number of investigations on light gauge steel frame / wood panel shear walls have been performed by researchers over the last 30 years. In this review only an overview of the main test programs, which are considered relevant to this thesis, is presented.

Some of the early research projects include that by McCreless & Tarpy (1978), in which tests on sixteen full size wall panels were conducted to determine the effect of various aspect ratios on the shear resistance of steel stud wall systems. They also investigated the effect of blocking and the degree of possible panel distortion before major wall panel damage occurred. Tarpy & Hauenstein (1978) tested eighteen full-scale walls with seven different types of wall panel construction and anchorage details. The research was oriented around two main objectives. 1) The first was to investigate the effect of different construction and anchorage details on the shear resistance of steel stud frames attached with gypsum wallboard, and to evaluate the damage threshold load level or the load that initially causes tearing of the wall panel diaphragm material. 2) The second was to compare the performance of steel framed shear walls with wood framed shear walls. Tarpy (1980) tested nine different types of wall panel construction and anchorage details. The purpose in this case was to determine the effect of cyclic loading versus monotonic unidirectional loading on the shear capacity of steel frame walls. Tarpy & Girard (1982) conducted another series of tests to determine the effect of different construction techniques and anchorage details on shear resistance of steel frame walls

sheathed with various materials, and to determine the threshold for damage in walls due to in-plane displacement.

Tissell (1993) completed eight tests of wall specimens sheathed with oriented strand board (OSB) or plywood and connected with different fastener sizes and spacing. The purpose of these tests was to investigate the effect of steel studs with different thicknesses.

Serrette et al. (1996a, b) and Serrette (1997) conducted a series of tests that were divided into three phases. The intent of the research program was to investigate the behaviour of light gauge steel framed shear walls sheathed with plywood, OSB, and gypsum wallboard (GWB). Serrette & Ogunfunmi (1996) tested 13 walls with different lateral bracing systems including X-bracing, gypsum sheathing board (GSB), GWB and the combination of X-bracing, GSB and GWB. Forty-four additional tests were conducted by Serrette et al. (1997b) to provide a wider range of design options for steel stud shear walls. Serrette et al. (1997a) tested a series of full-scale and small-scale walls to investigate the behaviour of the sheathing materials and fasteners. Plywood, OSB, Gypsum and fiberbond wallboards were attached to the steel stud frames on either one or both sides. Serrette et al. (2002) conducted 20 shear wall tests (10 monotonic and 10 cyclic) to investigate the performance of walls with configurations not covered by the 1997 Uniform Building Code (ICBO, 1997) and the 2000 International Building Code (ICC, 2000).

The National Association of Home Builders (NAHB) research centre (1997) carried out tests to assess the suitability of using the perforated shear wall design method for wood structures with light gauge steel framed shear walls, and to provide a direct

comparison between the performance of wood framed and steel framed shear walls. A method for designing perforated shear walls based on the same theory as found for wood framed shear wall design was recommended.

Salenikovich et al. (1999) conducted a series of shear wall tests using specimens which were 12.2 m (40') in length and 2.44 m (8') in height. One objective of this research was to determine the effect of opening size, cyclic loading, gypsum drywall sheathing and steel framing on shear wall performance. The other was to compare the experimental results with predicted capacities.

COLA-UCI (2001) tested four groups of shear walls sheathed with plywood and OSB panels attached to either light gauge steel stud framing or wood stud framing with different fastener schedules. The objective was to develop experimental shear strength values for light gauge steel framed walls and to compare the cyclic response of steel framed walls and wood framed walls.

In Australia, Gad et al. (1998, 1999a,b,c, 2000) tested one-room-houses constructed from full-scale components on a shake table. The research objective was to investigate the behaviour of Australian domestic structures constructed with cold formed steel stud walls, to identify the contribution of plasterboard to the lateral resistance and seismic design of the shear walls, and to provide a comparison between the lab-based tests with field tests using modal analysis.

In Romania, Fulop & Dubina (2002, 2003a,b) conducted a test program on shear wall panels and then compared the results with numerical solutions concerning expected earthquake performance. Alternative design methods and hysteretic modeling techniques were presented. Based on test results, a numerical equivalent model for hysteretic

behaviour of wall panels subject to shear was built and used in a 3D dynamic nonlinear analysis of cold formed steel framed buildings. Preliminary conclusions refer to the effect of over-strength and ductility upon the possible earthquake load reduction factor for the case of light-gauge steel shear wall structures.

In Canada, Kingsley (1996) carried out eighteen 1220mm x 2920mm cyclic racking tests. The test specimens consisted of a 1220mm x 2460mm steel stud wall with 200mm deep floor assemblies at the top and bottom. In order to investigate the effect of various wall configurations on the racking strength of the steel stud walls, Kingsley varied the orientation of exterior sheathing, the sheathing materials, the size of studs and web stiffeners, as well as fastener type and spacing.

Recently in Canada, Branston et al. (2003) completed a progress report based on the testing of twelve full-scale steel frame / wood panel shear walls (six monotonic and six reversed cyclic). Both OSB and plywood sheathing were included in the study. The aim was to reproduce the results of experiments completed by Serrette et al. (1996) and COLA-UCI (2001) in the USA.

In general, the performance of light gauge steel frame / wood shear walls, as observed during the test programs highlighted above, is dependant on such variables as aspect ratio, sheathing type and strength, stud size and thickness, connection type and size, as well as other construction details. These factors were considered in the planning of the light gauge steel frame / wood shear wall research program at McGill University.

### **2.2.1 CURRENT DESIGN PROCEDURES**

In Canada, no guide or code has yet been published for the design of light gauge steel frame / wood panel shear walls. In the USA, the American Iron and Steel Institute (AISI) has published a Shear Wall Design Guide (AISI, 1998) which lists the nominal strength for different wall configurations. The walls are constructed of steel studs sheathed with plywood, OSB, GWB or steel sheets, or braced by steel strip X-bracing. This guide was based on a large number of tests completed in the USA by Tissell (1993), Serrette (1994) and Serrette et al. (1996b, 1997b). In addition, nominal shear values for specific wall configurations are provided in model codes such as the *UBC* (ICBO, 1997), *IBC* (ICC, 2000) and *NEHRP* (FEMA, 1997a). Strict guidelines have been placed because of the limited scope of the tests. The AISI also has a new draft version of the Shear Wall Design Guide 2002 in progress, which contains additional wall configurations verified by Serrette et al (2002).

In Europe, the method from ECCS P88, *European Recommendations for the Application of Metal Sheeting Acting as a Diaphragm* (Fulop & Dubina, 2003a,b), can be used to predict initial rigidity and ‘elastic’ capacity of the panels, in the case of panels with corrugated sheeting. However, for wood panel sheathing, no guide exists and hence the results of full-scale tests would be needed to predict the shear capacity for a specific wall configuration.

As for components of shear walls, there exist codes and specifications to guide designers in North America. For example *the North American Specification for the Design of Cold-Formed Steel Structural Members* (2001) can be used to calculate the

capacity of steel studs and channels. *The CSA O86 Standard (2001) Engineering Design In Wood, the Standard for Load and Resistance Factor Design (LRFD) for Engineered Wood Construction* (AF&PA/ASCE, 1996), and *the National Design Specification (NDS) for Wood Construction* (AF&PA, 2001) can be adopted to determine the capacity of wood panels.

For wood framed shear walls, design methods and shear resistance values are provided in many codes and design manuals, such as UBC (1997), IBC (2000), CWC (2001), CSA O86 (2001), APA (1997) and AWC (1996). Furthermore, many analytical methods, including linear and nonlinear, closed formed and finite element analysis, can be used to predict the performance of wood framed shear walls.

*Prescriptive Method for Residential Cold Formed Steel Framing* (NASFA, 2000), a document published by the North American Steel Framing Alliance has incorporated the above USA codes and specifications into a practical construction manual. It is useful for homebuilders, design professionals, and building code officials. These provisions apply to the construction of detached one- or two-family dwellings, townhouses, attached multi-family dwellings, and other attached single-family dwellings not more than two storeys in height using in-line framing practice.

## **2.3 GENERAL REVIEW OF EXISTING ANALYTICAL APPROACHES FOR WOOD-FRAMED SHEAR WALLS**

### **2.3.1 *McCutcheon et al.***

Tuomi and McCutcheon (1978) developed an analytical procedure for calculating the racking strength of sheathed panels, removing the limitation where a set of tests are required for new combinations of sheathing, framing and fasteners. The assumed geometry and distortion of a panel are as shown in Figure 2.1.

This procedure is based on the following assumptions and limitations:

1. The lateral load versus deflection curve is linear for a single nail.
2. The frame becomes a parallelogram while the shape of the sheathing panel remains unchanged. The edges of the panel are free to rotate without interference from adjacent sheets and the foundation/lower storey.
3. The panel is parallel to the frame and is of the same height.
4. Nails are spaced evenly and symmetrically.
5. The loading speed is slow enough to eliminate dynamic or impact effects.
6. Distortions and deflections are small.
7. The four corner nails distort along the lines of the sheathing's diagonals.
8. All the external work is completely dissipated by the distortion of the nails.

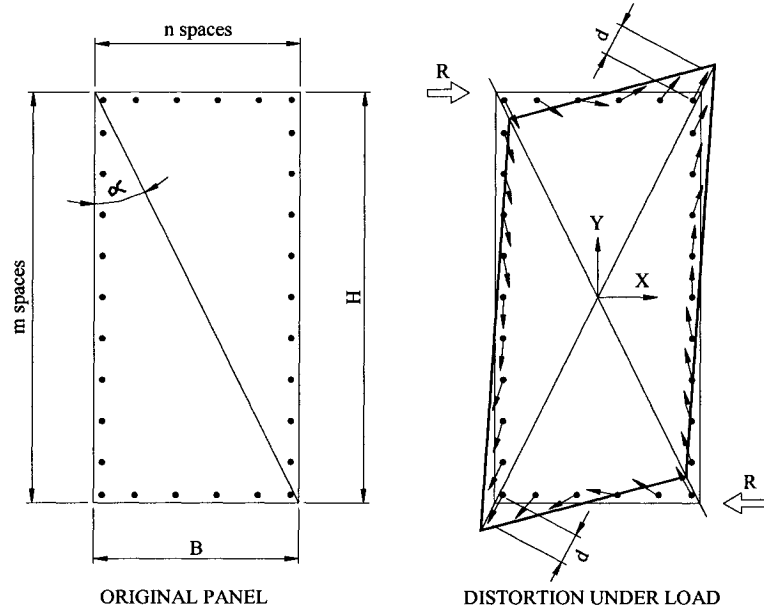


Figure 2.1 Geometry and Distortion of a Panel (Tuomi & McCutcheon, 1978)

The racking force of a panel with perimeter nailing was derived as:

$$R = r[(K_n + K_m)_p + (a^2 K_{na} + b^2 K_{nb} + a^2 K_{ma} + b^2 K_{mb})_f] \quad (2.1)$$

where:

$$K_n = K_{na} + K_{nb}; \quad K_m = K_{ma} + K_{mb}; \quad (2.2)$$

$$K_{na} = n \cdot \sin^3 \alpha; \quad K_{nb} = \frac{n^2 + 2}{3n} \sin \alpha \cdot \cos^3 \alpha; \quad (2.3)$$

$$K_{ma} = \frac{m^2 + 2}{3m} \sin^3 \alpha; \quad K_{mb} = m \cdot \cos^2 \alpha \cdot \sin \alpha; \quad (2.4)$$

R = theoretical racking load per panel;

r = lateral strength of single nail;

$\alpha$  = the angle between vertical and diagonal lines;

m = the number of fastener spaces along vertical side;

- n = the number of fastener spaces along horizontal side;
- p = subscript denoting nails around the perimeter of the panel;
- f = subscript denoting nails in the interior (field) of the panel;
- a = the ratio of “field height” to “perimeter height”,  $H_f / H_p$ ;
- b = the ratio of “field width” to “perimeter width”,  $B_f / B_p$ .

If a wall is composed of multiple panels, and the contribution from the wood framing is considered; the total racking resistance is the sum of the calculated racking forces for all the panels and the contribution from the frame itself, including the friction of the wood frame wall sliding over the support and other relatively minor considerations not measured in the lateral nail tests.

Tuomi and McCutcheon (1978) performed 34 full-scale tests and 29 small-scale tests to verify their analytical model. These tests adopted seven different sheathing materials with different grades, four different geometries and three different nail patterns. Theoretical and actual loads agreed with each other very well in the low load range (less than 7000 lb or 31.15 kN). Due to the linear assumption, this method cannot be used for the high load range.

McCutcheon (1985) presented a general approach for calculating racking deformations of wood framed shear walls, using the same energy approach employed by Tuomi and McCutcheon (1978) in the racking strength prediction, but removing the limitation that the behaviour of the nails is linear. The shear deformation of sheathing is also included when determining the total racking displacement.

If the load-slip curve of a nail can be expressed as a power curve

$$p = A \cdot x^B \tag{2.5}$$

the total racking displacement  $\Delta_t$  can be written as:

$$\Delta_t = \Delta_n + \Delta_s \quad (2.6)$$

where

$$\bar{A} = A \frac{(\sin \alpha)^{B+1}}{2^B} \cdot \sum_{rect} S; \quad (2.7)$$

$$S = \sum_{i=1}^{n_x} \left[ \sin^2 \alpha + \left( 2 \frac{i}{n_x} - 1 \right)^2 \cdot \cos^2 \alpha \right]^{(B+1)/2} + \sum_{j=1}^{n_y} \left[ \left( 2 \frac{j}{n_y} - 1 \right)^2 \cdot \sin^2 \alpha + \cos^2 \alpha \right]^{(B+1)/2} \quad (2.8)$$

$$\Delta_n = \left( \frac{R}{N \cdot \bar{A}} \right)^{1/B}, \text{ is the racking displacement caused by nail distortions;} \quad (2.9)$$

$$\Delta_s = \frac{RH}{NGtL}, \text{ is the racking displacement caused by shear in the sheathing;} \quad (2.10)$$

A, B = constants in the power curve used for expressing the load-slip relationship of nails, B is between zero and unity;

R = the racking resistance of the wall;

N = the number of independent vertical sheets;

H = the distance between top edge nail line and bottom edge nail line;

T = the thickness of the sheathing sheet;

L = the distance between side edge nail lines;

G = the shear modulus of the sheathing;

$r_x$  = the ratio of the reduced width of the interior rectangle to the width of the outer most rectangle;

$r_y$  = the ratio of the reduced height of the interior rectangle to the height of the outer most rectangle;

Alternative nonlinear nail load-slip curves have also been introduced by McCutcheon (1985) and Patton-Mallory & McCutcheon (1987). McCutcheon suggests that small-scale tests can be used to predict the racking deformation better because the connection tests demonstrate very high initial stiffness which greatly underestimates the racking displacements. The agreement between theoretical and test results is good up to moderate levels of deformation, however this method underestimates the deformation under high loads.

Hirashima (1981) applied the same method as McCutcheon (1985) to derive a racking deformation formula, where the racking force,  $R$ , of the shear wall was also assumed to be a power curve:

$$R = K \bullet \Delta_N^b \quad (2.11)$$

where  $K$  and  $b$  are constants;

$$P = a \bullet \delta^b \quad (2.12)$$

where  $P$  is the load and  $\delta$  is the deformation of a nail fastener;  $a$ ,  $b$  are constants.

An example of the assumed distortion of the wall is presented in Figure 2.2. After equating the internal and external work, the racking constant  $K$  is obtained as follows:

$$K = 2ak^f \left[ \begin{array}{l} nr^f \sin^f \alpha_T + n \sin^f \alpha_B + m_T r^f \cos \alpha_T + m_B \cos^f \alpha_B \\ + (r^f \cos^f \alpha_T + \cos^f \alpha_B) \sum \left| \frac{2i}{n} - 1 \right|^f + r^f \sin^f \alpha_T \sum \left| \frac{2j}{m_T} - 1 \right|^f \\ + \frac{1}{2} r^f \sin \alpha_T \sum \left| \frac{2i}{m_T} - 1 \right|^f + \sin^f \alpha_B \sum \left| \frac{2j}{m_T} - 1 \right|^f + \frac{1}{2} \sin^f \alpha_B \sum \left| \frac{2j}{m_B} - 1 \right|^f \end{array} \right]$$

(2.13)

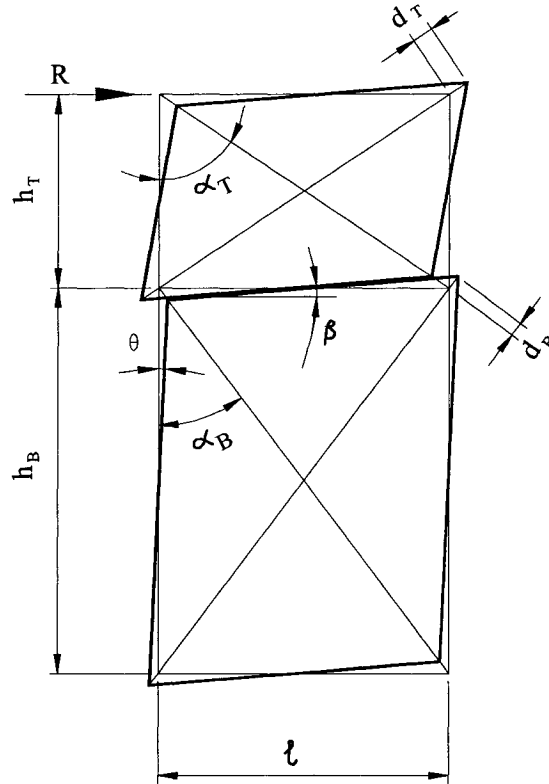


Figure 2.2 Deformation of Frame with Two Panels (Hirashima, 1981)

where

$$r = \frac{h_B h_T \cos \alpha_B + l \cdot h_T \sin \alpha_B}{h_B h_T \cos \alpha_T + l \cdot h_B \sin \alpha_T}; \quad (2.14)$$

$$k = \frac{1}{2[r \sin \alpha_T + \sin \alpha_B + \cot \alpha_B \cos \alpha_B + r \cot \alpha_T \cos \alpha_T]}; \quad (2.15)$$

$$f = b + 1; \quad (2.16)$$

$m$  = number of vertical nail spaces;

$n$  = number of horizontal nail spaces;

$m'$  = number of vertical nail spaces on centre stud.

The racking displacement of the panel can be obtained by adding the displacement due to the shear deformation of sheathing materials to  $\Delta_N$ . Corresponding tests show that the formula for calculating the racking displacement can be applied in practice.

Itani et al. (1982) present a methodology for calculating the racking performance of sheathed wood-stud walls, replacing each panel of sheathing with a pair of diagonal springs. The stiffness of each spring is calculated from the stiffness of a single sheathing-to-frame nail. The same assumptions as discussed by Tuomi and McCutcheon (1978) with respect to strength and stiffness were employed except that field nails applied at intermediate studs were ignored. The results were not significantly affected since the field nails contribute only about 5% to the overall stiffness of a standard size panel. The stiffness of each spring is determined by

$$K = \frac{k}{4} \left[ n + m - \frac{2}{3} \left( \frac{n^2 - 1}{n} \cdot \cos^2 \alpha + \frac{m^2 - 1}{m} \cdot \sin^2 \alpha \right) \right] \quad (2.17)$$

The connections between the bottom sill plate and supports are replaced with a series of springs. The stiffness of each spring is computed by summing the linear slip modulus of the nails connecting the sill plate to supports. Interior studs are not included in this model because they do not provide moment resistance at their end connections. Various computer programs can then perform the analysis of strength and deflection.

Analyses show that end panels need to be strengthened because they resist a higher ratio of the loads along a wall. Two additional findings were: the force distribution between panels is much influenced by openings, and in short walls containing few panels, the contribution from interior panels should not be minimized. This methodology allows

for complex wall configurations, containing window and door openings, to be analyzed quickly and easily by means of general purpose computer software.

### 2.3.2 *Easley et al.*

Easley et al. (1982) developed closed-form formulas for shear wall displacement and strength based on the deformation patterns of specimens observed in load tests. These formulas were derived following methods similar to those used by Easley for corrugated metal shear diaphragms (Easley, 1977), with some modification due to the different material components and connection details. Easley et al. observed that both the frame and sheathing deform as parallelograms. When subjected to lateral loading, the panel ends rotate relative to the end frame members and the panel side edges move along the side frame members and keep parallel to one another (Figure 2.3). Based on the above observations, Easley et al. assumed the following with respect to fastener forces and wall behaviour:

1. Fastener forces in the panel ends have both x-and y- components. The x-components along the end of the panel,  $F_{ex}$ , are uniform. The y-components,  $F_{eyi}$ , are proportional to the distances from the panel centreline,  $X_{ei}$ .
2. Fastener forces,  $F_{si}$  in the interior studs, and  $F_s$  in the panel sides, act only along the studs and are proportional to the distances from the panel centreline,  $X_{si}$ .
3. Nail force-slip curve is linear.

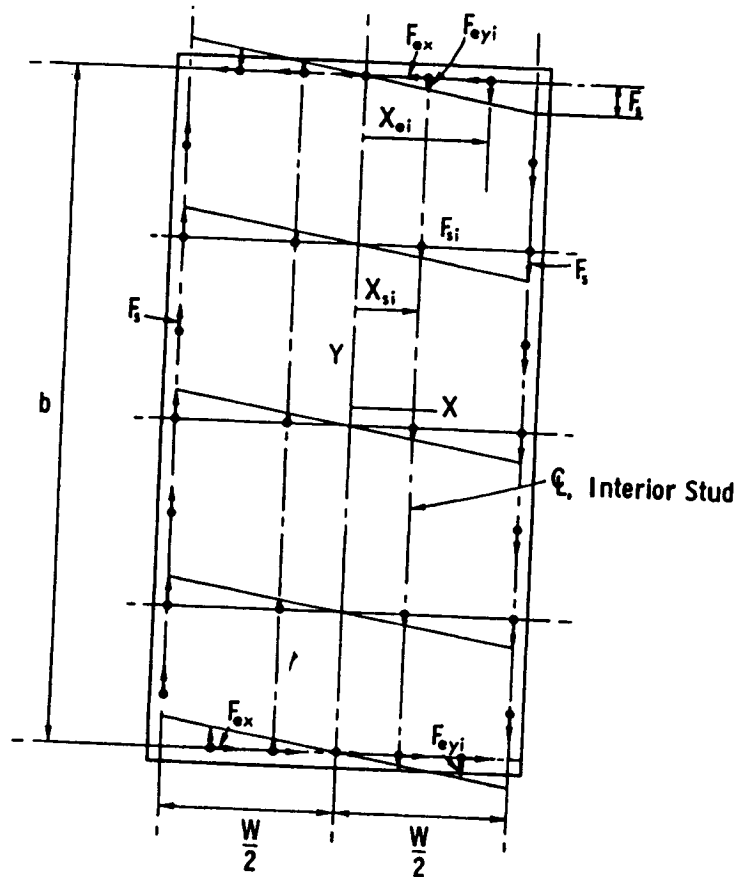


Figure 2.3 Nail Force Distribution of a Shear Wall Panel (Easley et al., 1982)

4. All the fasteners are identical, and all studs and nails are symmetrically located about the panel centreline.
5. Shear wall panels can be satisfactorily represented as isotropic materials;
6. When the wall is loaded, no separations occur in the framing member joints between the studs and the header or sill.

A closed-form equation was derived based on force and moment equilibrium for a particular panel. For side fasteners,

$$F_s = \frac{Nb}{\beta} \quad (2.18)$$

For end fasteners:

$$F_{ei} = [F_{ex}^2 + F_{eyi}^2]^{1/2} = N \left[ \left( \frac{w}{n_e} \right)^2 + \left( 2X_{ei} \frac{b}{w\beta} \right)^2 \right]^{1/2} \quad (2.19)$$

where

$$F_{ex} = Nw / n_e; \quad F_{eyi} = 2X_{ei} / w \bullet F_s; \quad F_{si} = 2X_{si} / wF_s; \quad (2.20)$$

$$\beta = n_s + \frac{4I_e + 2n_{si}I_s}{w^2}; \quad (2.21)$$

$$I_e = \sum_{i=1}^{n_e} X_{ei}^2; \quad I_s = \sum_{i=1}^m X_{si}^2; \quad (2.22)$$

$N$  = the shear force per unit length acting on the shear wall;

$n_s$  = the number of side fasteners;

$n_e$  = the number of end fasteners;

$n_{si}$  = the number of fasteners in each interior stud;

$m$  = the number of interior studs;

$w$  = the distance between two side fastener centrelines;

$b$  = the distance between two end fastener centrelines.

The largest nail force in the sheathing will occur either at the panel side fasteners or in two fasteners on each end located at the greatest distance from the panel centre line.

The shear strain  $\gamma$  is assumed to be the sum of  $\gamma_1$  and  $\gamma_2$ .

$$\gamma = \gamma_1 + \gamma_2 = N / G' \quad (2.23)$$

where

$$\gamma_1 = \frac{2\Delta_s}{w}, \quad (2.24)$$

$$\gamma_2 = \frac{N}{Gt}, \quad (2.25)$$

$$G' = \frac{1}{\left[ \frac{2b}{Kw\beta} + \frac{1}{Gt} \right]}, \quad (2.26)$$

$\gamma_1$  = the shear strain due to the localized deformations at the fasteners;

$\gamma_2$  = the shear strain in the individual panels;

$G'$  = the linear stiffness of a shear wall;

$\Delta_s$  =  $F_s/k$ , the total localized deformation at each side fastener; (2.27)

$G$  = the shear modulus of elasticity of the sheathing material;

$T$  = the thickness of the sheathing panels.

$k$  is derived from load-slip curves for connection tests which are typically nonlinear depending on the size and type of the fastener and the thickness and type of the sheathing material.

Prediction of the strength and stiffness behaviour of a series of 8' x 12' (2.44 x 3.66 m) shear walls using the above equations was compared with results from tests and finite element analyses. The following conclusions were provided by Easley et al.:

1. The accuracy of the prediction with these formulas is acceptable in engineering practice.
2. The nonlinear load-deflection relationship of connections, simply represented by the equations derived from connection test data, can be applied to calculate the nonlinear loads for a shear wall specified by the assumptions.

3. The theoretical results with the linear formula for stiffness have good agreement with the initial slope of the load-deflection relation from the test results of a shear wall.
4. The formulas for forces in the sheathing fasteners can be applied in calculating the shear walls loaded in the linear range.
5. Formulas for side fastener forces and the maximum end fastener force are applicable well into the nonlinear load-deflection range.

### *2.3.3 Gupta & Kuo*

In an attempt to create a model with higher accuracy than those described by Tuomi and McCutcheon (1978) and Easley et al. (1982), which could be applied in an iterative process, Gupta & Kuo (1985) developed an analytical approach based on the minimum potential energy principle. Elastic bending of the studs and shear energy of the sheathing were considered in this method. Some assumptions in the closed form models from Tuomi and McCutcheon (1978) and Easley et al. (1982) were eliminated and additional unknowns were introduced. In this method, there is no limitation on relative angles between the wood frame and the sheathing. The authors assumed that all the materials are linear elastic in one loading step, regardless of the nonlinearity of the nail load-slip curve. The stiffness matrix is obtained through differentiating the potential energy equation with respect to generalized coordinates,  $\gamma, \alpha, \beta$ , and  $w$ . These parameters and geometry of a typical sheathing panel are shown in Figure 2.4.

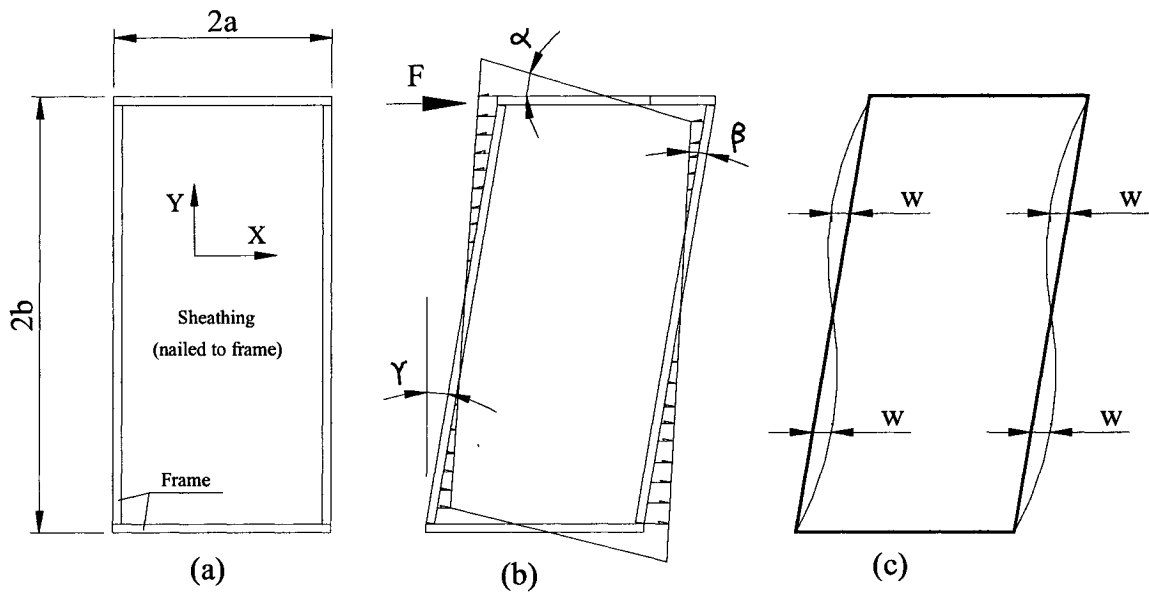


Figure 2.4 Deformation Pattern of a Typical Single Panel Wall (Gupta & Kuo, 1985)

For a multi-panel wall in a single-storey building,  $\alpha, \beta$  angles for all the panels are assumed to be the same; but three different  $w$ -amplitudes are considered:  $w_1$  for two end studs,  $w_2$  for studs at panel joints, and  $w_3$  for interior studs. The derivation of the stiffness matrix is the same as for a single panel wall.

Models that do not consider the deformation of the studs were also included in the paper by Gupta & Kuo. Comparison of the results using the model with those from tests and finite element analyses shows:

1. Proposed model is in good agreement with the results of shear wall tests.
2. Bending stiffness of the studs and the shear stiffness of the sheathing play an important role in providing the stiffness to the shear wall.
3. Bending stiffness of the studs and the shear stiffness of the sheathing provide little contribution to the load deformation properties of shear walls.

4. Constraining the stud deflection shape has the advantage of reducing the degrees-of-freedom from 6 to 3, making the calculation and computer program simpler.

Gupta & Kuo (1987a) applied their model, with some modifications, in the analysis of wood framed shear walls subject to uplift. A single-storey wall has five degrees of freedom: shear rotation of the frame, two relative rotations of the sheathing, uplift of the windward stud, and uplift of the windward panel. For walls of two or more storeys, two additional degrees of freedom were introduced for relative rotations of the sheathing in higher storeys. They verified the model by comparing the results with shear wall test data from the literature and found that vertical load and uplift restraint significantly increase the wall stiffness.

Gupta & Kuo (1987b) further applied their model to the analysis of a wood framed house. The analytical findings were in good agreement with the experimental results from Tuomi & McCutcheon (1974).

#### ***2.3.4 Kallsner & Lam***

Eurocode 5 (ENV 1995-1-1:1993) contains three models to predict shear wall performance as described by Kallsner & Lam (1995). All three models, one of which is elastic and the remaining two plastic, can be used for static analysis. In the elastic model analysis proposed by Kallsner (1984) and Akerlund (1984), the following assumptions were made:

1. Wood studs, top and bottom plates are rigid and hinged to each other.
2. Panels are rigid and free to rotate.

3. The load-displacement curve of sheathing-to-frame connections is linear and elastic until failure.
4. Relative displacements between the sheathing and the frame are small compared with the width and height of the sheets.
5. The centre points of the frame and the sheet have the same displacement, i.e. no relative translational displacement exists.

The fastener force distribution is shown in Figure 2.5. The deformation and shear resistance were determined based on the minimum potential energy principal.

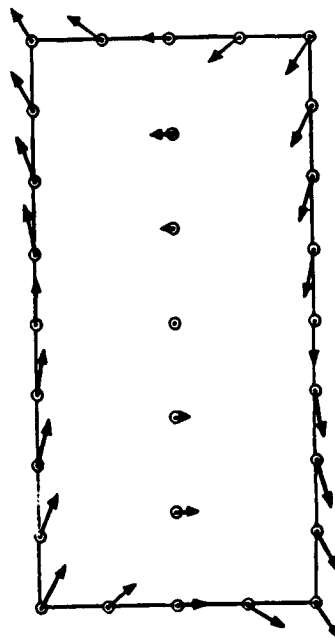


Figure 2.5 Linear Elastic Model Force Distribution (Kallsner & Lam, 1995)

The design racking load-carrying capacity  $H_d$  is

$$H_d = \frac{F_d}{h \cdot \sqrt{\left( \frac{x_{\max}}{\sum_{i=1}^N x_i^2} \right)^2 + \left( \frac{y_{\max}}{\sum_{i=1}^N y_i^2} \right)^2}} \quad (2.28)$$

The total horizontal displacement can be calculated as:

$$u_{frame} = (\gamma + \gamma_s)h = \frac{1}{K} Hh^2 \left( \frac{1}{\sum_{i=1}^N x_i^2} + \frac{1}{\sum_{i=1}^N y_i^2} \right) + \gamma_s h \quad (2.29)$$

In these two equations:

$x_i, y_i$  = coordinates referring to the centre of gravity of the fasteners;

$N$  = the number of all fasteners;

$K$  = the slip modulus for the fastener;

$H$  = the applied lateral load;

$H$  = the height of the wall;

$F_d$  = the design capacity per fastener;

$$\gamma_s = \frac{H}{Gbt}, \text{ is the shear deformation in the sheathing.} \quad (2.30)$$

In the lower bound method it is assumed that the load-displacement relationships of the fasteners are completely plastic. The force distribution also must satisfy the conditions of force and moment equilibrium. For a single panel sheet, the force distribution is shown in Figure 2.6.

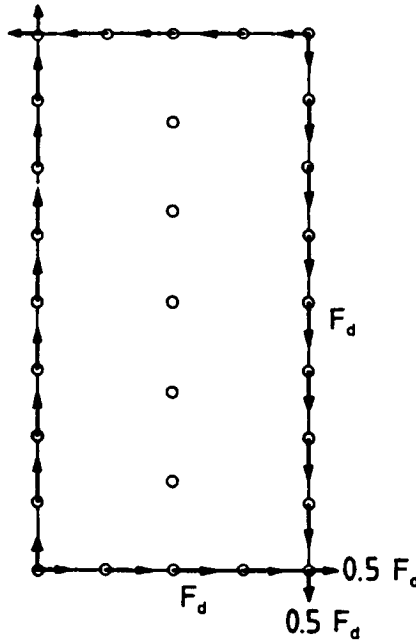


Figure 2.6 Lower Bound Model Force Distribution (Kallsner & Lam, 1995)

Each edge fastener carries the same load,  $F_d$ , except the corner fastener carries two load components, that is  $F_d/2$  parallel to the associated sides of the panel. The fasteners in the centre studs provide no contribution to the load carrying capacity. This force distribution, by itself, satisfies the force and moment equilibriums if the perimeter fastener spacing is constant. The design load carrying capacity is expressed by:

$$H_d = n \bullet F_d \quad (2.31)$$

where

$n$  = the number of fastener spaces along the top end of the panel;

$F_d$  = the design capacity per fastener.

The upper bound method is relatively complex if compared with the elastic method and the lower bound methods. Three assumptions exist:

1. Each frame member is regarded as a rigid body rotating around its own centre of rotation on the panel. The frame with one interior stud on the centre is composed of five members per panel (Figure 2.7), three vertical (AC, EF, BD) and two horizontal (AB, CD). Stud AC rotates about O1, similarly, BD about O2, CD about O3, AB about O4 and EF about O.
2. The frame members are hinged to each other. This requires that the rotation centres for frame members satisfy the condition shown in Figure 2.7. The straight lines between rotation centres must pass through the hinges. For example, the line linking O2 and O4 must pass through point B.
3. All fasteners can simultaneously reach their plastic capacity.

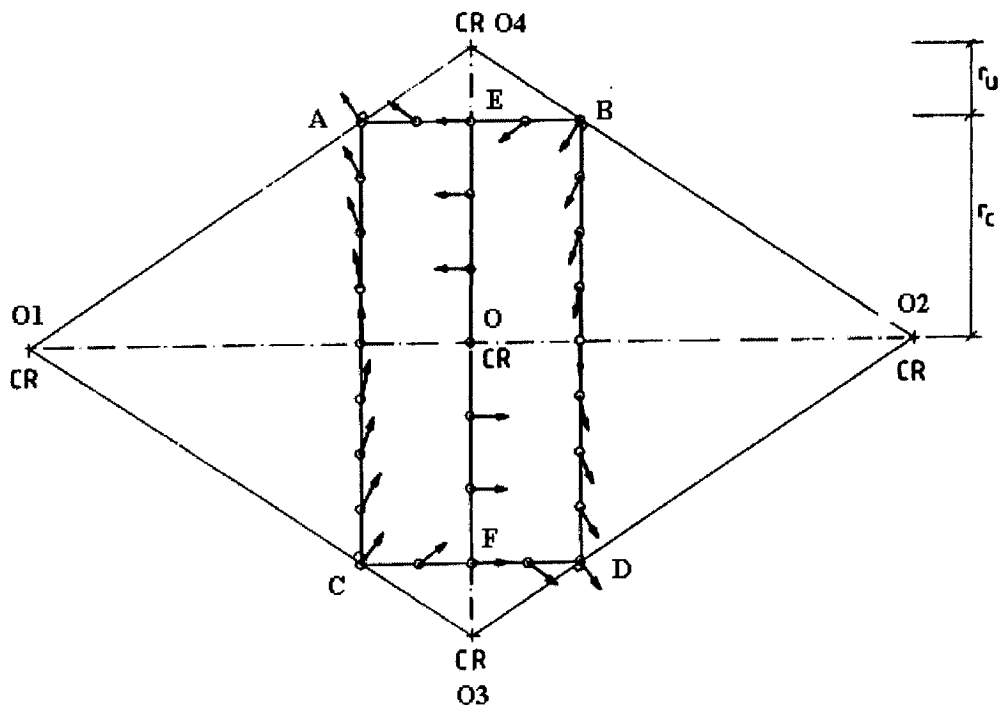


Figure 2.7 Upper Bound Model Force Distribution (Kallsner & Lam, 1995)

The design racking load carrying capacity is given by:

$$H_d = \frac{\sum_{hor} F_d \cdot r_i + \sum_{ver} F_d \cdot r_i \cdot \frac{r_u}{r_c}}{h \left( \frac{r_u}{r_c} + 1 \right)} \quad (2.32)$$

where

$$\frac{r_u}{r_c} = \frac{\gamma}{\varphi} - 1, \text{ is determined from the elastic model.}$$

$$\gamma = \frac{1}{k} H h \left( \frac{1}{\sum_{i=1}^N x_i^2} + \frac{1}{\sum_{i=1}^N y_i^2} \right), \text{ is the frame rotation;}$$

$$\varphi = \frac{1}{k} H h \frac{1}{\sum_{i=1}^N x_i^2}, \text{ is the sheathing rotation;}$$

$r_i$  is rotation radius of each fastener, which can be calculated after the rotation centres of frame members have been decided.

Kallsner & Lam concluded that the elastic model underestimated the capacity, and the upper bound plastic method overestimated the capacity of shear walls based on a comparison with full-scale tests. However, the difference in capacity obtained from these three methods is small, and the difference in the force distributions is moderate. Kallsner & Lam recommended as a general rule that the elastic model be used; however, the lower bound plastic method gives reasonable results and is very simple to incorporate into design.

### 2.3.5 Stewart

Stewart (1987) presented a relatively complete literature review and developed several models that could be used to predict the response of wood framed shear walls under racking loads. These models are simple and suitable for design office use. Both the elastic model and the ultimate strength model are based on the following assumptions:

1. The wood panels are rigid.
2. The framing members have the same cross section, and are hinged to one another. The top and bottom plates are rigid, and the studs behave linear elastically.
3. The sheathing-to-frame fasteners are evenly spaced along the perimeter of the panels, and the fastener spacing is close enough to be considered continuous.
4. The rotations of the panel and the frame are shown in Figure 2.8, in which  $\gamma_1$  and  $\gamma_2$  are independent and non zero.

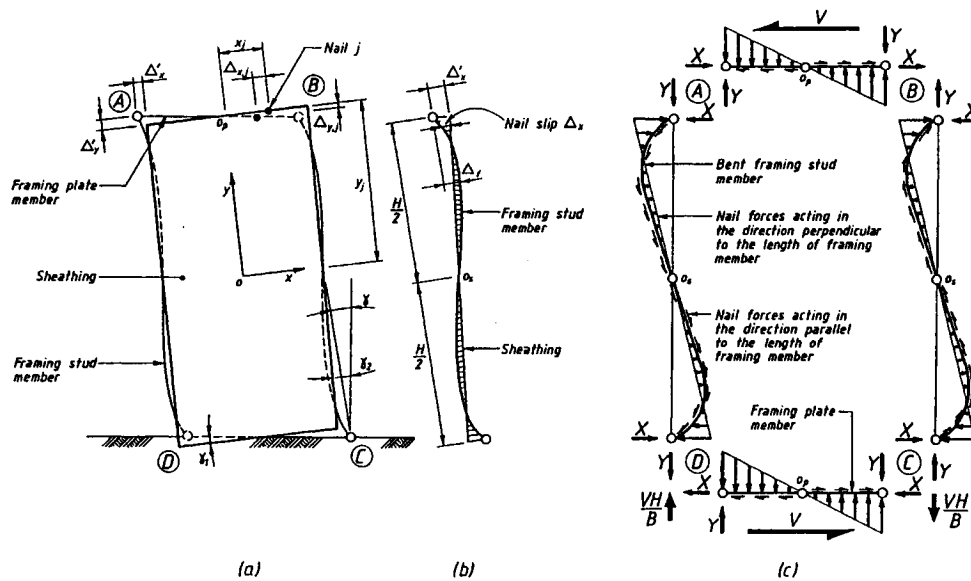


Figure 2.8 Shear Wall Deformation and Force Assumptions (Stewart, 1987)

An elastic shear wall model was developed to predict wall stiffness, framing joint forces, framing stress and sheathing stresses in the elastic range. An ultimate strength shear wall model was also developed to predict wall strength, framing joint forces, framing stresses and sheathing stresses corresponding to the ultimate strength of the wall. The two proposed models show that the load-slip characteristics of sheathing connections and their spacing have a dominant influence on wall strength and stiffness. The flexibility of the studs and separation of the framing joints have little influence on the stiffness and strength of a wall, but influence the framing flexural stress and frame joint forces. Analyses also show that the strength of a long wall with multiple panels is approximately proportional to wall length.

### **2.3.6 ANALYTICAL MODELS FROM OTHER RESOURECES**

The Timber Research and Development Association (TRADA) (1980) recommended a procedure for calculating the strength and stiffness of racking-resistant wall panels in the “*Timber Frame Housing Design Guide*” (1966). This guide provides calculation methods to determine the racking strength and stiffness based on material properties. The methods can be applied to walls with openings of any type given the following assumptions:

1. The frame is distorted into a parallelogram while the sheathing panels rotate relative to it until the load on the corner nails reaches its maximum capacity.
2. The frame members remain in contact.

Murakami et al. (1999) developed simple formulas for determining the nonlinear performance of a single-panel wall without limitations on fastener pattern and sizes of the sheathing panel. The nail load-slip curve is approximately represented by a bilinear elastic-plastic curve. Based on the forces and moment equilibrium, the moment on a wall at the yield point is determined by the yield strength and fastener pattern. In the nonlinear range, the calculation requires an iterative solution. A total of 759 models with different wall configurations were numerically solved to perform a regression analysis. The applied inelastic moment calculated with the closed-form equations was determined by rotation angles, and the moments at the yield point and at the plastic point. The accuracy of the approximate formulae has been verified by comparing with experimental results.

Salenikovich et al. (2000) completed 56 full-scale tests with different overturning restraints, as well as a series of connection tests. Mechanics-based analytical models were also developed to predict the strength and deflection of wood frame shear walls with or without overturning restraint. It was concluded that the models could accurately predict the load capacity and deflection of fully anchored and unrestrained wood frame shear walls.

## **2.4 FINITE ELEMENT ANALYSIS**

In order to overcome the limitations due to the assumptions made for closed-form models, discussed in the previous section, finite element analysis may be employed to predict the performance of wood framed shear walls. With the development of computer

techniques, more and more aspects can be taken into account in the analysis including nonlinear behaviour. Because the scope of this thesis is directed towards the closed-form analytical approaches, only a brief review of some finite element investigations will be presented.

Foschi (1977) presented formulations for the structural analysis of wood diaphragms incorporated in the computer program SADT, taking into account four different and basic structural elements:

1. The sheathing material was elastic, orthotropic and subjected to two-dimensional state of stress.
2. The framing members were linear beam elements, and higher accuracy can be obtained if more segments are used.
3. The connections between frame members were idealized as springs with three different loading conditions which are assumed to be nonlinear.
4. The sheathing-to-frame connections were represented by two-degree-of-freedom springs whose load-slip curve is based on an exponential function derived from test data.

Compared with test results, these formulations show good ability to predict diaphragm deformation and ultimate loads.

Dolan (1989) developed three numerical models to predict the behaviour of wood framed shear walls. One model, FREWALL, is a closed form mathematical model that was developed to predict the steady state response of shear walls to harmonic base excitations. The other two models are finite element models. One predicts the static behaviour of shear walls (also discussed in Dolan & Foschi (1991)) and the other predicts

the dynamic response to earthquakes. Both of Dolan's models are based on the model presented by Foschi (1977) with the following extension: 1) The programs can be used to predict the ultimate load capacity of the walls; 2) The adjacent sheathing panels can contact and press each other; 3) The sheathing is not rigid; 4) The effect of bearing and gap formation between framing elements is included. Two finite element programs were developed based on the modeling analyses. One is SHWALL for static analysis and the other is DYNWALL for dynamic analysis.

Tests were performed to determine the load-deflection characteristics of single nail connections. Forty-two full-size shear wall specimens were tested to verify the three numerical models. Dolan concluded that the analysis can be simplified and improved by eliminating minor variables to make the program more effective.

Itani & Cheung (1984) presented a finite element model to analyze the nonlinear load-deflection behaviour of sheathed wood diaphragms including walls, floors, ceilings, and roofs. Fasteners are represented by a series of mutually perpendicular nonlinear spring-pairs (single line of fasteners), which connect the sheathing and the frame. Plywood sheathing in diaphragms is modeled as two-dimensional linear plane stress element represented by a 4-node quadrilateral element. The studs of the diaphragm are modeled as linear beam elements. A computer program NONSAP with some modification was used to perform the analysis. The model is general and no restriction is imposed on sheathing arrangements, load application, and geometry of distorted diaphragms. Good agreement between experimental results and the analytical predictions was obtained.

Falk & Itani (1989) further simplified the model presented by Itani & Cheung (1984) in order to analyze a diaphragm with multiple sheets. A transfer element is linked between a single sheathing element and at least four beam elements. The number of nodes and the number of DOF are determined by these transfer elements, not by the number of fasteners.

Gutkowski & Castillo (1988) presented a finite element method specifically developed for shear walls, and compared experimental data with analytical results performed by the software WANELS. They concluded that the load-deflection relationship of walls sheathed with plywood and/or GWB could be predicted with good agreement, and the successful analysis of shear walls depends on the accuracy of the load-deformation of the panel-to-frame connections.

White & Dolan (1995) developed a finite element program WALSEIZ, which is a modification of the program developed by Dolan (1989). The modifications include:

1. The number of degrees of freedom in the plate, sheathing-bearing connector, and sheathing-to-framing connector is reduced;
2. The program can be used to perform load controlled monotonic analysis and calculate forces and stresses;
3. The program can perform the analysis of large walls with or without openings.

The results from the program were compared to experimental data from Dolan (1989). Good agreement was obtained for both monotonic and dynamic response.

Kasal & Leichti (1992) developed a nonlinear finite element model for light frame stud walls. They transformed a three-dimensional wood-frame stud wall into a simple

two-dimensional model with the application of energy concepts. The detailed model is used to simulate the simple tests of real substructure such as wood framed shear walls.

At the same time, several models for dynamic analysis have been developed by Stewart (1987), Filiatrault (1990), Dolan (1989) and other researchers. Models for the analysis of a wood framed house have also been developed by Gupta & Kuo (1987), Schmidt & Moody (1989) and Nelson et al. (1985).

## **2.5 ANALYTICAL APPROACHES FOR LIGHT GAUGE STEEL FRAME / WOOD PANEL SHEAR WALLS**

Fulop & Dubina (2003) recommended that the method from the “*European Recommendations for the Application of Metal Sheeting Acting as a Diaphragm, 1995*” (ECCS, 1995) be used for the situation where sheathing panels are made of corrugated steel sheeting, but only for an elastic range analysis. They also recommended that an acknowledged method used in wood framed shear walls can be applied in the case of OSB panels.

At present, no literature is available regarding analytical approaches specifically for light gauge steel frame/wood panel shear walls. Previous research has been focused on experimental study.

## CHAPTER 3 SHEAR WALL TESTS

### 3.1 INTRODUCTION

In the summer of 2003, a total 109 full-scale light gauge steel frame / wood panel shear walls were tested in the Jamieson Structures Laboratory of the Department of Civil Engineering and Applied Mechanics at McGill University. The wall test specimens were 8' (2440mm) in height with widths of 2' (610 mm), 4' (1220 mm) and 8' (2440 mm). In all cases, ASTM A653 (2002) Grade 230 steel was used (0.044"/1.12 mm) for the studs and tracks. Of the total number of tests, the author tested 46 walls that were constructed of various combinations of wood sheathing (CSP and OSB), which was connected to the light gauge steel frame with No. 8 sheathing screws at 3" (75 mm), 4" (100 mm) or 6" (150 mm) spacing around the panel perimeter. Each wall combination consisted of a minimum of six specimens, three of which were tested monotonically and three cyclically using the CUREE protocol for ordinary ground motions (Krawinkler et al., 2000; Boudreault, 2004). In some cases, additional tests were carried out because the measured shear loads were not within a 10% range, i.e. tests 31D, E, F and 34D.

The walls were tested in a self-equilibrating frame specifically designed for shear wall testing (Figure 3.1). The out-of-plane movement of the test specimens was limited by the HSS lateral bracing frames. A 250 kN (55 kip) dynamic actuator with a stroke of  $\pm 125$  mm ( $\pm 5$ " ) was used to provide lateral loading (Zhao, 2002).



Figure 3.1 Shear Wall Test Frame

In this thesis, only the 46 tests carried out by the author are reported in detail. The results from the other shear wall tests (Branston, 2004; Boudreault, 2004) are incorporated in a comparison of wall parameters and performance in Chapter 4. Furthermore, a detailed description of the wall components, construction sequence, instrumentation, testing protocols and data reduction is provided by Branston (2004) and Boudreault (2004), and hence is not repeated in this document.

### **3.2 TEST MATRIX**

The 46 specimens reported in this thesis were comprised of 24 monotonic tests and 22 cyclic tests of light gauge steel framed shear walls sheathed with Canadian

softwood plywood (CSP) or oriented strand board (OSB). A description of the variables included in the shear wall testing is provided in Table 3.1.

Table 3.1 Description of Wall Specimens

Specimen ID	Loading Protocol <sup>1,2</sup>	Length of Wall (ft)	Height of Wall (ft)	Panel Type	Thickness of Panel (mm)	Fastener Schedule <sup>3</sup> (in.)
15 – A,B,C	Monotonic <sup>1</sup>	2	8	CSP	12.5	6/12
16 – A,B,C	CUREE <sup>2</sup>	2	8	CSP	12.5	6/12
17 – A,B,C	Monotonic	2	8	CSP	12.5	4/12
18 – A,B,C	CUREE	2	8	CSP	12.5	4/12
19 – A,B,C	Monotonic	2	8	OSB	11	6/12
20 – A,B,C	CUREE	2	8	OSB	11	6/12
27 – A,B,C	Monotonic	2	8	OSB	11	4/12
28 – A,B,C	CUREE	2	8	OSB	11	4/12
29 – A,B,C	Monotonic	8	8	CSP	12.5	6/12
30 – A,B,C	CUREE	8	8	CSP	12.5	6/12
31 – A,B,C,D,E,F <sup>4</sup>	Monotonic <sup>5</sup>	8	8	CSP	12.5	4/12
32 – A,B,C	CUREE	8	8	CSP	12.5	4/12
33 – A,B,C	Monotonic	8	8	CSP	12.5	3/12
34 – A,B,C,D <sup>4</sup>	CUREE	8	8	CSP	12.5	3/12

<sup>1</sup>The monotonic testing protocol is explained in Section 3.4;

<sup>2</sup>The CUREE reversed cyclic protocol for ordinary ground motions is described in Section 3.4;

<sup>3</sup>Fastener schedule (e.g. 6"/12") refers to the spacing between sheathing to framing screws around the edge of each panel and along intermediate studs (field spacing), respectively;

<sup>4</sup>CSP used in 31E, F and 34D are from Richply; the remaining CSP panels are from Alberta plywood;

<sup>5</sup>In 31D,E, for the monotonic protocol the unloading to zero load at a displacement of 0.5" (12.5mm) and 1.5"(38mm) was removed.

1 foot (ft) = 305 mm

1 inch (in.) = 25.4 mm

Additional information on the materials used to construct the test specimens is listed below:

1. All the CSP panels were graded as sheathing conforming to CSA O151 (1978) with a thickness of 12.5 mm (1/2"). The CSP panels were from Alberta Plywood (Mill: AB 244) (Figure 3.2), except those in 31E, F and 34D, which were from Richply (Mill: AB 244) (Figure 3.3). The wood species contained in these two types of CSP panels were identified by CanPly based on samples obtained from the test specimens. The typical mechanical properties for these species are as listed in Table 3.2 (Forest Product Laboratory, 1999).

Table 3.2 Mechanical Properties of Wood Species in CSP Panels

Mill No.	Position	Wood Species	Specific Gravity	Static Bending		Compression Parallel to Grain (kPa)	Compression Perpendicular to Grain (kPa)	Shear Parallel to Grain (kPa)
				Modulus of Rupture (kPa)	Modulus of Elasticity (MPa)			
1/2" BC858	Face	DF	0.45	88000	13600	50000	6000	9500
	Inner	H/B	0.41	81000	12300	46700	4600	6500
	Inner	H/B	0.41	81000	12300	46700	4600	6500
	Back	DF	0.45	88000	13600	50000	6000	9500
1/2" AB244	Face	LPP	0.40	76000	10900	43200	3600	8500
	Inner	S	0.35	63000	10000	37000	3400	6800
	Inner	S	0.35	63000	10000	37000	3400	6800
	Back	S	0.35	63000	10000	37000	3400	6800

Notes:

1. Wood species as identified by CanPly. S = Western White Spruce; LPP = Lodgepole Pine; H/B = HemBal, mixture of Hemlock or Amabilis Fir; DF = Douglas Fir.
2. Specific gravity is based on weight when oven-dry and volume when green. All the specific gravities and mechanical properties are quoted from Forest Product Laboratory (1999).



Figure 3.2 Panel Markings of Alberta Plywood CSP (Mill: AB 244)



Figure 3.3 Panel Markings of Richply CSP (Mill: BC 858)

2. All the 11 mm (7/16") OSB panels were marked 1R24/2F16/W24 in accordance with CSA O325 (1992) (Figure 3.4). The panels were also stamped according to Grade O-2 following CSA O437 (2001) and 24/16 rated sheathing under US product standard PS 2 (APA, 1992).

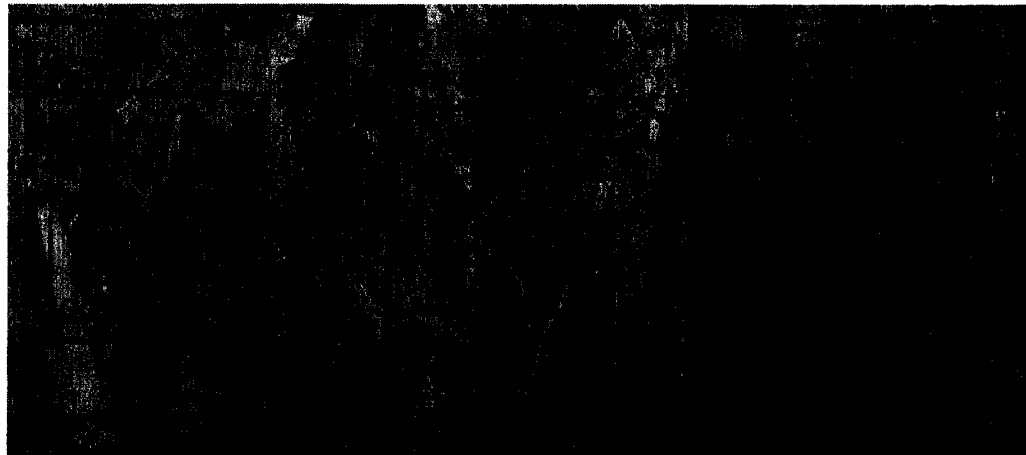


Figure 3.4 Panel Markings of OSB

3. Sheathing fasteners were No.8 x 1.5" self-piercing bugle head LOX drive screws (from Grabber Superdrive). The distance from the panel edges was 0.5" (12.7 mm).

4. Steel studs were 3-5/8"(W) x 1-5/8"(F) x 1/2"(Lip) in size, and tracks were 3-5/8"(W) x 1-3/16"(F). All steel was 0.044" (1.12 mm) thick Grade 230 ASTM A653 (2002).
5. Back-to-back studs were used at ends of the walls to prevent both flexural and local buckling failure of a single chord stud. These chord studs were connected with two No. 10-16 x 3/4" Hex washer head self drilling screws at 12" on centre.
6. Framing screws were No.8 x 0.5" self-drilling wafer head screws.
7. Hold-downs were Simpson Strong-Tie S/HD10 with ASTM A307 (2003) 7/8" anchor rods. Each hold-down was attached to the chord studs by 33 No. 10-16 x 3/4" Hex washer head self-drilling screws.
8. All panels were positioned vertically.
9. For 8' x 8' walls, a 1/8" gap was placed between the panels as recommended for the installation of wood sheathing.
10. In addition, back-to-back studs were used at the interior panel joint of the 8' x 8' walls so that the required 0.5" edge spacing could be maintained. These studs were also connected with two No. 10-16 x 3/4" Hex washer head self drilling screws at 12" on centre

### **3.3 FABRICATION AND TEST SETUP**

The configuration of an 8' x 8' test wall is shown in Figure 3.5. Each wall was first assembled on the floor of the structures lab. Chord members made of back-to-back studs

connected together with two No. 10 Hex head self-drilling screws spaced 12" on centre, were used at the ends of the wall and at the panel joint. Single studs spaced at 24" were used elsewhere. Studs and tracks were connected with No.8 gauge 0.5" self-drilling wafer head truss screws. The panels were then attached to the steel frame with No.8 x 1.5" Grabber self-drilling screws as per the wall configuration spacing requirement. During construction, the moisture content of the wood panel was measured with an electronic moisture meter (Delmhorst Instrument Co. RDM-2 (Delmhorst, 2003)). Readings were taken at various locations on the panel to ensure that the panel moisture content was not in excess of 10 %. In addition to recording the moisture content, all relevant information from the grade stamps on the panel, as well as imperfections in the assembled wall were recorded on the Test Data Sheets and Test Observation Sheets (Branston et al., 2004).

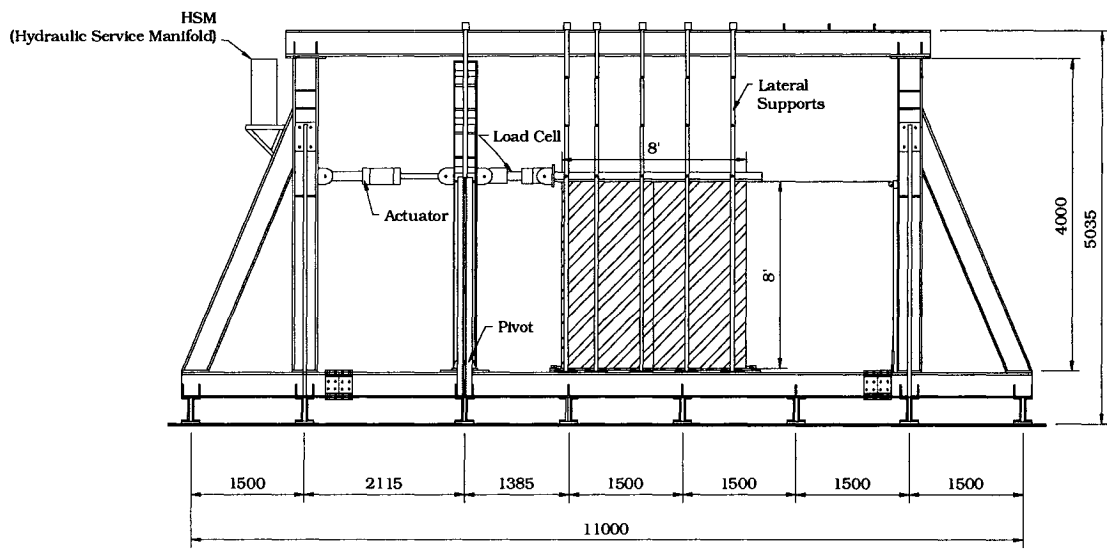


Figure 3.5 Test Frame with 8' x 8' Wall Specimen

After assembly, each 8' x 8' wall was then lifted and fixed into the test frame. The top track was connected to the loading beam (HSS 89x89x6.4 mm) with twelve 3/4"

A325 bolts (each bolt with a 2.5"x2.5"x1/8" steel washer). A 25 mm thick aluminum spacer was placed between the loading beam and the top track to allow the wood panels to rotate freely. The bottom track was fixed to the supporting frame with six 3/4" A325 shear anchors (each bolt with a 2.5"x2.5"x1/8" steel washer). A 25 mm thick steel plate was also placed as a spacer between the bottom track and the support. Two Simpson Strong-Tie S/HD10 hold downs with 7/8" anchor rods were placed at the ends of the wall. The nut on each anchor rod was first tightened by hand until snug, and then a wrench was used to turn the nut another half turn as per the manufacturer's instructions (Simpson, 2001).

The configuration of a 2' x 8' test wall is shown in Figure 3.6. The same setup procedure as followed for the 8' x 8' walls was adopted except that middle studs were not installed. The sheathing was cut from a standard 4' x 8' sheet, with the first half of the panel used for a monotonic specimen, while the second half was used for a cyclic wall in the same wall configuration group. The top track was connected to the load beam with three 3/4" A325 bolts. One 3/4" inch A325 shear anchor and two Simpson Strong-Tie S/HD10 hold downs were used to fix the bottom track to the support. The loading beam was the same as that used in the 4' x 8' wall tests (Branston, 2004).

Diagrams of screw spacing patterns for each wall configuration, as well as anchorage details are provided in Appendix I. Selected photographs of wall components are shown in Appendix II.

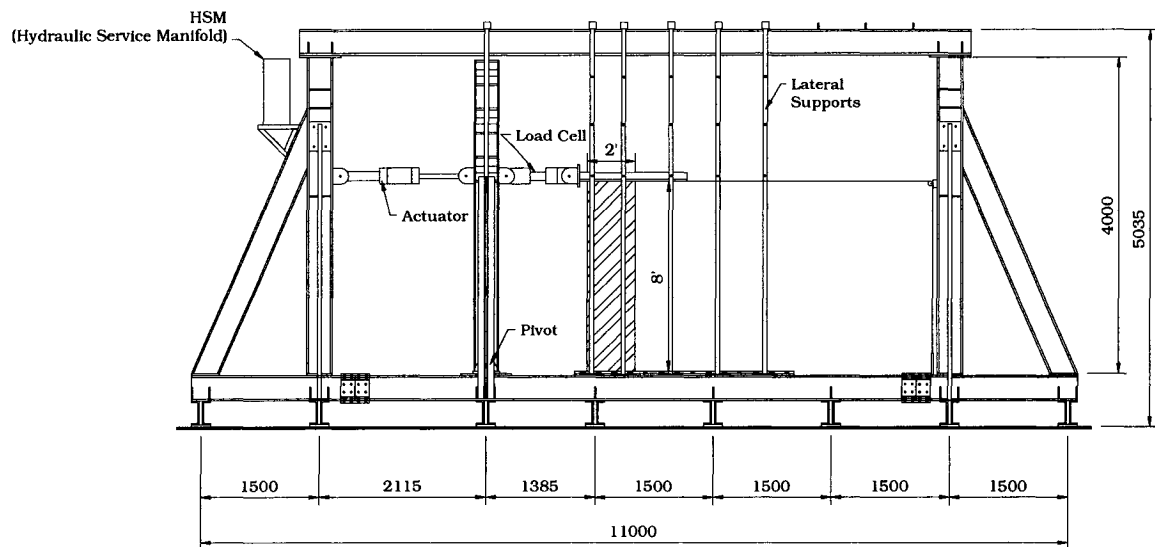


Figure 3.6 Test Frame with 2' x 8' Wall Specimen

### 3.4 LOAD PROTOCOLS

Two general displacement controlled test protocols were incorporated into this study: 1) a monotonic protocol similar to that used by Serrette et al. (1996), and 2) the CUREE ordinary ground motions reversed cyclic loading protocol (Krawinkler et al., 2000). In the case of the monotonic tests, the speed of loading was 7.5 mm per minute until the failure of the wall, which was defined as a sudden drop of the load carrying capacity. In order to evaluate the permanent set at 0.5" (12.7 mm, approximate 1/200 of the wall height 8') and 1.5" (38.0 mm, about 1/65 of the wall height), each test wall was unloaded to zero force once these two displacements were attained (Serrette et al., 1996b). Once the force in the wall was unloaded to zero, the loading was recommenced at the same rate (Figure 3.7). A modified monotonic protocol was also used for tests 31D

and E, in which the permanent set was not evaluated (Figure 3.8). The monotonic tests were carried out in order to obtain information on the static wind loading resistance of a shear wall, and in addition were necessary to establish the reversed cyclic testing protocols. The modified monotonic protocol was followed for the testing of two specimens to evaluate the effect of the two unloading cycles on the shear wall performance.

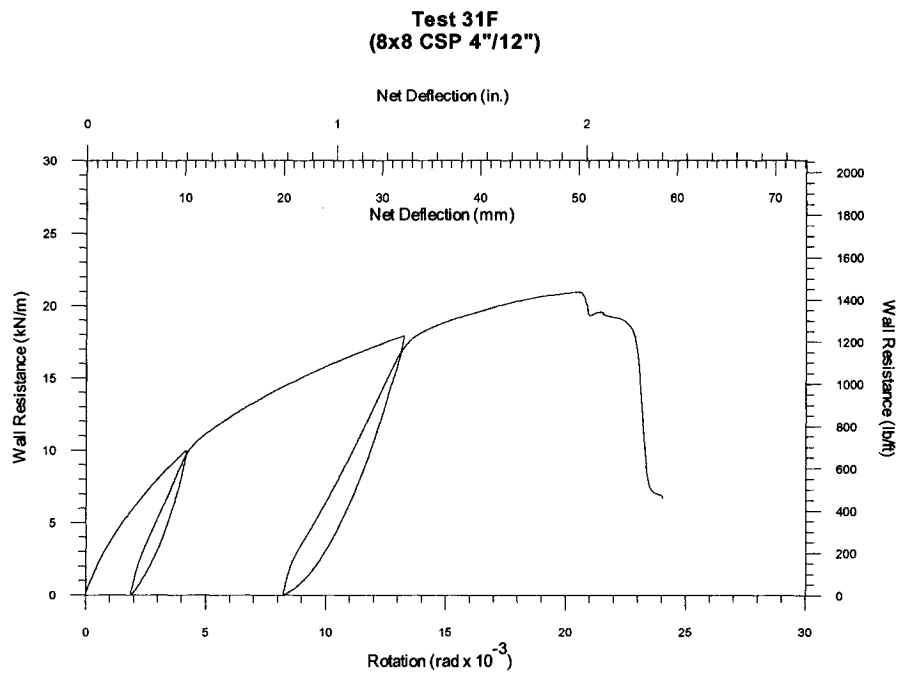
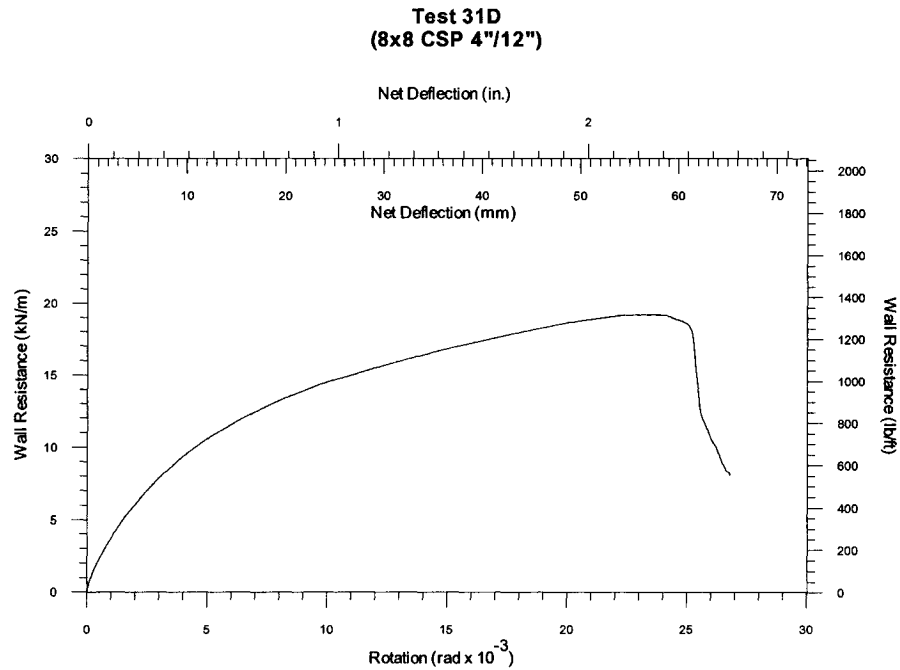


Figure 3.7 Typical Load-Deflection Curve for Monotonic Tests  
(with permanent set unloading)



**Figure 3.8 Modified Load-Deflection Curve for Monotonic Tests  
(without permanent set unloading)**

The CUREE ordinary ground motions reversed cyclic loading protocol was selected for use because it was developed to represent the demand on a light framed wood shear wall under seismic loading. The type of structure that these wood walls are used for is similar to what would be constructed with the steel frame / wood panel shear walls, and hence their behaviour under seismic loading is expected to be related. Additional information on the choice of a reversed cyclic loading protocol can be found in Boudreault (2004), and a detailed description of both protocols is provided in Branston (2004).

The cyclic protocol for each wall configuration was dependent on the maximum deformation capacity,  $\Delta_{max}$ , obtained from the matching monotonic tests. This maximum deformation refers to the post-peak wall displacement at a load of 80% of ultimate. A reference deformation,  $\Delta = 0.6 \Delta_{max}$ , was then relied on to determine the amplitude of the

different loading cycles. A typical reversed cyclic load vs. displacement test hysteresis is illustrated in Figure 3.9. All seven CUREE protocols used for the different wall configurations can be found in Appendix III.

The frequency of the reversed cyclic tests was kept at 0.5 Hz for most wall configurations, however in some cases this was changed to 0.25 Hz in the last sets of primary cycles and their trailing cycles because the required actuator input was greater than 100 mm. Furthermore, for the 2' long walls when the required input displacement was beyond 125 mm, the maximum range of the actuator, 125 mm was adopted as the input displacement. Additionally, if the  $1.5\Delta$  primary cycles were more than 125 mm, then the last set of cycles, that is  $2.0\Delta$  and  $1.5\Delta$  were omitted from the protocol (see Appendix III). A sine curve was used to connect the displacement amplitudes for the reversed cyclic protocol. As an example, the full protocol for wall configuration 8' x 8' CSP 6'/12' (Test 30A) is shown in Figure 3.10.

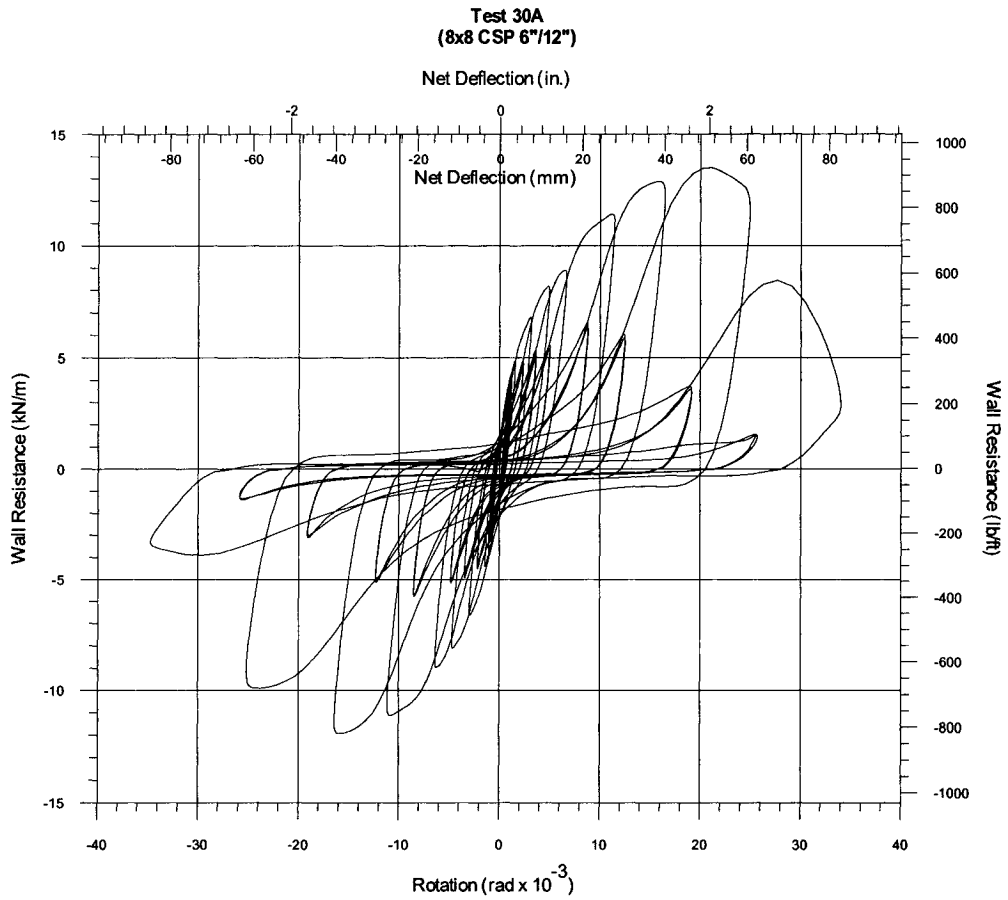


Figure 3.9 Typical Reversed Cyclic Load vs. Displacement Test Hysteresis

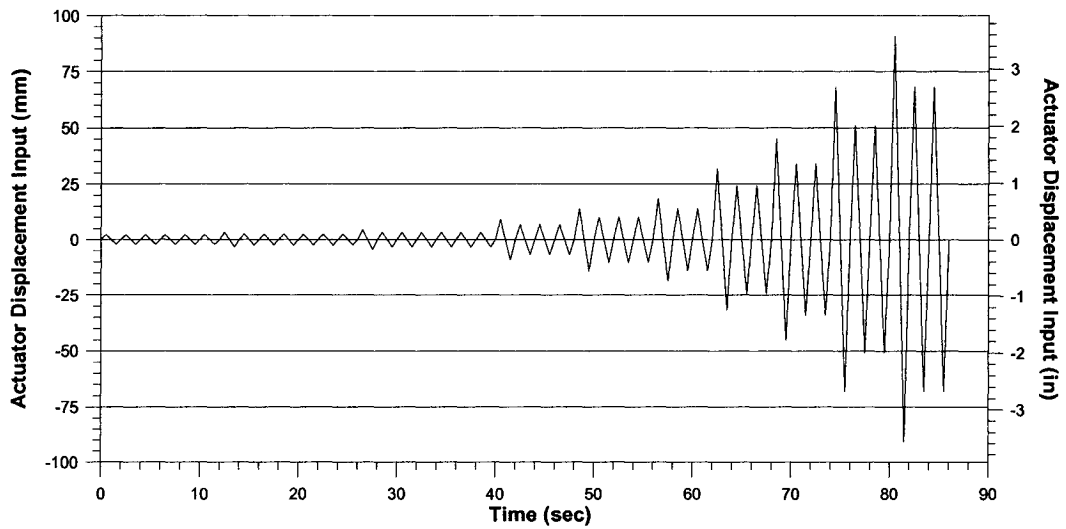


Figure 3.10 Typical Displacement-Time History Curve for Reversed Cyclic Tests

### 3.5 INSTRUMENTATION AND MEASUREMENT

Once each test wall had been installed in the test frame various LVDTs were placed on the specimen to measure displacements, including: wall slip, uplift, relative movement between the wood panel and steel track as well as top of wall movement and the movement of the braces. In addition, the displacement of the actuator was monitored. The arrangement of LVDTs is shown in Figure 3.11.

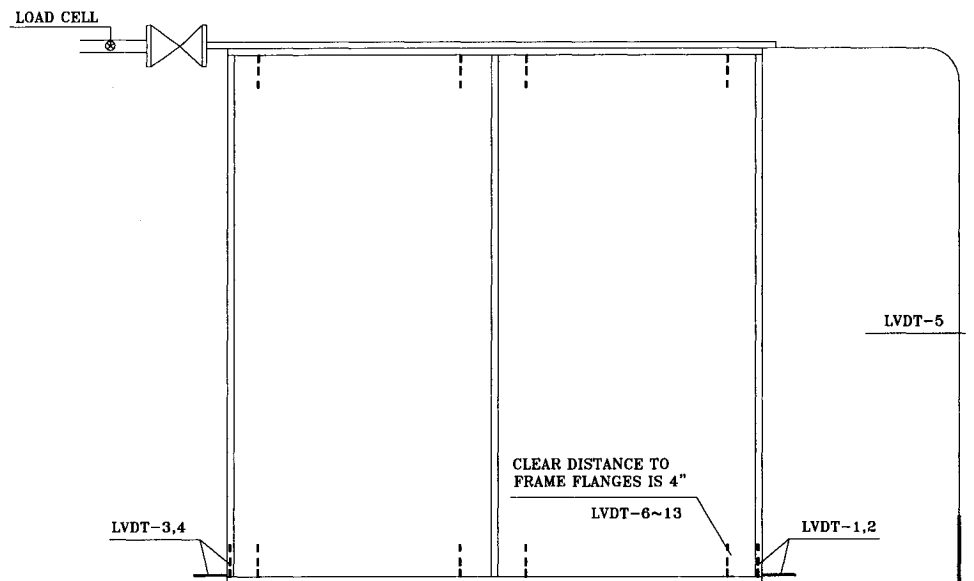


Figure 3.11 Layout of LVDTs on 8' x 8' Wall

A 250 kN capacity load cell was relied on to measure the force being applied on the wall by the actuator. In cyclic tests, an accelerometer was attached to the load cell assembly to measure the acceleration of the load beam. With this information and the mass of the load beam and load cell assembly (250 kg for a 8' x 8' Wall and 200 kg for a 2' x 8' Wall respectively), the inertial effect could be accounted for in reversed cyclic

tests. All LVDTs and load cells, as well as the accelerometer, were connected to Vishay Model 5100B scanners with data being recorded using the Vishay System 5000 StrainSmart software. For all monotonic tests, data was recorded at 2 scans per second, whereas for all reversed cyclic tests, data was recorded at 50 scans per second. Upon completion of each test, two samples were drilled from each wood panel to measure the moisture content according to APA Test Method P-6 (APA PRP-108, 2001). The moisture content of the wall test specimens ranged from 4.91% to 5.50% for the OSB panels and from 4.84% to 8.49% for the CSP panels.

### 3.6 GENERAL TEST RESULTS

A detailed description of the test data reduction method is provided by Branston (2004) and Boudreault (2004). Test results / curves for all of the author's wall specimens are presented in Branston et al. (2004), which also includes the test data sheet and test observations for each test. A summary of the parameters used to describe the wall behaviour in monotonic tests is given here:

1. Net deflection is defined by Equation (3.1) (Branston, 2004) as:

$$\Delta_{net} = \Delta_{walltop} - \left[ \left( \frac{\Delta_{baseslip1} + \Delta_{baseslip2}}{2} \right) \right] - \left[ (\Delta_{uplift1} - \Delta_{uplift2}) \times \frac{H}{L} \right] \quad (3.1)$$

where,

$\Delta_{net}$  = Net lateral in-plane displacement at the top of the wall

$\Delta_{walltop}$  = Total measured wall-top displacement

$\Delta_{base\ slip\ 1,2}$  = Measured slip at ends 1 and 2 of the wall specimen

$\Delta_{uplift\ 1,2}$  = Measured uplift at ends 1 and 2 of the wall specimen

$H$  = Height of the wall specimen (8' = 2440 mm)

$L$  = Length of the wall specimen

and the net rotation of the wall is defined by Equation (3.2) as:

$$\theta_{net} = \frac{\Delta_{net}}{H} \quad (3.2)$$

2. The shear strength is defined as unit shear load,  $S$ ,

$$S = \frac{F}{L}, \text{ kN/m} \quad (3.3)$$

where

$F$  = recorded load, kN,

3. Energy dissipation in a monotonic wall specimen is depicted as the shaded area in Figure 3.12. The unloading portions at  $\Delta = 12.5$  mm and  $\Delta = 38$  mm of the wall resistance vs. net deflection curve are not considered in the energy calculation.

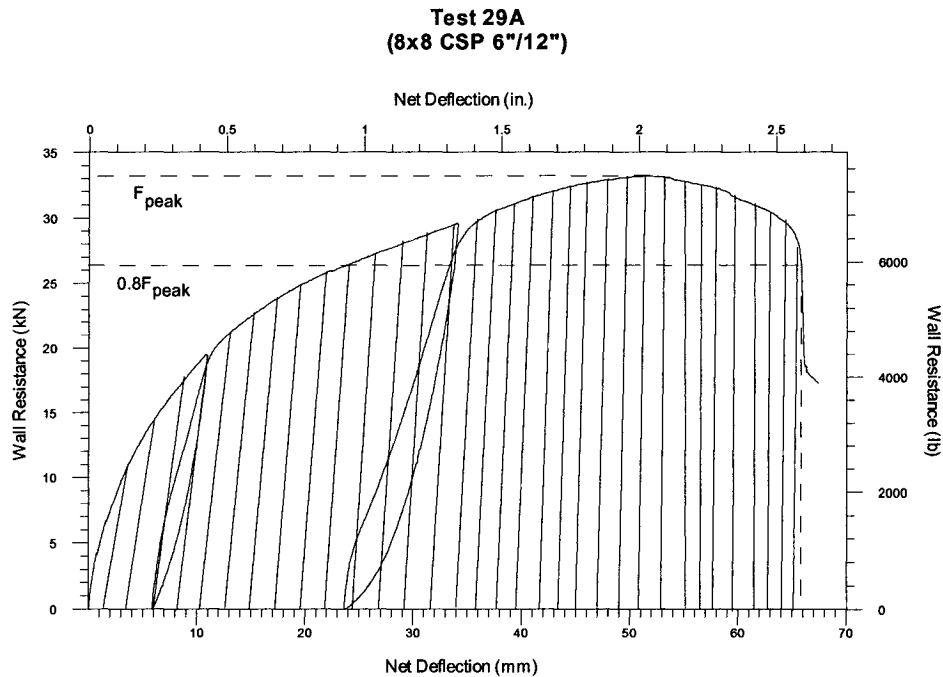


Figure 3.12: Energy Dissipation for a Monotonic Shear Wall Specimen

In cyclic tests, the parameters are as defined in monotonic tests, except that:

- 1) The parameters are determined independently for the positive and negative backbone curves;
- 2) The inertial effects are included in the shear strength calculation, using Equation (3.4):

$$S' = S \pm \left( \frac{a \times g \times m}{1000 \times L} \right) \quad (3.4)$$

where,

$S'$  = Wall resistance (corrected for inertia), kN/m;

$a$  = acceleration as measured by accelerometer, g;

$g$  = acceleration due to gravity (9.81 m/s<sup>2</sup>)

$m$  = mass (250 kg for a 8' long wall and 200 kg for a 2 long wall)

- 3) The energy dissipated by the wall specimen is defined as the area enclosed by the hysteretic loops. A single example loop is shown in Figure 3.13:

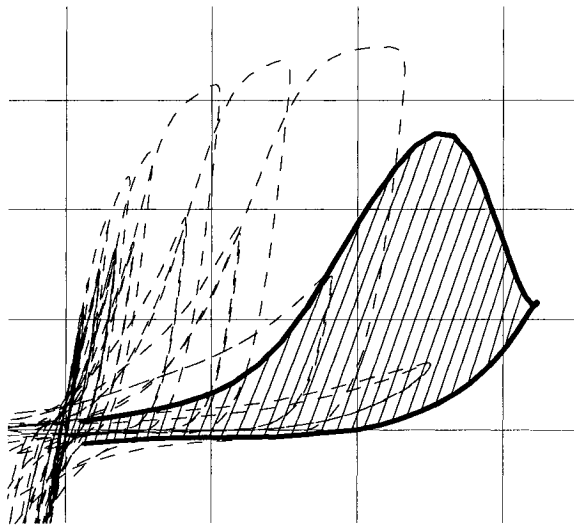


Figure 3.13: Energy Dissipation For a Reversed Cyclic Test (Branston, 2004)

Table 3.3 and 3.4 list the test results from monotonic and cyclic tests respectively. The performance of the light gauge steel frame / wood panel shear walls based on these data is to be evaluated in Chapter 4.

Table 3.3 Monotonic Shear Wall Test Results

TEST	PANEL TYPE	FASTENER SCHEDULE	MAXI. WALL RESISTANCE ( $S_u$ ) kN/m	DISP. AT $S_u$ ( $\Delta_{net,u}$ ) mm	DISP. AT 0.8 $S_u$ ( $\Delta_{net,0.8u}$ ) mm	ROT. AT $S_u$ ( $\theta_{net,u}$ ) RAD.	ROT. AT 0.8 $S_u$ ( $\theta_{net,0.8u}$ ) RAD.	ENERGY DISSIPATION, E JOULES
15A	CSP	6"/12"	11.8	99.3		0.0407		
15B	CSP	6"/12"	12.4	101.2	119.6	0.0415	0.0490	682
15C	CSP	6"/12"	12.5	109.6	143.7	0.0449	0.0589	776
<b>AVERAGE</b>	<b>CSP</b>	<b>6"/12"</b>	<b>12.2</b>	<b>103.3</b>	<b>131.7<sup>1</sup></b>	<b>0.0424</b>	<b>0.054<sup>1</sup></b>	<b>729<sup>1</sup></b>
17A	CSP	4"/12"	17.4	108.0	132.3	0.0443	0.0542	1027
17B	CSP	4"/12"	18.5	112.0	136.5	0.0459	0.0560	1130
17C	CSP	4"/12"	18.1	100.9	122.2	0.0414	0.0501	994
<b>AVERAGE</b>	<b>CSP</b>	<b>4"/12"</b>	<b>18.0</b>	<b>107.0</b>	<b>130.4</b>	<b>0.0439</b>	<b>0.0535</b>	<b>1050</b>
19A	OSB	6"/12"	12.5	78.1	99.9	0.0320	0.0410	596
19B	OSB	6"/12"	12.7	79.7	97.1	0.0327	0.0398	589
19C	OSB	6"/12"	12.2	77.5	101.0	0.0318	0.0414	616
<b>AVERAGE</b>	<b>OSB</b>	<b>6"/12"</b>	<b>12.5</b>	<b>78.4</b>	<b>99.3</b>	<b>0.0322</b>	<b>0.0407</b>	<b>600</b>
27A	OSB	4"/12"	19.5	80.1	96.9	0.0329	0.0398	922
27B	OSB	4"/12"	17.7	75.5	100.3	0.0310	0.0411	887
27C	OSB	4"/12"	17.9	78.4	97.3	0.0321	0.0399	839
<b>AVERAGE</b>	<b>OSB</b>	<b>4"/12"</b>	<b>18.4</b>	<b>78.0</b>	<b>98.2</b>	<b>0.0320</b>	<b>0.0403</b>	<b>882</b>
29A	CSP	6"/12"	13.6	51.7	65.8	0.0212	0.0270	1735
29B	CSP	6"/12"	13.8	49.6	66.3	0.0203	0.0272	1784
29C	CSP	6"/12"	13.3	50.3	69.0	0.0206	0.0283	1829
<b>AVERAGE</b>	<b>CSP</b>	<b>6"/12"</b>	<b>13.6</b>	<b>50.5</b>	<b>67.1</b>	<b>0.0207</b>	<b>0.0275</b>	<b>1783</b>
31A	CSP	4"/12"	21.8	58.1	71.3	0.0238	0.0292	2870
31B	CSP	4"/12"	18.7	58.5	71.9	0.0240	0.0295	2555
31C	CSP	4"/12"	19.8	58.9	81.8	0.0241	0.0335	3081
31D	CSP	4"/12"	19.2	55.9	61.9	0.0229	0.0254	2170
31E	CSP	4"/12"	22.6	52.5	61.9	0.0215	0.0254	2605
31F	CSP	4"/12"	20.9	50.0	56.1	0.0205	0.0230	2068
<b>AVERAGE(A,B,C)</b>	<b>CSP</b>	<b>4"/12"</b>	<b>20.5</b>	<b>55.6</b>	<b>67.5</b>	<b>0.0228</b>	<b>0.0277</b>	<b>2551</b>
33A	CSP	3"/12"	26.0	62.8	79.5	0.0258	0.0326	3831
33B	CSP	3"/12"	27.4	64.9	79.4	0.0266	0.0326	3976
33C	CSP	3"/12"	25.6	64.5	80.0	0.0265	0.0328	3790
<b>AVERAGE</b>	<b>CSP</b>	<b>3"/12"</b>	<b>26.3</b>	<b>64.1</b>	<b>79.5</b>	<b>0.0263</b>	<b>0.0326</b>	<b>3865</b>

<sup>1</sup>Based on tests 15 – B and 15 – C, test 15 – A did not reach 0.8  $S_u$  due to limited actuator displacement

Table 3.4 Reversed Cyclic Shear Wall Test Results

TEST	PANEL TYPE	FASTENER SCHEDULE	MAXI. WALL RESISTANCE (S <sub>w</sub> ) (POSITIVE CYCLE) kN/m	DISP. AT S <sub>w</sub> (Δ <sub>net,u+</sub> ) mm	ROT. AT S <sub>w</sub> (θ <sub>net,u+</sub> ) RAD.	MAXI. WALL RESISTANCE (S <sub>w</sub> ) (NEGATIVE CYCLE) kN/m	DISP. AT S <sub>w</sub> (Δ <sub>net,u-</sub> ) mm	ROT. AT S <sub>w</sub> (θ <sub>net,u-</sub> ) RAD.	ENERGY DISSIPATION, E JOULES
16A	CSP	6"/12"	11.3	66.8	0.0274	-10.7	-62.6	-0.0257	2887
16B	CSP	6"/12"	11.4	99.9	0.0410	-10.3	-61.2	-0.0251	2806
16C	CSP	6"/12"	11.0	87.4	0.0358	-10.0	-55.0	-0.0226	2210
<b>AVERAGE</b>	<b>CSP</b>	<b>6"/12"</b>	<b>11.2</b>	<b>84.7</b>	<b>0.0347</b>	<b>-10.3</b>	<b>-59.6</b>	<b>-0.0245</b>	<b>2637</b>
18A	CSP	4"/12"	16.2	102.0	0.0418	-15.3	-73.1	-0.0300	3528
18B	CSP	4"/12"	16.9	88.0	0.0361	-15.5	-72.4	-0.0297	4005
18C	CSP	4"/12"	18.6	95.2	0.0390	-15.9	-72.3	-0.0296	4184
<b>AVERAGE</b>	<b>CSP</b>	<b>4"/12"</b>	<b>17.2</b>	<b>95.1</b>	<b>0.0390</b>	<b>-15.5</b>	<b>-72.6</b>	<b>-0.0296</b>	<b>3906</b>
20A	OSB	6"/12"	11.8	87.9	0.0360	-10.1	-53.0	-0.0217	2728
20B	OSB	6"/12"	11.6	86.4	0.0354	-9.8	-55.0	-0.0226	3096
20C	OSB	6"/12"	10.5	80.1	0.0247	-10.3	-34.6	-0.0142	2385
<b>AVERAGE</b>	<b>OSB</b>	<b>6"/12"</b>	<b>11.3</b>	<b>78.1</b>	<b>0.0320</b>	<b>-10.0</b>	<b>-47.5</b>	<b>-0.0195</b>	<b>2737</b>
28A	OSB	4"/12"	17.5	76.1	0.0312	-15.7	-59.9	-0.0246	4288
28B	OSB	4"/12"	17.6	84.7	0.0347	-15.5	-86.9	-0.0356	4172
28C	OSB	4"/12"	19.0	79.6	0.0326	-16.4	-86.9	-0.0356	4403
<b>AVERAGE</b>	<b>OSB</b>	<b>4"/12"</b>	<b>18.0</b>	<b>80.1</b>	<b>0.0328</b>	<b>-15.9</b>	<b>-77.9</b>	<b>-0.0319</b>	<b>4288</b>
30A	CSP	6"/12"	13.5	51.3	0.0210	-11.9	-38.9	-0.0160	9031
30B	CSP	6"/12"	13.0	52.6	0.0216	-11.6	-39.3	-0.0161	8926
30C	CSP	6"/12"	13.3	51.7	0.0212	-12.1	-36.3	-0.0157	8615
<b>AVERAGE</b>	<b>CSP</b>	<b>6"/12"</b>	<b>13.3</b>	<b>51.9</b>	<b>0.0213</b>	<b>-11.9</b>	<b>-38.6</b>	<b>-0.0159</b>	<b>8957</b>
32A	CSP	4"/12"	20.0	54.0	0.0221	-18.1	-43.1	-0.0177	11875
32B	CSP	4"/12"	20.7	54.1	0.0222	-17.3	-43.5	-0.0178	12059
32C	CSP	4"/12"	20.3	53.4	0.0219	-17.8	-43.0	-0.0176	11876
<b>AVERAGE(A,B,C)</b>	<b>CSP</b>	<b>4"/12"</b>	<b>20.3</b>	<b>53.6</b>	<b>0.0221</b>	<b>-17.7</b>	<b>-43.2</b>	<b>-0.0177</b>	<b>11937</b>
34A	CSP	3"/12"	26.7	60.3	0.0247	-23.7	-45.4	-0.0186	14504
34B	CSP	3"/12"	29.1	60.8	0.0249	-25.0	-45.9	-0.0188	17366
34C	CSP	3"/12"	28.0	60.3	0.0247	-23.9	-46.8	-0.0192	16043
34D	CSP	3"/12"	30.4	58.0	0.0238	-27.5	-46.4	-0.0190	17069
<b>AVERAGE</b>	<b>CSP</b>	<b>3"/12"</b>	<b>28.6</b>	<b>59.9</b>	<b>0.0245</b>	<b>-25.0</b>	<b>-46.1</b>	<b>-0.0189</b>	<b>16243</b>

### 3.7 PRELIMINARY VALUES FOR SHEAR WALL DESIGN

An Equivalent Energy Elastic-Plastic (EEEP) curve, reviewed by Branston (2004), is an idealized curve applied in this thesis to determine strength and stiffness parameters (Figure 3.14). The area bounded by the EEEP curve, the x-axis, and the limiting displacement, is equal to the area below the observed test curve or backbone curve.

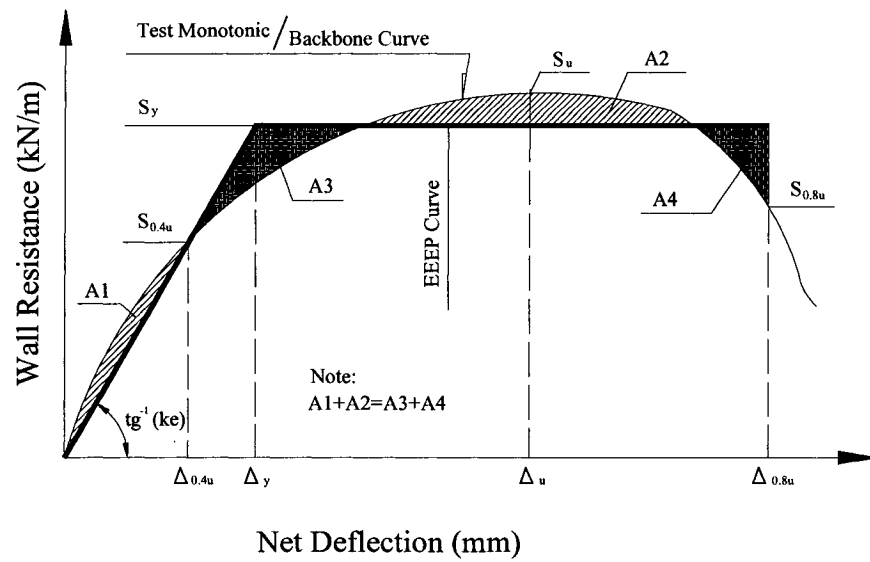


Figure 3.14: EEEP Model (Park, 1989; Salenikovich et al., 2000b)

Typical EEEP curves for the monotonic and reversed cyclic tests are shown in Figures 3.15 and 3.16, respectively.

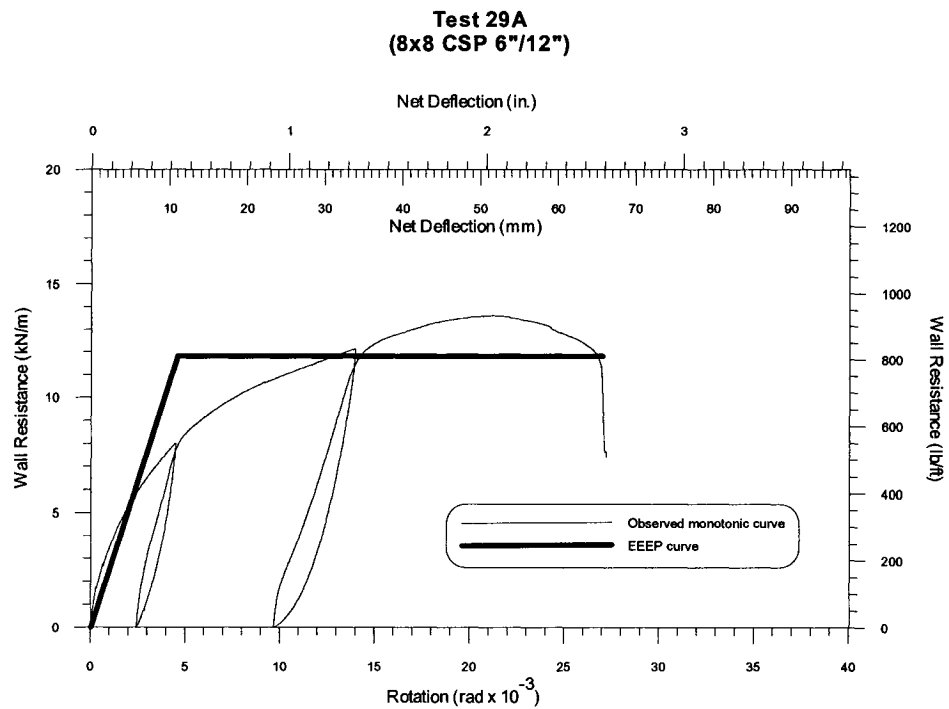


Figure 3.15: EEEP Analysis for a Monotonic Test (test 29A)

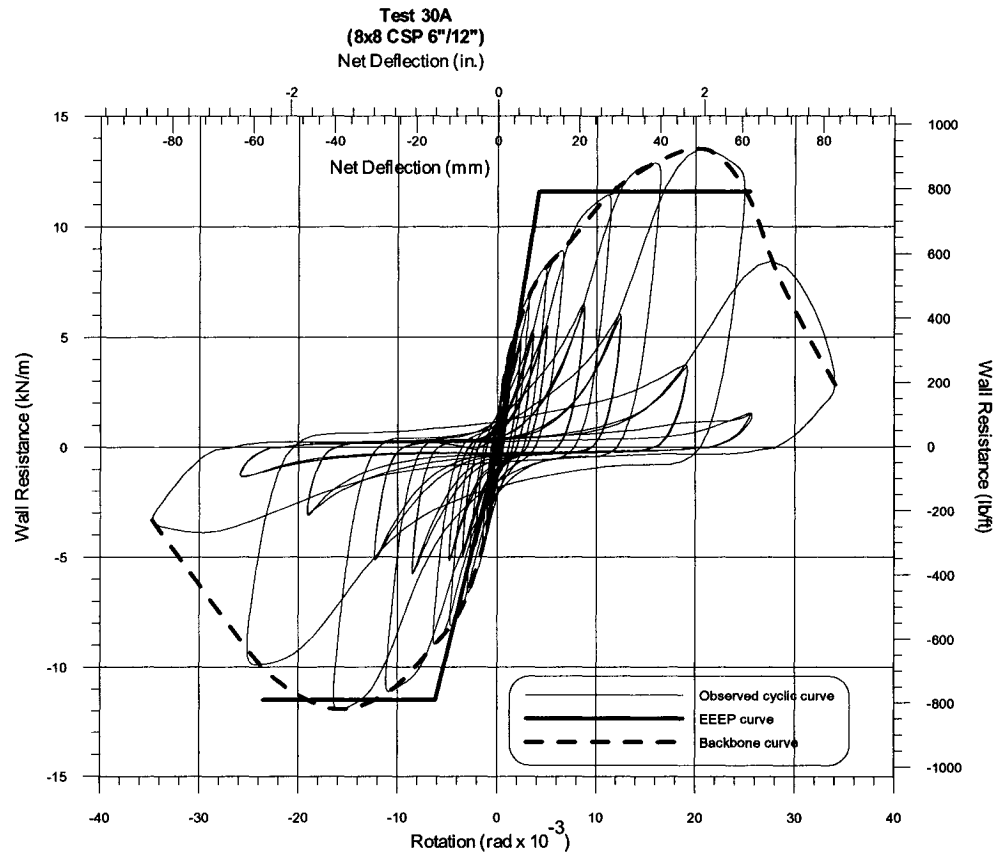


Figure 3.16: EEEP Analysis for a Reversed Cyclic Test (test 30A)

The horizontal line depicting the plastic portion of the EEEP curve is restricted in length due to the inelastic inter-storey deflection limit of 2.5% of the storey height for buildings of normal importance (NRCC, 2001). For an 8' (2440 mm) high shear wall this inelastic inter-storey drift limit is 61 mm. Two cases exist where the design of a light gauge steel frame / wood panel shear wall would be influenced by the inelastic drift limit of 61 mm: Case I:  $61 \text{ mm} < \Delta_{\text{net},u}$  and Case II:  $\Delta_{\text{net},u} < 61 \text{ mm} < \Delta_{\text{net},0.8u}$ . A third case also exists in which the failure displacement of the test specimen at  $S_{0.8u}$  (post-peak) is below the seismic drift limit. In this situation, a restriction on the design capacity was not necessary and no modification to the EEEP curve procedure detailed above was utilized.

A more complete discussion of the approach used to interpret the test data for the development of design values can be found in Branston (2004).

The following parameters are then determined from an EEEP curve:

- 1) The initial elastic stiffness,  $K_e$ , which is equal to  $S_{0.4u}/\Delta_{net, 04u}$ ;
- 2)  $S_y$  and  $\Delta_{net,y}$ : the yield shear strength and corresponding net deflection, which are determined using the EEEP curve; where:

$$S_y = \frac{-\Delta_{net, failure} \pm \sqrt{\Delta_{net, failure}^2 - \frac{2A}{k_e}}}{-\frac{1}{k_e}} \quad (3.5)$$

A is the area under backbone curve which terminates at  $\Delta_{net,0.8u}$  or  $\Delta=2.5\% H$ , whichever is smaller.

- 3) Ductility ( $\mu$ ):

$$\mu = \frac{\Delta_{net, failure}}{\Delta_{net,y}} \quad (3.6)$$

Design parameters based on the above approach are given in Table 3.5 for monotonic tests and in Tables 3.6 and 3.7 for reversed cyclic tests.

Table 3.5 Design Parameters Resulting from Monotonic Tests

TEST	PANEL TYPE	FASTENER SCHEDULE	YIELD LOAD (Sy) kN/m	DISP. AT Sy ( $\Delta_{net,y}$ ) mm	DISP. AT 0.4Su ( $\Delta_{net,0.4u}$ ) mm	STIFFNESS (ke) kN/m	ROT. AT Sy ( $\theta_{net,y}$ ) RAD.	DUCTILITY $\mu$	ENERGY DISSIPATION, E Joules
15A <sup>1</sup>	CSP	6"12"	7.71	17.0	10.4	0.276	0.0070	3.58	246
15B <sup>1</sup>	CSP	6"12"	8.75	20.8	11.7	0.257	0.0085	2.94	270
15C <sup>1</sup>	CSP	6"12"	7.52	40.0	26.6	0.115	0.0164	1.52	188
<b>AVERAGE</b>	<b>CSP</b>	<b>6"12"</b>	<b>8.23</b>	<b>18.9</b>	<b>16.3</b>	<b>0.270</b>	<b>0.0077</b>	<b>3.26</b>	<b>258</b>
17A <sup>1</sup>	CSP	4"12"	11.8	30.5	17.9	0.237	0.0125	2.00	330
17B <sup>1</sup>	CSP	4"12"	12.4	30.3	18.1	0.250	0.0124	2.01	347
17C <sup>1</sup>	CSP	4"12"	12.6	25.8	14.9	0.297	0.0106	2.36	368
<b>AVERAGE</b>	<b>CSP</b>	<b>4"12"</b>	<b>12.3</b>	<b>28.9</b>	<b>17.0</b>	<b>0.263</b>	<b>0.0118</b>	<b>2.12</b>	<b>348</b>
19A <sup>1</sup>	OSB	6"12"	10.1	20.5	10.2	0.299	0.0084	2.97	312
19B <sup>1</sup>	OSB	6"12"	10.0	16.6	8.37	0.369	0.0068	3.68	322
19C <sup>1</sup>	OSB	6"12"	10.0	13.7	6.69	0.446	0.0058	4.45	330
<b>AVERAGE</b>	<b>OSB</b>	<b>6"12"</b>	<b>10.0</b>	<b>16.9</b>	<b>8.40</b>	<b>0.373</b>	<b>0.0069</b>	<b>3.70</b>	<b>321</b>
27A <sup>1</sup>	OSB	4"12"	15.7	15.5	7.70	0.618	0.0064	3.93	510
27B <sup>1</sup>	OSB	4"12"	14.7	15.9	7.70	0.582	0.0065	3.83	474
27C <sup>1</sup>	OSB	4"12"	14.2	16.4	8.24	0.530	0.0067	3.72	458
<b>AVERAGE</b>	<b>OSB</b>	<b>4"12"</b>	<b>14.9</b>	<b>15.9</b>	<b>7.90</b>	<b>0.570</b>	<b>0.0065</b>	<b>3.83</b>	<b>481</b>
29A	CSP	6"12"	11.8	11.1	5.11	2.60	0.0045	5.94	1735
29B	CSP	6"12"	12.1	12.1	5.47	2.45	0.0050	5.49	1784
29C	CSP	6"12"	11.8	11.5	5.17	2.51	0.0047	6.00	1829
<b>AVERAGE</b>	<b>CSP</b>	<b>6"12"</b>	<b>11.9</b>	<b>11.6</b>	<b>5.30</b>	<b>2.52</b>	<b>0.0047</b>	<b>5.81</b>	<b>1783</b>
31A	CSP	4"12"	18.6	16.5	7.74	2.75	0.0068	4.32	2870
31B	CSP	4"12"	16.4	15.8	7.24	2.53	0.0085	4.54	2555
31C	CSP	4"12"	17.4	18.1	8.22	2.34	0.0074	4.53	3081
31D	CSP	4"12"	16.4	15.1	7.06	2.65	0.0062	4.11	2170
31E	CSP	4"12"	19.3	15.2	7.14	3.08	0.0063	4.14	2605
31F	CSP	4"12"	17.7	16.5	7.83	2.61	0.0068	3.40	2068
<b>AVERAGE(A,B,C)</b>	<b>CSP</b>	<b>4"12"</b>	<b>17.6</b>	<b>16.2</b>	<b>7.50</b>	<b>2.66</b>	<b>0.0066</b>	<b>4.17</b>	<b>2558</b>
33A <sup>1</sup>	CSP	3"12"	21.6	19.1	9.23	2.75	0.0078	3.19	2702
33B <sup>1</sup>	CSP	3"12"	22.1	18.4	9.13	2.93	0.0076	3.31	2788
33C <sup>1</sup>	CSP	3"12"	21.1	19.8	9.59	2.60	0.0081	3.08	2632
<b>AVERAGE</b>	<b>CSP</b>	<b>3"12"</b>	<b>21.6</b>	<b>19.1</b>	<b>9.30</b>	<b>2.76</b>	<b>0.0078</b>	<b>3.19</b>	<b>2707</b>

<sup>1</sup> Capacity governed by 2.5% inelastic drift limit (Case I)

Table 3.6 Design Parameters Resulting from Reversed Cyclic Tests (Positive Cycles)

TEST	PANEL TYPE	FASTENER SCHEDULE	YIELD LOAD (Sy+) kN/m	DISP. AT Sy+ ( $\Delta_{net,y+}$ ) mm	STIFFNESS (ke) kN/m	ROT. AT Sy+ ( $\theta_{net,y+}$ ) RAD.	DUCTILITY $\mu$	ENERGY DISSIPATION <sup>2</sup> , E JOULES
16A <sup>1</sup>	CSP	6"/12"	8.78	17.2	0.312	0.0070	3.55	280
16B <sup>1</sup>	CSP	6"/12"	8.44	24.4	0.210	0.0100	2.49	251
16C <sup>1</sup>	CSP	6"/12"	8.68	26.2	0.202	0.0108	2.32	253
<b>AVERAGE</b>	<b>CSP</b>	<b>6"/12"</b>	<b>8.63</b>	<b>22.6</b>	<b>0.240</b>	<b>0.0093</b>	<b>2.79</b>	<b>261</b>
18A <sup>1</sup>	CSP	4"/12"	11.0	28.8	0.233	0.0118	2.12	313
18B <sup>1</sup>	CSP	4"/12"	13.5	27.5	0.299	0.0113	2.22	388
18C <sup>1</sup>	CSP	4"/12"	13.5	24.6	0.334	0.0101	2.47	400
<b>AVERAGE</b>	<b>CSP</b>	<b>4"/12"</b>	<b>12.7</b>	<b>27.0</b>	<b>0.287</b>	<b>0.0111</b>	<b>2.27</b>	<b>367</b>
20A <sup>1</sup>	OSB	6"/12"	9.04	17.5	0.315	0.0072	3.49	288
20B <sup>1</sup>	OSB	6"/12"	9.21	12.3	0.455	0.0051	4.94	308
20C <sup>1</sup>	OSB	6"/12"	9.63	18.4	0.320	0.0075	5.19	506
<b>AVERAGE</b>	<b>OSB</b>	<b>6"/12"</b>	<b>9.29</b>	<b>16.1</b>	<b>0.363</b>	<b>0.0066</b>	<b>4.54</b>	<b>367</b>
28A <sup>1</sup>	OSB	4"/12"	15.0	14.8	0.619	0.0061	4.11	491
28B <sup>1</sup>	OSB	4"/12"	14.3	17.5	0.499	0.0072	3.49	456
28C <sup>1</sup>	OSB	4"/12"	15.7	14.9	0.643	0.0061	4.10	512
<b>AVERAGE</b>	<b>OSB</b>	<b>4"/12"</b>	<b>15.0</b>	<b>15.7</b>	<b>0.587</b>	<b>0.0064</b>	<b>3.90</b>	<b>480</b>
30A	CSP	6"/12"	11.6	10.1	2.80	0.0041	6.15	1612
30B	CSP	6"/12"	11.3	9.5	2.89	0.0039	6.54	1589
30C	CSP	6"/12"	11.4	12.4	2.24	0.0051	5.34	1671
<b>AVERAGE</b>	<b>CSP</b>	<b>6"/12"</b>	<b>11.4</b>	<b>10.7</b>	<b>2.64</b>	<b>0.0044</b>	<b>6.01</b>	<b>1624</b>
32A	CSP	4"/12"	17.4	15.5	2.74	0.0064	4.29	2498
32B	CSP	4"/12"	17.6	15.3	2.80	0.0063	4.48	2629
32C	CSP	4"/12"	17.3	16.1	2.61	0.0066	4.26	2560
<b>AVERAGE(A,B,C)</b>	<b>CSP</b>	<b>4"/12"</b>	<b>17.5</b>	<b>15.7</b>	<b>2.72</b>	<b>0.0064</b>	<b>4.34</b>	<b>2563</b>
34A	CSP	3"/12"	23.2	18.0	3.14	0.0074	3.92	3475
34B	CSP	3"/12"	25.3	18.3	3.38	0.0075	3.94	3889
34C	CSP	3"/12"	24.0	18.9	3.10	0.0077	3.86	3715
34D	CSP	3"/12"	25.8	14.2	4.43	0.0058	4.31	3405
<b>AVERAGE</b>	<b>CSP</b>	<b>3"/12"</b>	<b>24.6</b>	<b>17.3</b>	<b>3.51</b>	<b>0.0071</b>	<b>4.01</b>	<b>3621</b>

<sup>1</sup> Capacity governed by 2.5% inelastic drift limit (Case I)

<sup>2</sup> Energy calculation based on area under backbone curve

Table 3.7 Design Parameters Resulting from Reversed Cyclic Tests (Negative Cycles)

TEST	PANEL TYPE	FASTENER SCHEDULE	YIELD LOAD (Sy) kN/m	DISP. AT Sy- ( $\Delta_{net,y}$ ) mm	STIFFNESS (ke) kN/m	ROT. AT Sy- ( $\theta_{net,y}$ ) RAD.	DUCTILITY $\mu$	ENERGY DISSIPATION <sup>2</sup> , E JOULES
16A <sup>1</sup>	CSP	6"/12"	-9.12	-15.8	0.353	-0.0065	3.87	295
16B <sup>1</sup>	CSP	6"/12"	-9.12	-14.6	0.382	-0.0060	4.18	298
16C	CSP	6"/12"	-9.36	-17.2	0.333	-0.0070	5.26	466
<b>AVERAGE</b>	<b>CSP</b>	<b>6"/12"</b>	<b>-9.20</b>	<b>-15.8</b>	<b>0.353</b>	<b>-0.0065</b>	<b>4.44</b>	<b>353</b>
18A <sup>1</sup>	CSP	4"/12"	-12.6	-16.5	0.465	-0.0068	3.70	404
18B <sup>1</sup>	CSP	4"/12"	-12.3	-17.9	0.419	-0.0073	3.41	390
18C <sup>1</sup>	CSP	4"/12"	-12.3	-20.9	0.359	-0.0086	2.92	379
<b>AVERAGE</b>	<b>CSP</b>	<b>4"/12"</b>	<b>-12.4</b>	<b>-18.4</b>	<b>0.417</b>	<b>-0.0076</b>	<b>3.34</b>	<b>391</b>
20A	OSB	6"/12"	-9.47	-13.4	0.430	-0.0055	6.79	488
20B	OSB	6"/12"	-9.33	-15.9	0.357	-0.0065	5.82	482
20C	OSB	6"/12"	-9.29	-9.1	0.625	-0.0037	6.39	302
<b>AVERAGE</b>	<b>OSB</b>	<b>6"/12"</b>	<b>-9.36</b>	<b>-12.8</b>	<b>0.470</b>	<b>-0.0052</b>	<b>6.34</b>	<b>424</b>
28A	OSB	4"/12"	-14.6	-17.0	0.524	-0.0070	6.06	844
28B <sup>1</sup>	OSB	4"/12"	-13.7	-14.2	0.589	-0.0058	4.31	449
28C <sup>1</sup>	OSB	4"/12"	-14.4	-16.7	0.527	-0.0068	3.66	462
<b>AVERAGE</b>	<b>OSB</b>	<b>4"/12"</b>	<b>-14.2</b>	<b>-15.9</b>	<b>0.547</b>	<b>-0.0065</b>	<b>4.68</b>	<b>585</b>
30A	CSP	6"/12"	-11.5	-15.2	1.85	-0.0062	3.78	1402
30B	CSP	6"/12"	-11.4	-15.7	1.77	-0.0064	3.86	1470
30C	CSP	6"/12"	-11.7	-15.9	1.79	-0.0065	3.69	1448
<b>AVERAGE</b>	<b>CSP</b>	<b>6"/12"</b>	<b>-11.5</b>	<b>-15.6</b>	<b>1.80</b>	<b>-0.0064</b>	<b>3.78</b>	<b>1440</b>
32A	CSP	4"/12"	-15.7	-11.3	3.39	-0.0046	4.90	1892
32B	CSP	4"/12"	-16.6	-19.8	2.04	-0.0081	3.49	2394
32C	CSP	4"/12"	-17.2	-19.6	2.15	-0.0080	3.60	2546
<b>AVERAGE(A,B,C)</b>	<b>CSP</b>	<b>4"/12"</b>	<b>-16.5</b>	<b>-16.9</b>	<b>2.53</b>	<b>-0.0069</b>	<b>4.00</b>	<b>2277</b>
34A	CSP	3"/12"	-20.3	-14.3	3.46	-0.0059	3.78	2321
34B	CSP	3"/12"	-24.0	-21.4	2.74	-0.0088	3.54	3802
34C	CSP	3"/12"	-21.2	-16.0	3.24	-0.0065	4.15	3018
34D	CSP	3"/12"	-23.1	-14.3	3.95	-0.0059	3.60	2494
<b>AVERAGE</b>	<b>CSP</b>	<b>3"/12"</b>	<b>-22.2</b>	<b>-16.5</b>	<b>3.35</b>	<b>-0.0068</b>	<b>3.77</b>	<b>2909</b>

<sup>1</sup> Capacity governed by 2.5% inelastic drift limit (Case I)

<sup>2</sup> Energy calculation based on area under backbone curve

### 3.8 FAILURE MODES OBSERVED DURING FULL-SCALE TESTING

Once each test had been completed the damage to the specimen, which was typically localized to the sheathing-to-frame screw connections, was recorded on test data sheets (Branton et al., 2004). Definitions of each failure mode are described as follows, with accompanying photographs contained in Appendix IV.

- 1) Tear-out of Sheathing (TO): This failure mode occurred at screws located along the edges of a sheathing panel. The screw head in this case would tear out of the side of the panel due to high bearing stress on the wood (Figure A.IV-1).
- 2) Pull-through Sheathing (PT): In this failure mode, the shank of a screw rotated about the flanges of the steel framing members. The failure was characterized by the screw pulling through the sheathing. At the end of each test, the panel side where the screws pulled through the sheathing always separated from the steel studs or tracks. In no case did the screw pull out of the steel frame (Figure A.IV-2 and 3).
- 3) Screw Shear Failure (S): This condition generally occurred in cyclic tests. The corner screws were often sheared at the contact surface of the sheathing and steel framing under reversed cyclic loading. The failure was due to the shear in the neck of the screws, which was beyond the shear capacity of the fastener. The screws at these locations penetrated through the wood sheathing and two layers of steel (track & stud). The double steel layer did not allow for the screw to rotate, and hence the shear force in the fastener became large enough for failure to occur (Figure A.IV-5).
- 4) Wood Bearing Failure (WB): This failure mode took place in walls that were sheathed with plywood. Typically one or two of the interior plies failed in bearing while the outer plies remained intact. Further loading of the connection would usually lead to complete tear-out failure (Figure A.IV-8).
- 5) Partial pull-through Sheathing (PPT): This failure occurred when the head of a screw was partially pulled through the sheathing. A gap between the

sheathing and steel framing was always visible in this failure mode (Figure A.IV-4).

In certain cases several failure modes occurred simultaneously at a screw connection. For example, the edge of the sheathing might be torn out and the screws might be partially pulled through the sheathing at the same time. Some local buckling or twist of the track was also observed during the tests.

In most cases, all of the screws along the sides or edges of a panel rotated or tilted about the flanges of the studs or tracks as the wall was loaded in shear. The corner screws always failed first due to pull-through-sheathing or tear-out of sheathing. Then the sheathing to track connections next to these corner connections began to fail. With a further increase in panel rotation, the screws along the panel edges began to partially pull through the sheathing. Finally, when one side or edge of a panel separated from the studs or tracks, the shear capacity of the wall began to degrade rapidly. No pullout of screws from the steel framing was observed. Screw connections on the centrelines of the panels remained in good condition without visible damage. The sheathing panels did not exhibit any form of shear buckling.

In one 8' x 8' test, the flange of the top track became separated from the studs below because the wafer head screws in this instance were placed too close to the edge of the track flange. It is recommended that stud to track screws should generally be located at the middle lines of the flanges of tracks or closer to the track webs, as was done for the other walls constructed for this test program.

### 3.9 MATERIAL TESTING

In this section, the mechanical properties of the light gauge steel frame / wood panel shear wall components are reported, including the wood sheathing and steel framing. The material properties will later be used in the analyses of results from full-scale tests, and then as the basic data for the analytical models discussed in Chapter 5.

Shear tests were carried out by Boudreault (2004) on the CSP and OSB sheathing following the ASTM D1037 (1999) edgewise shear method. Wood specimens perpendicular and parallel to the grain of the outer plies or strands were used, with average values found in Table 3.8.

Table 3.8 Specified Strength and Rigidity Capacities for Sheathing Panels (Boudreault, 2004)

		Shear Through Thickness, $V_p$ , N/mm	Shear Through Thickness Rigidity, $B_v$ , N/mm	Minimum Nominal Thickness, mm
OSB	From Table 7.3D CSA O86	46	11000	11
	Test Results	101	10303	11.15
CSP	From Table 7.3B CSA O86	30	5700	12.5
	Test Results	$51^1/64^2$	5738/6520	11.56/11.69

Note: <sup>1</sup> Alberta Plywood <sup>2</sup> Richply.

Coupons from the ASTM A653 Grade 230 (33 ksi) (2002) steel studs and tracks were tested following the ASTM A370 (2002) procedure. All coupons were cut from the web of the stud and track components in the rolling direction. A 50 mm gauge length extensometer was used to measure the extension, and hence, determine the Young's

Modulus. Upon completion of the coupon tests, the zinc coating was removed with a 10% hydrochloric acid (HCl) solution to obtain the base metal thickness, which was then used to determine the material properties. Test results are shown in Table 3.9. The average yield strength exceeded the specified minimum strength 230 MPa (33 ksi) by approximately 13.7%. The measured average base metal thickness was less than the specified nominal thickness (1.12 mm) by approximately 3.1%. The average percent elongation (10%) and  $F_u / F_y$  ratio (1.08) requirements set by the North American Specification for Cold-Formed Steel Members (AISI, 2002) were met for all steel coupons

Table 3.9 Material Properties from Coupon Tests of Steel Framing Members

Coupon	Specimen	Member	Base Metal Thickness (mm)	Yield Stress ( $F_y$ - MPa)	Ultimate Stress ( $F_u$ - MPa)	$F_u/F_y$	Modulus of elasticity (E - MPa)	% Elong.
AVG	18 gauge 230 MPa	Stud	1.09	251	335	1.34	197667	38.5%
AVG	18 gauge 230 MPa	Track	1.08	272	344	1.26	203667	41.6%

## **CHAPTER 4**

### **PERFORMANCE EVALUATION OF TESTED SHEAR WALLS**

#### **4.1 INTRODUCTION**

In this chapter, the performance of all 109 monotonic and reversed cyclic tests (Table 4.1), carried out by Branston (2004), Boudreault (2004) and the author, is evaluated in detail based on both the test results and the design parameters determined from the EEEP curves, as documented in Chapter 3. The evaluation includes five indices of light gauge steel frame / wood panel shear wall performance, which are: ultimate shear strength, yield shear strength, stiffness, ductility and energy dissipation ability. Furthermore, each index is compared with respect to the variables associated with the different wall configurations, which are: screw spacing, sheathing type and aspect ratio. Monotonic and reversed cyclic loading protocols are also incorporated in the following comparisons. Each data point in the graphs contained in this chapter represents the average of the three or more tests of the same wall configuration. In addition, for reversed cyclic tests, the parameters are determined independently for the positive and negative displacement regions, and then the average value is used to represent the wall behaviour. In Section 4.7 the measured deflection of the test walls is discussed in order to give a complete explanation of the performance of light gauge steel frame / wood panel shear walls.

Table 4.1: Light Gauge Steel Frame / Wood Panel Shear Wall Test Program Matrix

Branston et al. (2004)

Specimen	Protocol	Wall Length (ft)	Wall Height (ft)	Sheathing Type	Sheathing Thickness (mm)	Fastener <sup>2</sup> Schedule (in.)
1 <sup>3</sup> – A,B,C,D,E,F	Monotonic	4	8	CSP	12.5	4/12
4 <sup>3</sup> – A,B,C	CUREE <sup>1</sup>	4	8	CSP	12.5	4/12
5 <sup>3</sup> – A,B,C,D	Monotonic	4	8	DFP	12.5	4/12
6 <sup>3</sup> – A,B,C	CUREE	4	8	DFP	12.5	4/12
7 <sup>4</sup> – A,B,C	Monotonic	4	8	CSP	12.5	6/12
8 <sup>4</sup> – A,B,C	CUREE	4	8	CSP	12.5	6/12
9 <sup>4</sup> – A,B,C	Monotonic	4	8	CSP	12.5	3/12
10 <sup>4</sup> – A,B,C	CUREE	4	8	CSP	12.5	3/12
11 <sup>4</sup> – A,B,C	Monotonic	4	8	DFP	12.5	6/12
12 <sup>4</sup> – A,B,C	CUREE	4	8	DFP	12.5	6/12
13 <sup>4</sup> – A,B,C	Monotonic	4	8	DFP	12.5	3/12
14 <sup>4</sup> – A,B,C,D	CUREE	4	8	DFP	12.5	3/12
15 <sup>5</sup> – A,B,C	Monotonic	2	8	CSP	12.5	6/12
16 <sup>5</sup> – A,B,C	CUREE	2	8	CSP	12.5	6/12
17 <sup>5</sup> – A,B,C	Monotonic	2	8	CSP	12.5	4/12
18 <sup>5</sup> – A,B,C	CUREE	2	8	CSP	12.5	4/12
19 <sup>5</sup> – A,B,C	Monotonic	2	8	OSB	11.0	6/12
20 <sup>5</sup> – A,B,C	CUREE	2	8	OSB	11.0	6/12
21 <sup>4</sup> – A,B,C	Monotonic	4	8	OSB	11.0	6/12
22 <sup>4</sup> – A,B,C	CUREE	4	8	OSB	11.0	6/12
23 <sup>4</sup> – A,B,C	Monotonic	4	8	OSB	11.0	4/12
24 <sup>4</sup> – A,B,C	CUREE	4	8	OSB	11.0	4/12
25 <sup>4</sup> – A,B,C	Monotonic	4	8	OSB	11.0	3/12
26 <sup>4</sup> – A,B,C	CUREE	4	8	OSB	11.0	3/12
27 <sup>5</sup> – A,B,C	Monotonic	2	8	OSB	11.0	4/12
28 <sup>5</sup> – A,B,C	CUREE	2	8	OSB	11.0	4/12
29 <sup>5</sup> – A,B,C	Monotonic	8	8	CSP	12.5	6/12
30 <sup>5</sup> – A,B,C	CUREE	8	8	CSP	12.5	6/12
31 <sup>5</sup> – A,B,C,D,E,F	Monotonic	8	8	CSP	12.5	4/12
32 <sup>5</sup> – A,B,C	CUREE	8	8	CSP	12.5	4/12
33 <sup>5</sup> – A,B,C	Monotonic	8	8	CSP	12.5	3/12
34 <sup>5</sup> – A,B,C,D	CUREE	8	8	CSP	12.5	3/12

<sup>1</sup>CUREE reversed cyclic protocol for ordinary ground motions.<sup>2</sup>Fastener schedule (e.g. 3"/12") refers to the spacing between sheathing to framing screws around the edge of the panel and along intermediate studs (field spacing), respectively.<sup>3</sup>Boudreault (2004).<sup>4</sup>Branston (2004).<sup>5</sup>The author.

## 4.2 ULTIMATE SHEAR STRENGTH ( $S_u$ )

The ultimate shear strength,  $S_u$ , is the maximum shear wall strength that was recorded during the testing of each monotonic test (Figure 3.14), and is the average of the maximum positive and negative shear resistance ( $S'_{u+}$  and  $S'_{u-}$ ) in each reversed cyclic test (Figure 3.16). Further details are provided in Section 3.7.

### 4.2.1 ULTIMATE SHEAR STRENGTH vs. SCREW SPACING

Screw spacing along the panel edges is one of the major factors which affects the behaviour of a light gauge steel frame / wood panel shear wall. The screw spacing was not directly used in this comparison; rather, the number of screws on the perimeter of the panel(s) was plotted against the measured ultimate shear capacity of the test walls. The graphs in Figure 4.1 contain the test results for walls constructed of the three sheathing types, having different aspect ratios and for the two loading cases.

In most cases  $S_u$  was found to be approximately proportional to the number of perimeter screws per panel for walls with the same aspect ratio, both in monotonic tests and reversed cyclic tests. A few exceptions occurred for walls of 4' x 8' CSP M and 4' x 8' OSB M, where a nonlinear increase with the decrease of the screw spacing can be seen, however the general proportional trend is still evident. These special cases may be explained by two reasons, one of which is the limited number of walls that were tested and the other is the inherent variability in the wood sheathing. In the case of the 2' x 8'

walls only two screw spacings were tested, hence the line plotted is only an estimate of the possible effect of placing fasteners at intermediate distances.

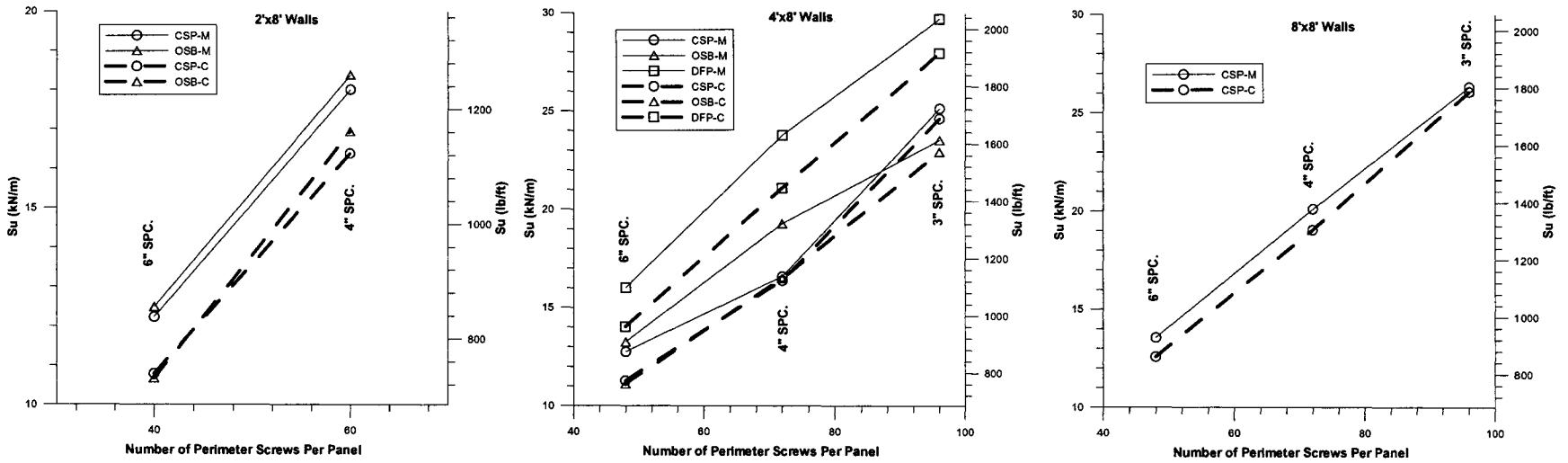


Figure 4.1 Ultimate Shear Strength,  $S_u$ , vs. Number of Perimeter Screws Per Panel

#### **4.2.2 *ULTIMATE SHEAR STRENGTH vs. SHEATHING TYPE***

The sheathing panels used in this research project included CSP from Alberta Plywood, CSP from Richply, DFP and OSB. The material properties of the wood sheathing play an important role in the behaviour of a shear wall. Comparisons are presented in the form of bar charts in Figure 4.2. Test results for walls constructed having different aspect ratios and screw spacing, as well as the two loading cases are presented.

The ultimate shear capacity for walls with 11 mm OSB panels is typically very close to that measured for 12.5 mm CSP walls having the same aspect ratio and screw pattern. Shear walls (4' x 8' in size) with DFP panels showed an elevated resistance of approximately 25% compared with the matching CSP walls. It is expected that this increased capacity would also occur in the 2' x 8' and 8' x 8' walls. The higher capacity can be attributed to the increased bearing resistance of DFP adding to the overall strength of the shear walls (Branston, 2004).

The 4' x 8' and 8' x 8' CSP wall configurations were composed of wood panels from two mills, that is Alberta Plywood (AB 244) and Richply (BC 858). Even though the plywood from both mills is manufactured to CSA Standard O151 (1978) the measured strength was not consistent. In all situations where Richply panels were tested a higher capacity was measured (approx. 22%). This finding was similar to that obtained for the material tests, which showed that the Richply panels have approximately 25% higher shear strength (Table 3.7). The wood species used in Richply generally has a higher dry density (Table 3.2) and mechanical properties, hence this makes the sheathing connections reach higher lateral resistance (Forest Products laboratory, 1999).

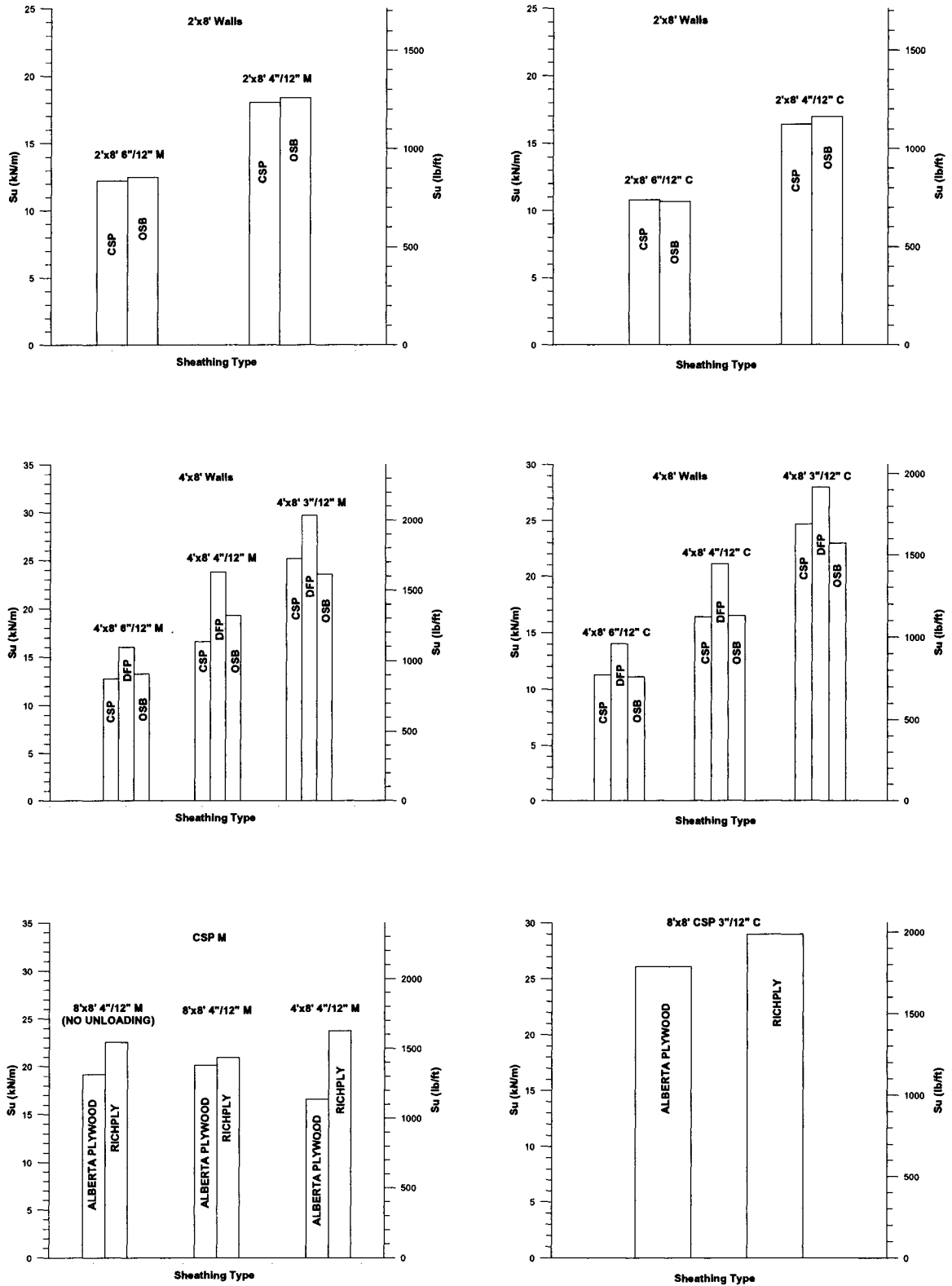


Figure 4.2 Ultimate Shear Strength,  $S_u$ , vs. Sheathing Type

### **4.2.3 ULTIMATE SHEAR STRENGTH vs. ASPECT RATIO**

The ratio of the height to the length of a wall segment (aspect ratio) was considered in the comparison of the light gauge steel frame / wood panel shear wall performance. Three different wall sizes were tested, i.e. 2' x 8', 4' x 8' and 8' x 8', although not all screw spacing distances and sheathing types were included for each size. The results obtained from the test data are presented in Figure 4.3.

The ultimate shear capacity per unit length that was reached was reasonably consistent for walls with different widths (2, 4 and 8-foot walls) both in monotonic tests and reversed cyclic tests, if screw spacing along panel edges and sheathing type stay unchanged. As can be seen in Figure 4.3 there is only a slight increase in strength for the longer walls. Only results for the CSP and OSB walls are shown because tests were carried out on different size specimens, whereas, for DFP walls the specimen size was limited to 4' x 8'. Some exceptions exist due to the same reasons explained in Section 4.2.1, that is the limited number of tests carried out and the variability of the wood properties. It should be noted that although the ultimate capacity of the different size walls in kN/m was similar, the level of deformation required to reach  $S_u$  varied significantly for the 2' x 8' walls. A more detailed discussion on this topic can be found in Section 4.7.

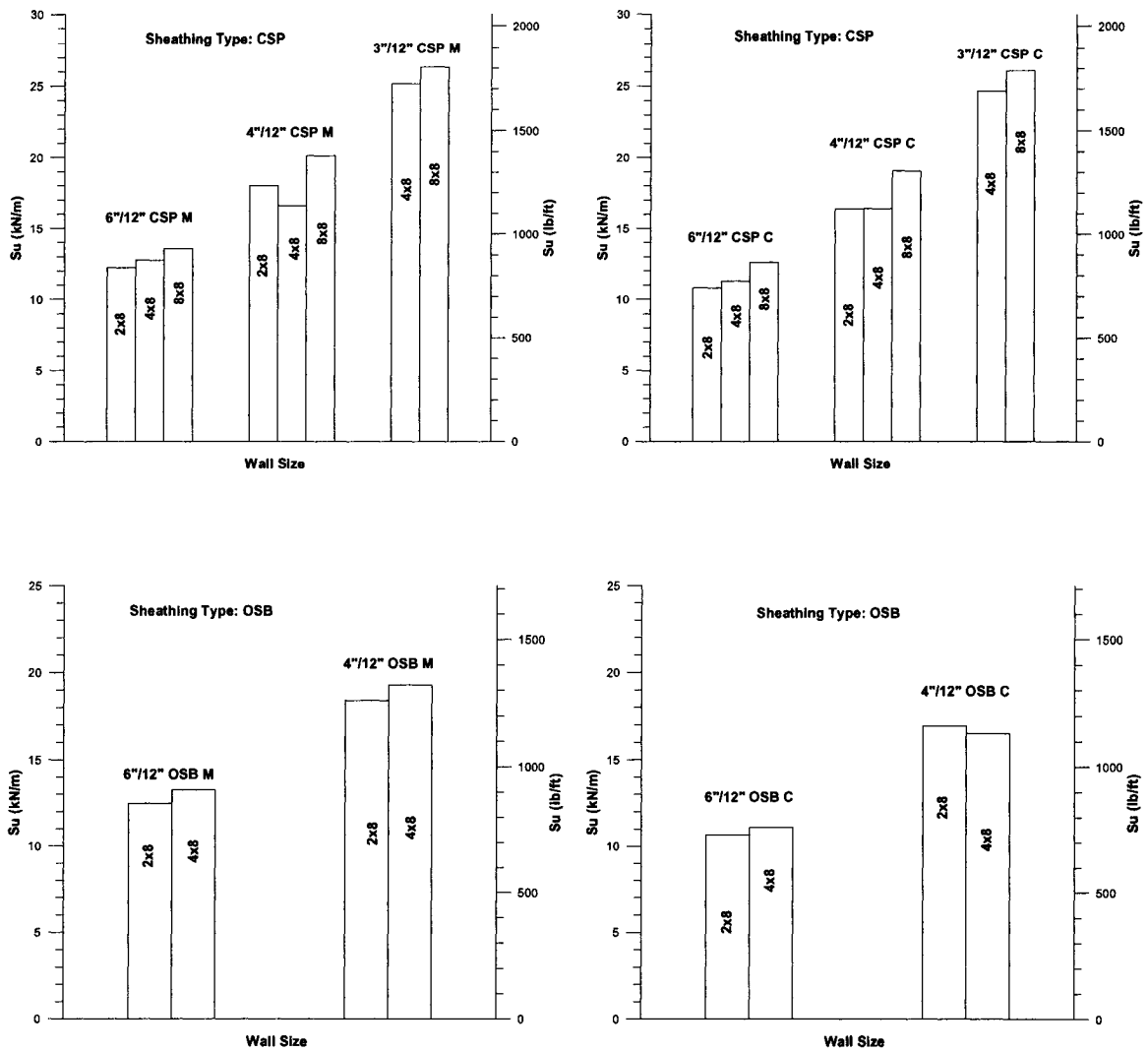


Figure 4.3 Ultimate Shear Strength,  $S_u$ , vs. Aspect Ratio

#### 4.2.4 *ULTIMATE SHEAR STRENGTH vs. LOAD PROTOCOL*

In order to account for the different behaviour of walls under monotonic and reversed cyclic testing and to determine if a relationship exists between the two loading cases, test results are analyzed and compared in this section (Figure 4.4). Detailed information on the different loading protocols can be found in Section 3.4.

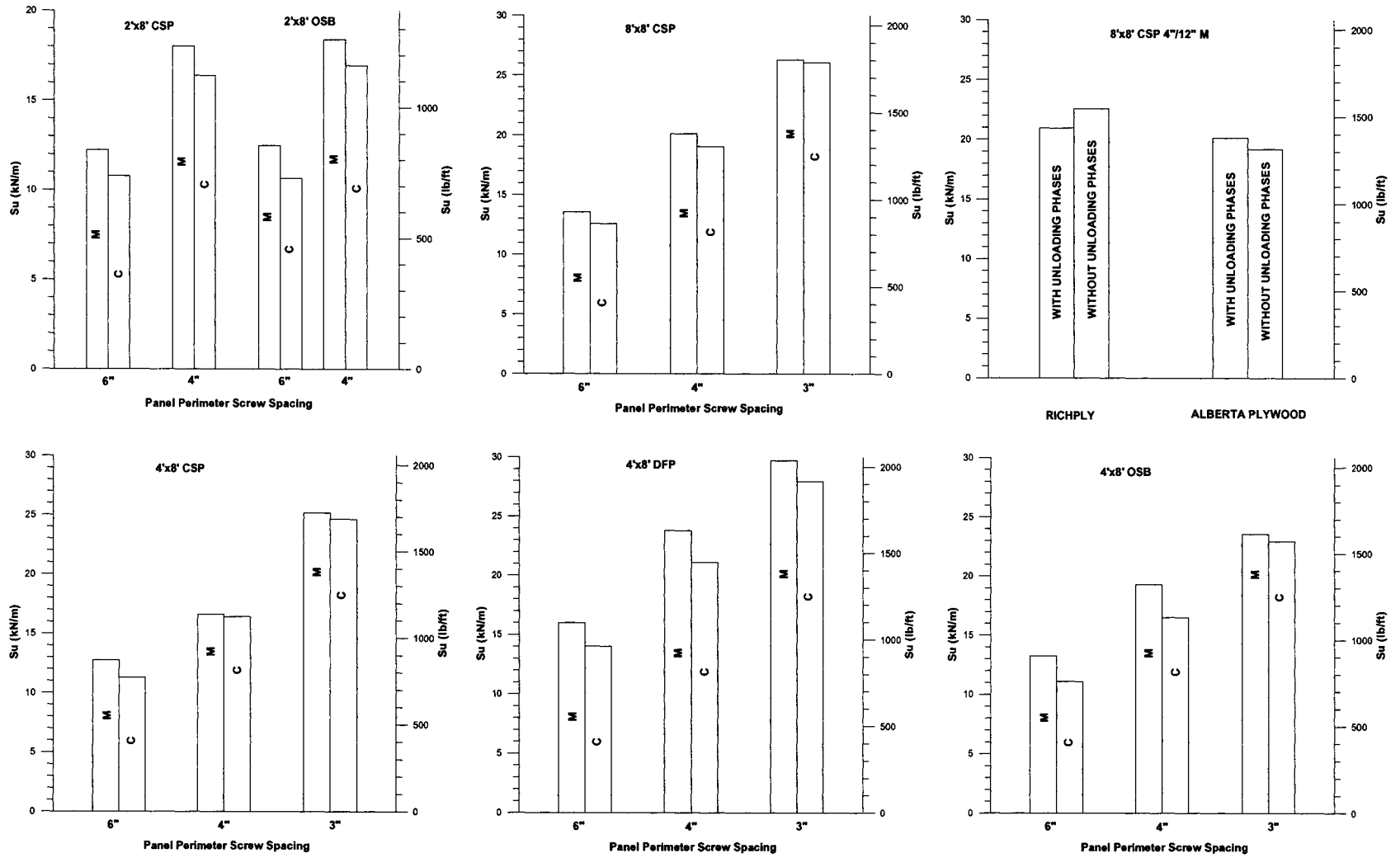


Figure 4.4 Ultimate Shear Strength,  $S_u$ , vs. Load Protocol

In general, the  $S_u$  values measured for the reversed cyclic tests are somewhat less (average 8%) than those obtained for the monotonic tests with the same wall configuration. This is due to the enlargement of the holes in the sheathing around the sheathing screws during the initial cycles in the reversed cyclic loading protocol, which caused a decrease of the bearing resistance of the wood sheathing, and hence the connection.

Figure 4.4 also provides a comparison of the 8' x 8' CSP monotonic tests that were carried out with slightly different protocols. In one situation the permanent offset unloading was included at 12.5 and 38 mm, while for the other tests no unloading took place. The results provide no evidence that the two unloading cycles in the monotonic protocol affected the ultimate shear capacity that was measured.

### **4.3 YIELD SHEAR STRENGTH ( $S_y$ )**

The yield shear strength,  $S_y$ , is defined as the force corresponding to the design level displacement, which is determined by the EEEP method (Equation (3.5), Figure 3.14). Detailed information is contained in Section 3.7.

#### ***4.3.1 YIELD SHEAR STRENGTH vs. SCREW SPACING***

As found for the ultimate shear capacity,  $S_u$ , of the test walls, the yield shear strength,  $S_y$ , follows a similar trend (Figure 4.5). The yield shear strength of the wall increases approximately linearly with the number of perimeter screws per panel. Test results are shown for walls constructed of the three sheathing types, having different aspect ratios and for the two loading cases. As previously stated, only two screw spacings were tested for the 2' x 8' walls, hence the line plotted is only an estimate of the possible effect of placing fasteners at intermediate distances.

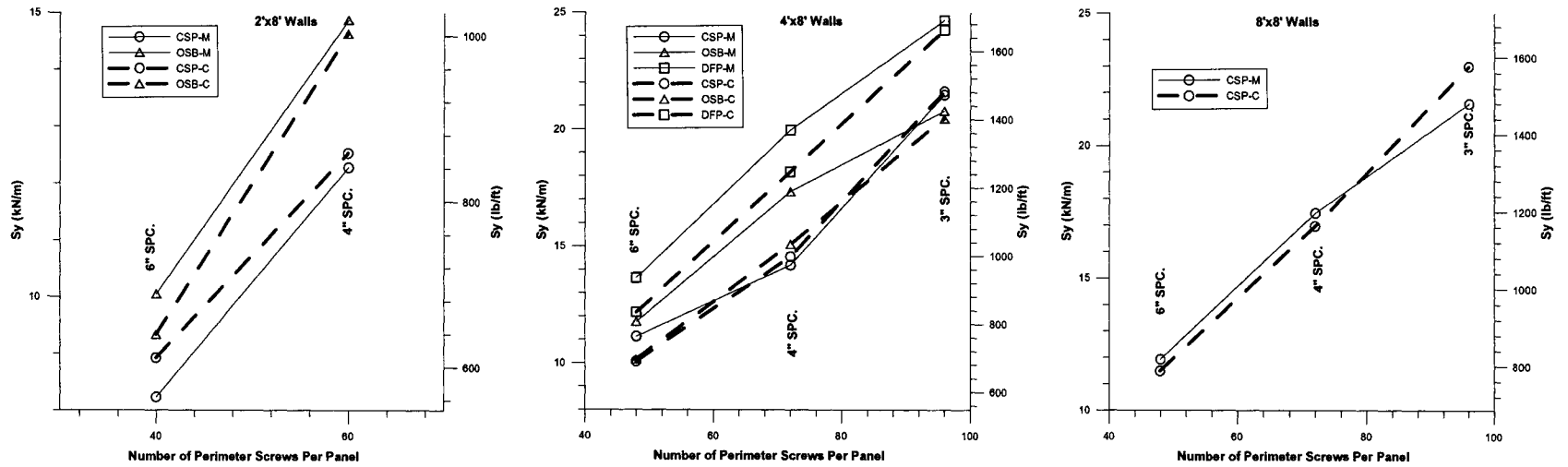


Figure 4.5 Yield Shear Strength,  $S_y$ , vs. Number of Perimeter Screws Per Panel

#### **4.3.2 YIELD SHEAR STRENGTH vs. SHEATHING TYPE**

The shear yield capacity,  $S_y$ , for OSB walls was found to be consistently higher than that measured for the CSP walls in all except for two cases (4'x8' 3"/12" M&C) (Figure 4.6). Overall, this increase in capacity was in the range of 14% for monotonic tests and 5% for cyclic tests. This increase can be attributed to the higher ductility  $\mu$  (Section 4.5.2) and simultaneously higher energy under the backbone curve  $E_b$  (Section 4.6.2) of OSB walls. As previously noted, for the ultimate shear strength the walls with DFP sheathing possessed a higher shear yield capacity and bearing capacity compared with the CSP walls (average 25% for monotonic tests and 20% for cyclic tests). In the comparison of Alberta Plywood vs. Richply tests, walls with sheathing of the later type exhibit a higher shear yield capacity. This can be attributed to the higher specific gravity and mechanical properties of the Richply sheathing itself (Table 3.2). Richply panels are made of the same wood species as DFP panels, which was identified by Canply.

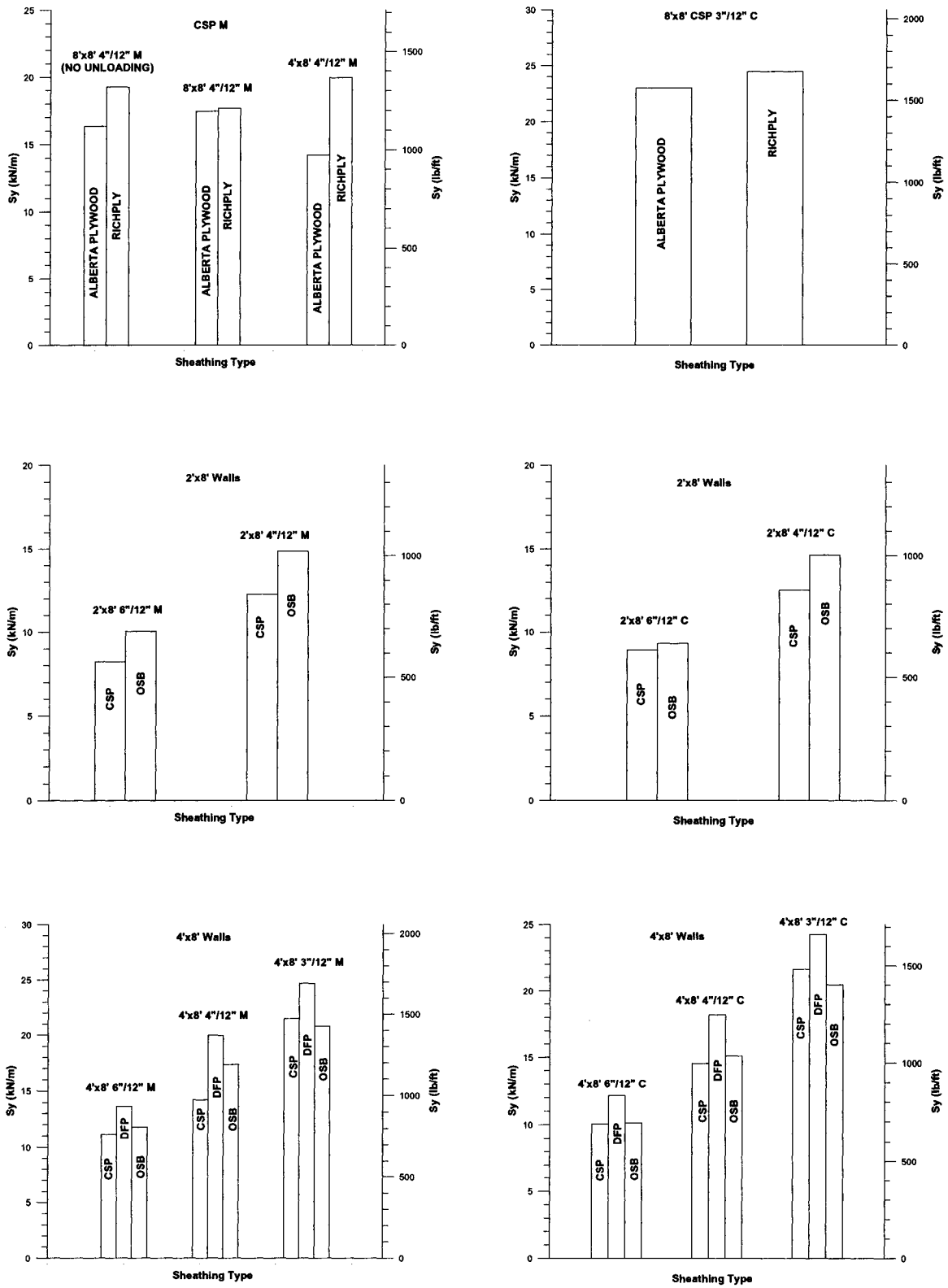


Figure 4.6 Yield Shear Strength,  $S_y$ , vs. Sheathing Type

### 4.3.3 YIELD SHEAR STRENGTH vs. ASPECT RATIO

The effect of the aspect ratio on the yield shear strength,  $S_y$ , is shown in Figure 4.7. On average,  $S_y$  increases by approximately 10% with each change in wall length. This is due to the increase of initial stiffness  $K_e$  with the longer walls (Section 4.4.3) and the effect of having a lower yield displacement in the EEEP analysis approach.

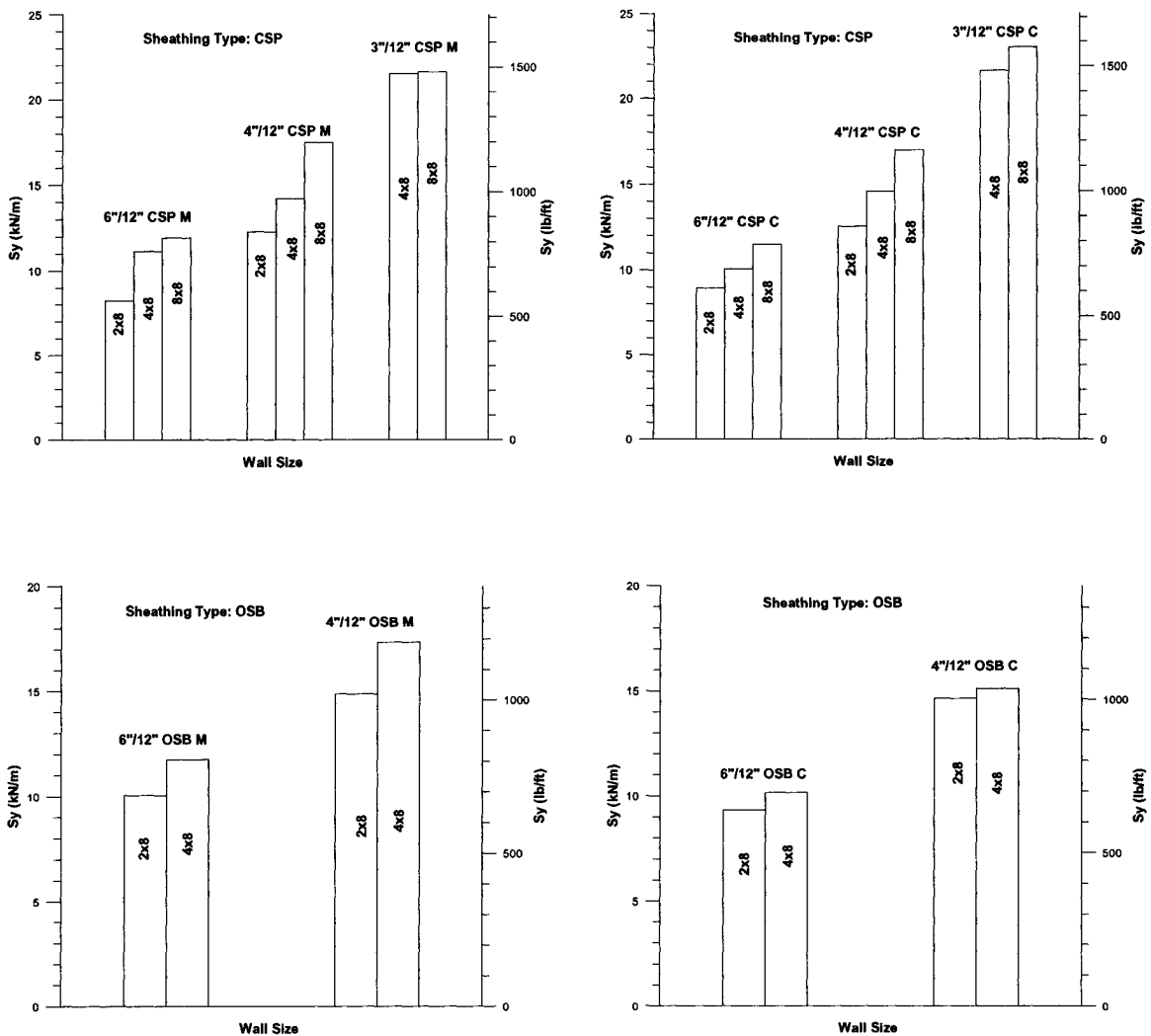


Figure 4.7 Yield Shear Strength,  $S_y$ , vs. Aspect Ratio

#### **4.3.4 YIELD SHEAR STRENGTH vs. LOAD PROTOCOL**

It was found that the  $S_y$  values obtained from the reversed cyclic tests are close to those measured for the monotonic tests with the same wall configuration (Figure 4.8). Even though in some cases one load protocol is higher than the other, no fixed trend is apparent. Similarly, for the 8' x 8' walls made of different types of CSP sheathing the unloading phases in the monotonic protocol did not create a consistent difference in the measured wall properties.

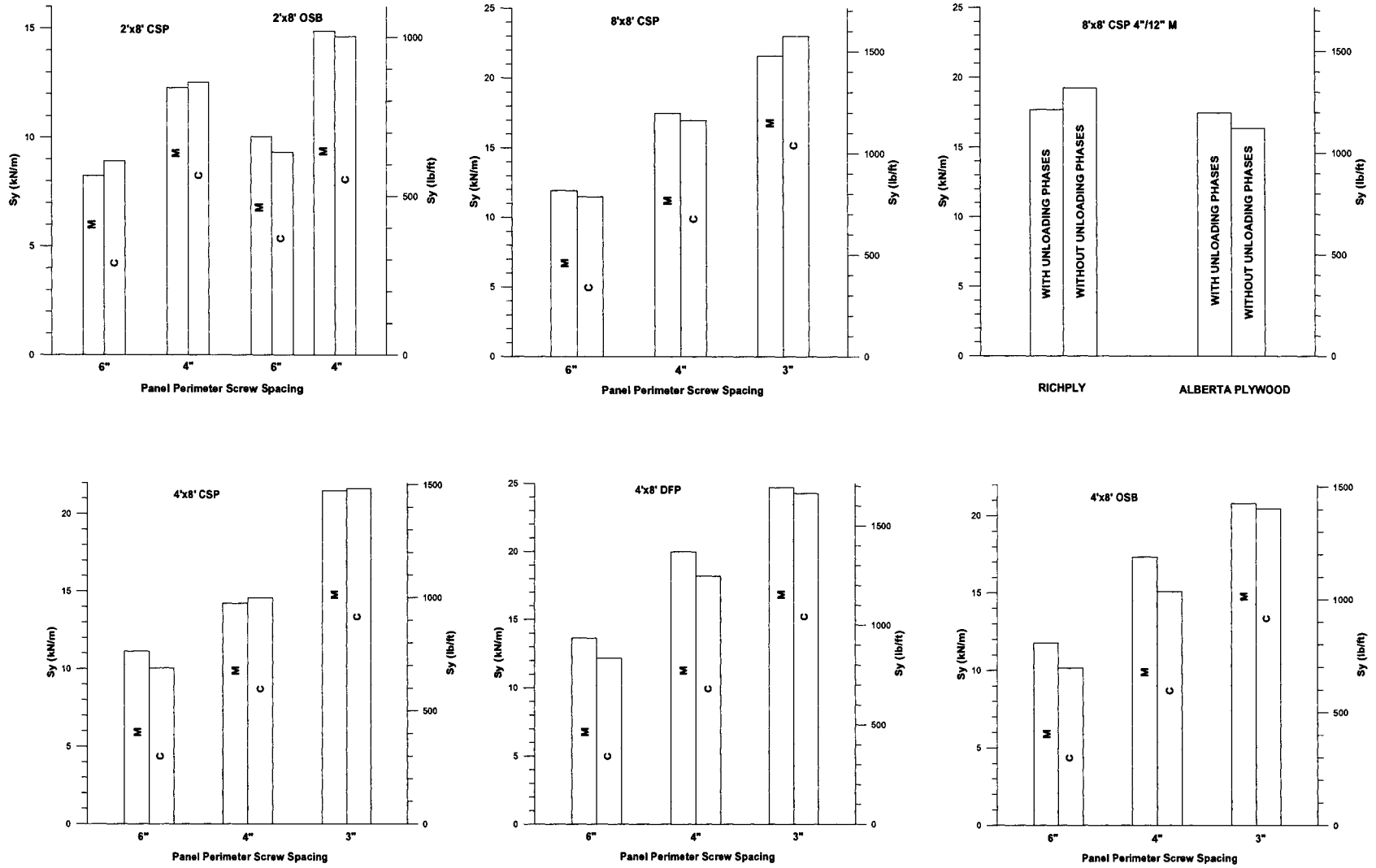


Figure 4.8 Yield Shear Strength,  $S_y$ , vs. Load Protocol

#### 4.4 STIFFNESS ( $K_e$ )

The initial elastic stiffness of a shear wall,  $K_e$ , which is equal to  $S_{0.4u}/\Delta_{net, 0.4}$ , is determined from its EEEP curve. Details can be found in Section 3.7 and Figure 3.14.

##### 4.4.1 *STIFFNESS vs. SCREW SPACING*

Generally, the idealized initial elastic stiffness,  $K_e$ , increased with the decrease of screw spacing as shown in Figure 4.9, however, this increase is not linear, and in some cases it decreased with the addition of perimeter screws. The lack of a definite trend is due to the nonlinearity of the connection performance and the sheathing panel shear stiffness. Moreover, the use of different types of CSP panels affected the measured results.

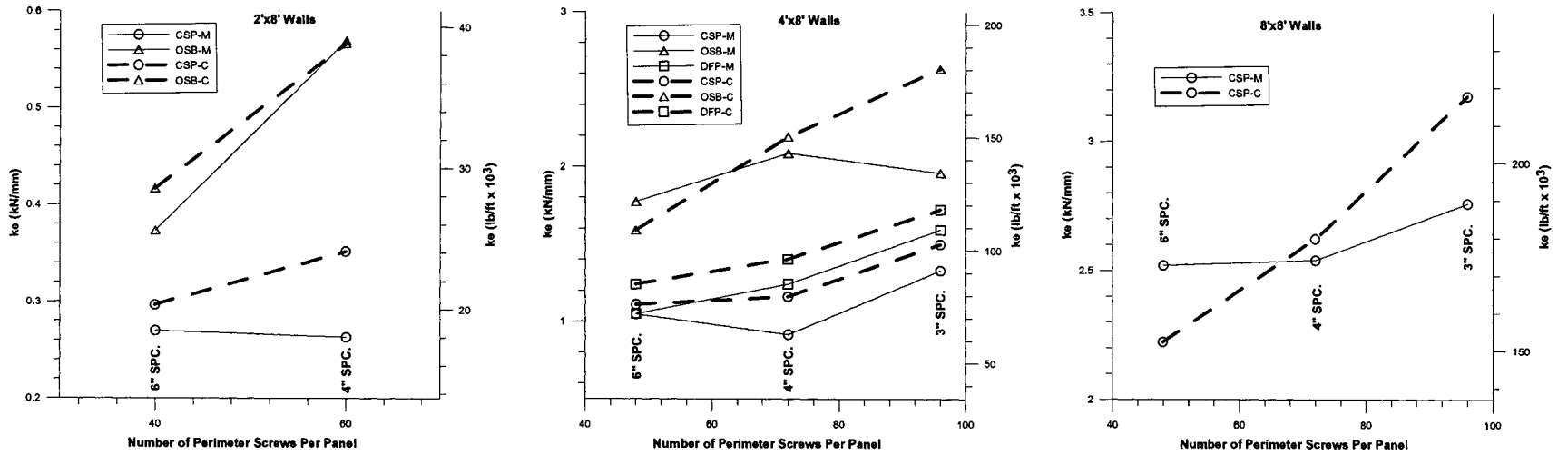


Figure 4.9 Stiffness,  $K_e$ , vs. Screw Spacing

#### **4.4.2 STIFFNESS vs. SHEATHING TYPE**

The measured stiffness,  $K_e$ , for the OSB walls is much higher than that obtained for the CSP and DFP walls with the same connection configuration (Figure 4.10). DFP walls exhibited a higher initial stiffness than CSP walls; however, the increase from one wall configuration to another was not fixed. For the two types of CSP panels that were tested, the measured stiffness for the Richply sheathed walls is higher (Figure 4.10). The higher stiffness of the shear walls may be attributed to the higher mechanical properties of the sheathing material, which increased the stiffness of the sheathing connections. Wood species, which made of the layers of Richply, have higher mechanical properties than those in Alberta Plywood panels (Table 3.2).

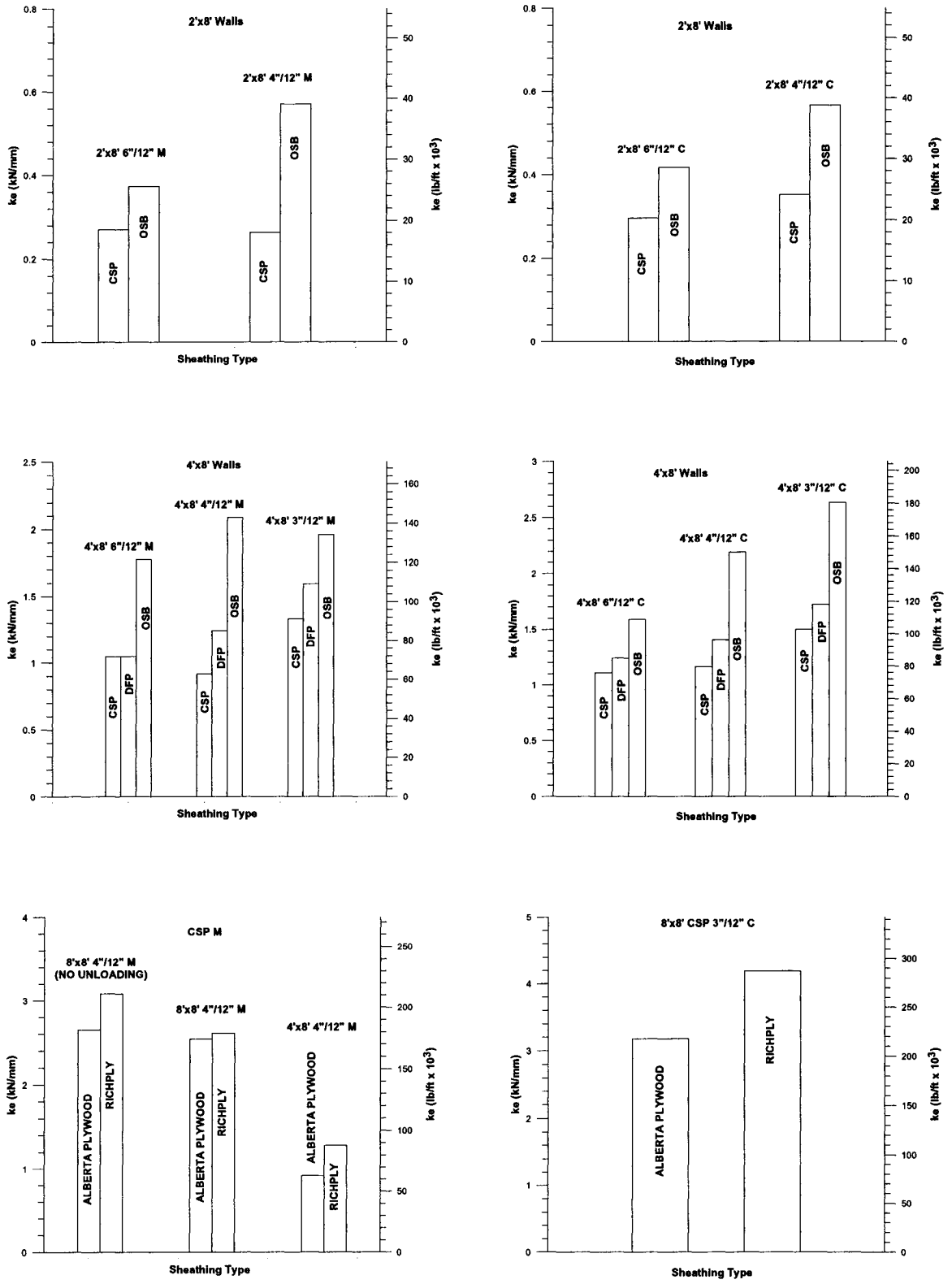


Figure 4.10 Stiffness,  $K_e$ , vs. Sheathing Type

### 4.4.3 STIFFNESS vs. ASPECT RATIO

The test results illustrated in Figure 4.11 show that  $K_e$  increases with an increase of the wall length for both monotonic and reversed cyclic tests. This can be explained using a cantilever beam theory: the test walls can be taken as vertically placed cantilever beams with the same length, so the wider beam has larger lateral stiffness. As well, in the longer walls, the hold-downs will make more contribution to the lateral stiffness.

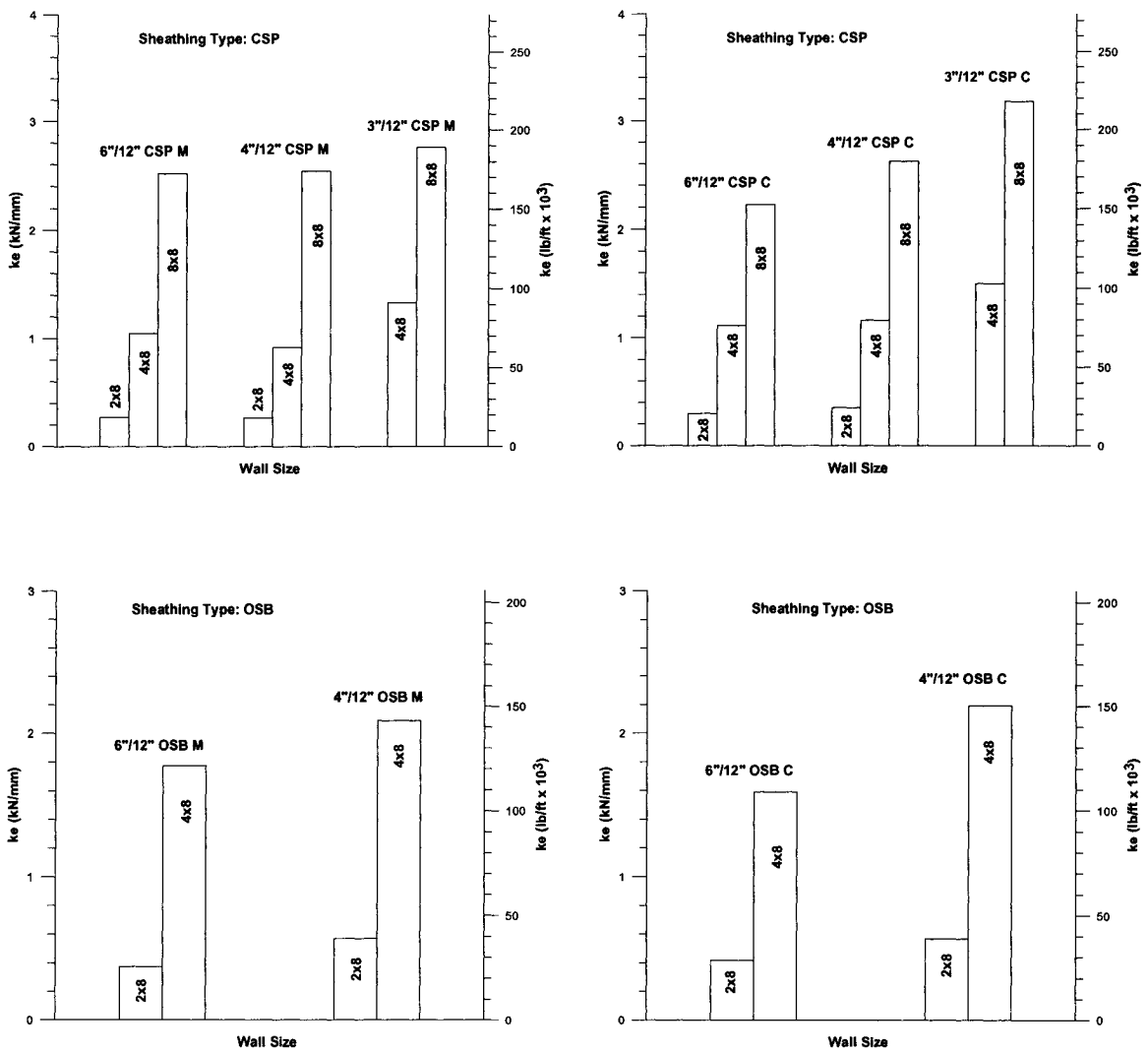


Figure 4.11 Stiffness,  $K_e$ , vs. Aspect Ratio

#### **4.4.4 STIFFNESS vs. LOAD PROTOCOL**

The  $K_e$  values for cyclic tests are generally higher than those measured for the monotonic tests with the same wall configuration, with some exceptions (Figure 4.12). This may be attributed to the faster loading speed used in the cyclic testing, which on average was 20 mm/ sec versus 7.5 mm/min for the monotonic protocol. This comparison is valid if the lateral displacement  $\Delta_{net, 0.4u}$  is taken in the range of 10 mm (Table 3.4).

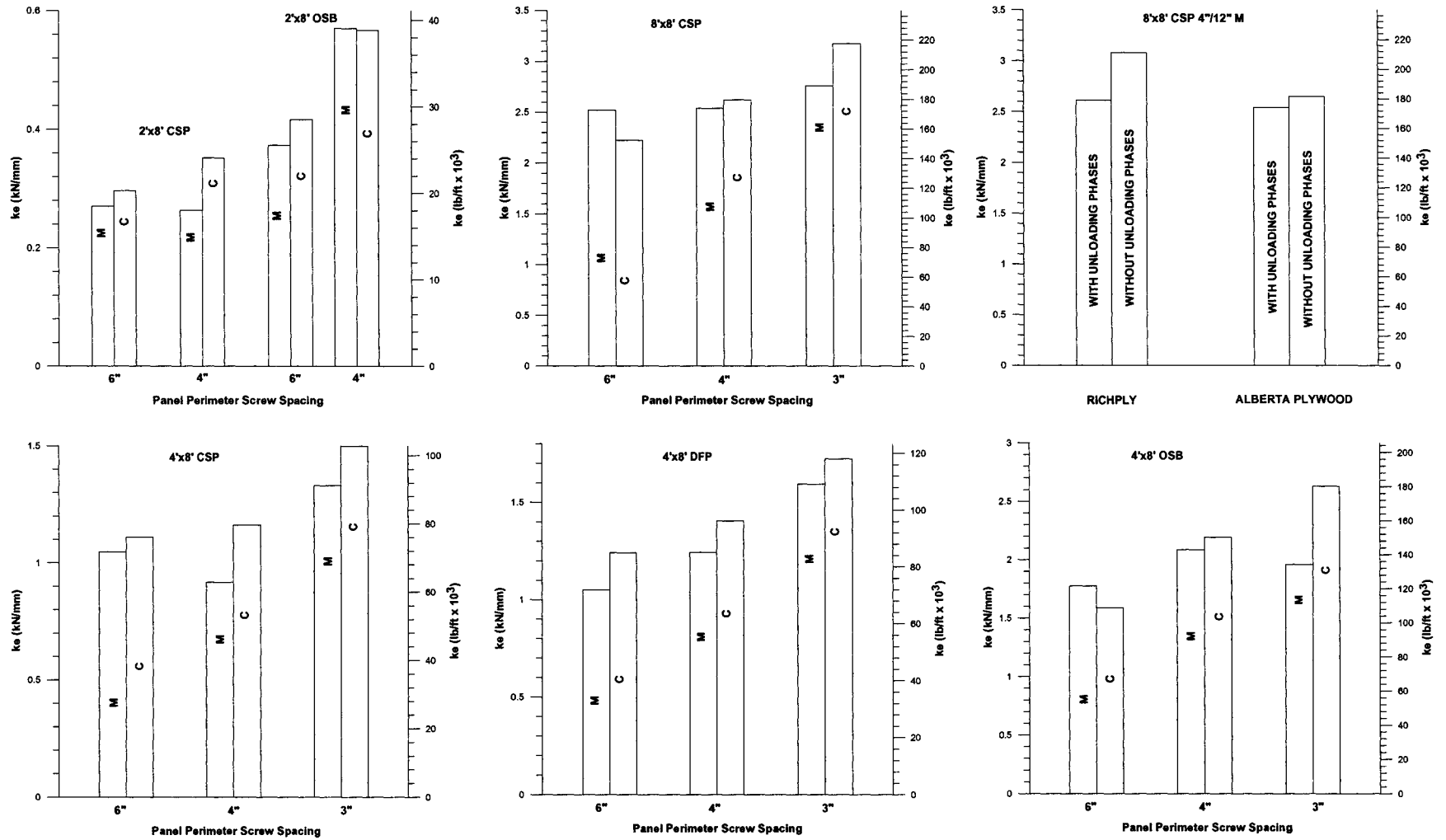


Figure 4.12 Stiffness,  $K_e$ , vs. Load Protocol

## 4.5 DUCTILITY ( $\mu$ )

The ductility  $\mu$  is defined as  $\Delta_{\text{net, failure}}/\Delta_{\text{net, y}}$  as in Equation (3.6). Detailed information is given in Branston (2004).

### 4.5.1 DUCTILITY vs. SCREW SPACING

It was found that the ductility,  $\mu$ , decreases along with the decrease of the panel edge screw spacing distance as shown in Figure 4.13, with the exception of the 2' x 8' OSB monotonic tests. A more pronounced decrease in ductility occurred when changing from the 6" to 4" spacing, while the measured  $\mu$  values were similar for the walls with 4" and 3" screw spacing. These results can be explained as follows: the closer screw spacing makes the force distribution between the screws more even and eventually makes the wall able to undergo larger lateral deflection; however, this benefit will become less dominant when the screw spacing becomes very close. When the screw spacing reduces to an extent, most of the screws can reach their full capacity at the same time; however, the ultimate capacity of single screw cannot be improved by reducing the screw spacing. As well, the failure of the wall may be governed by the buckling of end chords when the screw spacing becomes less than 3".

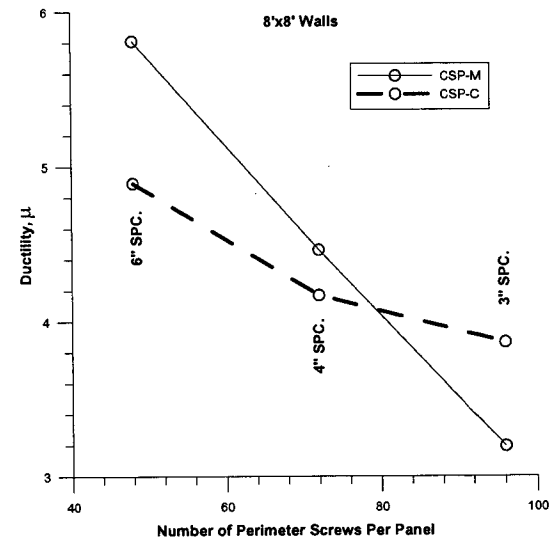
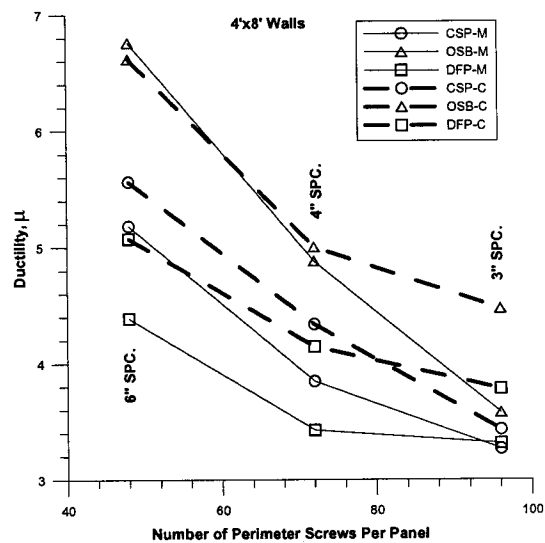
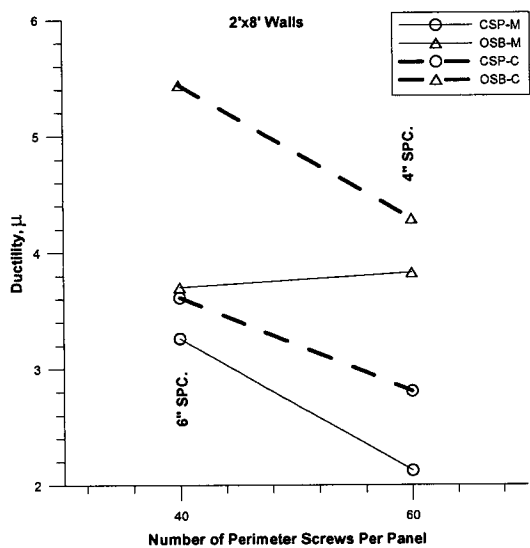


Figure 4.13 Ductility,  $\mu$ , vs. Number of Perimeter Screws Per Panel

#### **4.5.2 DUCTILITY vs. SHEATHING TYPE**

In a comparison of ductility versus sheathing type, the OSB walls possessed the highest  $\mu$  values (Figure 4.14). For most of the 4' x 8' wall configurations the CSP walls showed a greater ductility compared with the DFP walls, except in the case of the 3"/12" screw pattern. The ductility of the walls sheathed with Richply CSP panels is slightly less than that of walls constructed with Alberta Plywood CSP panels. The OSB panels, which are composed of glued small strands of wood have less defects overall than CSP and DFP panels. Plywoods are made of veneers peeled from logs and hence the probability of a defect at a connection is greater, which would result in less ductility. That is, the sheathing with higher bearing deformability will cause the walls made of it to have higher ductility.

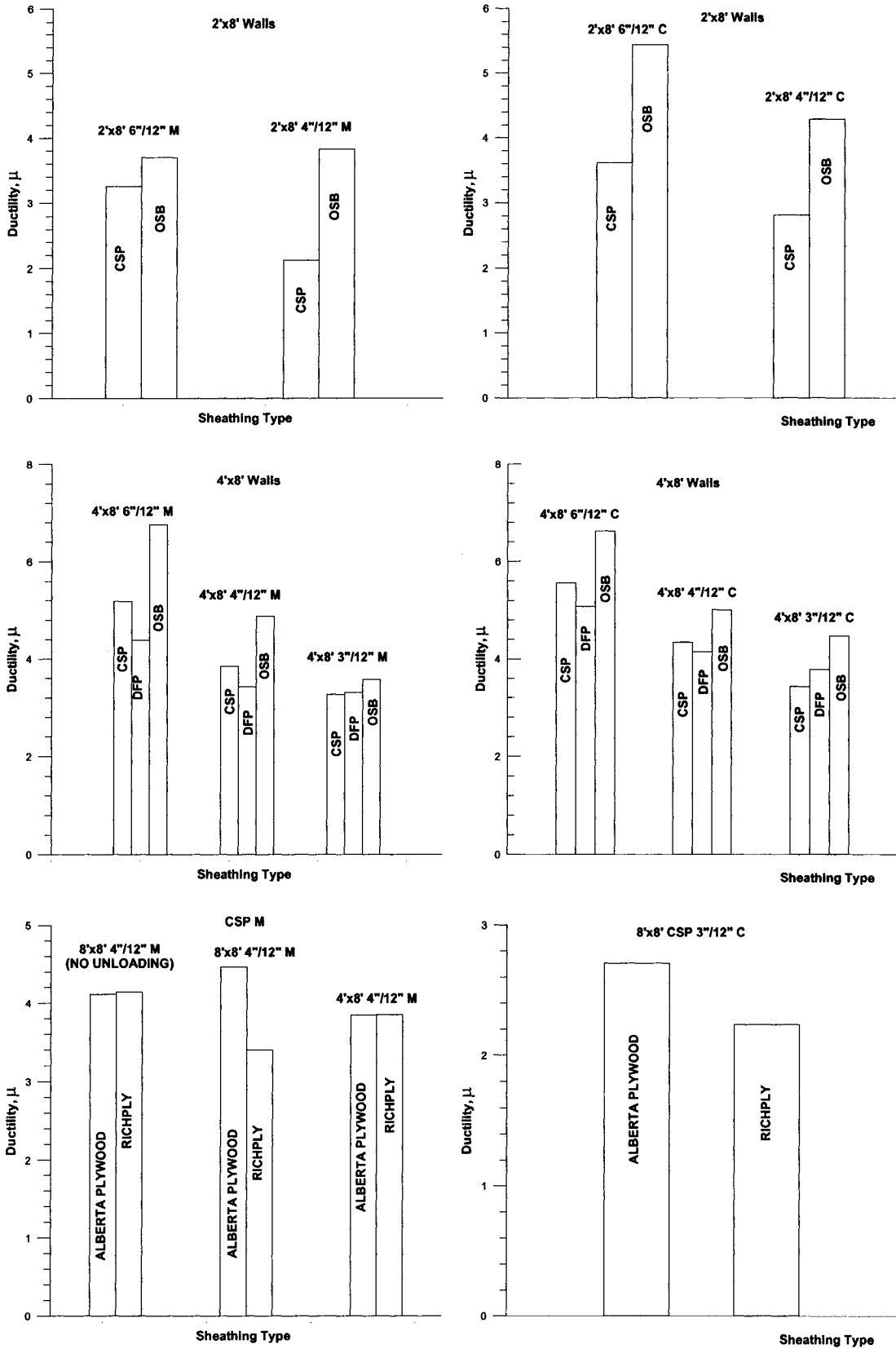


Figure 4.14 Ductility,  $\mu$ , vs. Sheathing Type

#### **4.5.3 DUCTILITY vs. ASPECT RATIO**

The ductility of the 2' walls was found to be much less than that of the 4' and 8' walls mainly because of the drift limit ( $2.5\%h_s$ ) that was incorporated into the EEEP analysis procedure (Section 3.7) (Figure 4.15). The 2' long walls would have possessed greater ductility measures if this limit had not been imposed, i.e. on average an increase of 40% would have been obtained. Moreover, without the limit the ductility of the 2' long walls would become close to that of the 4' walls. Ductility values for the 4' and 8' CSP walls with same screw spacing are close to each other. No consistent trend exists in terms of which of these wall lengths provides the greatest ductility.

#### **4.5.4 DUCTILITY vs. LOAD PROTOCOL**

The ductility measured for the reversed cyclic tests is generally higher than that recorded for the monotonic tests with the same wall configuration (Figure 4.16). However, this observation did not hold true for the 8' x 8' CSP 6"/12" and 4"/12" walls, nor for the 4' x 8' OSB 6"/12" specimens. It is likely that during the initial small amplitude cycles of the reversed cyclic protocol a redistribution of the demand on sheathing connections takes place. This allows for a more even distribution of the forces between each of the connections in comparison to what would typically occur in a monotonically loaded wall specimen. The more even demand on the connections provides for greater ductility of the cyclically loaded shear walls. The comparisons shown in Figure 4.16 where this did not hold true, i.e. the monotonic walls were more

ductile, was probably caused by variations in the quality of the wood sheathing and in the placement of the screw fasteners.

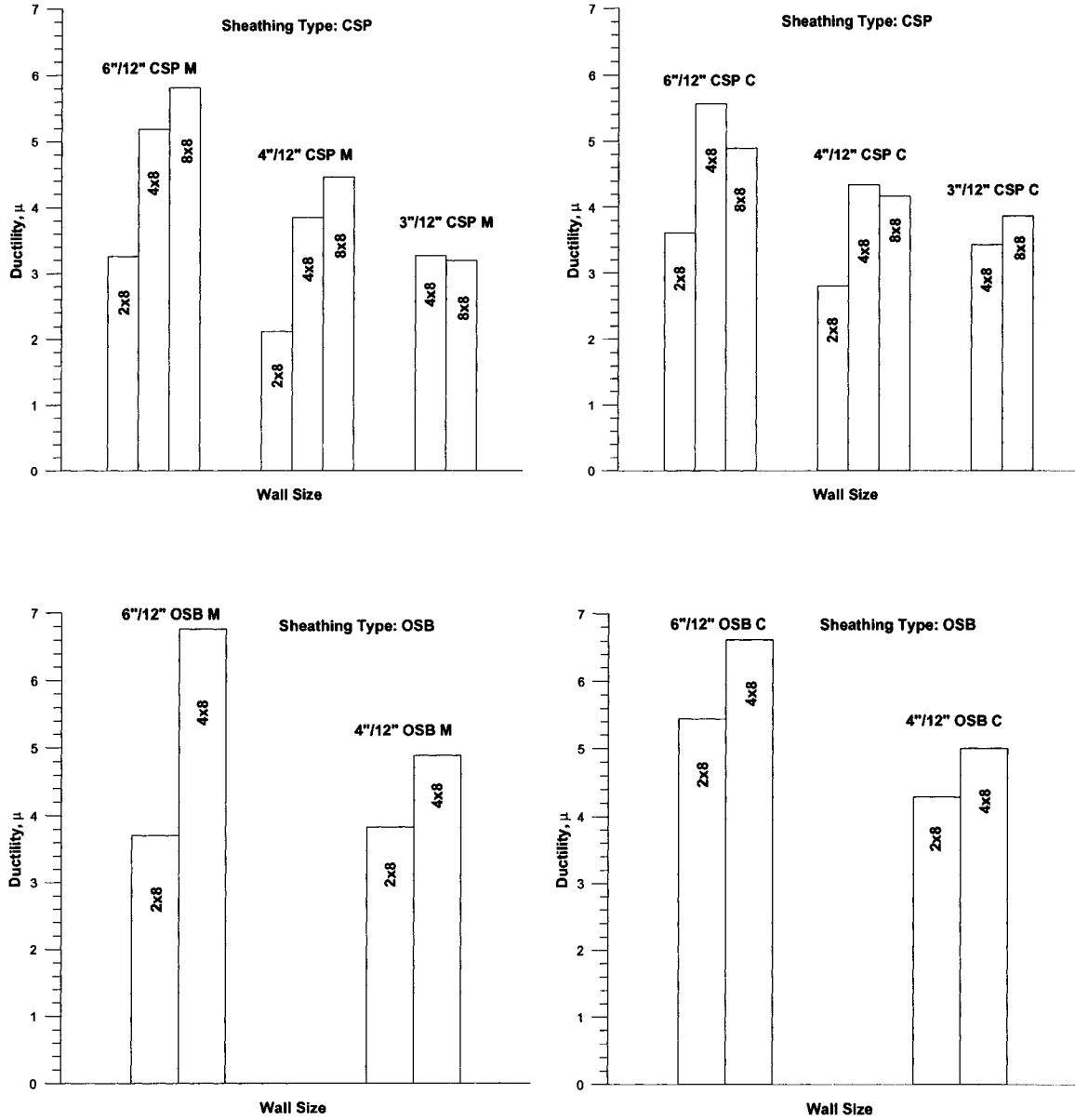


Figure 4.15 Ductility,  $\mu$ , vs. Aspect Ratio

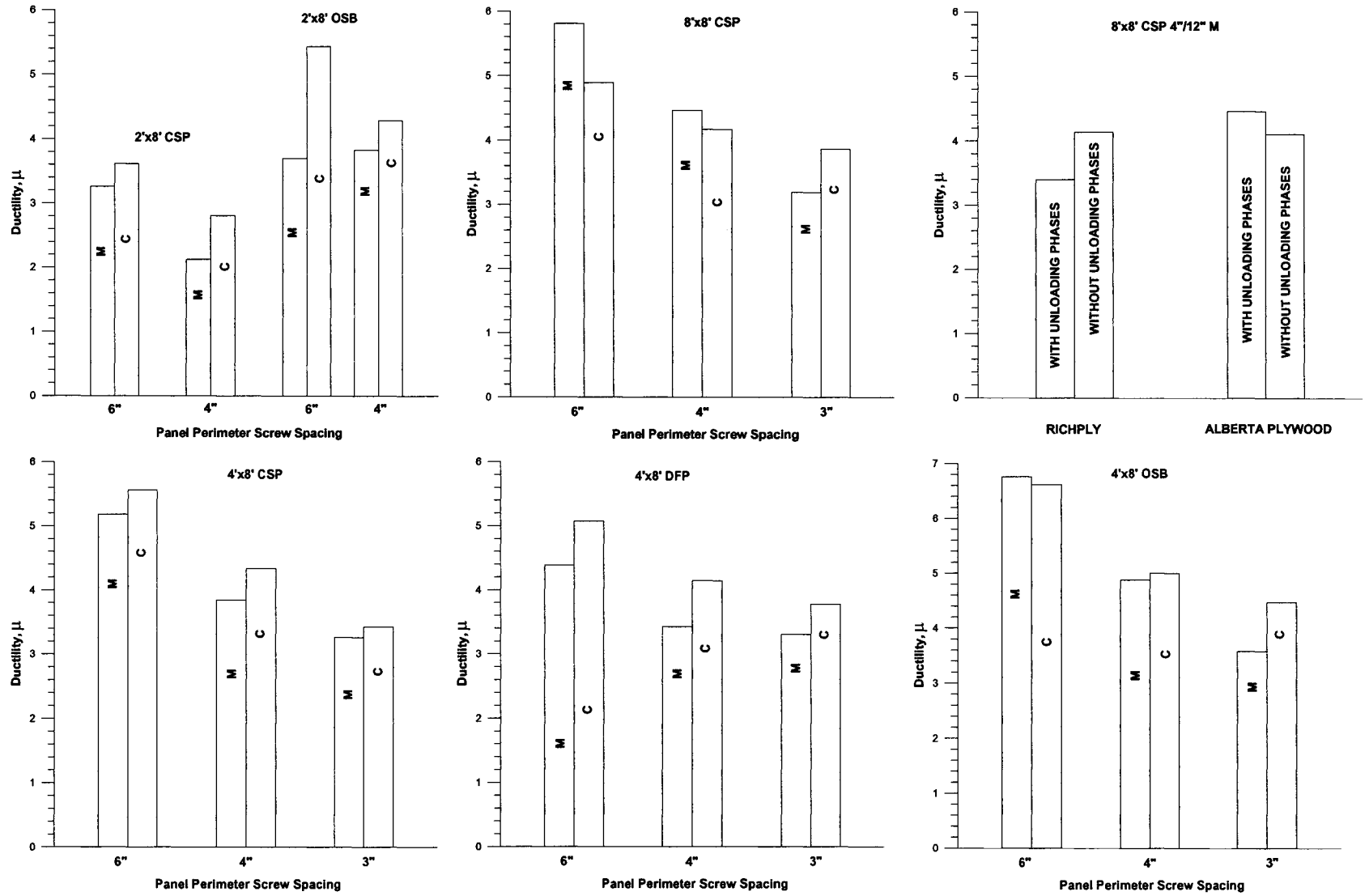


Figure 4.16 Ductility,  $\mu$ , vs. Load Protocol

## 4.6 ENERGY DISSIPATION ABILITY ( $E_r$ & $E_b$ )

Two indices are used to evaluate the energy dissipation ability of the shear walls; this includes the real energy,  $E_r$ , and the energy under the backbone curve,  $E_b$  (Figures 3.12 and 3.13, Tables 3.2-3.6). In the case of monotonic tests these two energy measures are the same, except when the EEEP analysis is governed by the 2.5%  $h_s$  inelastic drift limit (Table 3.4). However, for reversed cyclic tests the real energy includes all of the cycles in the protocol, which provides for significantly higher measures of energy compared with the backbone approach. Similarly, when comparing real cyclic with monotonic energy values, it is expected that the cyclic specimens will dissipate significantly more energy due to the repeated displacements in the loading protocol. In some comparisons a normalized energy value is used, where  $E_r$  or  $E_b$  is divided by the number of perimeter screws in a wall; in order to provide for a comparison of the efficiency of the individual fasteners as more are added to a shear wall. Additional details on the energy measurements are provided in Sections 3.6 and 3.7 (Figure 3.12 ~ 3.16).

### 4.6.1 ENERGY DISSIPATION ABILITY vs. SCREW SPACING

Figures 4.17 ~ 4.20 show the energy dissipation trend of the shear walls as a function of the sheathing perimeter screw spacing. The real energy dissipation,  $E_r$ , is approximately proportional to the number of perimeter screws with the exception of 4' x 8' DFP 3"/12" M tests. These walls failed by local buckling of the compression chords rather than at the sheathing connections, and hence the full energy dissipating ability of

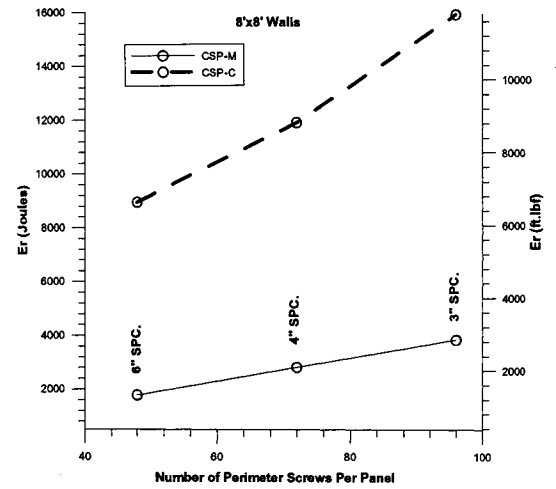
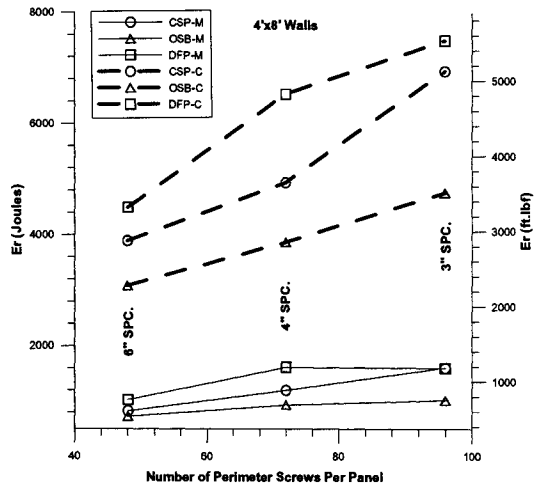
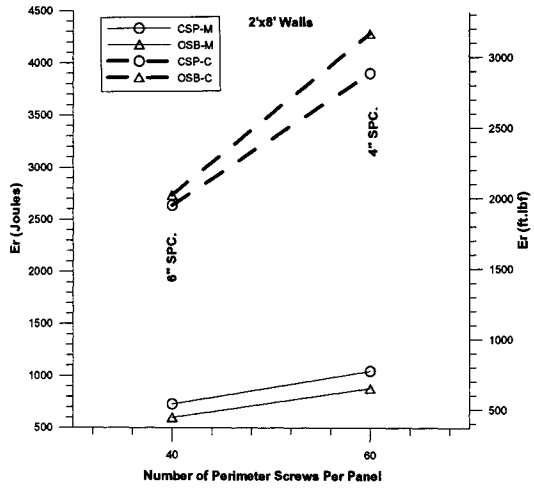


Figure 4.17 Energy,  $E_r$ , vs. Number of Perimeter Screws Per Panel

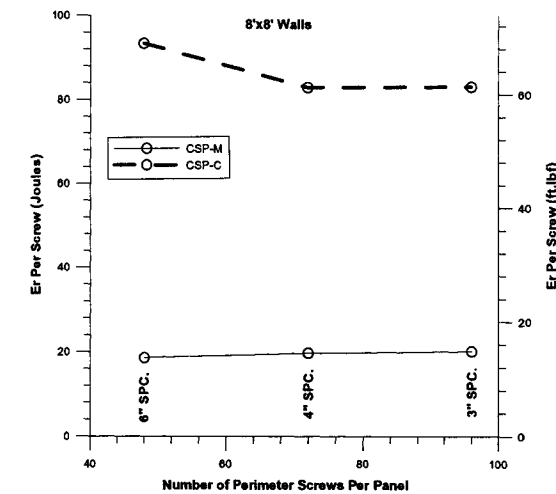
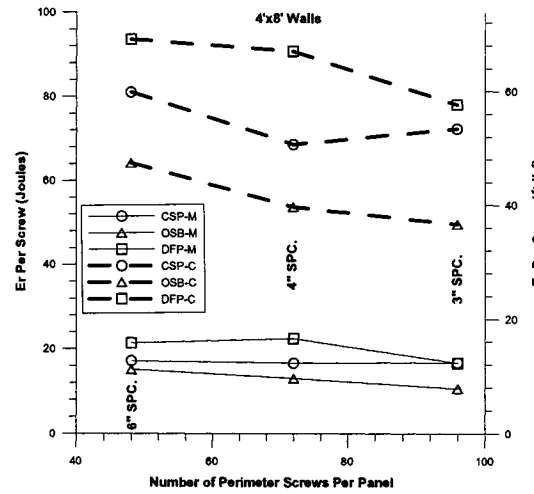
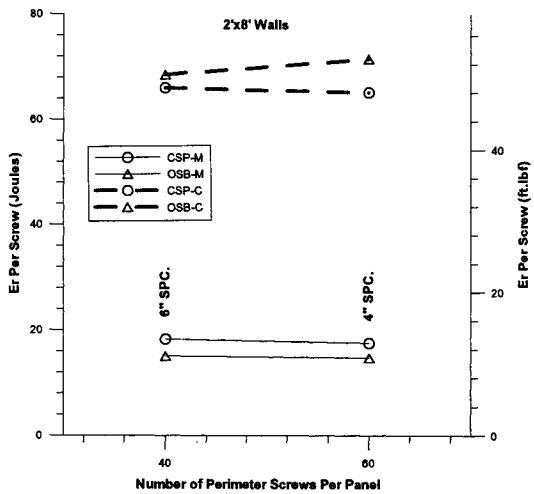


Figure 4.18 Normalized Energy,  $E_r$ , vs. Number of Perimeter Screws Per Panel

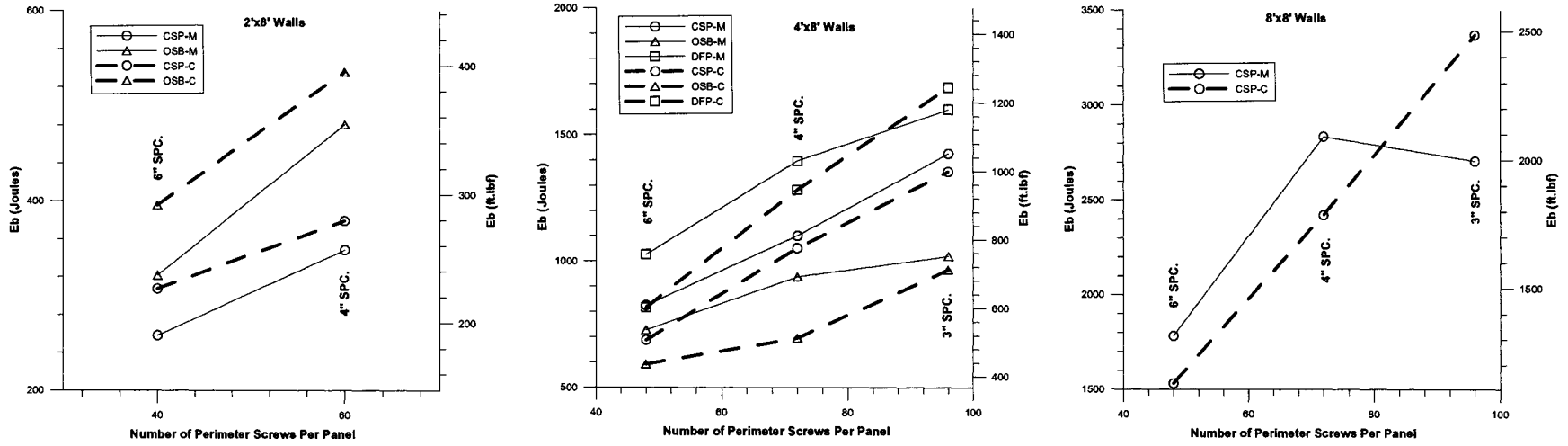


Figure 4.19 Energy,  $E_b$ , vs. Number of Perimeter Screws Per Panel

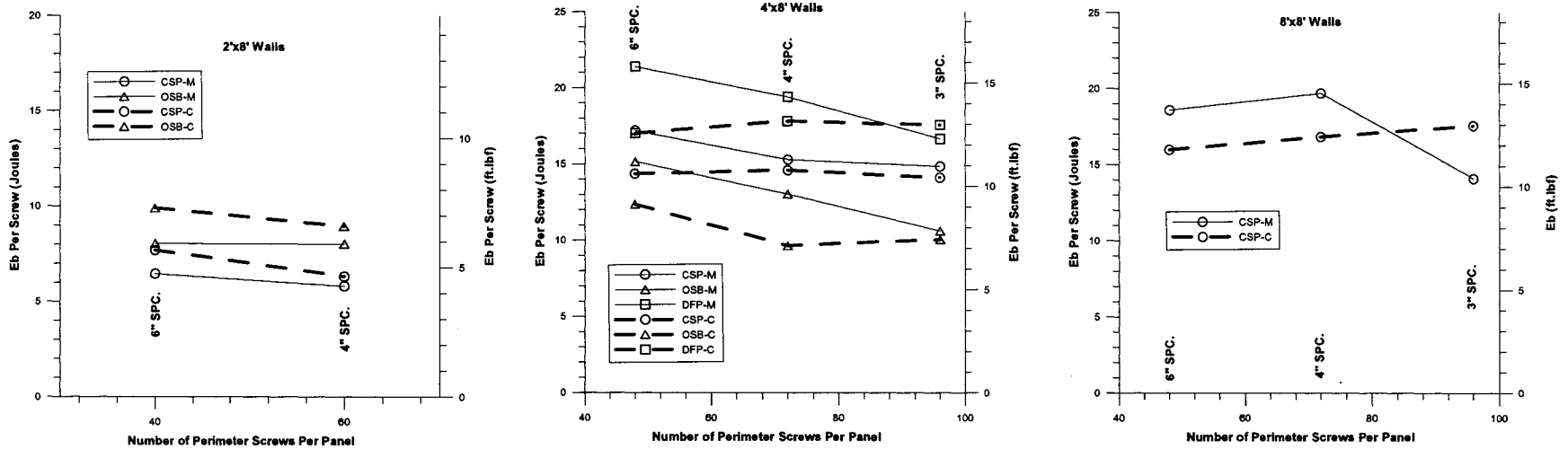


Figure 4.20 Normalized Energy,  $E_b$ , vs. Number of Perimeter Screws Per Panel

the individual connections was not achieved. The measured energy dissipation ability of these walls was similar to the 4' x 8' DFP 4"/12" M specimens (Figure 4.17). The energy under the backbone curve,  $E_b$ , increases with the decrease of the screw spacing for walls with the same width. However, the  $E_b$  values for the 8' x 8' CSP 3"/12" M walls are less than that of the same wall with a 4" perimeter screw spacing (Figure 4.19), because the former are governed by the 2.5%  $h_s$  drift limit in the calculation of energy.

If normalized energy values are compared, the energy per screw remains quite level as the spacing between perimeter screws is decreased (Figure 4.18 & 4.20). Only a slight decrease in the measured energy values per screw occurs as the number of screws is increased. This shows that each screw seems to be able to develop near to its full energy dissipation capacity, and hence the wall energy dissipation is essentially a summation of the individual screw fastener energy dissipation. The sheathing screws in those walls whose calculated energy dissipation is governed by the 2.5%  $h_s$  drift limit have not yet reached their full load carrying capacity at the deflection level considered.

#### **4.6.2 ENERGY DISSIPATION ABILITY vs. SHEATHING TYPE**

The real energy,  $E_r$ , dissipated by the OSB walls is less than that dissipated by the CSP walls with the same wall configuration, except for 2' x 8' walls in cyclic tests. The DFP walls have a larger capacity to dissipate the energy than both the CSP and OSB walls with the exception of the 4' x 8' 3"/12" M walls. As noted previously, this was due to the different failure mode of these three DFP shear walls. The difference between the walls with Richply panels and those with Alberta Plywood panels presented no fixed trend (Figure 4.21). The energy under the backbone,  $E_b$ , shows similar findings to those noted for the  $E_r$  measurements, except that the 2' x 8' OSB walls have a higher energy dissipation both in monotonic and cyclic tests (Figure 4.22). The energy dissipation ability of shear walls with the same wall configuration is mainly affected by three factors: the shear capacity, stiffness and deformability of the sheathing connections. However, these three factors show different trends with the change of sheathing types, so the energy capacity cannot be simply determined by any one factor.

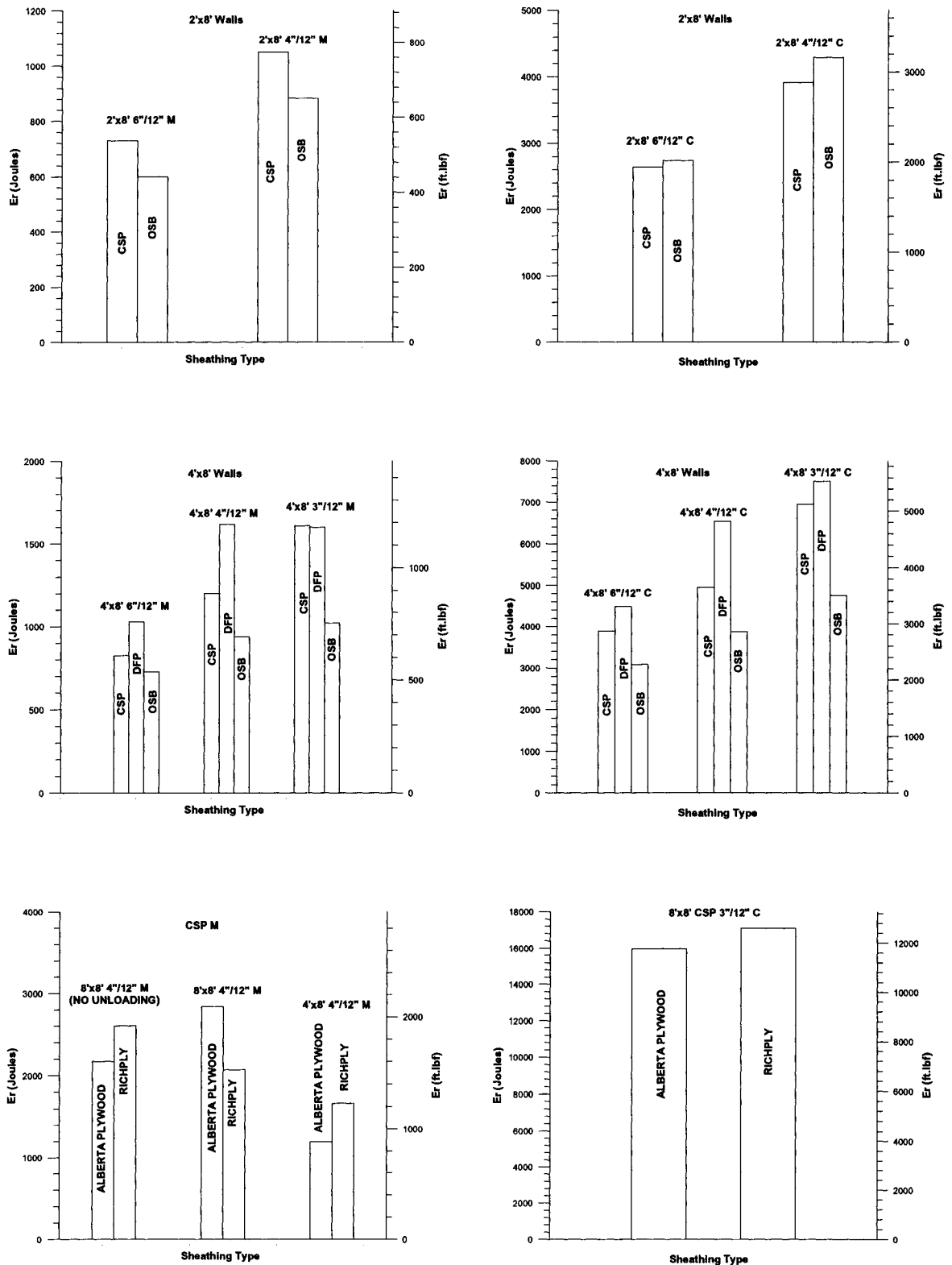


Figure 4.21 Energy,  $E_r$ , vs. Sheathing Type

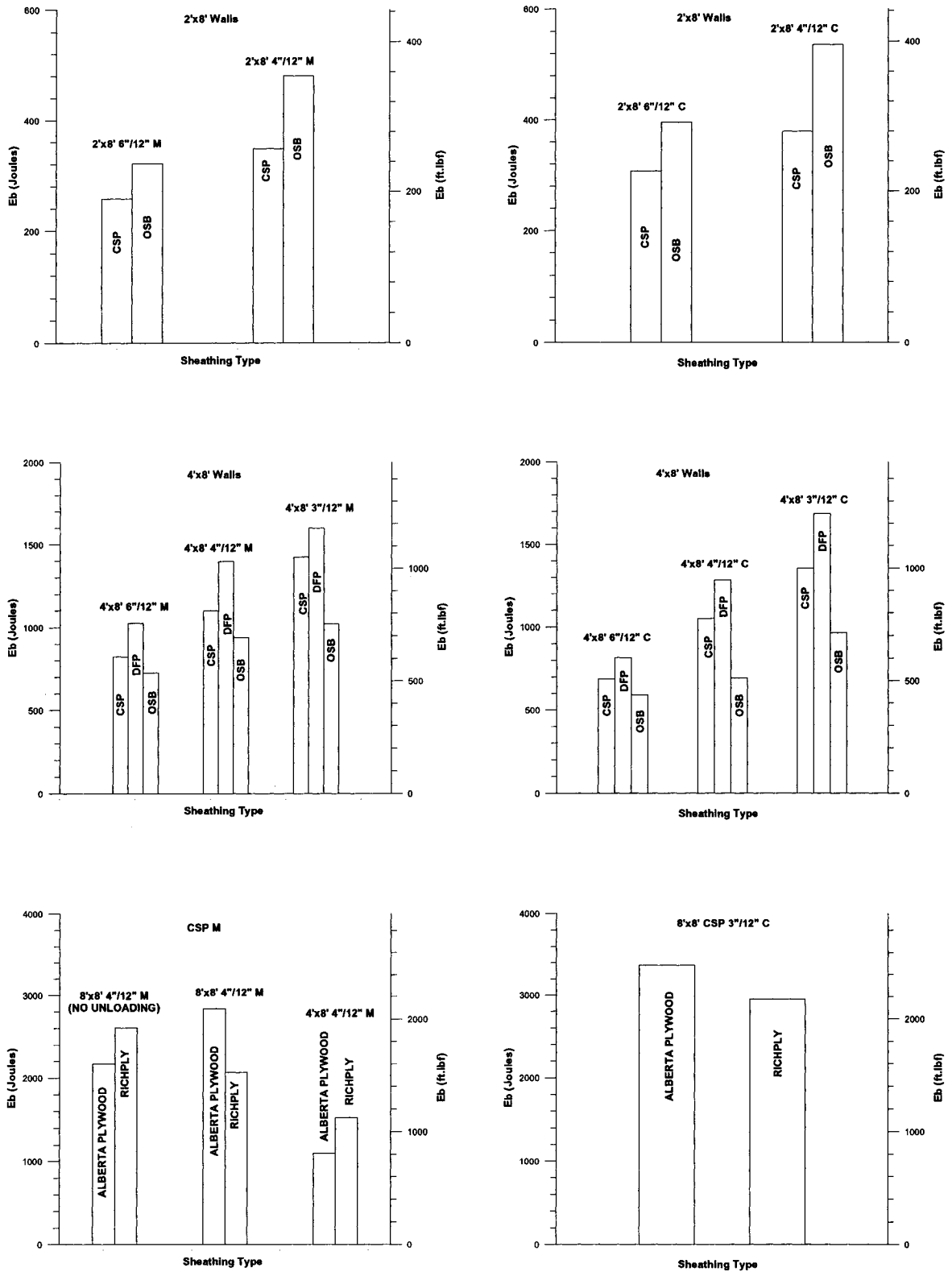


Figure 4.22 Energy,  $E_b$ , vs. Sheathing Type

### 4.6.3 ENERGY DISSIPATION ABILITY vs. ASPECT RATIO

Given walls with the same screw pattern, the real energy dissipation,  $E_r$ , generally increases with the wall length, however, the increase is not proportional to the ratio of wall length. An exception exists in the group OSB 4"/12" C, in which the energy dissipated by the 4' x 8' walls is less than that dissipated by the 2' x 8' walls (Figure 4.23). With the same screw pattern, a longer wall has more perimeter screws. This provides a larger energy dissipation capacity, since the overall ability to dissipate energy is based on the sum of the contribution of the individual screw connections.

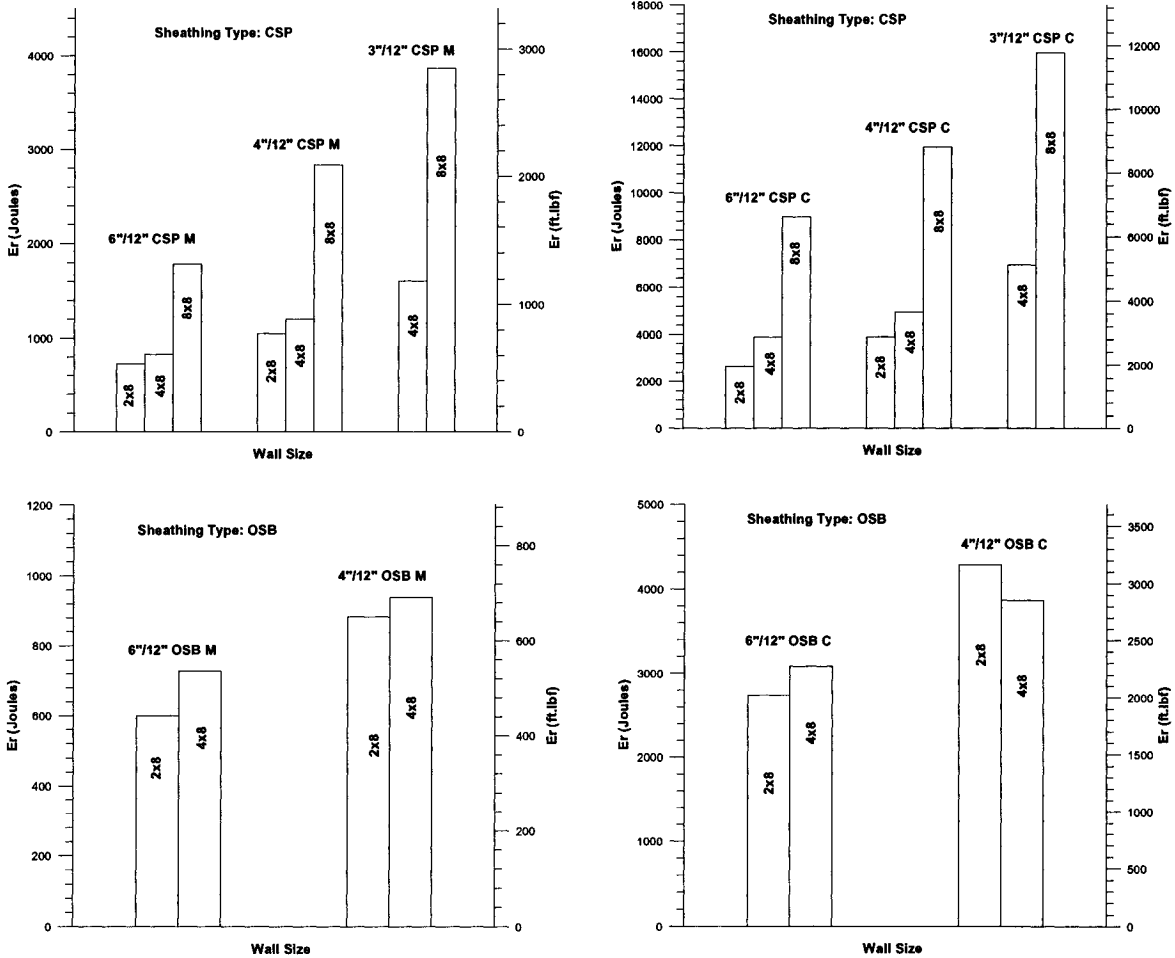


Figure 4.23 Energy,  $E_r$ , vs. Aspect Ratio

The energy under the backbone curve,  $E_b$ , is approximately proportional to the ratio of wall length if the same screw pattern is specified, except for the OSB walls in cyclic tests (Figure 4.24). The 2.5%  $h_s$  drift limit causes the 2' x 8' walls not to reach their full energy dissipation ability, while this limit usually did not apply for 4' x 8' and 8' x 8' walls.

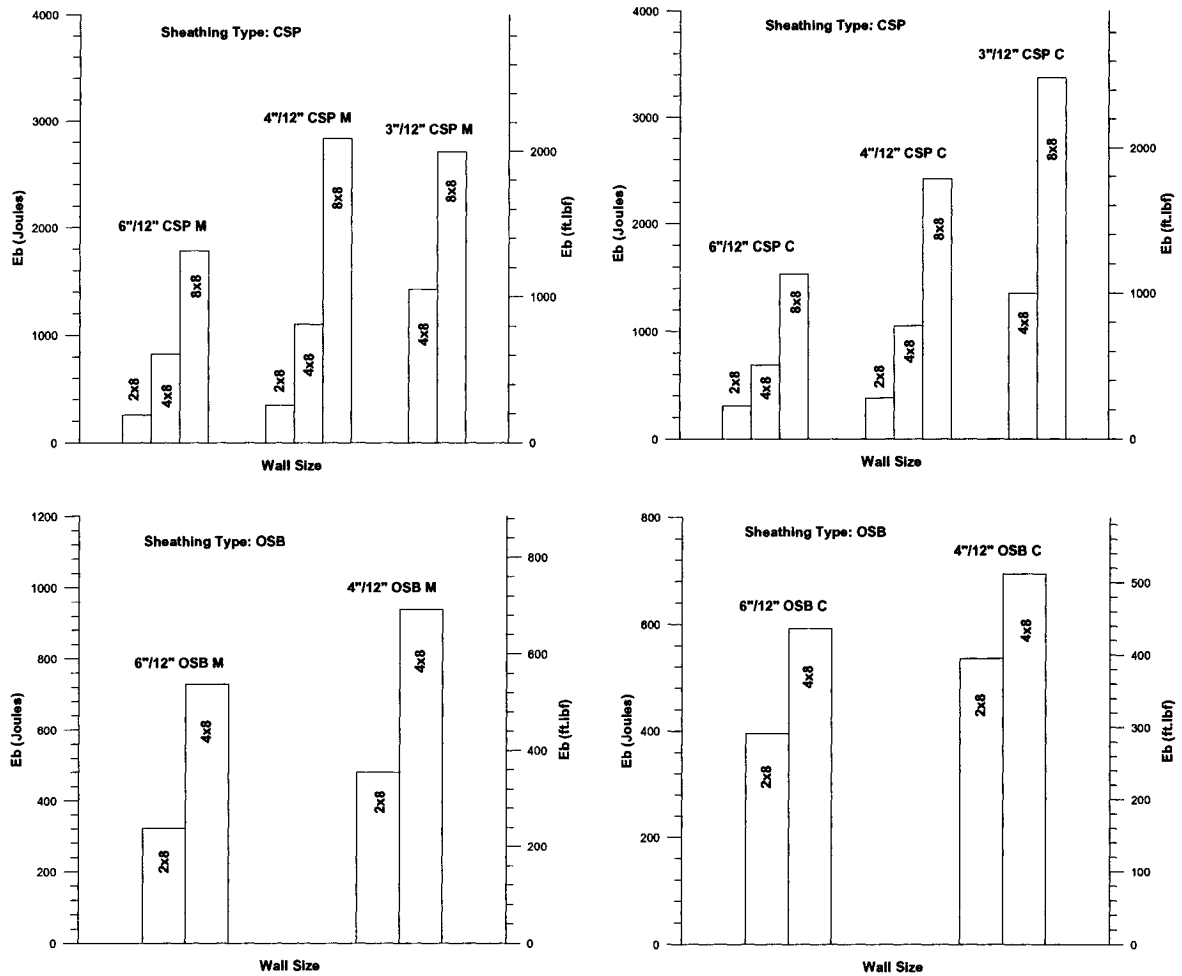


Figure 4.24 Energy,  $E_b$ , vs. Aspect Ratio

The normalized energy values,  $E_r$ , determined for the test walls are nearly at the same level for specimens with the same type of sheathing, which is reasonable, because each screw can reach its full capacity during lateral loading (Figure 4.25).

Normalized Energy,  $E_b$ , for 4' x 8' and 8' x 8' walls with the same type of sheathing are very close to each other, however, the values for 2' x 8' walls are much less than those for 4' x 8' and 8' x 8' walls (Figure 4.26), since the failure of the 2' x 8' walls are governed by the 2.5%  $h_s$  drift limit. Hence, the sheathing screws cannot reach their full capacity at the deflection level considered.

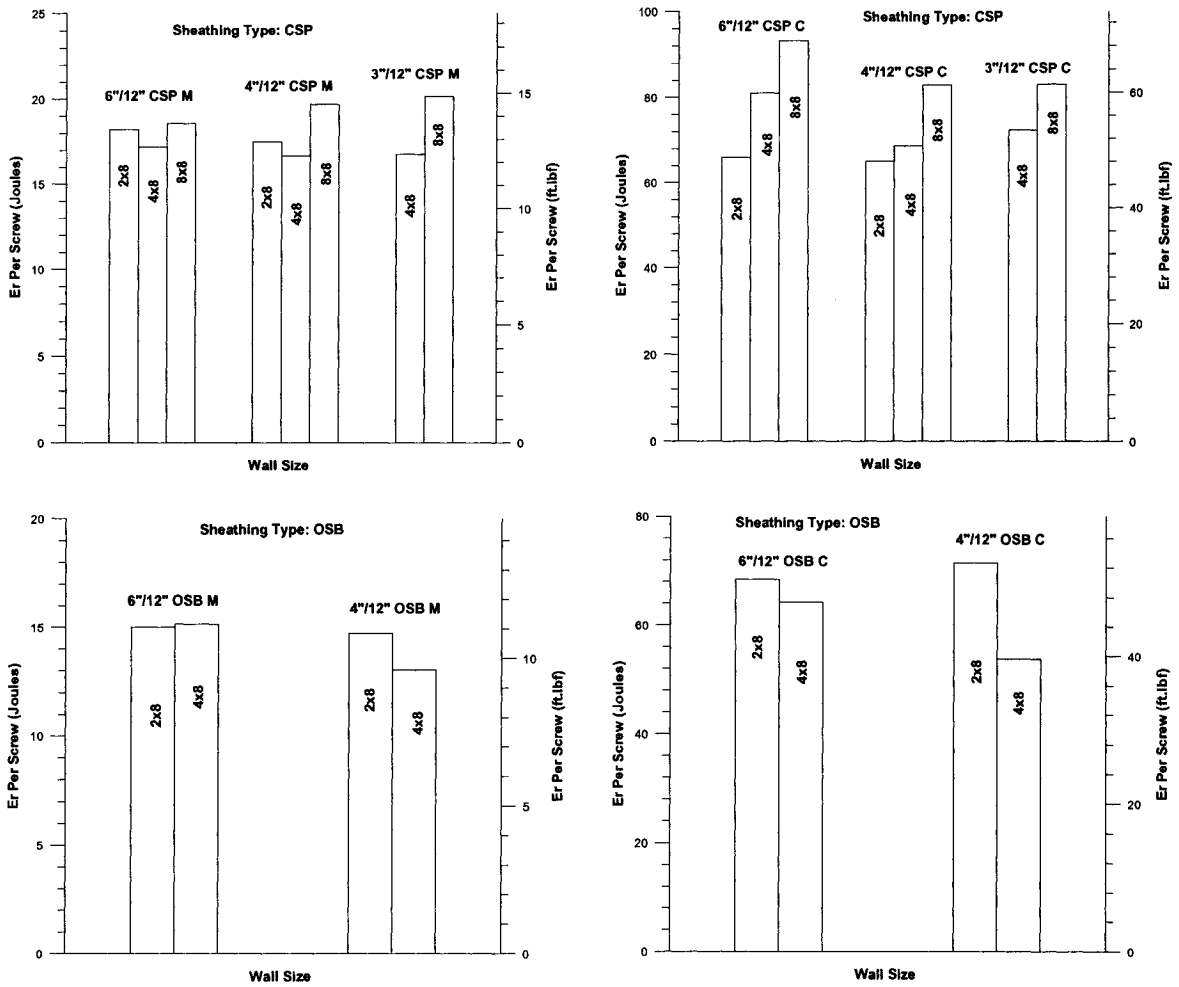


Figure 4.25 Normalized Energy,  $E_r$ , vs. Aspect Ratio

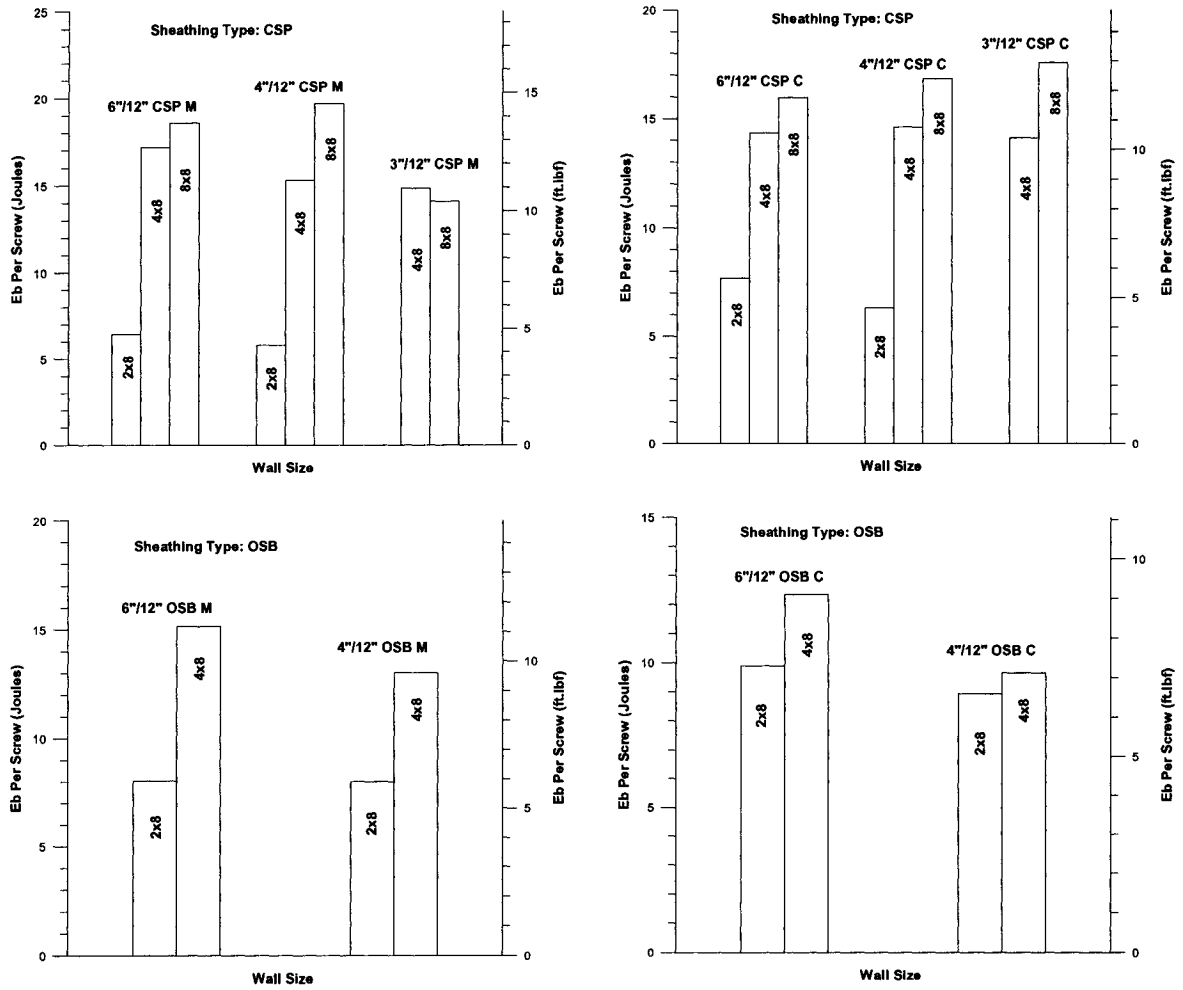


Figure 4.26 Normalized Energy,  $E_b$ , vs. Aspect Ratio

#### 4.6.4 ENERGY DISSIPATION ABILITY vs. LOAD PROTOCOL

The real energy,  $E_r$ , dissipated in each cyclic test is significantly higher than that dissipated in monotonic tests due to the repeated displacements (Figure 3.13) in the loading protocol (Figure 4.27). It is therefore, not appropriate to draw any conclusions from these results.

The energy measured under the backbone curve,  $E_b$ , provides a more equitable comparison between the performance of the monotonic and reversed cyclic test specimens.

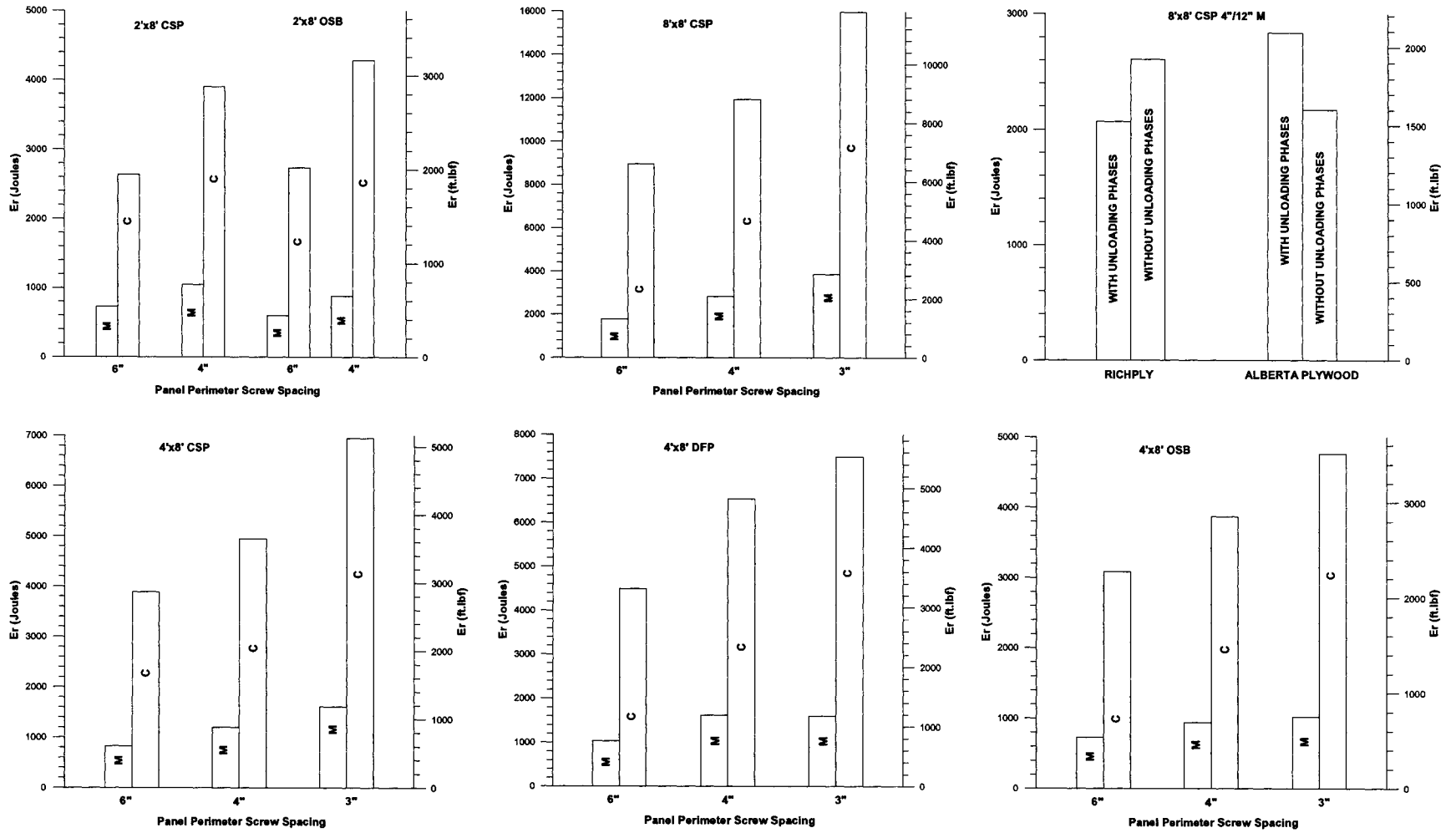


Figure 4.27 Energy,  $E_r$ , vs. Load Protocol

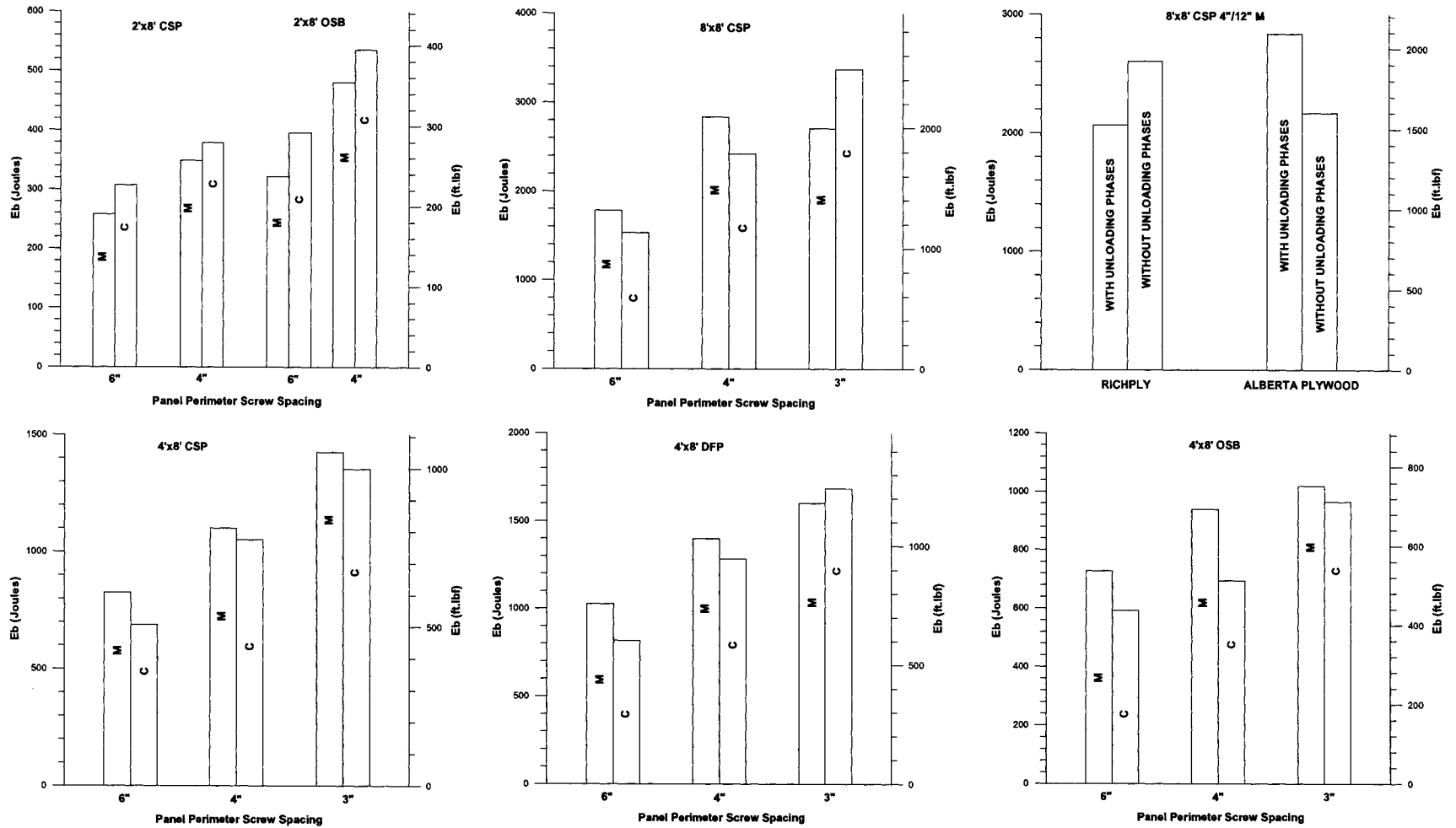


Figure 4.28 Energy,  $E_b$ , vs. Load Protocol

The dissipated energy for cyclic tests is generally less than that determined for monotonic tests with the same wall configuration; this is due to the decrease of stiffness of the sheathing connections as the deformation cycles are repeated (Tables 5.1 and 5.3). However, an exception exists for the 2' x 8' CSP and OSB walls, for which the energy values in cyclic tests are more than those in monotonic tests (Figure 4.28). In the calculation of energy the maximum deflection that could be considered was governed by the 2.5%  $h_s$  drift limit. In addition, the 4' x 8' DFP 3"/12" walls and 8' x 8' CSP 3"/12" walls showed higher energy dissipation for the cyclic tests. For the DFP walls this was caused by the change in failure mode of the monotonically tests specimens, from connection failure to chord buckling, which resulted in a lower energy dissipation level (Branston, 2004). The last exception of 8' x 8' CSP 3"/12" walls may be due to the fluctuation of the sheathing strength and quality. In general, when the drift limit is not applied the energy under the backbone curve,  $E_b$ , in cyclic tests can be assumed to reach the same level as in the monotonic tests.

## 4.7 DEFLECTION

The lateral in plane deflection of a shear wall is determined using Equation (3.1). Typical monotonic load-deflection curves of walls with different wall lengths are shown in Figure 4.29.

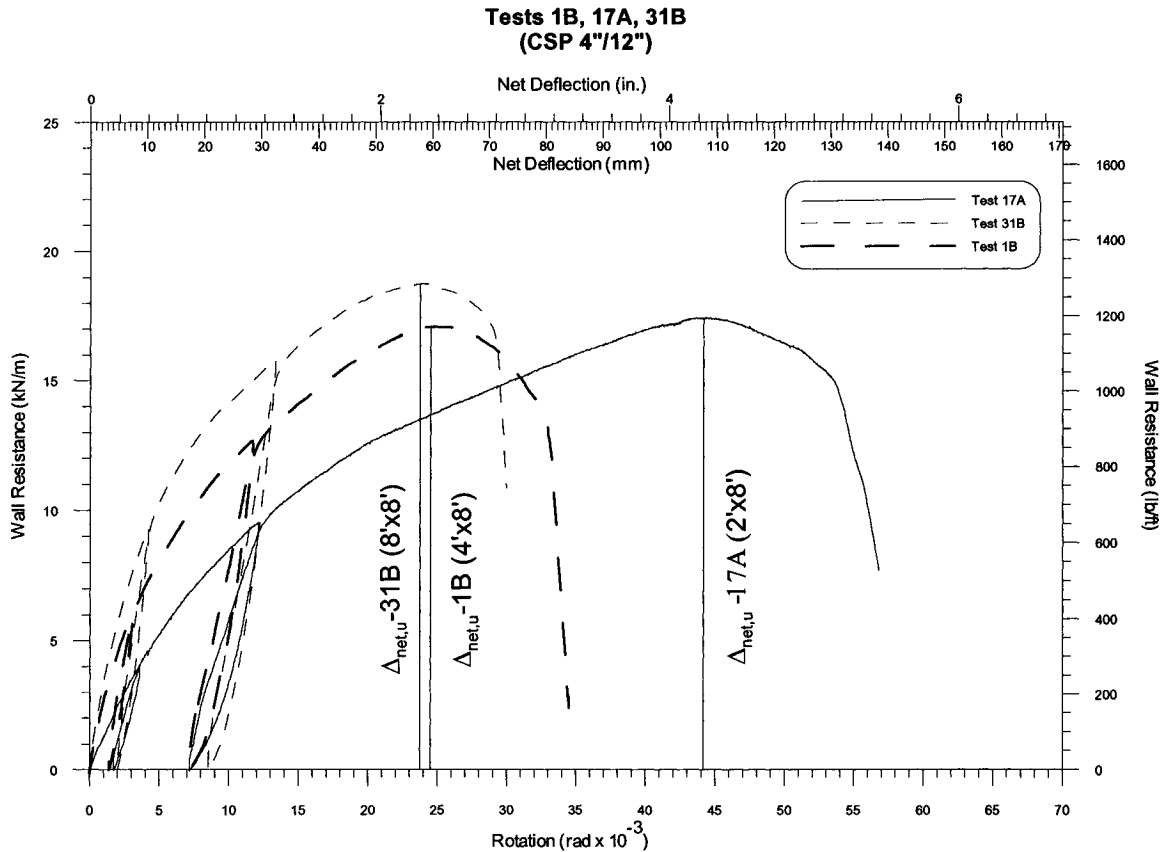


Figure 4.29 Deflection vs. Wall Length

This comparison of representative shear wall test specimens reveals the following rules: The 8' x 8' and 4' x 8' walls reached their maximum load capacity at nearly the same deflection level. However, the deflection of the 2' x 8' wall was almost twice that of the two longer walls at its ultimate load position. This indicates that the 2' x 8' walls are much more flexible than the 8' x 8' walls and 4' x 8' walls due to the higher aspect ratio.

The same results occurred for the walls tested with the reversed cyclic protocol. Table 4.2 provides a comparison of the deflection measured at ultimate load between the 4' and 8' long walls and the 2' walls. In each case the longer wall(s) for a certain configuration are compared with the shortest that was tested, either 2' or 4'. The ratios show that the 4' and 8' walls typically reach their ultimate load carrying level at the same displacement, whereas values that range between 0.42 and 0.63 show that the 2' long walls always reach their ultimate shear capacity at much greater lateral displacements.

Figure 4.29 and Table 4.2 show that in a design situation the 2' x 8' walls should not be expected to develop their full capacity together with either a 8' x 8' or a 4' x 8' wall. Hence, it is recommended that the shear capacity of a 2' long wall when constructed in tandem with a longer wall should not be relied on. In the case of a structure that consists solely of 2' long shear walls, then the 2.5%  $h_s$  drift limit must be considered in the determination of the lateral load carry capacity. A more detailed discussion of a recommended design approach has been provided by Branston (2004)

Table 4.2 Comparison of Deflection at Ultimate Load,  $\Delta_{net,u}$ , vs. Wall Length

	ID	$\Delta_{net,u}$	Ratio		ID	$\Delta_{net,u}$	Ratio
		mm				mm	
CSP 6"/12"				CSP 6"/12"			
2x8 CSP 6"/12" M	15A,B,C	103.3	1.00	2x8 CSP 6"/12" C	16A,B,C	72.2	1.00
4x8 CSP 6"/12" M	7A,B,C	50.7	0.49	4x8 CSP 6"/12" C	8A,B,C	44.3	0.61
8x8 CSP 6"/12" M	29A,B,C	50.5	0.49	8x8 CSP 6"/12" C	30A,B,C	45.4	0.63
8x8/4x8			1.00	8x8/4x8			1.02
CSP 4"/12"				CSP 4"/12"			
2x8 CSP 4"/12" M	17A,B,C	107.0	1.00	2x8 CSP 4"/12" C	18A,B,C	83.8	1.00
4x8 CSP 4"/12" M	1A,B,C	60.6	0.57	4x8 CSP 4"/12" C	4A,B,C	50.4	0.60
8x8 CSP 4"/12" M	31A,B,C	58.5	0.55	8x8 CSP 4"/12" C	32A,B,C	48.5	0.58
8x8/4x8			0.97	8x8/4x8			0.96
CSP 3"/12"				CSP 3"/12"			
4x8 CSP 3"/12" M	9A,B,C	61.0	1.00	4x8 CSP 3"/12" C	10A,B,C	48.3	1.00
8x8 CSP 3"/12" M	33A,B,C	64.1	1.05	8x8 CSP 3"/12" C	34A,B,C	53.3	1.10
OSB 6"/12"				OSB 6"/12"			
2x8 OSB 6"/12" M	19A,B,C	78.4	1.00	2x8 OSB 6"/12" C	20A,B,C	62.8	1.00
4x8 OSB 6"/12" M	21A,B,C	41.1	0.52	4x8 OSB 6"/12" C	22A,B,C	36.1	0.57
OSB 4"/12"				OSB 4"/12"			
2x8 OSB 4"/12" M	27A,B,C	78.0	1.00	2x8 OSB 4"/12" C	28A,B,C	79.0	1.00
4x8 OSB 4"/12" M	23A,B,C	39.5	0.51	4x8 OSB 4"/12" C	24A,B,C	32.8	0.42

#### 4.8 STUD CAPACITY

The maximum axial load  $P_{max}$  (kN) acting on the end studs in each test is determined with Equation (4.1):

$$P_{max} = \frac{S_u * L * H}{(L - 85 * 2) * 1000} \quad (4.1)$$

where

$S_u$  = The ultimate shear strength, kN/m;

L = The wall length, mm;

H = The wall height, mm;

85 = The distance from the centre of a hold-down to the adjacent outer wall side, mm.

Similarly, the axial load  $P_y$  acting on the end studs in each test, corresponding to the yield shear strength of the wall, is determined with Equation (4.2):

$$P_y = \frac{S_y * L * H}{(L - 85 * 2) * 1000} \quad (4.2)$$

where

$S_y$  = The yield shear strength, kN/m;

Summarized in Table 4.3 are the average axial loads on the end studs when the walls, which were of the same configuration, reached their ultimate and yield strength level during monotonic and cyclic tests. In addition, the theoretical axial compression capacity of the end chord studs, calculated according to CSA S136 (2001), is listed in the table, as well as the ratio of actual axial loads to the theoretical capacity. The table shows the yield loads measured for specimens 13A,B,C (4x8 DFP 3"/12" walls) are beyond the axial compression capacity of the studs, which is in accordance with the observations made during monotonic testing where the chord studs failed by local buckling (Branston, 2004). However, the chords did not fail in the matching cyclic tests with the same wall configuration. This may have been attributed to the fact that the maximum lateral load only lasted for a very short time in the cyclic tests, or that the actual stud capacity is higher than that determined following the CSA S136 prescribed calculations (see Appendix V) because of strain rate effects.

Table 4.3 Ratios of Chord Stud Loads in Tests to the Capacity Determined by CSA S136

ID	Maximum Load in Test (kN)	$P_n$ (kN)	Ratio	Yield Load in Test (kN)	$P_n$ (kN)	Ratio
2x8 CSP 6"/12" M	41.3	62.0	0.667	27.8	62.0	0.449
2x8 CSP 6"/12" C	36.4	62.0	0.588	30.2	62.0	0.486
2x8 CSP 4"/12" M	60.9	62.0	0.983	41.5	62.0	0.670
2x8 CSP 4"/12" C	55.4	62.0	0.894	42.4	62.0	0.683
2x8 OSB 6"/12" M	42.2	62.0	0.681	34.0	62.0	0.548
2x8 OSB 6"/12" C	36.0	62.0	0.581	31.5	62.0	0.509
2x8 OSB 4"/12" M	62.2	62.0	1.003	50.3	62.0	0.811
2x8 OSB 4"/12" C	57.3	62.0	0.924	49.5	62.0	0.798
4x8 CSP 6"/12" M	36.1	62.0	0.583	31.5	62.0	0.509
4x8 CSP 6"/12" C	31.9	62.0	0.515	28.5	62.0	0.460
4x8 CSP 4"/12" M	47.0	62.0	0.759	40.2	62.0	0.649
4x8 CSP 4"/12" C	46.4	62.0	0.749	41.3	62.0	0.666
4x8 CSP 3"/12" M	71.3	62.0	1.150	60.9	62.0	0.982
4x8 CSP 3"/12" C	69.8	62.0	1.126	61.3	62.0	0.989
4x8 DFP 6"/12" M	45.4	62.0	0.732	38.6	62.0	0.623
4x8 DFP 6"/12" C	39.7	62.0	0.640	34.5	62.0	0.556
4x8 DFP 4"/12" M	67.4	62.0	1.087	56.6	62.0	0.913
4x8 DFP 4"/12" C	59.8	62.0	0.964	51.5	62.0	0.831
4x8 DFP 3"/12" M	84.2	62.0	1.358	69.9	62.0	1.128
4x8 DFP 3"/12" C	79.2	62.0	1.278	68.8	62.0	1.109
4x8 OSB 6"/12" M	37.6	62.0	0.606	33.3	62.0	0.538
4x8 OSB 6"/12" C	31.5	62.0	0.507	28.8	62.0	0.464
4x8 OSB 4"/12" M	54.7	62.0	0.882	49.1	62.0	0.793
4x8 OSB 4"/12" C	46.7	62.0	0.753	44.1	62.0	0.712
4x8 OSB 3"/12" M	66.7	62.0	1.076	58.9	62.0	0.951
4x8 OSB 3"/12" C	65.0	62.0	1.048	58.0	62.0	0.935
8x8 CSP 6"/12" M	35.5	62.0	0.573	31.3	62.0	0.504
8x8 CSP 6"/12" C	33.0	62.0	0.532	30.1	62.0	0.486
8x8 CSP 4"/12" M	52.7	62.0	0.850	45.8	62.0	0.739
8x8 CSP 4"/12" C	49.9	62.0	0.805	44.5	62.0	0.717
8x8 CSP 3"/12" M	69.0	62.0	1.113	56.6	62.0	0.913
8x8 CSP 3"/12" C	68.4	62.0	1.102	60.3	62.0	0.972

Note:  $P_n$  is the axial capacity of the end studs determined following CSA S136 (2001).

# CHAPTER 5 ANALYTICAL APPROACH

## 5.1 GENERAL INTRODUCTION

A review of various analytical approaches that can be relied on to determine the strength and stiffness of wood framed shear walls has been presented in Chapter 2. In this chapter these analytical models are used with the light gauge steel frame / wood panel shear walls tested by Branston et al. (2004). Moreover, the models are used to predict the lateral load capacity and deflection of walls at the design load level, which is defined as the yield shear strength  $S_y$  (Figure 3.14 and Equation (3.5)). As well, comparisons between the tests results and the theoretical prediction are conducted to verify the effectiveness of the different analytical approaches.

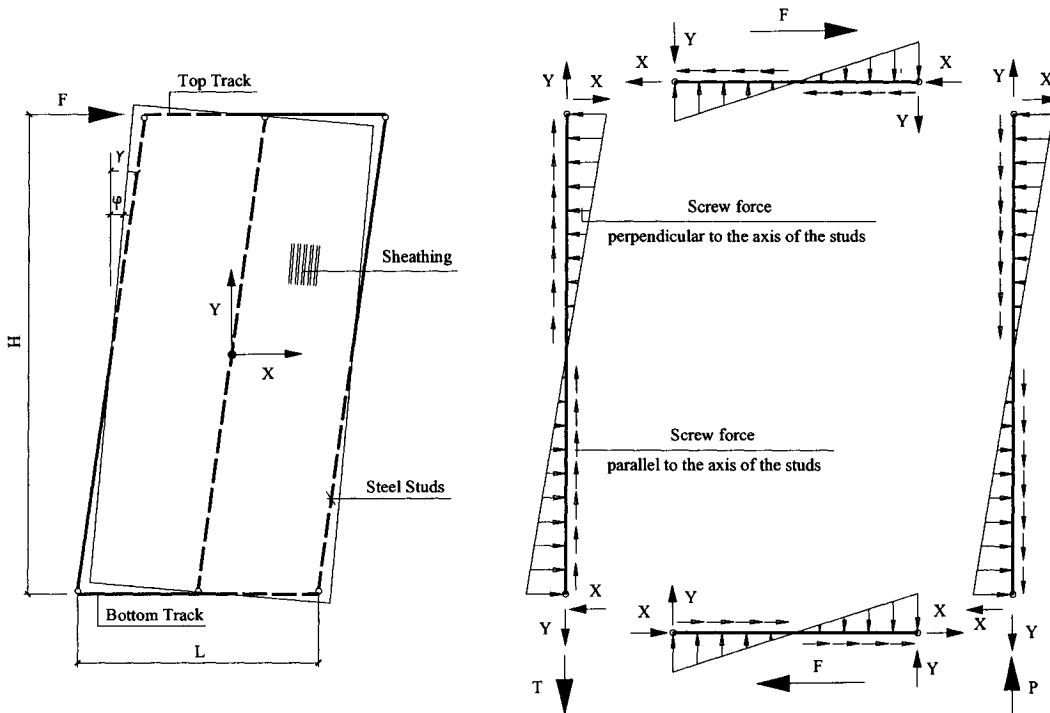


Figure 5.1 Deformations and Force Distribution in Rigid Framing Members

Figure 5.1 shows the assumed deformations and force distribution of a typical light gauge steel frame / wood panel shear wall with height  $H$  and width  $L$ . The lateral load at the top of the wall produces a moment  $M_f (= F \bullet H)$  and a horizontal force  $F$  on the wall bottom. If the hold-downs are designed to fully transfer the tension force into the support through the end studs, the vertical forces ( $T = P$ ) acting on the end studs are equal to  $M_f / L$ , and balanced by shear flow along the screw lines on the end studs, which is produced by sheathing rotation relative to the steel frame. The shear flow causes the axial forces in the end studs to distribute triangularly, with the maximum forces ( $M_f / L$ ) at the bottom of the end studs (Stewart, 1987). With respect to the top track, if the screw spacing along the top edge of the sheathing and the spacing for anchors to the load beam are both small enough to assume the applied force is uniform, then no axial force exists in the top track. Similar for the bottom track, the applied force can be considered uniform if the screw and shear anchor spacing is small. The interior studs at the centreline of a panel or at the joint of two panels with the same width are assumed to carry no axial forces due to lateral loads causing in-plane shearing of the wall. However, the interior studs need to be designed to support gravity loads as well as transverse lateral loads. The interior studs also provide out-of-plane support to stiffen the sheathing panel against shear buckling. The studs at the panel joints act as splices between adjacent wood panels; hence the design of the back-to-back studs needs to incorporate the shear force due to the opposite rotation of the two adjacent panels. Triangularly distributed forces also act perpendicular to the axes of the studs and tracks attached to the edges of panels, due to the relative displacements between studs and panels. In a capacity based design approach the size of the steel frame members is selected such that the frame itself does

not fail. Given this information, and for simplification purposes, the frame members can be assumed to be rigid in the analytical model.

The relative displacements and rotations between the studs and panels introduce forces into the sheathing screws. These screws, which allow for the sheathing and framing to act together as a type of composite system, are under complex loading, including shear, bending and tension.

As for shear wall deflection, the total horizontal displacement of a wall can be determined using Equation (5.1).

$$\Delta_{walltop} = \Delta_{net} + \left[ \left( \frac{\Delta_{baseslip1} + \Delta_{baseslip2}}{2} \right) \right] + \left[ (\Delta_{uplift1} - \Delta_{uplift2}) \times \frac{H}{L} \right] \quad (5.1)$$

where the sheathing screw slip, shear distortion of the sheathing panel (panels) and deformation of framing members all contribute to  $\Delta_{walltop}$ . In this thesis, the analytical model for predicting a shear wall deflection only considers the corrected displacement  $\Delta_{net}$ , for which the movement due to the base slip and uplift of the wall is removed.

## **5.2 PERFORMANCE OF INDIVIDUAL SCREWED SHEATHING CONNECTIONS**

As noted in the discussion above, the sheathing-to-frame connections are a major factor in the performance of a light gauge steel frame / wood panel shear wall. Background information that describes the performance of individual sheathing connections is necessary to carry out an analytical prediction of a wall's performance. For this reason a series of monotonic and cyclic connection tests was performed by Okasha

(2004) using the same wood sheathing, steel studs and screws as for the full-scale wall tests. In this section a brief description of the failure modes of the connection tests is presented to establish a relationship between the full-scale tests and the connection tests.

The connection tests were conducted in accordance with the ASTM Standard D1761 (1988). The monotonic tests were run at a rate of 2 mm/min, and the corresponding cyclic tests were performed by using the same CUREE test protocol as incorporated into the full-scale wall test program. Two failure modes were observed during the connection tests. One was that screws were pulled through the sheathing; the other was that the sheathing edge was torn out by a screw. The screws were never pulled out of the steel studs. These observations were in accordance with what was observed in the full-scale tests (see Section 3.8). The monotonic load capacity in connections loaded perpendicular-to-grain was higher (average 15%) than that in connections loaded parallel-to-grain. The results of the lower capacity parallel-to-grain specimens were therefore selected in order to establish the connection properties required for the wall analyses.

A typical monotonic test curve is shown in Figure 5.2. The monotonic test and analysis results that were considered relevant to the analyses contained in this thesis are quoted in Table 5.1.

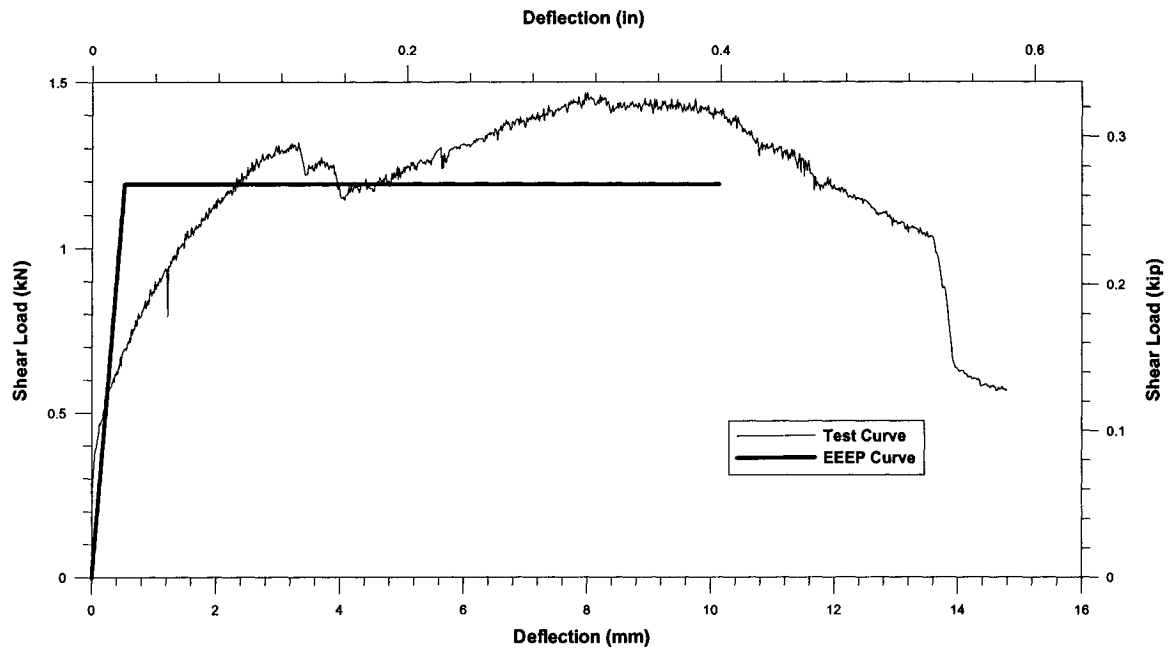


Figure 5.2 Typical Monotonic Test Curve for Connection Tests (Okasha, 2004)

Table 5.1 Parameters from Monotonic Connection Tests (Okasha, 2004)

ID <sup>1</sup>	TEST NO.	MAX. LOAD (kN)	EEEP YIELD LOAD (kN)	$k_e$ (0.4max load) (kN/mm)	$k_s$ (max load) (kN/mm)
CSP12.5-PR M <sup>2</sup>	38A,B,C	1.376	1.192	2.383	0.210
CSP25-PR M	7A,B,C	1.740	1.487	1.513	0.197
OSB12.5-PR M	34A,B,C	1.754	1.487	2.683	0.376
OSB25-PR M	16A,B,C	1.955	1.643	1.168	0.194
DFP25-PR M	25A,B,C	2.860	2.367	1.513	0.242

<sup>1</sup> ID is used in this thesis for convenience; <sup>2</sup> CSP represents the sheathing material, 12.5 represents the edge distance, PR represents the loading direction parallel to the sheathing grain, and M means monotonic tests.

A typical cyclic test curve is shown in Figure 5.3. The cyclic connection test and analysis results that were considered relevant to the modeling are quoted in Table 5.2.

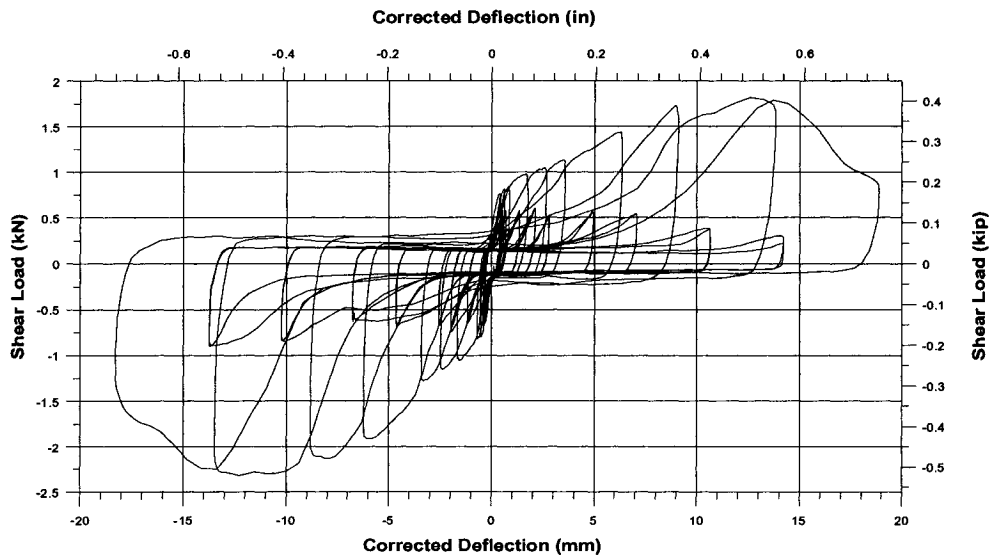


Figure 5.3 Typical Cyclic Test Curve for Connection Tests (Okasha, 2004)

Table 5.2 Parameters from Cyclic Connection Tests (Okasha, 2004)

ID	TEST NO.	MAX. LOAD (kN)	EEEP YIELD LOAD (kN)	$k_e$ (0.4max load) (kN/mm)	$k_s$ (max load) (kN/mm)
CSP25-PR C	7D,E,F	2.228	2.024	0.691	0.209
OSB25-PR C	16D,E,F	2.152	1.956	0.927	0.242
DFP25-PR C	25D,E	3.186	2.785	0.735	0.311

The load capacities listed in Table 5.2 for the cyclic tests are much higher than those in Table 5.1 for the monotonic tests. This is not in accordance with the full-scale test results listed in Chapter 3, in which the shear strength for cyclic tests are lower or close to those for the corresponding monotonic tests. There are two explanations for this phenomenon, one of which is that the loading speed for the cyclic tests was much faster than that used for the monotonic tests and the other is the large variance in wood panels, which may have a more noticeable effect when only single connections are tested. In

order to obtain a reasonable prediction of the wall behaviour, the load capacities for the monotonic tests were used. At the same time, the stiffness was taken as the average of the absolute values of the positive and negative results from the cyclic tests. This average value was used to take into account the possible change in connection stiffness as the load in the wall changed direction. Modified values are listed in Table 5.3.

Table 5.3 Modified Connection Parameters for Prediction of Cyclic Tests

ID	TEST NO.	MAX. LOAD (kN)	EEEE YIELD LOAD (kN)	$k_e$ (0.4max load) (kN/mm)	$k_s$ (max load) (kN/mm)
CSP25-PR C	7D,E,F	1.740	1.487	0.702	0.197
OSB25-PR C	16D,E,F	1.955	1.643	0.926	0.230
DFP25-PR C	25D,E	2.860	2.367	0.793	0.301

The parameters listed in Table 5.1 were adopted for the prediction of lateral resistance and deflection of full-scale shear walls under monotonic loading, and those in Table 5.3 were utilized for the shear walls under cyclic loading.

### 5.3 SIMPLIFIED STRENGTH MODEL

#### 5.3.1 ASSUMPTIONS

Based on the failure observations described in Chapter 3, the racking performance of the light gauge steel frame / wood panel shear walls was similar to that of the wood framed shear walls. When a shear wall is subjected to lateral loading, the steel frame distorted as a parallelogram in which the top and bottom tracks maintained a horizontal

position. The screws along the perimeter of a panel rotated about the flange of the studs; however, no obvious rotation of the screws connected to the interior studs was observed. The connections of the steel frame members are assumed to act as hinges, which means that no lateral resistance develops in the frame itself. The lateral load was resisted by the composite action of the wood panels and steel framing through their relative rotation. The external work applied to the shear wall was assumed to be absorbed by two components: the rotation of the screws and the shear deformation of the sheathing panels.

In order to develop a strength model which can be conveniently used to predict the shear capacity of a light gauge steel frame / wood panel shear wall, some secondary factors in the performance of a shear wall need to be neglected or simplified. The following assumptions are applied in the model, which are similar to what was proposed by Kallsner (1984) and Akerlund (1984):

- ❖ No deformation exists in the studs and tracks. These steel members are hinged to each other. The studs and tracks retain their original section shape and straightness. Although the studs or tracks may deform or buckle at the maximum load, under low or intermediate loads, this assumption can be considered reasonable.
- ❖ The panels are rigid in their own plane and adjacent panels have no contact or overlap with each other. The panels also have enough space to rotate without contact with the test support. In tests, and in engineering practice, a 1/8" vertical gap between the panels is specified to allow the expansion of the panels when subjected to elevated moisture content level. A gap of this size

also allows for the free rotation of the panels. The horizontal gaps provided by 1" thick spacers have the same function as the vertical ones.

- ❖ The load-displacement curves of the sheathing-to-frame connections are idealized as EEEP curves, bilinear elastic and plastic curves. Although the actual load-displacement curves show obvious nonlinear characteristics, the purpose of this thesis is to develop a simple analytical model.
- ❖ The relative displacements between the sheathing and framing are small compared with the panel size. The wood and steel also do not separate from each other during loading. Even at the maximum load, the relative rotation between the sheathing and the framing is very small. For studs, the maximum average relative rotation is  $0.899^\circ$  for monotonic tests; for tracks, the maximum average relative rotation is  $0.962^\circ$  for 4' x 8' and 8' x 8' walls and  $2.415^\circ$  for 2' x 8' walls in monotonic tests. Appendix VIII contains detailed information about the relative rotation in both monotonic and reversed cyclic tests.
- ❖ No relative displacement exists between the centre of the sheathing panel and the corresponding point on the steel frame, which means the origin of the assumed coordinate system on the panel and on the frame coincide during lateral displacements, as shown in Figure 5.1.
- ❖ No horizontal panel joints exist in the same storey, which means the height of the sheathing is almost equal to the height of the frame. Although in engineering practice, such joints are allowed or arranged, no tests with such configuration were included in this research.

- ❖ The shear wall is fully anchored onto the support or lower storey. No rotation of the bottom track occurs.
- ❖ The external work done by the racking loads is completely absorbed by the distortion of the sheathing-to-frame connections. This means the small amount of energy absorbed by the deformation of the steel framing members and the friction between a wall and its supports can be neglected.
- ❖ The sheathing-to-frame connections have the same capacity in all directions.

### **5.3.2 DETAILS OF THE SIMPLIFIED MODEL**

The displacement of the sheathing relative to the steel frame can be viewed in Figure 5.1. All of the studs have rotated about their bottom ends through the angle  $\gamma$  and the sheathing panel has rotated as a rigid body to an angle  $\phi$  relative to its original position. In the simplified model these two rotations, which are taken as independent variables, result in the force distribution of the sheathing-to-frame connections as shown in Figure 5.4.

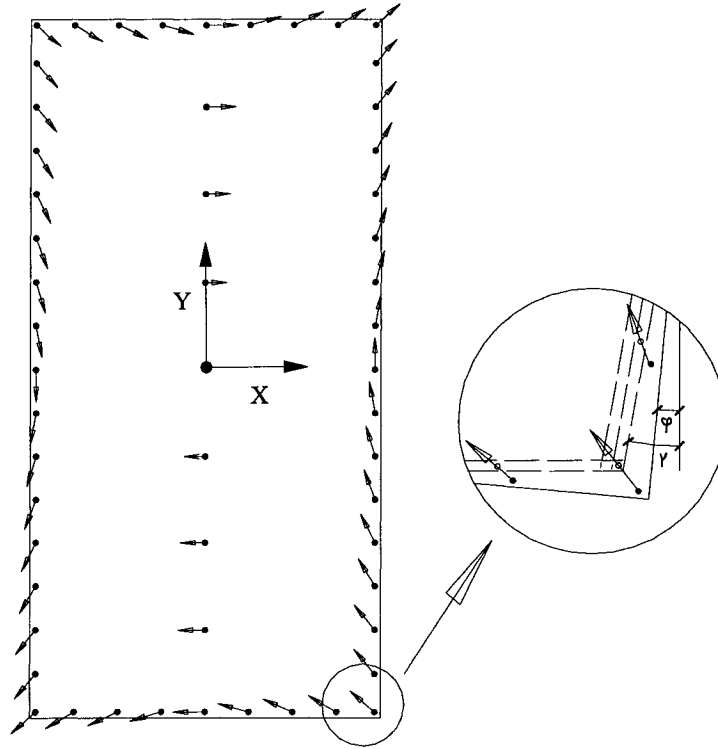


Figure 5.4 Assumed Force Distribution in Sheathing Connections

By defining the positive angles as clockwise, the relative displacements of the steel framing members to the panel at any point are given by the following:

$$\text{Along X, } u = u_{frame} - u_{panel} = (\gamma - \varphi) \cdot y \quad (5.2)$$

$$\text{Along Y, } v = v_{frame} - v_{panel} = \varphi \cdot x \quad (5.3)$$

The force components of each sheathing-to-frame connection can then be expressed as:

$$S_{xi,conn} = k \cdot u_i = k \cdot (\gamma - \varphi) \cdot y \quad (5.4)$$

$$S_{yi,conn} = k \cdot v_i = k \cdot \varphi \cdot x \quad (5.5)$$

where

$i$ : the number of the fasteners;

$k$ : the racking stiffness of sheathing-to-frame connections.

These two force components are symmetrically distributed on the panel, and hence satisfy the force and moment equilibrium conditions.

The potential energy due to the elastic deformations of all the sheathing-to-frame connections can be summed as:

$$U_1 = \sum_{i=1}^N \frac{1}{2} \cdot k \cdot (u_i^2 + v_i^2) \quad (5.6)$$

where, N is the total number of the sheathing-to-frame connections.

The potential energy due to the displacement  $\gamma \cdot H$  of the racking load F is determined by:

$$U_2 = -F \cdot \gamma \cdot H \quad (5.7)$$

The total potential energy of the wall system is the sum of  $U_1$  and  $U_2$ :

$$U = U_1 + U_2 = \frac{1}{2} k \sum_{i=1}^N \left\{ y_i^2 \cdot (\gamma - \varphi)^2 + x_i^2 \cdot (\varphi)^2 \right\} - F \cdot \gamma \cdot H \quad (5.8)$$

The force distribution must satisfy the minimum potential energy principle, which is expressed by the two partial derivations below which are set to equal to zero.

$$\frac{\partial U}{\partial \gamma} = 0 \quad \text{and} \quad \frac{\partial U}{\partial \varphi} = 0 \quad (5.9)$$

This results in:

$$k \cdot (\gamma - \varphi) \cdot \sum_{i=1}^N y_i^2 - F \cdot H = 0 \quad (5.10)$$

$$k \cdot [-(\gamma - \varphi) \cdot \sum_{i=1}^N y_i^2 + (\varphi) \cdot \sum_{i=1}^N x_i^2] = 0 \quad (5.11)$$

Solving Equation (5.10) ~ (5.11), the following solution is obtained:

$$\gamma = \frac{1}{k} \bullet F \bullet H \bullet \left( \frac{1}{\sum_{i=1}^N x_i^2} + \frac{1}{\sum_{i=1}^N y_i^2} \right) \quad (5.12)$$

$$\varphi = \frac{1}{k} \bullet F \bullet H \bullet \frac{1}{\sum_{i=1}^N x_i^2} \quad (5.13)$$

It is now possible to determine the force components by substituting Equations (5.12) and (5.13) into Equations (5.4) and (5.5), respectively.

$$S_{x_i,conn} = F \bullet H \bullet \frac{y_i}{\sum_{i=1}^N y_i^2} \quad (5.14)$$

$$S_{y_i,conn} = F \bullet H \bullet \frac{x_i}{\sum_{i=1}^N x_i^2} \quad (5.15)$$

The resultant connection force is then given by:

$$S_{i,conn} = \sqrt{S_{x_i,conn}^2 + S_{y_i,conn}^2} = F \bullet H \bullet \sqrt{\left( \frac{x_i}{\sum_{i=1}^N x_i^2} \right)^2 + \left( \frac{y_i}{\sum_{i=1}^N y_i^2} \right)^2} \quad (5.16)$$

The maximum connection force occurs at the four corners where  $x_i$  and  $y_i$  reach their highest values:

$$S_{max,conn} = F \bullet H \bullet \sqrt{\left( \frac{x_{max}}{\sum_{i=1}^N x_i^2} \right)^2 + \left( \frac{y_{max}}{\sum_{i=1}^N y_i^2} \right)^2} \quad (5.17)$$

A wall is considered to have failed when the maximum connection force reaches its design capacity, which is quoted as  $S_{y,conn}$ . Therefore, the shear capacity of the wall

segment,  $S_{y,wall}$ , which is defined as the product of  $S_y$  (Section 3.7) and the wall length  $L$ , can be expressed as:

$$S_{y,wall} = \frac{S_{y,conn}}{H \cdot \sqrt{\left(\frac{x_{max}}{\sum_{i=1}^N x_i^2}\right)^2 + \left(\frac{y_{max}}{\sum_{i=1}^N y_i^2}\right)^2}} \quad (5.18)$$

Equation (5.18) shows that the shear capacity is dependent on two factors, the first being the wall configuration including the connection pattern and the second the shear capacity per connection. Equations (5.12) ~ (5.18) were originally presented by Kallsner and Lam (1995) in their elastic model for wood framed shear walls.

If the assumption that the sheathing panels are rigid is removed, and the uniform shear strain of the sheathing is expressed as  $\gamma_s$ , three unknown variables now exist. Since  $\gamma_s$  is usually small, it can be taken as another independent variable. The potential energy due to the shear deformation of the sheathing panel is then given by:

$$U_3 = \frac{1}{2} \cdot G \cdot \gamma_s^2 \cdot L \cdot H \cdot t \quad (5.19)$$

where:

$G$  is the shear modulus of the sheathing;

$t$  is the thickness of the sheathing;

The displacement of the wall due to the shear deformation of the sheathing can be taken as  $\gamma_s \cdot H$ . The potential energy due to  $\gamma_s \cdot H$  can be expressed as:

$$U_4 = -F \cdot \gamma_s \cdot H \quad (5.20)$$

With the same procedure as followed above Equation (5.13) becomes:

$$\varphi = \frac{1}{k} \cdot F \cdot H \cdot \frac{1}{\sum_{i=1}^N x_i^2} - \frac{F \cdot H}{G \cdot L \cdot t} \quad (5.13a)$$

and  $\gamma_s$  is expressed as:

$$\gamma_s = \frac{F \cdot H}{G \cdot L \cdot t} \quad (5.21)$$

Equations (5.12) ~ (5.18) remain as shown previously.

In the development of the analytical method up to this point, the load capacity of the studs and tracks has not been considered. In tests and engineering practice the top tracks are connected to the load beam or upper floor elements with screws or shear anchors, which are placed reasonably close in order to transfer the lateral load uniformly. The bottom tracks are similarly fastened onto the supporting or lower floor elements, and the hold-downs are installed to constrain the uplift of the ends of the tracks (Bateman, 1996). Hence, it is assumed that the tracks have enough capacity to resist the applied loads, and as such they can be taken as rigid elements.

The end studs are subject to axial compression or tension force under applied racking loads. Lateral loads are not considered to produce axial force in the studs on the centreline of the panels or at the interior panel joints. At the same time, all the studs need to support the gravity loads on the wall and out-of-plane loads, e.g. wind pressure normal to the surface of the wall. In this model, only the axial force in the end studs is considered. At this stage gravity loads on the wall were not accounted for in the analytical model because no gravity loads were applied in the tests related to this thesis.

The lateral resistance of a shear wall is then determined as the minimum of that obtained from Equation (5.18) and the resistance which is related to the axial load

capacity of the end studs. The axial load capacity of an end chord is the minimum of the capacity of a hold-down connection, the capacity of the back-to-back stud connections, as well as tension and compression capacity of the stud (or studs) calculated according to the *North American Specification for the Design of Cold-formed Steel Structural Members* (CSA, 2001). The capacity of the back-to-back studs is taken as 62.0 kN (Appendix V).

### **5.3.3 COMPARISON OF SHEAR WALL CAPACITY BETWEEN TEST RESULTS AND ANALYTICAL APPROACHES**

Comparisons between the shear wall capacity measured during the laboratory testing and that predicted using the analytical models are performed to validate the accuracy of the model introduced in Section 5.3.2. The intent is for the model to predict the shear wall capacity  $S_{y,wall}$  at the level of the yield shear strength,  $S_y$  (Section 3.7). At the same time, in order to verify that Kallsner's & Lam's elastic model is the most reasonable and effective solution to predict the shear wall capacity of light gauge steel frame / wood panel shear walls, other models that are based on different assumptions and which have been applied in the prediction of wood frame shear walls are also contained in the comparisons. These models, which are reviewed in Chapter 2, include Kallsner's & Lam's lower and upper plastic models, as well as models by Easley and McCutcheon.

In order to find the best matching connection test condition to predict the shear capacity accurately, six cases were considered in each model for monotonic loading, which are EEEP12.5, EEEP25, Max.load12.5&ke, Max.load12.5&ks, Max.load25&ke and Max.load25&ks; and three for cyclic loading, which are EEEP25, Max.load25&ke

and Max.load25&ks; and three for cyclic loading, which are EEEP25, Max.load25&ke and Max.load25&ks. Based on the preliminary evaluation of the predictions of monotonic tests, the three cases with edge distance 12.5 mm are not included in the predictions of cyclic tests. For each of these nine cases the relevant test parameters can be found in Tables 5.1 and 5.3. The shear capacity per connection was represented by the EEEP yield capacity or the maximum shear load, and the stiffness was represented by the EEEP elastic stiffness  $k_e$  or the secant stiffness  $k_s$ . At the same time, two edge distances (namely 12.5 mm and 25 mm) were considered in order to find the effect due to the edge distance. All of these nine cases were considered in each model because it was not known which ones would best represent the behaviour of the connection in the prediction of the performance of a full-size shear wall. The most appropriate case to use, in terms of connection characteristics, is determined through a comparison of the test to predicted results for the shear wall specimens.

In each case, the five models were applied in the analysis of the 32 wall configurations adopted for the comparison. This included both monotonic and cyclic tests, which represented 103 of the total 109 full-scale tests in Branston et al. (2004). Tests referred from Branston (2004) and Boudreault (2004) are listed in Table 5.4. The prediction using each model under each case was then compared with the average shear capacity  $S_{y,wall}$  of the tested full-scale walls with the matching wall configuration. This average shear capacity was obtained from the three or more tests that were performed for each configuration. Due to the large amount of the data, only the combined ratio of the shear capacity from all full-scale tests to the prediction with each model is listed in Table

5.5. Appendix VI and VII contain the details of the comparison in tabular and graphical format, respectively.

Table 5.4 Description of Wall Specimens Used in Analytical Comparison  
( Branston (2004) and Boudreault (2004) )

Specimen ID	Loading Protocol	Length of Wall (ft)	Height of Wall (ft)	Panel Type	Thickness of Panel (mm)	Fastener Schedule (in.)
1 – A,B,C	Monotonic	4	8	CSP	12.5	4/12
4 – A,B,C	CUREE	4	8	CSP	12.5	4/12
5 – A,B,C,D	Monotonic	4	8	DFP	12.5	4/12
6 – A,B,C	CUREE	4	8	DFP	12.5	4/12
7 – A,B,C	Monotonic	4	8	CSP	12.5	6/12
8 – A,B,C	CUREE	4	8	CSP	12.5	6/12
9 – A,B,C	Monotonic	4	8	CSP	12.5	3/12
10 – A,B,C	CUREE	4	8	CSP	12.5	3/12
11 – A,B,C	Monotonic	4	8	DFP	12.5	6/12
12 – A,B,C	CUREE	4	8	DFP	12.5	6/12
13 – A,B,C	Monotonic <sup>5</sup>	4	8	DFP	12.5	3/12
14 – A,B,C,D	CUREE	4	8	DFP	12.5	3/12
21 – A,B,C	Monotonic	4	8	OSB	11	6/12
22 – A,B,C	CUREE	4	8	OSB	11	6/12
23 – A,B,C	Monotonic	4	8	OSB	11	4/12
24 – A,B,C	CUREE	4	8	OSB	11	4/12
25 – A,B,C	Monotonic	4	8	OSB	11	3/12
26 – A,B,C	CUREE	4	8	OSB	11	3/12

See Table 3.1 for a description of the parameters.

Table 5.5 Combined Ratios of Full-Scale Shear Wall Test to Predicted Shear Capacity

Monotonic Loading Cases	Kallsner's & Lam's Elastic Model			Kallsner's & Lam's Lower Plastic Model			Kallsner's & Lam's Upper Plastic Model			Easley's Model			McCutcheon's Model		
	Ratio	SD	COV	Ratio	SD	COV	Ratio	SD	COV	Ratio	SD	COV	Ratio	SD	COV
EEEE12.5	1.270	0.181	0.143	1.232	0.178	0.145	1.091	0.126	0.116	1.646	0.210	0.128	1.235	0.196	0.158
EEEE25	1.050	0.122	0.116	1.022	0.120	0.117	0.927	0.098	0.106	1.336	0.152	0.114	1.025	0.132	0.129
Max.load12.5&ke	1.093	0.162	0.148	1.063	0.157	0.148	0.950	0.109	0.114	1.415	0.190	0.134	1.065	0.173	0.162
Max.load12.5&ks	1.093	0.162	0.148	1.063	0.157	0.148	0.950	0.109	0.114	1.415	0.190	0.134	1.065	0.173	0.162
Max.load25&ke	0.918	0.117	0.128	0.900	0.119	0.133	0.835	0.129	0.155	1.142	0.127	0.112	0.902	0.127	0.140
Max.load25&ks	0.918	0.117	0.128	0.900	0.119	0.133	0.835	0.129	0.155	1.142	0.127	0.112	0.902	0.127	0.140
Cyclic Loading Cases	Kallsner's & Lam's Elastic Model			Kallsner's & Lam's Lower Plastic Model			Kallsner's & Lam's Upper Plastic Model			Easley's Model			McCutcheon's Model		
	Ratio	SD	COV	Ratio	SD	COV	Ratio	SD	COV	Ratio	SD	COV	Ratio	SD	COV
EEEE25	1.012	0.129	0.127	0.985	0.125	0.126	0.893	0.107	0.120	1.288	0.162	0.126	0.988	0.135	0.136
Max.load25&ke	0.885	0.122	0.137	0.868	0.123	0.141	0.806	0.138	0.171	1.102	0.141	0.128	0.869	0.128	0.148
Max.load25&ks	0.885	0.122	0.137	0.868	0.123	0.141	0.806	0.138	0.171	1.102	0.141	0.128	0.869	0.128	0.148

Note: Each ratio and the associated statistical information represent the 16 wall configurations and a total of 103 individual shear wall test specimens.

From Table 5.5, the following observations can be made:

- ❖ Predictions in the case of EEEP12.5 always underestimate the load capacity of the shear walls, except for Kallsner's & Lam's upper plastic model, which gave results close to the values from the full-scale tests. The ratio of test to predicted shear resistance is between 1.091 and 1.646 for monotonic wall specimens. Due to the unsatisfactory predictions of monotonic tests, the cases with edge distance 12.5 mm are not included in the predictions of cyclic tests. The predictions using Max.load25 always overestimate the load capacity of the shear walls except for in the case of Easley's model. The test to predicted ratio falls between 0.835 and 0.918 for specimens tested monotonically, and between 0.806 and 0.885 for those walls tested cyclically. An exception exists for Easley's model, which gave a test to predicted result of 1.142 and 1.102 for monotonic and cyclic tests, respectively.
- ❖ For monotonic loading cases, the prediction with EEEP25 and Max.load12.5 both gives good agreement except for those with Easley's model. The ratio with EEEP25 is between 0.927 and 1.050, and in the case of Easley's model 1.336; the ratio with Max.load12.5 is between 0.950 and 1.093, except for 1.415 for Easley's model.
- ❖ For cyclic loading cases, the prediction with EEEP25 shows good consistency with the test results, except for that with Easley's model. The ratio is between 0.893 and 1.012, and for Easley's model 1.288.
- ❖ The predictions provided by McCutcheon's model and Kallsner's & Lam's lower plastic model are very close to those given by Kallsner's & Lam's

elastic model. Kallsner's & Lam's upper plastic model gives a higher prediction than other models, while the prediction from Ealsey's model is much lower. As an example, Table 5.6 lists  $S_{y,wall}$  predicted by these five models and the ratio based on Kallsner's & Lam's elastic model. The average ratios for monotonic loading cases with EEEP25 are both 1.03 for McCutcheon's model and for Kallsner's & Lam's lower plastic model. The same conclusion can be obtained in cyclic loading cases, since the connection shear capacities in Table 5.3 adopt the same values as in Table 5.1 for monotonic loading.

- ❖ McCutcheon's model places a strict limitation in the assumption, which requires that the screws on the panel corners must rotate along the diagonal lines. This behaviour was not typically observed during testing. As for Kallsner's & Lam's lower plastic model, it requires the screw spacing is uniform along the panel edges and cannot be used to predict the deflection of shear walls, which will be discussed in the next section. So Kallsner's & Lam's elastic model with the connection shear capacity from the case of EEEP25 is recommended as the selected model to predict the shear capacity of light gauge steel frame / wood panel shear walls.

Table 5.6  
Comparisons between Different Models in Predicting  $S_{y,wall}$  for Tests with EEEP25

ID	$S_{y,wall}$ (kN)	$S_{y,wall}$ (kN)	$S_{y,wall}$ (kN)	$S_{y,wall}$ (kN)	$S_{y,wall}$ (kN)
	with Kallsner's & Lam's Elastic Model	with Kallsner's & Lam's Lower Plastic Model	with Kallsner's & Lam's Upper Plastic Model	with McCutcheon's Model	with Easley's Model
2x8 CSP 6"/12" M/C	5.76	5.95	6.32	6.14	4.19
Ratio	1.00	1.03	1.10	1.07	0.726
2x8 CSP 4"/12" M/C	8.61	8.92	9.46	9.16	6.52
Ratio	1.00	1.04	1.10	1.06	0.757
2x8 OSB 6"/12" M/C	6.37	6.57	6.98	6.78	4.62
Ratio	1.00	1.03	1.10	1.07	0.726
2x8 OSB 4"/12" M/C	9.52	9.86	10.5	10.1	7.20
Ratio	1.00	1.04	1.10	1.06	0.757
4x8 CSP 6"/12" M/C	11.6	11.9	13.9	11.8	9.02
Ratio	1.00	1.02	1.20	1.01	0.776
4x8 CSP 4"/12" M/C	17.3	17.8	20.6	17.6	13.6
Ratio	1.00	1.03	1.19	1.02	0.785
4x8 CSP 3"/12" M/C	23.0	23.8	27.3	23.4	18.1
Ratio	1.00	1.04	1.19	1.02	0.788
4x8 DFP 6"/12" M/C	18.5	18.9	22.1	18.7	14.4
Ratio	1.00	1.02	1.20	1.01	0.776
4x8 DFP 4"/12" M/C	27.5	28.4	32.8	28.0	21.6
Ratio	1.00	1.03	1.19	1.02	0.785
4x8 DFP 3"/12" M/C	36.6	37.9	43.4	37.3	28.8
Ratio	1.00	1.04	1.19	1.02	0.788
4x8 OSB 6"/12" M/C	12.8	13.1	15.4	13.0	10.0
Ratio	1.00	1.02	1.20	1.01	0.776
4x8 OSB 4"/12" M/C	19.1	19.7	22.7	19.4	15.0
Ratio	1.00	1.03	1.19	1.02	0.785
4x8 OSB 3"/12" M/C	25.4	26.3	30.1	25.9	20.0
Ratio	1.00	1.04	1.19	1.02	0.788
8x8 CSP 6"/12" M/C	23.2	23.8	27.8	23.5	18.0
Ratio	1.00	1.02	1.20	1.01	0.776
8x8 CSP 4"/12" M/C	34.6	35.7	41.2	35.2	27.2
Ratio	1.00	1.03	1.19	1.02	0.785
8x8 CSP 3"/12" M/C	45.9	47.6	54.5	46.9	36.2
Ratio	1.00	1.04	1.19	1.02	0.788
<b>Average Ratio</b>	<b>1.00</b>	<b>1.03</b>	<b>1.17</b>	<b>1.03</b>	<b>0.773</b>
Standard Deviation	0.0000	0.00469	0.0407	0.0211	0.0199
COV	0.0000	0.00455	0.0349	0.0205	0.0258

## 5.4 SIMPLIFIED DEFLECTION MODEL

### 5.4.1 INTRODUCTION

In the simplified deflection model, the same assumptions as adopted in the simplified strength model are made, except that the sheathing panels are not assumed to be rigid. In contrast, the sheathing panels are taken as isotropic and deformable materials, and hence the shear strain can be assumed to be uniform over a whole panel. The purpose of the deflection model is to predict the deflection of the wall  $\Delta_y$  corresponding to the yield strength  $S_y$  (or yield load capacity  $S_{y,wall}$ ).

### 5.4.2 DETAILS OF THE SIMPLIFIED MODEL

The total displacement of the steel frame can be determined by considering the rotation of the frame due to  $\gamma$  and  $\gamma_s$ , and the bottom slippage on the support. Equation (5.1) can be rewritten as:

$$\Delta_{walltop} = \frac{1}{k} FH^2 \cdot \left( \frac{1}{\sum_{i=1}^N x_i^2} + \frac{1}{\sum_{i=1}^N y_i^2} \right) + \frac{F}{GLt} + \left[ \left( \frac{\Delta_{baseslip1} + \Delta_{baseslip2}}{2} \right) \right] + \left[ (\Delta_{uplift1} - \Delta_{uplift2}) \times \frac{H}{L} \right] \quad (5.22)$$

The final two components in Equation (5.22) can be affected by many factors, such as the type of frame-to-support connections/anchorage, the shear modulus of these connections, the friction between a wall and its support, extension and slippage of the hold-down connections, and the deformation of the steel frame. Although these factors have an

impact on the behaviour of a tested wall, their inclusion would overly complicate the model, and hence they were not considered. Therefore, the deflection model used herein to predict the net lateral deflection, which was defined in Equation (5.1), was based on the following equation:

$$\Delta_{net} = \frac{1}{k} FH^2 \cdot \left( \frac{1}{\sum_{i=1}^N x_i^2} + \frac{1}{\sum_{i=1}^N y_i^2} \right) + \frac{F}{GLt} \quad (5.23)$$

which is similar to that presented by Kallsner & Lam (1995) for predicting the deflection of wood framed shear walls.

#### **5.4.3 COMPARISON OF SHEAR WALL DEFLECTION BETWEEN TEST RESULTS AND ANALYTICAL APPROACHES**

As described in Section 5.3.3, comparisons between the deflections measured during testing and the predictions made with the analytical approaches are performed to verify the effectiveness of the model introduced above. Meanwhile, in order to verify that Kallsner's & Lam's elastic model is more appropriate for the prediction of shear wall deflection than other models, Easley's model and McCutcheon's model are included in the comparison.

The same nine cases of connection properties, as described in the comparison of strength models, are incorporated in the deflection models. Each combination of the listed deflection models and loading cases included all the sixteen wall configurations. Only the combined ratio of the full-scale test to the predicted deflection in each combination is listed in Table 5.7. More detailed information is provided in Appendix VI and VII.

Table 5.7 Combined Ratios of Full-Scale Shear Wall Test to Predicted Deflection

Monotonic Loading Cases	Kallsner's & Lam's Elastic Model			Easley's Model			McCutcheon's Model		
	Ratio	SD	COV	Ratio	SD	COV	Ratio	SD	COV
EEEE12.5	2.236	0.380	0.170	3.150	0.521	0.166	2.205	0.365	0.165
EEEE25	1.441	0.303	0.210	2.059	0.385	0.187	1.432	0.300	0.209
Max.load12.5&ke	1.923	0.339	0.176	2.709	0.464	0.171	1.899	0.324	0.171
Max.load12.5&ks	0.431	0.075	0.174	0.677	0.122	0.181	0.432	0.075	0.173
Max.load25&ke	1.263	0.301	0.238	1.763	0.339	0.192	1.261	0.297	0.235
Max.load25&ks	0.307	0.096	0.313	0.467	0.131	0.281	0.309	0.096	0.312
Cyclic Loading Cases	Kallsner's & Lam's Elastic Model			Easley's Model			McCutcheon's Model		
	Ratio	SD	COV	Ratio	SD	COV	Ratio	SD	COV
EEEE25	0.886	0.124	0.139	1.311	0.144	0.110	0.884	0.124	0.140
Max.load25&ke	0.775	0.133	0.171	1.123	0.143	0.128	0.778	0.134	0.172
Max.load25&ks	0.293	0.092	0.313	0.445	0.116	0.260	0.295	0.093	0.313

Note: Each ratio and the associated statistical information represent the 16 wall configurations and a total of 103 individual shear wall test specimens.

Based on the data in Table 5.7, the observations are summarized as follows:

- ❖ For the most part, the prediction of lateral deflections is not as accurate as that of the lateral shear wall resistance. This can be attributed to the strong nonlinear behaviour of the sheathing-to-frame connections (Figures 5.2 and 5.3), the nonlinearity of the wood panels and the effect of hold-down connections, the combination of which causes the nonlinear performance of the shear walls (Figures 3.7-3.9).
- ❖ The predictions based on the initial stiffness  $k_e$  of a connection always underestimate the lateral deflection under monotonic loading. The ratio of test to predicted deflection is 2.205 ~ 3.150 for EEE12.5, 1.432 ~ 2.059 for EEE25, 1.899 ~ 2.709 for Max.Load12.5 and 1.261 ~ 1.763 for Max.Load25.

In contrast, the predictions that incorporate  $k_s$  overestimate the wall deflection under monotonic loading, as indicated by the test to predicted ratios which range between 0.307 and 0.677.

- ❖ In the case of cyclic loading, the prediction with EEEP25 gives good agreement in both Kallsner's & Lam's model and McCutcheon's model. The average test to predicted ratios are 0.886 and 0.884, respectively. However, Easley's model only provides a good prediction in the case where the Max.Load25 and  $k_e$  are utilized. The prediction with  $k_s$  overestimates the wall deflection by a significant amount, as can be seen by the range of the test to predicted deflection ratio (0.293 ~ 0.445).
- ❖ The predictions with McCutcheon's model are very close to that given by Kallsner's & Lam's elastic model. The average ratio is 1.008 for monotonic loading cases with EEEP25 and 1.004 for corresponding cyclic loading cases. The prediction from Easley's model is much lower than the other two models. Table 5.8 shows the predictions and relative ratios between these three deflection models under monotonic loading in EEEP25 case and Table 5.9 for cyclic loading in the case of EEEP25.
- ❖ As discussed in Section 5.3.3, the assumption in McCutcheon's model that the screws on the panel corners must rotate along the diagonal lines, is not always the truth in this series of tests. On the other hand, Kallsner's & Lam's elastic model does not put similar strict limitation in the prediction, so this model is more reasonable in predicting the lateral deflection of a light gauge steel

frame / wood panel shear wall. At the same time, the connection parameters in the case of EEEP25 are recommended as the input data.

Table 5.8 The Relative Ratio of the Net Lateral Deflections Using Different Models with EEEP25 (Monotonic)

ID	Predicted Deflection (mm) with Kallsner's & Lam's Model	Predicted Deflection (mm) with McCutcheon' Model	Predicted Deflection (mm) with Ealsey's Model
2x8 CSP 6"/12" M	12.5	12.6	8.48
Ratio	1.000	1.013	0.679
2x8 CSP 4"/12" M	14.6	14.8	10.4
Ratio	1.000	1.020	0.715
2x8 OSB 6"/12" M	14.5	14.5	9.65
Ratio	1.000	1.001	0.668
2x8 OSB 4"/12" M	15.7	15.8	11.0
Ratio	1.000	1.006	0.701
4x8 CSP 6"/12" M	8.58	8.62	5.82
Ratio	1.000	1.005	0.679
4x8 CSP 4"/12" M	10.6	10.7	7.46
Ratio	1.000	1.010	0.704
4x8 CSP 3"/12" M	12.6	12.8	9.06
Ratio	1.000	1.013	0.719
4x8 DFP 6"/12" M	10.7	10.8	7.00
Ratio	1.000	1.003	0.652
4x8 DFP 4"/12" M	12.5	12.6	8.45
Ratio	1.000	1.007	0.676
4x8 DFP 3"/12" M	14.3	14.4	9.86
Ratio	1.000	1.010	0.691
4x8 OSB 6"/12" M	8.91	8.93	5.72
Ratio	1.000	1.002	0.642
4x8 OSB 4"/12" M	10.1	10.2	6.74
Ratio	1.000	1.006	0.664
4x8 OSB 3"/12" M	11.4	11.5	7.72
Ratio	1.000	1.009	0.678
8x8 CSP 6"/12" M	8.58	8.62	5.82
Ratio	1.000	1.005	0.679
8x8 CSP 4"/12" M	10.6	10.7	7.46
Ratio	1.000	1.010	0.704
8x8 CSP 3"/12" M	12.6	12.8	9.06
Ratio	1.000	1.013	0.719
<b>Average Ratio</b>	<b>1.000</b>	<b>1.008</b>	<b>0.685</b>
Standard Deviation	0.0000	0.0048	0.0225
COV	0.0000	0.0048	0.0329

Table 5.9 The Relative Ratio of the Net Lateral Deflections  
Using Different Models with EEEP25 (Reversed Cyclic)

ID	Predicted Deflection (mm) with Kallsner's & Lam's Model	Predicted Deflection (mm) with McCutcheon' Model	Predicted Deflection (mm) with Ealsey's Model
2x8 CSP 6"/12" C	22.1	22.1	14.76
Ratio	1.000	1.002	0.669
2x8 CSP 4"/12" C	24.1	24.3	17.0
Ratio	1.000	1.007	0.702
2x8 OSB 6"/12" C	17.6	17.5	11.69
Ratio	1.000	0.998	0.666
2x8 OSB 4"/12" C	18.8	18.9	13.1
Ratio	1.000	1.002	0.698
4x8 CSP 6"/12" C	13.72	13.75	8.84
Ratio	1.000	1.002	0.645
4x8 CSP 4"/12" C	15.7	15.8	10.50
Ratio	1.000	1.006	0.667
4x8 CSP 3"/12" C	17.7	17.9	12.10
Ratio	1.000	1.009	0.682
4x8 DFP 6"/12" C	17.2	17.2	10.78
Ratio	1.000	1.001	0.628
4x8 DFP 4"/12" C	18.9	19.0	12.25
Ratio	1.000	1.004	0.647
4x8 DFP 3"/12" C	20.7	20.8	13.66
Ratio	1.000	1.007	0.660
4x8 OSB 6"/12" C	10.58	10.59	6.70
Ratio	1.000	1.001	0.633
4x8 OSB 4"/12" C	11.8	11.9	7.72
Ratio	1.000	1.005	0.654
4x8 OSB 3"/12" C	13.0	13.1	8.70
Ratio	1.000	1.008	0.667
8x8 CSP 6"/12" C	13.72	13.75	8.84
Ratio	1.000	1.002	0.645
8x8 CSP 4"/12" C	15.7	15.8	10.50
Ratio	1.000	1.006	0.667
8x8 CSP 3"/12" C	17.7	17.9	12.10
Ratio	1.000	1.009	0.682
<b>Average Ratio</b>	<b>1.000</b>	<b>1.004</b>	<b>0.663</b>
Standard Deviation	0.0000	0.0031	0.0205
COV	0.0000	0.0031	0.0309

## 5.5 DISCUSSION

One of the objectives of this thesis was to recommend an analytical method with which a prediction of light gauge steel frame / wood panel shear wall behaviour could be

made. A comparison of the test results with the predicted shear capacity and deflections allowed for the following conclusions / discussions to be presented.

1. The yield strength and initial stiffness per connection with 25 mm edge distance can be relied on to predict the yield lateral resistance and deflection of full-scale shear walls, if both the connection and full-scale test results are analyzed using the EEEP methods.

2. Comparisons of the test to predicted results show that Kallsner's & Lam's elastic strength model has excellent ability to predict the lateral resistance. Although McCutcheon's model also gives very close results, it places a strict limitation on the assumption which requires that the screws on the panel corners must rotate along the diagonal lines. This behaviour was not typically observed during testing.

3. The deflection predictions using Kallsner's & Lam's elastic model also show satisfactory agreement with the test results, especially for the cyclic loading cases. For monotonic tests, the deviation can be attributed to the nonlinearity of the connection and wood panels, as well as the effect of tightening the hold-down connections. The high initial stiffness measured in connection tests, due to the faster loading speed, causes the analytical methods to underestimate the deflection of shear walls.

4. In order to better predict the performance of the full-scale shear walls, the conditions for connection tests need to be kept consistent with those in full-scale tests, such as the loading speed and edge distance.

Based on the observation (Sections 5.3 and 5.4) and discussion above, the elastic models, presented by Kallsner & Lam (1995) to predict the lateral resistance and deflection of wood framed shear walls, are recommended to predict the lateral resistance

and deflection of light gauge steel frame / wood panel shear walls under monotonic and cyclic loading. At the same time, the connection shear capacity ( $S_{y, conn}$ ) and initial stiffness ( $k_e$ ) in the case of EEEP25 are also recommended as the input connection parameters in both the strength and deflection models.

## CHAPTER 6 SUMMARY AND CONCLUSIONS

### 6.1 SUMMARY

A total of 46 full-scale light gauge steel frame / wood panel shear wall tests were conducted for and described in this thesis. Design strength and stiffness values were determined for these test walls following the Equivalent Energy Elastic-Plastic (EEEP) data analysis approach. A comparison involving the behavioural properties of the 109 shear walls, tested by Branston (2004), Boudreault (2004) and the author, with different configurations and loading protocols was presented in detail. The variation in the ultimate shear strength, shear yield strength, stiffness, ductility and energy dissipation ability was documented with respect to the sheathing fastener spacing, sheathing type, wall aspect ratio and loading protocol.

A detailed literature review that covers the use of analytical models to predict the shear strength and deflection of wood framed shear walls was also presented. A number of analytical models were evaluated in their ability to predict the light gauge steel frame / wood panel shear wall test specimen results. Based on this, a simple analytical model is then recommended for design. As well, the failure of a shear wall due to the compression chord buckling is included both in the evaluation of the shear wall performance and in the analytical prediction.

## 6.2 PERFORMANCE OF LIGHTGAUGE STEEL FRAME / WOOD PANEL SHEAR WALLS

Based on the evaluation of the performance of all 109 monotonic and reversed cyclic full-scale wall tests presented in detail in Chapter 4, it can be concluded that light gauge steel frame / wood panel shear walls show good lateral resistance and ductility during racking tests. The performance of this type of structure is characterized by the following comments.

- ❖ The shear walls show a strong nonlinear load-deflection behaviour, both in monotonic and cyclic testing. This may be explained by the nonlinearity of the sheathing-to-steel framing connections and wood panels under shear loading.

- ❖ The ultimate shear strength  $S_u$  is approximately proportional to the number of perimeter screws per panel for walls with the same aspect ratio and same sheathing type, both in monotonic tests and reversed cyclic tests.  $S_u$  for walls with 11 mm OSB panels is typically very close to that measured for the matching 12.5 mm CSP walls. Shear walls with 12.5mm DFP panels showed an elevated resistance of approximately 25% compared with the matching CSP walls. If perimeter screw spacing and sheathing type stay unchanged,  $S_u$  is reasonably consistent for walls with different aspect ratios both in monotonic tests and reversed cyclic tests.  $S_u$  values measured for the cyclic tests are generally less (average 8%) than those for monotonic tests with the same wall configuration.

- ❖ The yield shear strength,  $S_y$ , of a wall increases approximately linearly with the number of perimeter screws per panel both in monotonic tests and reversed cyclic

tests if the aspect ratio and sheathing type stay unchanged.  $S_y$  for the 11mm OSB walls was found to be consistently higher than that measured for the matching 12.5mm CSP walls. The walls with 12.5mm DFP sheathing possess a higher (about 25%) shear yield capacity compared with the matching CSP walls.  $S_y$  increases by approximately 10% with each change in wall length (2', 4' and 8'). The reversed cycling loading protocol has no obvious effect on  $S_y$ . As well, the unloading phases in the monotonic protocol do not create a notable difference in the measured wall properties.

❖ The idealized initial elastic stiffness,  $K_e$ , increased with the decrease of screw spacing; however, this increase is nonlinear.  $K_e$  for the 11mm OSB walls is much higher than that determined for the 12.5mm CSP and 12.5mm DFP walls with the same wall configuration. In addition, the DFP walls exhibited a higher initial stiffness than the CSP walls.  $K_e$  increases with an increase of the wall length for both monotonic and reversed cyclic tests if the same screw pattern is used.  $K_e$  values for cyclic tests are generally higher than those measured for the monotonic tests with the same wall configuration.

❖ The ductility,  $\mu$ , decreases along with the decrease of the panel edge screw spacing distance. The 11mm OSB walls possess the highest  $\mu$  values and the 12.5mm CSP walls show a greater ductility compared with the matching 12.5mm DFP walls. The ductility of 2' walls was found to be much less than that of the matching 4' and 8' walls; however, the values for 4' and 8' CSP walls with same screw spacing are close to each other. The ductility measured for the cyclic tests are generally higher than those recorded for the monotonic tests with the same wall configuration.

❖ The real energy dissipation,  $E_r$ , is approximately proportional to the number of perimeter screws, however, the normalized energy,  $E_r$  per screw remains relatively consistent regardless of the connection pattern. The energy under the backbone curve,  $E_b$ , increases with the decrease of the screw spacing for walls with the same width, however, when failure occurs due to buckling of the chord studs or when the drift limit must be considered in the evaluation of results the value of  $E_b$  will reduce to a much lower level. The real energy,  $E_r$ , dissipated by the 11mm OSB walls is less than that dissipated by the 12.5mm CSP walls, and the 12.5mm DFP walls have larger capacity to dissipate the energy than both the CSP and OSB walls. The energy under the backbone curve,  $E_b$ , shows similar trends as noted for  $E_r$ , except that the OSB walls have a higher energy dissipation ability for both the monotonic and cyclic test specimens.

❖ When comparing walls with the same screw pattern, the real energy dissipation,  $E_r$ , generally increases with the wall length, however, the increase is not proportional to the ratio of wall length. The energy under the backbone curve,  $E_b$ , is approximately proportional to the ratio of wall length if the same screw pattern is specified. The real energy,  $E_r$ , in cyclic tests is significantly higher than that in monotonic tests due to the repeated displacements in the loading protocol; however, the energy under the backbone curve,  $E_b$ , in cyclic tests can be taken as the same level as in monotonic tests.

❖ As for wall deflection in plane, the 2' walls exhibited approximately twice as much flexibility as the matching 4' or 8' walls both in monotonic and cyclic tests. Hence, the lateral resistance of a 2' wall is based on the drift limit and for design it cannot be expected to develop its full capacity when placed in tandem with a longer wall

- ❖ When the perimeter screw spacing becomes less than 3 in., the buckling of the end chords under the compression force may govern the failure modes both in monotonic and reversed cyclic tests.

### 6.3 ANALYTICAL MODELS

Analytical models by Kallsner & Lam, Easley and McCutcheon, which were originally intended to predict the strength and displacement of wood framed shear walls, were presented and a comparison with the test results was completed. Based on the comparison and observations made during testing, the elastic model recommended for use with light gauge steel frame / wood panel shear walls is similar to that presented by Kallsner & Lam (1995). The most salient findings are as follows:

- ❖ The lateral shear yield resistance,  $S_y$ , and the deflection of full-scale walls can be effectively predicted with the models, if appropriate connection test data is available.
- ❖ The yield strength and initial stiffness of connection tests with 25 mm edge distance and loading parallel to the panel grain are recommended for use in the models.
- ❖ Good agreement was obtained between the prediction and test strength values in both monotonic and cyclic cases using the Kallsner & Lam approach.
- ❖ The deflection model showed satisfactory agreement with the test results, especially for cyclic loading cases.

## 6.4 RECOMMENDATIONS

In order to better understand the behaviour of light gauge steel frame / wood panel shear walls other factors need to be considered in future research, involving both physical testing and analytical models.

- ❖ Wall length. In this thesis, the effect of height-to-width ratios was investigated; however, the length of the test specimens was far less than that of an actual wall in a building. Further research is needed to investigate the effect due to the length of a shear wall, such as the variation of the force distribution in different wall panels in a long wall, the variation of the hold-down forces due to the height-to-width ratios, and the relationship between a whole wall and its wall segments.

- ❖ Wall openings. Windows and doors usually exist in an actual light gauge steel frame / wood panel shear wall structure. A conservative design method is to neglect the contribution from the parts above or beneath the openings. In order to utilize this contribution, perforated shear wall tests need to be performed to verify the effect of openings and analytical models need to be developed for use in a design office. Construction details commonly used in actual light gauge steel frame / wood panel shear walls should be incorporated into the tests.

- ❖ Gravity loads. Gravity loads acting on the top of a shear wall will contribute to the restraint of the rotation of the wall under lateral loading and may cause an increase in the shear strength and racking stiffness of the shear wall. Gravity loads will also increase the axial compression forces in the studs. In some cases, the steel studs will fail

due to local or overall buckling under combined gravity and lateral loading. This needs to be considered in design and further tests should be carried out.

- ❖ Force perpendicular to the plane of a shear wall. Only in-plane loading was considered for the tests documented in this thesis; however, an actual wall is also subjected to loads perpendicular to its plane. The perpendicular loading will cause bending deformation and stress in the sheathing and steel studs. Further research needs to incorporate the perpendicular loading in tests and analytical models.

- ❖ The axial compression behaviour of the back-to-back studs with sheathing on one side needs to be better understood. At present, no equations in the CSA S136 Design Standard are suitable for their calculation.

- ❖ The connection data used in the models needs to be improved. This would allow for a more accurate prediction of the shear wall deflection. Different loading speeds in the connection tests need to be performed to find the most suitable one. In future connection tests, it is suggested that the edge distance parallel to the loading direction be the same as the perimeter screw spacing in the full-scale shear wall tests. As well, in order to obtain a better prediction of the full-scale tests, each connection test specimen should contain at least 3 screws to account for the variation of sheathing material nonuniformity.

## REFERENCES

American Iron and Steel Institute (1998). "Shear Wall Design Guide", Publication RG-9804, American Iron and Steel Institute, Washington DC, USA.

American Iron and Steel Institute (2002). "Standard for Cold-formed Steel Framing Design Provisions Lateral Resistance", Feb 2002 Draft, Washington, DC, USA.

American Plywood Association (2001). "Design / Construction Guide Diaphragms and Shear Walls", The Engineered Wood Association, Tacoma, WA, USA.

American Society for Testing and Materials, A653. (2002). "Standard Specification for Steel Sheet, Zinc-Coated (Galvanized) or Zinc-Iron Alloy-Coated (Galvannealed) by the Hot-Dip Process", West Conshohocken, PA, US.

American Wood Council (1996). "Load and Resistance Factor Design Manual for Engineered Wood Construction", 1996 Edition, American Forest & Paper Association.

Bateman B. W., (1996). "Light-gauge Steel verses Conventional Wood Framing in Residential Construction". ASC Proceeding of the 33rd Annual Conference, Texas A&M University-College Station, Texas. April 18-20, 1996. pp 203-210.

Boudreault, F. A., (2004). "Seismic Analysis of Steel Frame / Wood Panel Shear Walls", Master's Thesis, Dept. of Civil Engineering and Applied Mechanics, McGill University, Montreal, Canada.

Branston A. E., Boudreault F. A., and Rogers C. A. (2003). "Testing of Steel Frame/Wood Panel Shear Walls (Matching Tests of Existing Shear Wall Experiments) - Progress Report". McGill University, Montreal, Canada.

Branston, A.E., Boudreault, F.A., Chen, C.Y., Rogers, C.A. (2004). "Light Gauge Steel Frame / Wood Panel Shear Wall Test Data: Summer 2003", Department of Civil

Engineering and Applied Mechanics, McGill University, Montreal, QC, Canada.

Branston, A. E. (2004). "Development of a Design Methodology for Steel Frame / Wood Panel Shear Walls", Master's Thesis, Dept. of Civil Engineering and Applied Mechanics, McGill University, Montreal, Canada.

Breyer, D. E., Fridley, K. J. and Cobeen, K. E. (1998). "Design of Wood Structures ASD", Fourth Edition, McGraw-Hill, Inc.

Canadian Standards Association, O121. (1978). "Douglas Fir Plywood", Rexdale, ON, Canada.

Canadian Standards Association, O151. (1978). "Canadian Softwood Plywood", Rexdale, ON, Canada.

Canadian Standards Association, O325. (1992). "Construction Sheathing", Rexdale, ON, Canada.

Canadian Standards Association, S136-01 (2001). "North American Specification for the Design of Cold-Formed Steel Structural Members", Mississauga, ON, Canada.

Canadian Standards Association, 086-01 (2001). "Engineering Design in Wood", Toronto, ON, Canada.

Canadian Wood Council (2001). "Wood Design Manual 2001", Nepean, ON, Canada.

Canadian Wood Council (2002). "Introduction to Wood Design, A Learning Guide to Complement the Wood Design Manual", Ottawa, ON, Canada.

Ceccotti, A., and Karacabeyli, E. (2000). "Dynamic Analysis of Nailed Wood-Frame Shear Walls", Proceedings of the 12th World Conference on Earthquake Engineering, Auckland, New Zealand, Paper (0720) 1-8.

COLA-UCI (2001). "Report of a Testing Program of Light-Framed Walls with Wood-Sheathed Shear Panels", Final Report to the City of Los Angeles Department of Building and Safety, Light Frame Test Committee Subcommittee of Research

Committee, Structural Engineers Association of Southern California, Department of Civil and Environmental Engineering, University of California, Irvine, CA, USA.

Dolan, J. D., Johnson, A. C. (1997). "Long Shear Walls with Openings", Report No. TE-1996-002, Department of Wood Science and Forest Products, Virginia Polytechnic Institute and State University, Blacksburg, Virginia, USA.

Dolan, J. D., Foschi, R. O. (1991). "Structural Analysis Model for Static Loads on Timber Shear Walls", Journal of Structural Engineering, ASCE, Vol. 117, No 3, March 1991, 851-861.

Dolan, J. D. and Gutshall, S. T. (1994). "Monotonic and Cyclic Tests to Determine Short-term Duration-of-Load Performance of Nail and Bolt Connections: Volume I: Summary Report", Virginia Polytechnic Institute and State University Timber Engineering Report No. TE-1994-001.

Dolan, J. D., and White, M. W. (1992). "Design Consideration for Using Adhesives in Shear walls", Journal of Structural Engineering, ASCE, Vol. 118, No 12, P3473-3479.

Durham, J., Prion, H. G. L., Lam, F, and He, M. (1999). "Earthquake Resistance of Shear Walls with Oversize Sheathing Panels", 8th Canadian Conference on Earthquake Engineering Vancouver, BC, Canada, 161-166.

Easley, J. T, Foomani, M., and Dodds, R. H. (1982). "Formulas for Wood Shear Walls", Journal of Structural Division, ASCE, 108(ST11), 2460-2478.

Easley, J.T., 1977. "Strength and Stiffness of Corrugated Metal Shear Diaphragm", Journal of the Structural Division, ASCE, Vol. 103, No. ST1, January 1977, 169-180.

ECCS P88, 1995. "European Recommendations for the application of metal sheeting acting as a diaphragm". Publication 88, European Convention for Constructional Steelwork, Brussels, 1995.

ENV 1995-1-1:1993, "Eurocode 5 – Design of Timber Structures – Part 1-1: General Rules and Rules for Buildings".

Faherty, K. F. and Williamson T. G. (1999). "Wood Engineering and Construction Handbook", Third Edition, McGraw-Hill.

Falk, R. H. and Itani, R. Y. (1989). "Finite Element Modeling of Wood Diaphragms", Journal of Structural Engineering, ASCE, Vol.115, No.3, March 1989, P1722-1733.

Filiatrault, A. (1990). "Static and Dynamic Analysis of Timber Shear Walls", Canadian Journal of Civil Engineering, Vol.17, 643-651.

Folz, B. and Filiatrault, A. (2001). "Cyclic Analysis of Wood Shear Walls", Journal of Structural Engineering, ASCE, Vol. 127, No. 4, 433-441.

Forest Products Laboratory (1999) "Wood handbook—Wood as an Engineering Material". Gen. Tech. Rep. FPL–GTR–113. Madison, WI:U.S. Department of Agriculture, Forest Service, Forest Products Laboratory.

Fosci, R. O. (1977). "Analysis of Wood Diaphragms and Trusses. Part I: Diaphragms", Presented to the Meeting of the International Union of Forest Research Organizations, Wood Engineering Group, Aalborg, Denmark, June 17-18, 1976. Can. J. Civ. Eng. 4, 345(1977).

Fulop L. A. and Dubina D. (2003). "Performance of Wall-stud Cold-formed Shear Panels under Monotonic and Cyclic Loading, Part II: Numerical Modelling and Performance Analysis" Thin-walled Structures.2003.

Fulop L.A. and Dubina D. (2003). "Performance of Wall-stud Cold-formed Shear Panels under Monotonic and Cyclic Loading, Part I: Experimental Research" Thin-walled Structures.2003.

Gad, E. F., Duffield, C. F., Chandler, A. M. and Stark, G. (1998). "Testing of Cold-formed Steel Framed Domestic Structures", Proceedings of the 11th European Conference on Earthquake Engineering, Paris, France.

Gad, E. F., Chandler, A. M., Duffield, C. F. and Hutchinson, G. L. (1999a). "Earthquake Ductility and Over-strength in Residential Structures". Structural

Engineering and Mechanics, Vol. 8, No. 4, 361-382.

Gad, E.F., Duffield, C.F., Hutchinson, G.L, Mansell, D.S. and Stark, G. (1999b). "Lateral Performance of Cold-formed Steel-framed Domestic Structures", Engineering Structures, Elsevier Science Ltd., Vol. 21, 83-95.

Gad, E. F., Chandler, A. M., Duffield, C. F. and Stark, G. (1999c). "Lateral Behaviour of Plasterboard-clad Residential Steel Frames", Journal of Structural Engineering, ASCE, Vol. 125, No. 1,32-39.

Gad, E. F., Duffield and C. F. (2000). "Lateral Behaviour of Light Framed Walls in Residential Structures", Proceedings of the 12th World Conference on Earthquake Engineering, Auckland, New Zealand, Paper 1663.

Sherwood, G. and Moody, R. C. (1989). "Light-Frame Wall and Floor Systems Analysis and Performance". General Technical Report FPL-GTR-59, Madison, WI: U.S. Department of Agriculture, Forest Service, Forest Products Laboratory.

Gupto, A. K. and Kuo, G. P. (1985). "Behavior of Wood-Framed shear Walls", Journal of Structural Engineering, ASCE, Vol.111, No.8, August 1985, P1722-1733.

Gupto, A. K. and Kuo, G. P. (1987a). "Wood Framed shear Walls with Uplifting", Journal of Structural Engineering, ASCE, Vol.113, No.2, February 1987, P241-259.

Gupto, A. K. and Kuo, G. P. (1987b). "Modeling of a Wood-framed House", Journal of Structural Engineering, ASCE, Vol.113, No.2, P260-278.

Gutkowski, R. M. and Castillo, A. L. (1988). "Single and Double Sheathed Wood Shear Wall Study", Journal of Structural Engineering, ASCE, Vol. 114, No. 6, 1268-1284.

He, M., Magnusson, H., Lam, F. and Prion, H. G. L. (1999). "Cyclic Performance of Perforated Wood Shear Walls with Oversize OSB Panels", Journal of Structural Engineering, ASCE, Vol. 125, No.1, P10-18.

Heine, C. P. and Dolan, J. D. (2001). "Dynamic Performance of Perforated Light-frame Shear Walls with Various End Restraints", *Forest Products Journal*, Vol.50, No.7/8, July/August 2001, P65-72.

Hirashima Y. (1981) "Derivation of Racking Deformation Formula of Nailed Frame Panel". *Mokuzai Gakkaishi* 1981, Vol.27, NO. 2. p141-143.

International Code Council (2000). "International Building Code 2000", 3rd Printing, Falls Church, VA, USA.

International Conference of Building Officials (1997). "Uniform Building Code - ICBO", Whittier, CA, USA.

Itani, R. Y., Tuomi, R. L., and McCutcheon W. J. (1982). "Methodology to Evaluate Racking Resistance of Nailed Walls", *Forest Products Research Society* 1982. *Forest Prod J.*32 (1):30-36.

Itani, R.Y. and Cheung, C. K. (1984). "Nonlinear Analysis of Sheathed Wood Diaphragm", *Journal of Structural Engineering*, ASCE, Vol.110, No.9, September 1984, P2137-2147.

Kaellsner B. and Lam F. (1995) "Diaphragms and Shear Walls". STEP Lectures: *Holzbauwerke nach Eurocode 5-Grundlagen, Entwicklungen, Ergaenzungen*, Fachverlag Holz, Duesseldorf, Germany, pp. 15/1-15/19.

Kasal B. and Leichti R. J. (1992) "Nonlinear Finite-Element Model For Light-Frame Stud Walls", *Journal of Structural Engineering*, ASCE, Vol.118, No.11. November 1992, pp3122-3135.

Kingsley, C. (1996). "Structural Tests of Light Gauge Steel Stud Panels", Internal Report No. 726. National Research Council Canada, Ottawa, ON, Canada.

Lam, F., Prion, H. G. L., and He, M. (1997). "Lateral Resistance of Wood Shear Walls with Large Sheathing Panels", *Journal of Structural Engineering*, Vol. 123, No.12, December, 1997. P1666-1673.

McCreless, C. S. and Tarpy, T. S. (1978). "Experimental Investigation of Steel Stud Shear Wall Diaphragms", Proceedings of the 4th International Speciality Conference on Cold-Formed Steel Structures, St. Louis, MO, USA, 647-672.

McCutcheon, W. J., (1985). "Racking deformation in Wood Shear Walls", Journal of Structural Engineering, Vol.111, No.2, February 1985, P257-269.

Murakami, M., Moss, P. J., Carr, A. J., and Inayama, M. (1999). "Formulae to Predict Non-Linear Behaviour of Sheathed Walls with Any Nailing Arrangement Pattern". *In*: Walford, G. B. and Gaunt, D. J. (Ed.) Proceedings of the Pacific Timber Engineering Conference. Rotorua, New Zealand, Vol. 3: 189-196.

National Association of Home Builders Research Center (1997). "Monotonic Tests of Cold-formed Steel Shear Walls with Openings", Report prepared for the American Iron and Steel Institute, the U.S. Department of Housing and Urban Development and the National Association of Home Builders, NAHB Research Center Inc., Upper Marlboro, MD, USA.

National Research Council of Canada (1995). "National Building Code of Canada, 1995". 11th Edition, Ottawa, ON, Canada.

National Research Council of Canada (2004). "National Building Code of Canada, 2004". 12th Edition Draft, Ottawa, ON, Canada.

Nelson, E. L., Wheat, D. L. and Fowler, D. W. (1985). "Structural Behaviour of Wood Shear Wall Assemblies". ASCE, Vol.111, No.3, March 1985, pp654-666.

North American Steel Framing Alliance, "Prescriptive Method for Residential Cold-Formed Steel Framing". Year 2000 Edition, Publication NT3.00 NASFA, October 2000.

Okasha, A. (2004) "Evaluation of Connection Performance for Steel Frame / Wood Panel Shear Walls" M.Eng. Project Report, Department of Civil Engineering and Applied Mechanics, McGill University

Robertson, R. A. (1981). Discussion of "Racking Strength of Light-Frame Nailed Walls". ASCE, Vol.106, No. ST9, Sep. 1980, pp1981-1985.

Ruben, C. T. F. (1992). "Buckling of Lipped Flanges in Cold-formed Steel Studs with Web Cut-outs", Master Thesis, Concordia University, Canada.

Salenikovich, A. J., Dolan, J. D. and Easterling, W. S. (1999). "Monotonic and Cyclic Tests of Long Steel-frame Shear Walls with Openings", Report No. TE-1999-001, Department of Wood Science and Forest Products, Virginia Polytechnic Institute and State University, Blacksburg, Virginia, USA.

Salenikovich, A. J., Dolan, J. D., Loferski, J. R., Easterling, W. S., Woeste, P., and White, M.W. (2000). "The Racking Performance of Light-Frame Shear Walls", PhD. Dissertation, Department of Wood Science and Forest Products, Virginia Polytechnic Institute and State University, Blacksburg. Virginia, USA.

Schmidt R. J. and Moody R. C. (1989) "Modeling Laterally Loaded Light-Frame Buildings", Journal of Structural Engineering, ASCE, Vol.115, No.1, January, 1989. pp 201-217.

Serrette, R. L. (1994). "Light Gauge Steel Shear Wall Tests", Light Gauge Steel Research Group, Department of Civil Engineering, Santa Clara University, Santa Clara, CA: USA.

Serrette, R. L. (1997). "Behaviour of Cyclically Loaded Light Gauge Steel Framed Shear Walls", Proceedings of Structures Congress XV sponsored by The Structural Engineering Institute of ASCE, Portland, OR, USA, 443-448.

Serrette, R. L., Encalada, J., Juadines, M. and Nguyen, H. (1997a). "Static Racking Behaviour of Plywood, OSB, Gypsum, and FiberBond Walls with Metal Framing", Journal of Structural Engineering, ASCE, Vol. 123, No. 8, 1079-1086

Serrette, R., Encalada, J., Hall, G., Matchen, B., Nguyen, H. and Williams, A. (1997b). "Additional Shear Wall Values for Light Weight Steel Framing", Report No.

LGSRG-1-97, Light Gauge Steel Research Group, Department of Civil Engineering, Santa Clara University, Santa Clara, CA, USA.

Serrette, R. L., Ogunfunmi, K. (1996). "Shear Resistance of Gypsum-sheathed Light-gauge Steel Stud Walls", *Journal of Structural Engineering*, ASCE, Vol. 122, No. 4, 383-389.

Serrette, R., Hall, G., Nguyen, H. (1996a). "Dynamic Performance of Light Gauge Steel Framed Shear Walls", *Proceedings of the 13<sup>th</sup> International Speciality Conference on Cold-Formed Steel Structures*, St. Louis, MO, USA, 487-498.

Serrette, R., Nguyen, H., Hall, G. (1996b). "Shear Wall Values for Light Weight Steel Framing", Report No. LGSRG-3-96, Light Gauge Steel Research Group, Department of Civil Engineering, Santa Clara University, Santa Clara, CA, USA.

Serrette, R. L., Morgan, K. and Sorhouet, M. (2002). "Performance of Cold-formed Steel-framed Shear Walls: Alternative Configurations", Final Report: LGSRG-06-02, Submitted to NAHB Research Center, July 12, 2002. , Light Gauge Steel Research Group, Department of Civil Engineering, Santa Clara University, Santa Clara, CA, USA.

Stewart, W. G., (1987). "The Seismic Design of Plywood Sheathed Shear Walls", PHD thesis, Civil Engineering, University of Canterbury, Christchurch, New Zealand.

Sugiyama, H. and Matsumoto, T. (1994). "Empirical Equations for the Estimation of Racking Strength of A Plywood-sheathed Shear Wall with Openings", *Summaries of Technical Papers of Annual Meeting, Transactions of the Architectural Institute of Japan*.

Tarpy, T. S. (1980). "Shear Resistance of Steel-stud Wall Panels", *Proceedings of the 5<sup>th</sup> International Speciality Conference on Cold-Formed Steel Structures*, St. Louis, MO, USA, 331-348.

Tarpy, T. S., and Girard, J. D. (1982). "Shear Resistance of Steel-stud Wall Panels", Proceedings of the 6th International Speciality Conference on Cold-Formed Steel Structures, St. Louis, MO, USA, 449-465.

Tarpy, T. S., and Hauenstein, S. F. (1978). "Effect of Construction Details on Shear Resistance of Steel-Stud Wall Panels", Vanderbilt University, Nashville, TN, USA. A Research Project Sponsored by the American Iron and Steel Institute. Project No. 1201-412.

Timber Research and Development Association, (1980) "Calculations for the racking Resistance of Timber Framed Walls/TRADA". High Wycombe, Buckinghamshire: TRADA, 1980. TA666 T763 Section 1, Sheet 18.

Tissell, J. R. (1993). "Wood Structural Panel Shear Walls". Report No. 154, APA – The Engineered Wood Association, Tacoma, WA, USA.

Tuomi, R. L. and McCutcheon, W. J. (1974). "Testing of a Full-scale House under Simulated Snowloads and Windloads". Research Paper FPL 234, U.S. Department of Agriculture, Forest Products Laboratory, Madison, Wisc., 1974.

Tuomi, R. L. and McCutcheon, W. J. (1978). "Racking Strength of Light-Frame Nailed Walls". ASCE, Vol. 104, No. ST7, July 1978. P1131-1140.

Waite T. J., NAHB Research Center, (2000) "Steel-Frame House Construction", Craftsman Book Company, CA, USA.

White, M. W., and Dolan, J. D., (1995), "Nonlinear Shear-Wall Analysis", Journal of Structural Engineering, Vol.121, No.11, P1629-1635.

Yu, W.W. (2000). "Cold-formed Steel Design", Third Edition, John Wiley & Sons, Inc., NY, USA.

Zhao, Y. (2002), "Cyclic Performance of Cold-formed Steel Stud Shear Walls", Master Thesis. McGill University, Montreal, Canada.

# APPENDIX I WALL CONFIGURATIONS

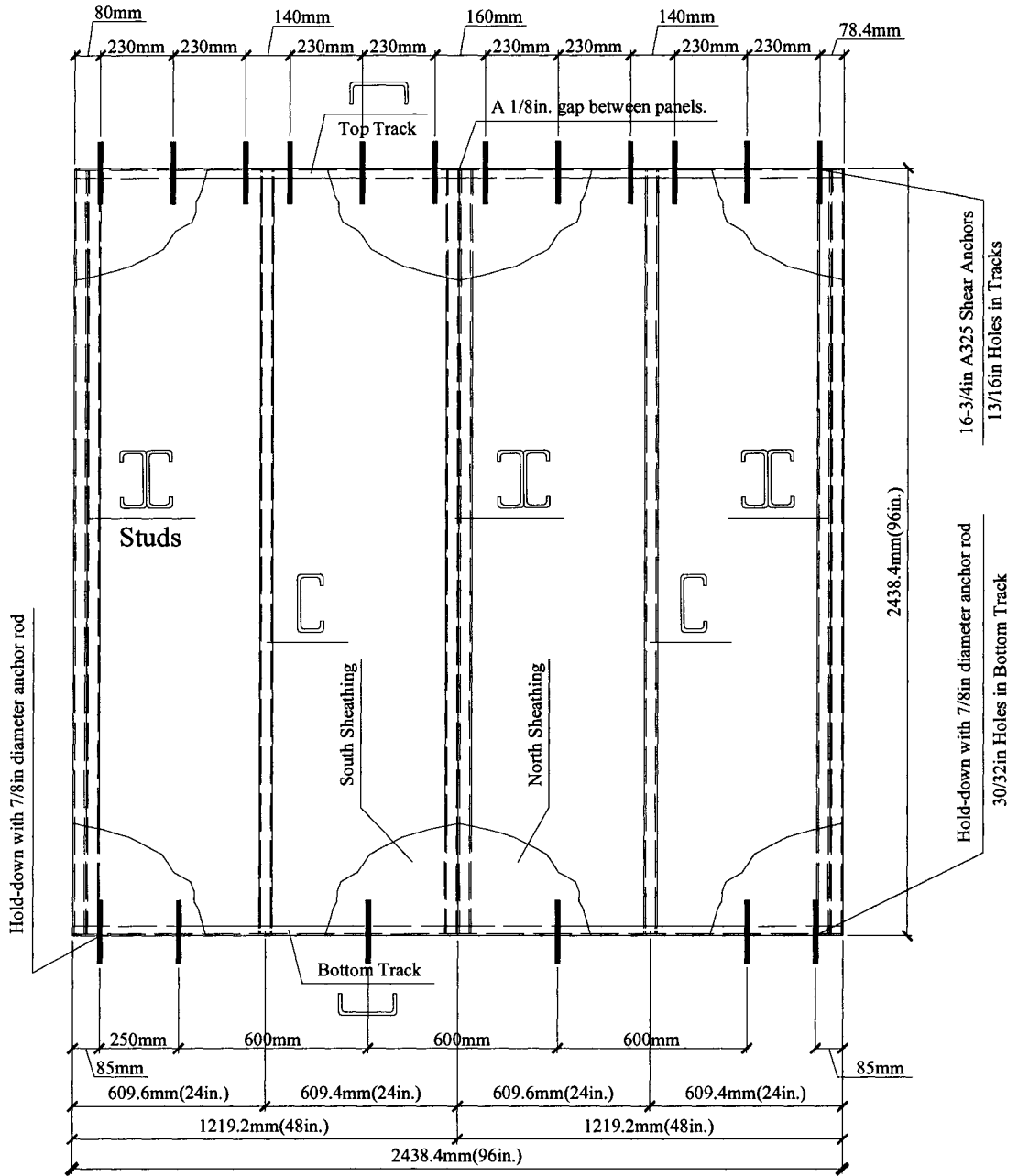


Figure A-I.1 8' x 8' Wall Configuration

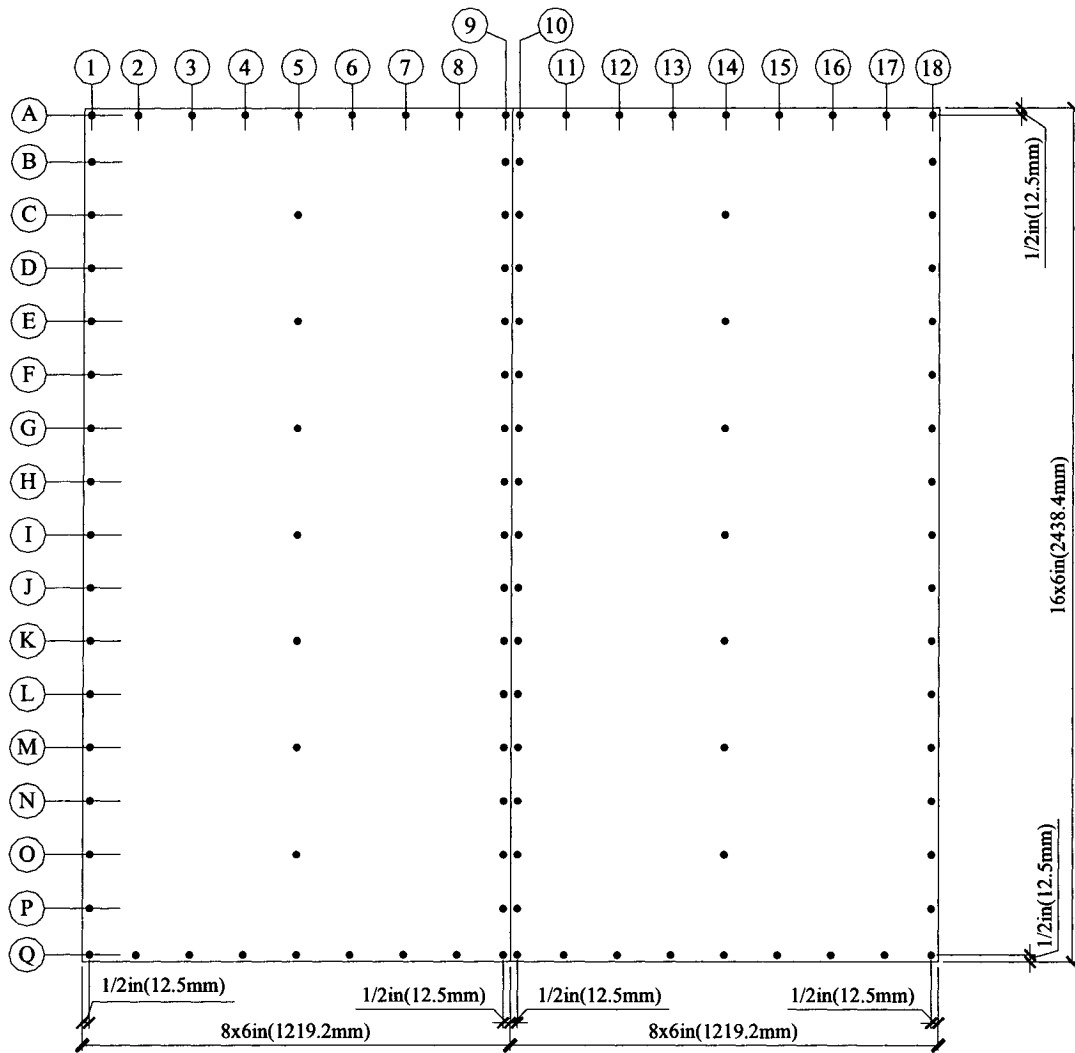


Figure A-I.2 6/12 Screw Pattern for All 8' x 8' Walls

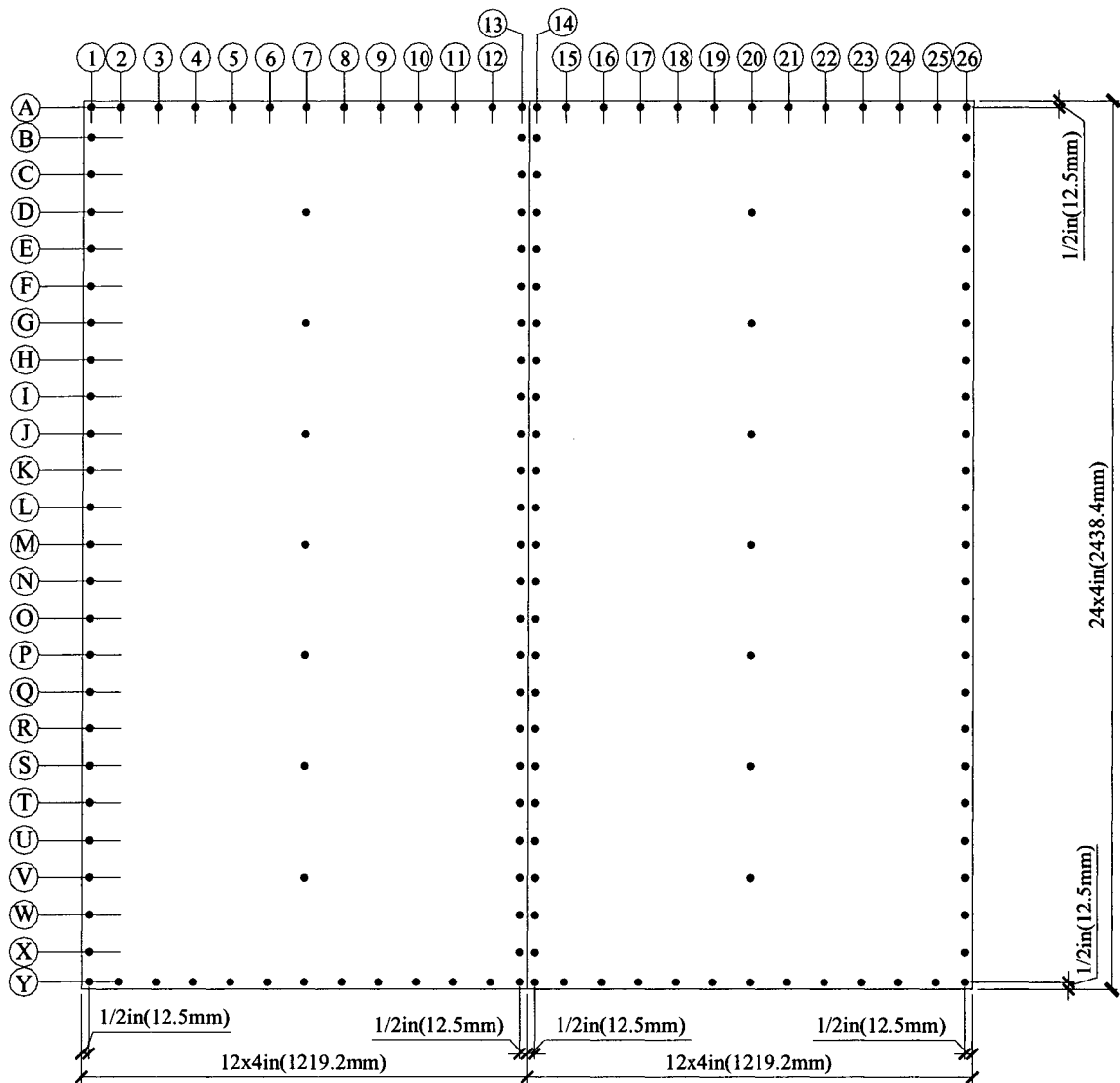


Figure A-I.3 4/12 Screw Pattern for All 8' x 8' Walls

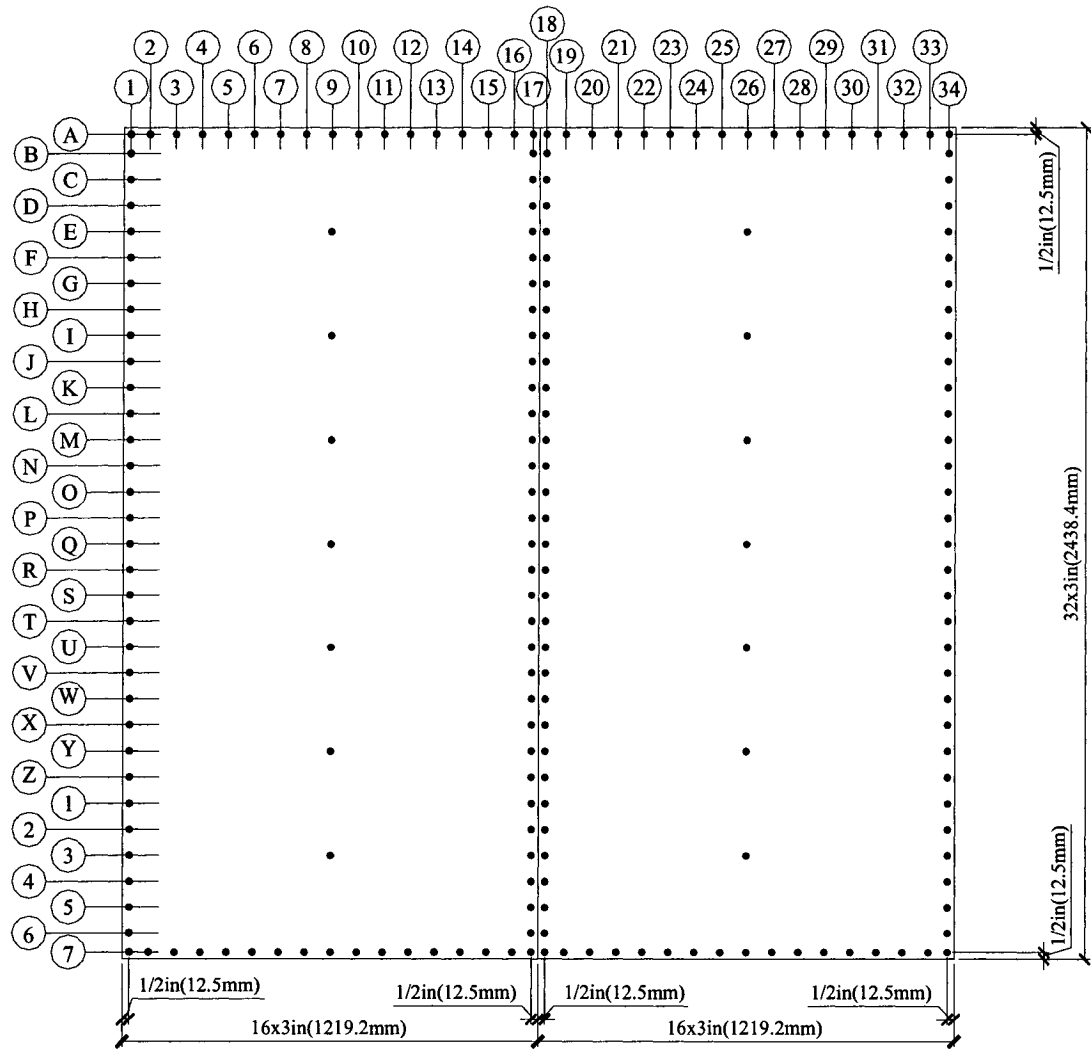


Figure A-I.4 3/12 Screw Pattern for All 8' x 8' Walls

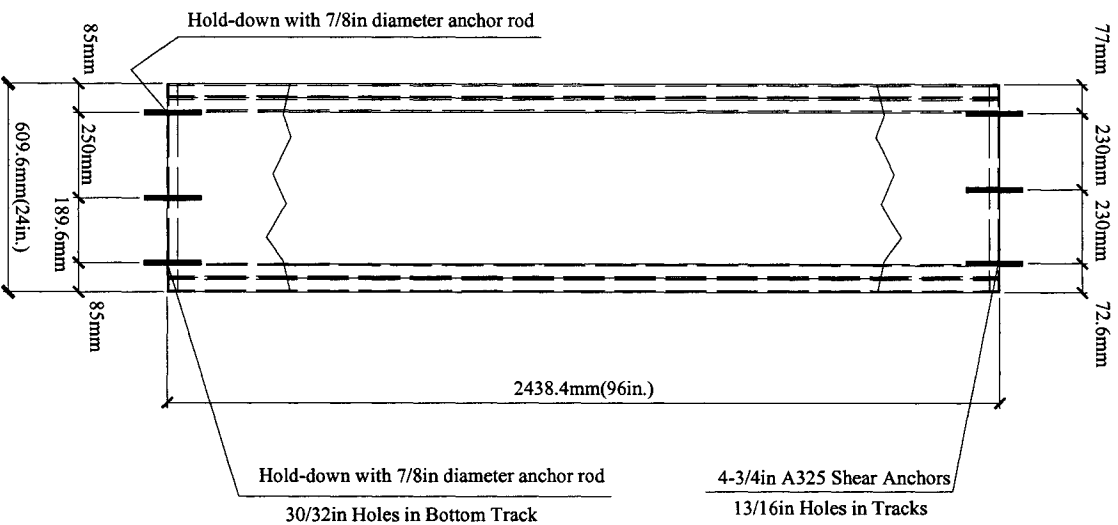
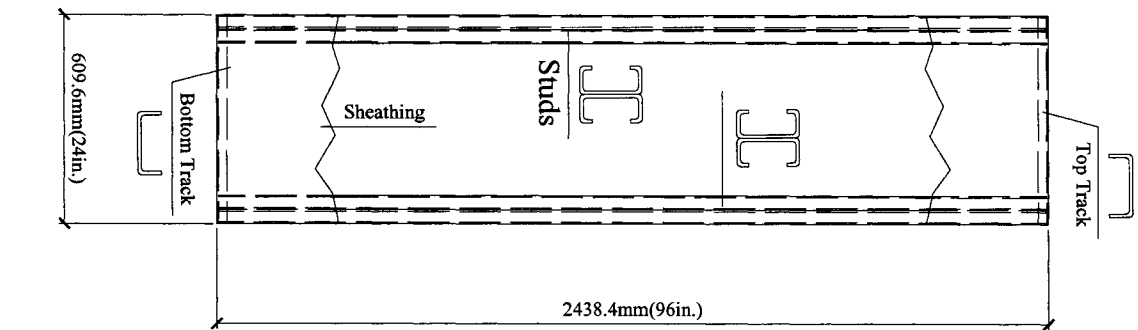


Figure A-1.5 2' x 8' Wall Configuration

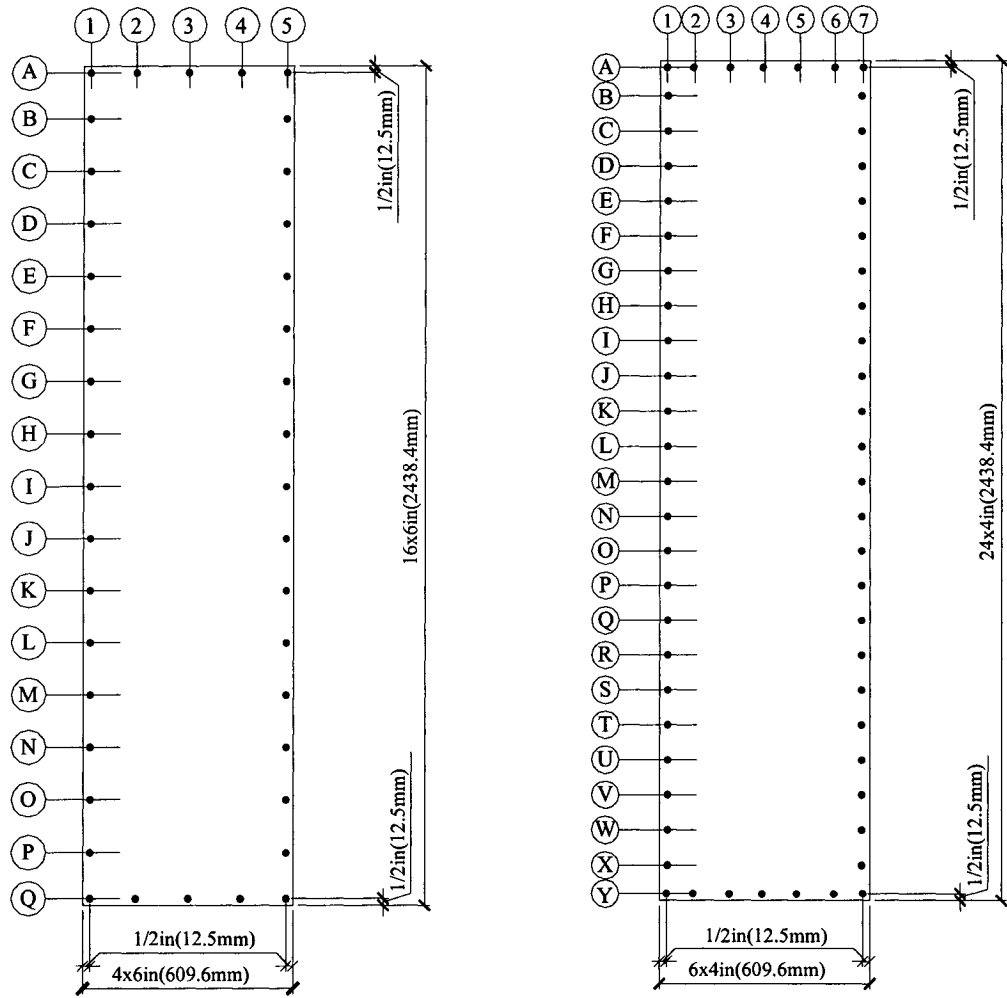


Figure A-I.6 Screw Patterns for All 2' x 8' Walls

## APPENDIX II COMPONENTS OF TEST SPECIMENS

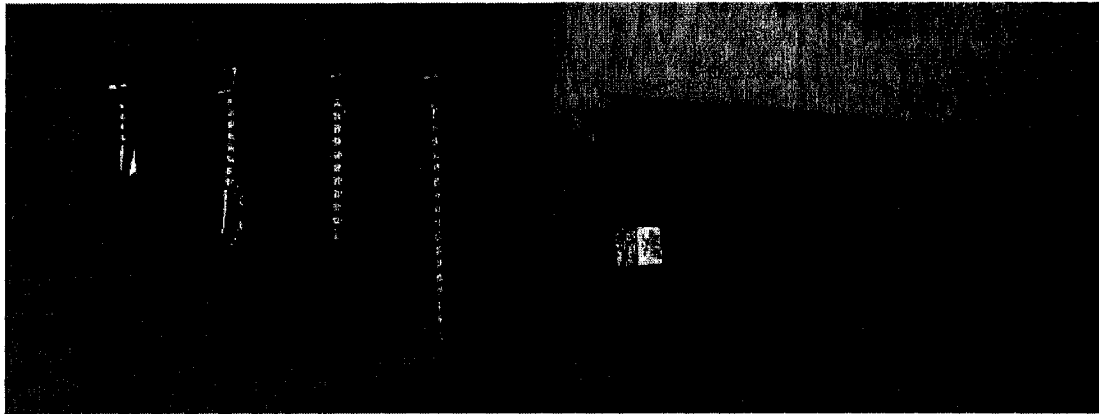


Figure A-II.1 Screws

Figure A-II.2 Hold-down

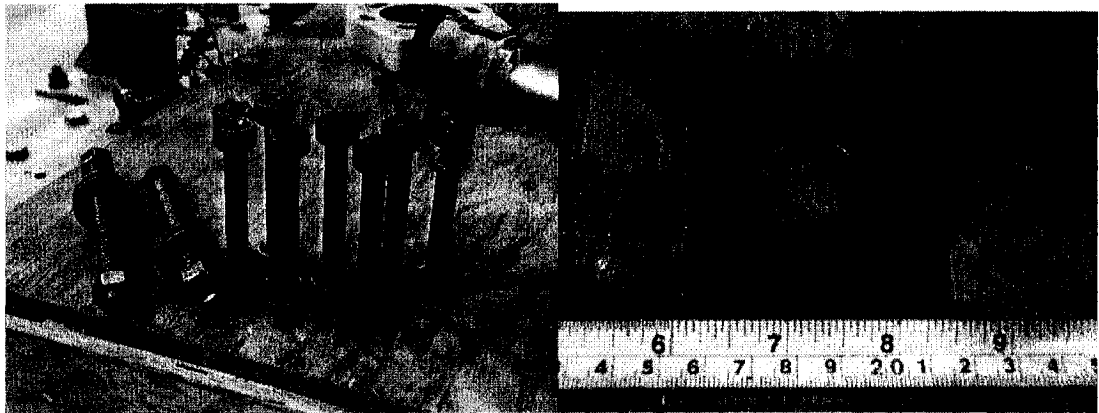


Figure A-II.3 Anchor Rods and Shear Anchors

Figure A-II.4 Washers

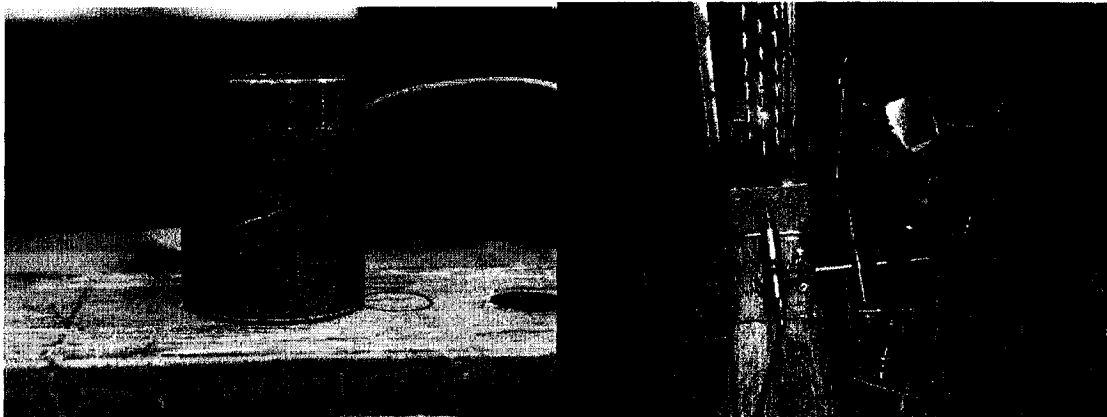


Figure A-II.5 Load Cell

Figure A-II.6 LVDTs



Figure A-II.7 Sheathing

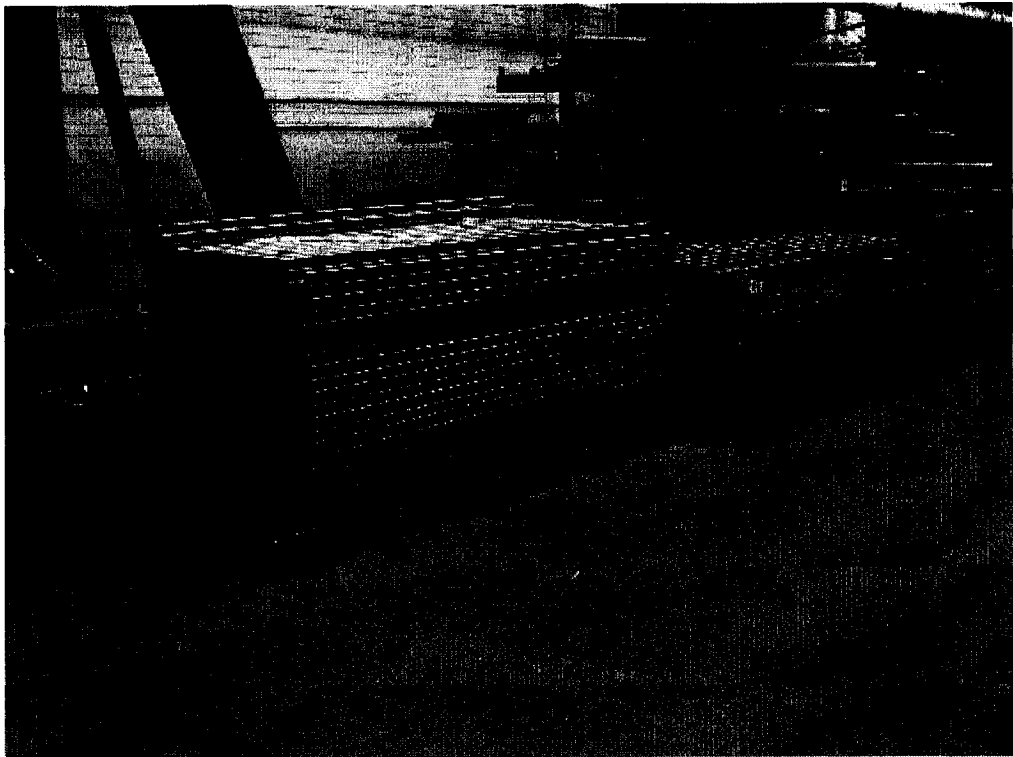


Figure A-II.8 Studs and tracks



Figure A-II.9 2' x 8' Wall Specimens



Figure A-II.10 8' x 8' CSP Wall Specimen in Test Frame

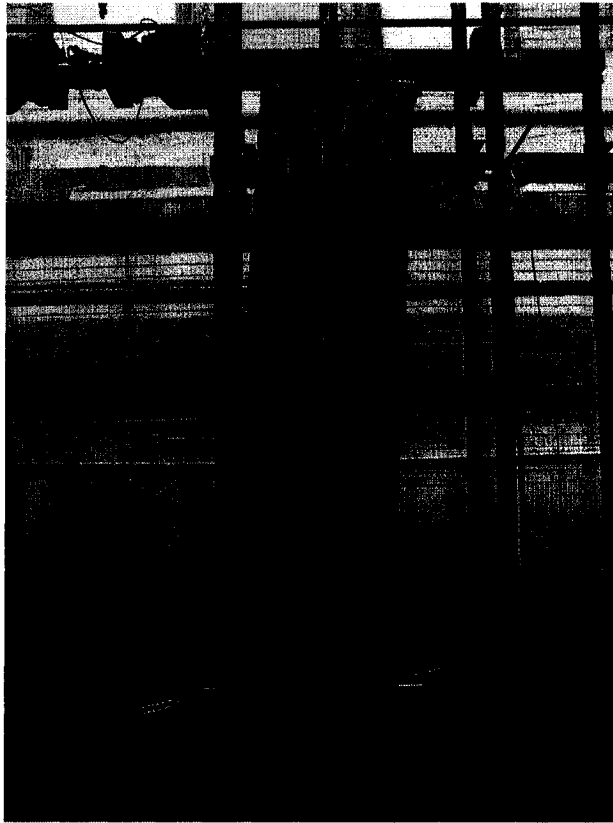


Figure A-II.11 2' x 8' OSB Wall Specimen in Test Frame (post test)

## APPENDIX III REVERSED CYCLIC TEST PROTOCOLS

Table III.1: CUREE Cyclic Protocol for Tests 16-A,B,C  
(2x8 CSP 6"/12")

$\Delta=0.6*\Delta_m$	72.035	Screw Pattern:	6"/12"
		Sheathing:	CSP

Displ.	Target (corr.)	Actuator Input	No. Of cycles
	mm	mm	
0.050 $\Delta$	3.602	4.452	6
0.075 $\Delta$	5.403	6.450	1
0.056 $\Delta$	4.052	4.948	6
0.100 $\Delta$	7.203	8.466	1
0.075 $\Delta$	5.403	6.450	6
0.200 $\Delta$	14.407	17.078	1
0.150 $\Delta$	10.805	12.760	3
0.300 $\Delta$	21.610	26.002	1
0.225 $\Delta$	16.208	19.187	3
0.400 $\Delta$	28.814	35.174	1
0.300 $\Delta$	21.610	26.002	2
0.700 $\Delta$	50.424	62.150	1
0.525 $\Delta$	37.818	46.339	2
1.000 $\Delta$	72.035	87.860	1
0.750 $\Delta$	54.026	66.359	2
1.500 $\Delta$	108.052	125.000	1**
1.125 $\Delta$	81.039	99.320	2*

\*: The displacement is beyond the displacement at the maximum load capacity.  
 \*\*: The displacement is beyond the range of the actuator.

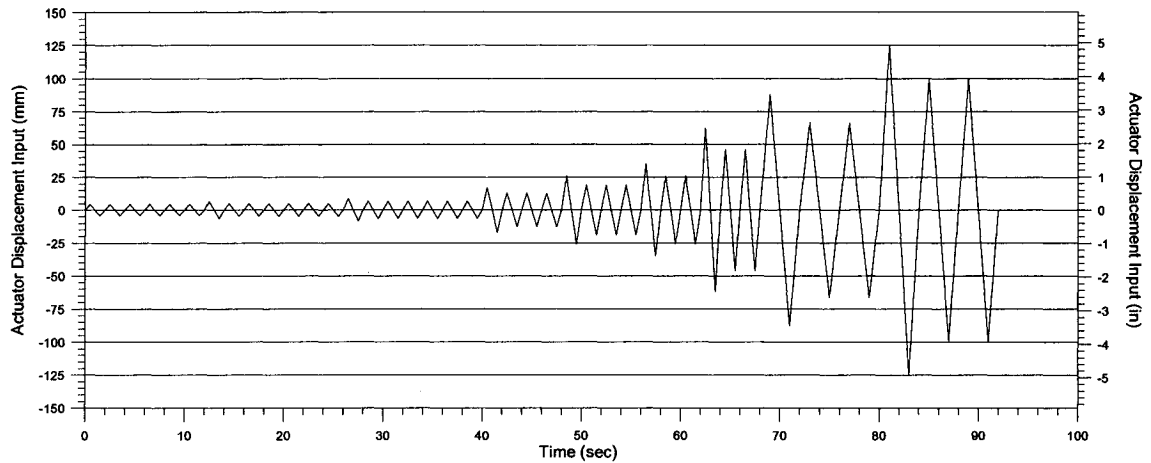


Table III.2: CUREE Cyclic Protocol for Tests 18-A,B,C  
(2x8 CSP 4"/12")

$\Delta=0.6*\Delta_m$	78.194	Screw Pattern:	4"/12"
		Sheathing:	CSP

Displ.	Target (corr.)	Actuator Input	No. Of cycles
	mm	mm	
0.050 $\Delta$	3.910	5.981	6
0.075 $\Delta$	5.865	8.279	1
0.056 $\Delta$	4.398	6.558	6
0.100 $\Delta$	7.819	10.498	1
0.075 $\Delta$	5.865	8.279	6
0.200 $\Delta$	15.639	19.913	1
0.150 $\Delta$	11.729	14.996	3
0.300 $\Delta$	23.458	29.844	1
0.225 $\Delta$	17.594	22.445	3
0.400 $\Delta$	31.277	38.912	1
0.300 $\Delta$	23.458	29.844	2
0.700 $\Delta$	54.736	66.968	1
0.525 $\Delta$	41.052	50.292	2
1.000 $\Delta$	78.194	95.889	1
0.750 $\Delta$	58.645	71.515	2
1.500 $\Delta$	117.290	125.000	1**
1.125 $\Delta$	87.968	108.666	2

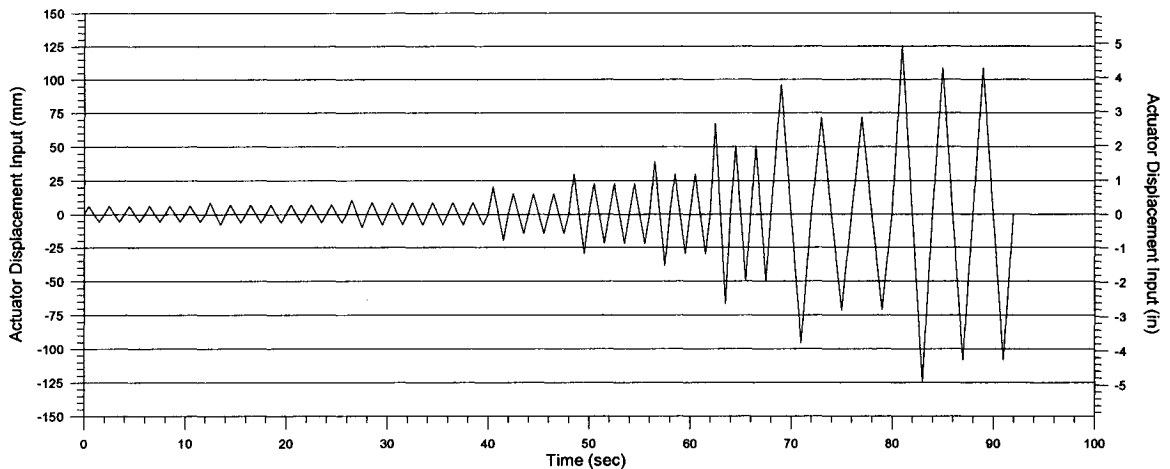


Table III.3: CUREE Cyclic Protocol for Tests 20-A,B,C  
(2x8 OSB 6"/12")

$\Delta=0.6*\Delta_m$	59.591	Screw Pattern:	6"/12"
		Sheathing:	OSB

Displ.	Target (corr.)	Actuator Input	No. Of cycles
	mm	mm	
0.050 $\Delta$	2.980	4.951	6
0.075 $\Delta$	4.469	6.804	1
0.056 $\Delta$	3.352	5.430	6
0.100 $\Delta$	5.959	8.595	1
0.075 $\Delta$	4.469	6.804	6
0.200 $\Delta$	11.918	16.125	1
0.150 $\Delta$	8.939	12.163	3
0.300 $\Delta$	17.877	23.782	1
0.225 $\Delta$	13.408	18.011	3
0.400 $\Delta$	23.836	31.087	1
0.300 $\Delta$	17.877	23.782	2
0.700 $\Delta$	41.714	51.605	1
0.525 $\Delta$	31.285	39.387	2
1.000 $\Delta$	59.591	73.143	1
0.750 $\Delta$	44.693	55.323	2
1.500 $\Delta$	89.386	109.072	1*
1.125 $\Delta$	67.040	82.020	2
2.000 $\Delta$	119.182	125.000	1**
1.500 $\Delta$	89.386	109.072	2*

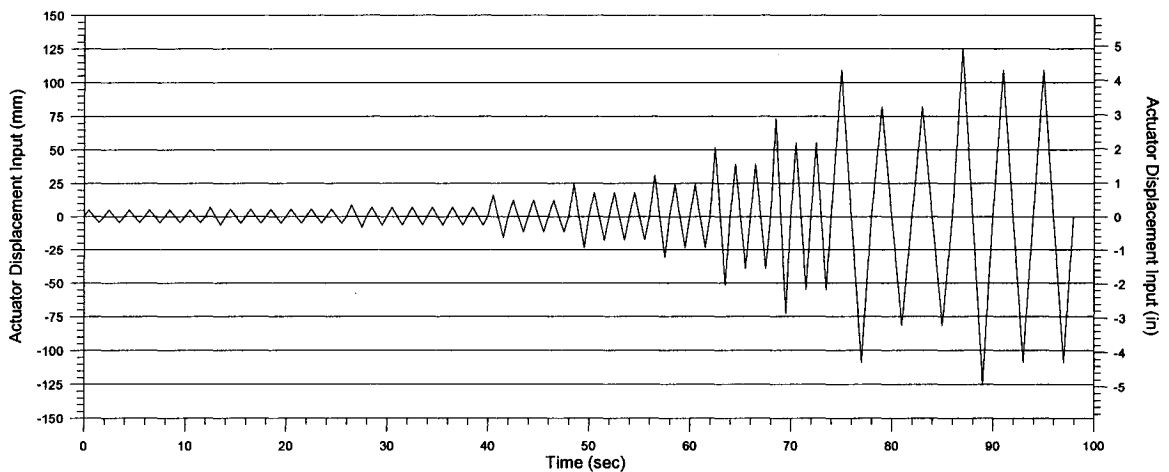


Table III.4: CUREE Cyclic Protocol for Tests 28-A,B,C  
(2x8 OSB 4"/12")

$\Delta=0.6*\Delta_m$	58.271	Screw Pattern:	4"/12"
		Sheathing:	OSB

Displ.	Target (corr.)	Actuator Input	No. Of cycles
	mm	mm	
0.050 $\Delta$	2.914	3.400	6
0.075 $\Delta$	4.370	5.098	1
0.056 $\Delta$	3.278	3.816	6
0.100 $\Delta$	5.827	6.802	1
0.075 $\Delta$	4.370	5.098	6
0.200 $\Delta$	11.654	13.231	1
0.150 $\Delta$	8.741	10.126	3
0.300 $\Delta$	17.481	20.328	1
0.225 $\Delta$	13.111	14.995	3
0.400 $\Delta$	23.308	27.792	1
0.300 $\Delta$	17.481	20.328	2
0.700 $\Delta$	40.790	50.753	1
0.525 $\Delta$	30.592	37.681	2
1.000 $\Delta$	58.271	72.765	1
0.750 $\Delta$	43.703	54.413	2
1.500 $\Delta$	87.407	109.164	1*
1.125 $\Delta$	65.555	81.638	2
2.000 $\Delta$	116.542	125.000	1**
1.500 $\Delta$	87.407	109.164	2*

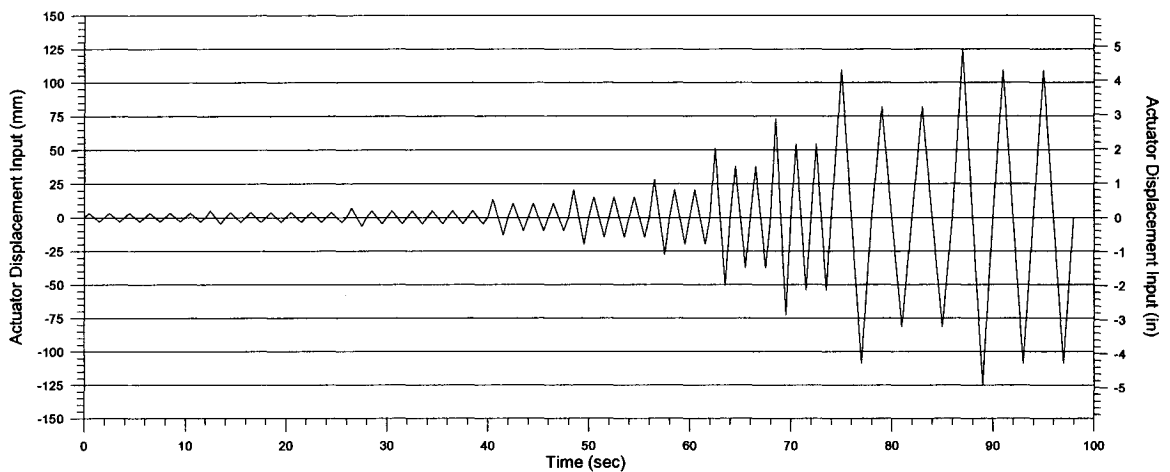


Table III.5: CUREE Cyclic Protocol for Tests 30-A,B,C  
(8x8 CSP 6"/12")

$\Delta=0.6*\Delta_m$	40.220	Screw Pattern:	6"/12"
		Sheathing:	CSP

Displ.	Target (corr.)	Actuator Input	No. Of cycles
	mm	mm	
0.050 $\Delta$	2.011	2.245	6
0.075 $\Delta$	3.017	3.382	1
0.056 $\Delta$	2.262	2.538	6
0.100 $\Delta$	4.022	4.494	1
0.075 $\Delta$	3.017	3.382	6
0.200 $\Delta$	8.044	9.129	1
0.150 $\Delta$	6.033	6.766	3
0.300 $\Delta$	12.066	14.046	1
0.225 $\Delta$	9.050	10.342	3
0.400 $\Delta$	16.088	18.650	1
0.300 $\Delta$	12.066	14.046	2
0.700 $\Delta$	28.154	31.790	1
0.525 $\Delta$	21.116	24.151	2
1.000 $\Delta$	40.220	45.284	1
0.750 $\Delta$	30.165	34.046	2
1.500 $\Delta$	60.331	68.052	1*
1.125 $\Delta$	45.248	50.908	2
2.000 $\Delta$	80.441	90.698	1*
1.500 $\Delta$	60.331	68.052	2*

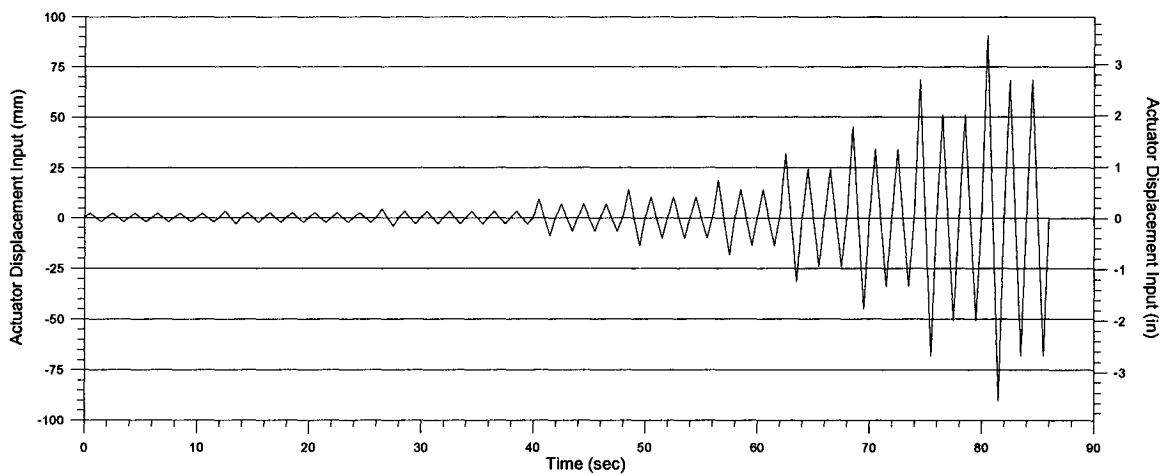


Table III.6: CUREE Cyclic Protocol for Tests 32-A,B,C  
(8x8 CSP 4"/12")

$\Delta=0.6*\Delta_m$	44.978	Screw Pattern:	4"/12"
		Sheathing:	CSP

Displ.	Target (corr.)	Actuator Input	No. Of cycles
	mm	mm	
0.050Δ	2.249	2.485	6
0.075Δ	3.373	3.747	1
0.056Δ	2.530	2.793	6
0.100Δ	4.498	5.042	1
0.075Δ	3.373	3.747	6
0.200Δ	8.996	10.583	1
0.150Δ	6.747	7.707	3
0.300Δ	13.493	16.148	1
0.225Δ	10.120	12.019	3
0.400Δ	17.991	21.255	1
0.300Δ	13.493	16.148	2
0.700Δ	31.484	36.421	1
0.525Δ	23.613	27.467	2
1.000Δ	44.978	52.073	1
0.750Δ	33.733	39.030	2
1.500Δ	67.466	78.167	1*
1.125Δ	50.600	58.496	2
2.000Δ	89.955	104.206	1*
1.500Δ	67.466	78.167	2*

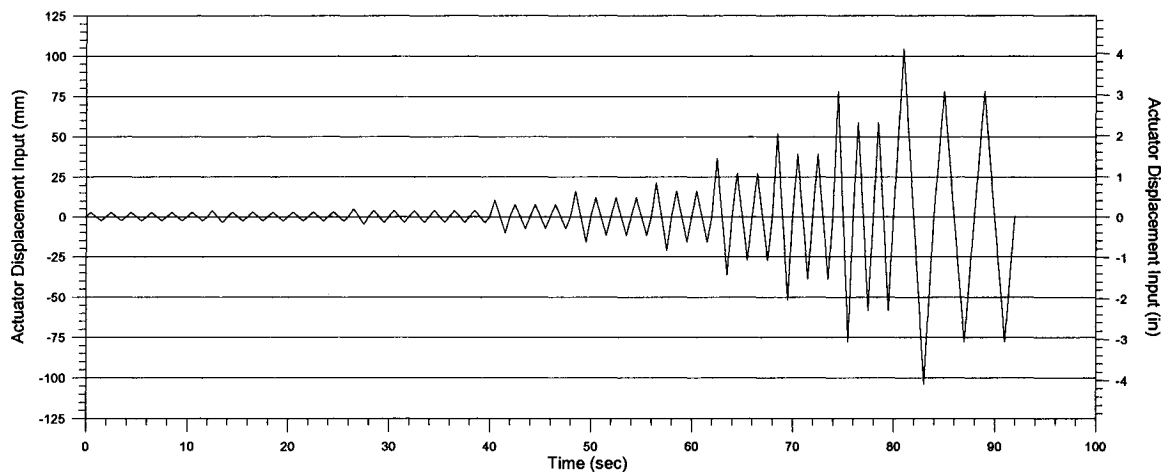
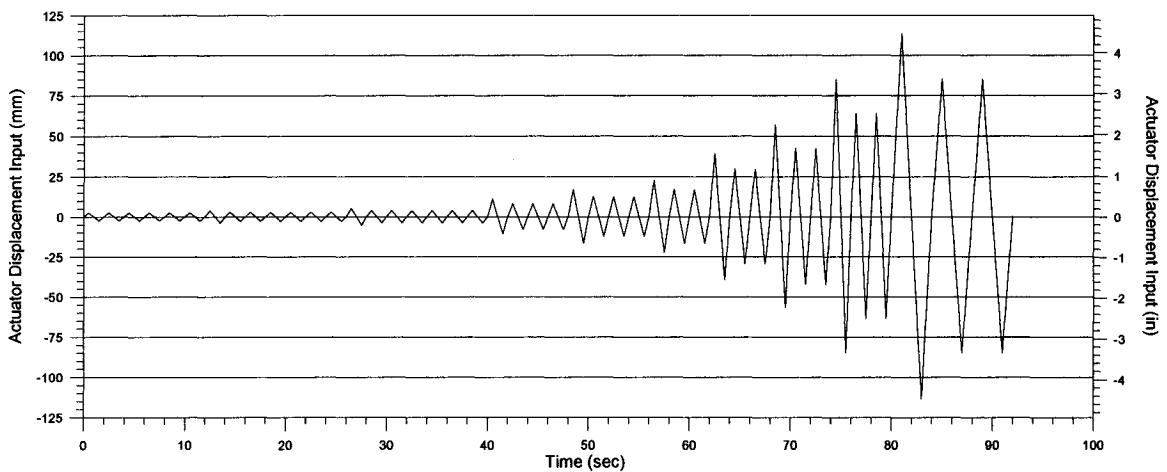


Table III.7: CUREE Cyclic Protocol for Tests 32-A,B,C  
(8x8 CSP 3"/12")

$\Delta=0.6*\Delta_m$	47.768	Screw Pattern:	3"/12"
		Sheathing:	CSP

Displ.	Target (corr.)	Actuator Input	No. Of cycles
	mm	mm	
0.050 $\Delta$	2.388	2.636	6
0.075 $\Delta$	3.583	3.938	1
0.056 $\Delta$	2.687	2.937	6
0.100 $\Delta$	4.777	5.287	1
0.075 $\Delta$	3.583	3.938	6
0.200 $\Delta$	9.554	10.983	1
0.150 $\Delta$	7.165	8.023	3
0.300 $\Delta$	14.330	16.790	1
0.225 $\Delta$	10.748	12.478	3
0.400 $\Delta$	19.107	22.478	1
0.300 $\Delta$	14.330	16.790	2
0.700 $\Delta$	33.438	39.368	1
0.525 $\Delta$	25.078	29.560	2
1.000 $\Delta$	47.768	56.665	1
0.750 $\Delta$	35.826	42.285	2
1.500 $\Delta$	71.652	85.060	1*
1.125 $\Delta$	53.739	63.761	2
2.000 $\Delta$	95.536	113.529	1*
1.500 $\Delta$	71.652	85.060	2*



**APPENDIX IV PICTURES OF FAILURE MODES**

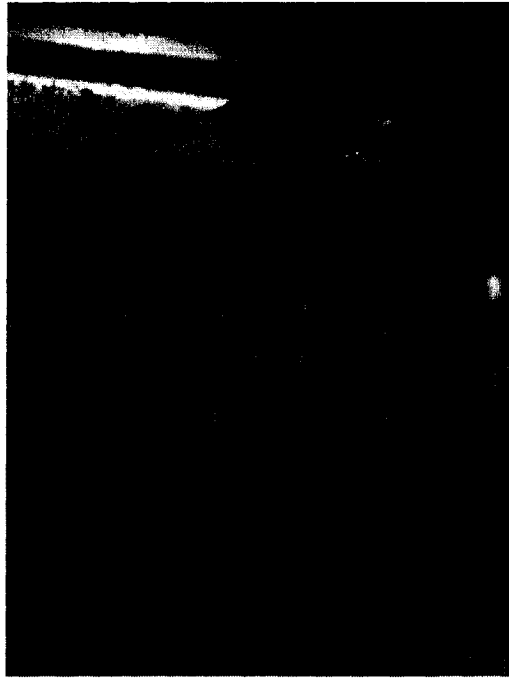


Figure A.IV-1 Tear-out of Sheathing

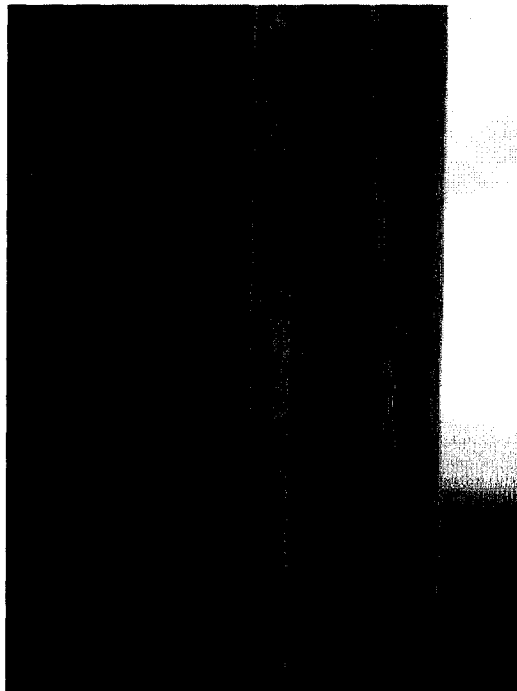


Figure A.IV-2 Pull-Through Sheathing (1)

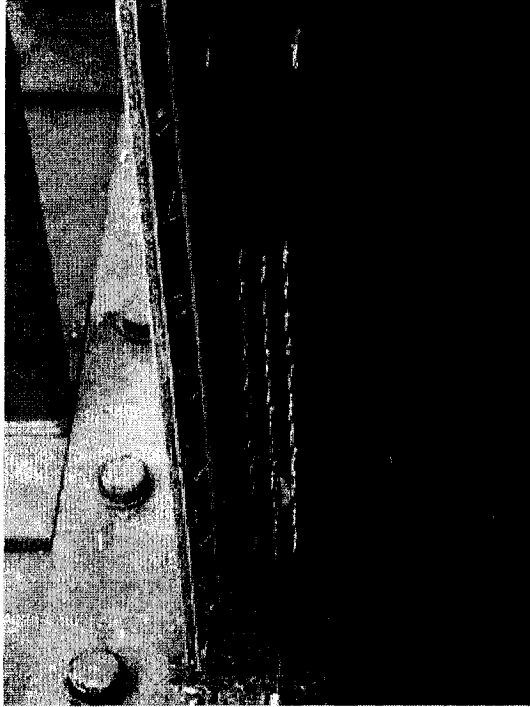


Figure A.IV-3 Pull-Through Sheathing (2)



Figure A.IV-4 Partial-Pull-Through Sheathing



Figure A.IV-5 Screw Shear Failure



Figure A.IV-6 Buckling of Track



Figure A.IV-7 Twist of Steel Track



Figure A.IV-8 Wood Bearing Failure

## APPENDIX V CALCULATION OF CAPACITY OF STUDS

The axial load capacity of an end chord is the minimum of the capacity of a hold-down connection, the capacity of the back-to-back stud connections, as well as tension and compression capacity of the stud (or studs) calculated according to the *North American Specification for the Design of Cold-formed Steel Structural Members* (CSA, 2001). The composite action of the studs and wood sheathing is neglected, however, the wood sheathing is assumed to act as the lateral brace in the minor axis of the built-up chord section. Calculations for the built-up chord section are first shown for the case when no web perforations exist, and then the case where web perforations are accounted for.

The sizes of a chord are shown in Figure A-V.1&2, and the longitudinal screw spacing along the axis of the stud is 12”.

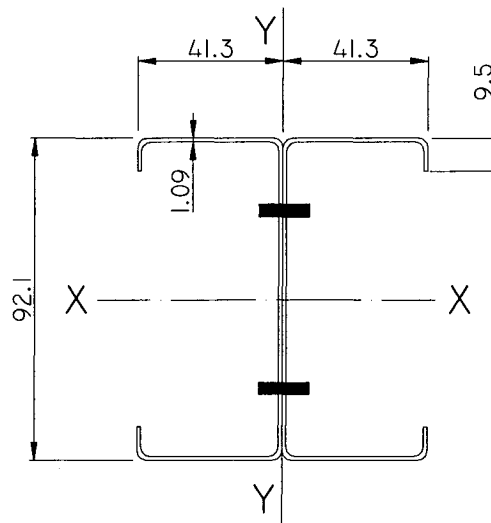


Figure A-V.1 Cross-Section of Chord Studs

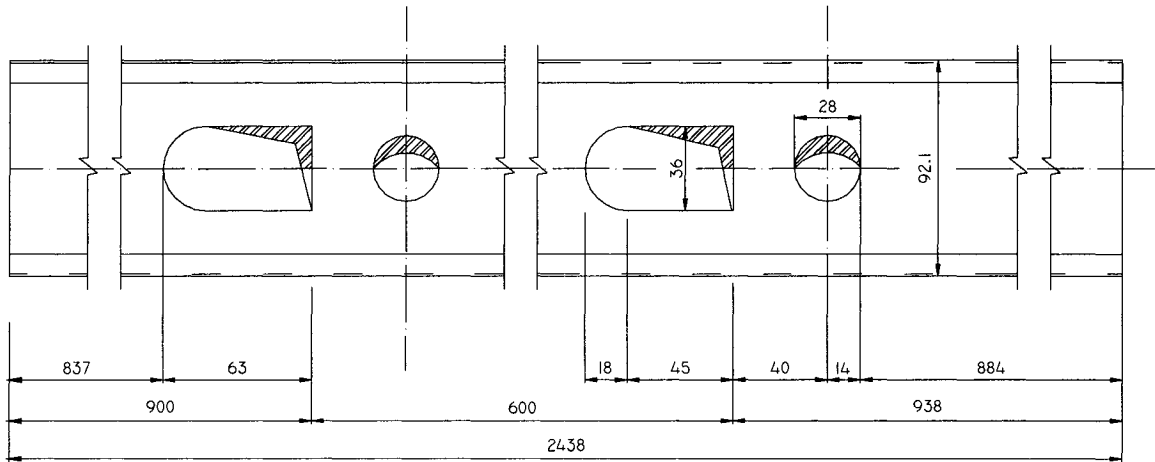


Figure A-V.2 Stud Dimensions and Hole Locations

The dimensions of a chord are shown in Figure A-V.1&2. The inside bend radius of the corners is assumed to be  $2 \times 1.09 = 2.18 \text{ mm}$  and hence  $r = 2.5 \times 1.09 = 2.725 \text{ mm}$ .

The mechanical properties:

$$F_y = 250.9 \text{ MPa}; F_u = 335.2 \text{ MPa}; F_u / F_y = 1.34; E = 197667 \text{ MPa};$$

$$\text{Elongation} = 38.5\%$$

$$\text{Web slenderness ratio: } w/t = (92.1 - 6 \times 1.09) / 1.09 = 78.5 < 500;$$

$$\text{Flange slenderness ratio: } w/t = (41.3 - 6 \times 1.09) / 1.09 = 31.9 < 60;$$

$$\text{Lip slenderness ratio: } w/t = (9.5 - 3 \times 1.09) / 1.09 = 5.72 < 60.$$

$$A_g = 2 \times 201.3 = 402.6 \text{ mm}^2; I_x = 2 \times 272254 = 544508 \text{ mm}^4; R_x = 36.8 \text{ mm}$$

$$I_y = 2 \times 77347 = 154694 \text{ mm}^4; R_y = 19.6 \text{ mm}.$$

$$\text{Distance between centroid of single stud and web centerline is: } \bar{x} = 12.691 \text{ mm};$$

1) Calculate  $P_n$  (CSA S136-01 Clause 4 (a), 4.5)

**Wall studs without perforation:**

$$k = 1.0;$$

$$k \times L_x / R_x = 1 \times 2438.4 / 36.8 = 66.3 < 200;$$

$$r_i = \sqrt{\frac{77347 - 201.3 \times 12.691^2}{201.3}} = 14.9; \quad \frac{a}{r_i} = \frac{12 \times 25.4}{14.9} = 20.5 < 0.5 \times 66.3 = 33.15;$$

$$(kL/R)_m = \sqrt{(66.3)^2 + (20.5)^2} = 69.4;$$

for studs with sheathing screws in 6-in spacing

$$k \times L_y / R_y = 1 \times 152.4 / 19.6 = 7.78 < 200;$$

for studs with sheathing screws in 4-in spacing

$$k \times L_y / R_y = 1 \times 101.6 / 19.6 = 5.18 < 200;$$

for studs with sheathing screws in 3-in spacing

$$k \times L_y / R_y = 1 \times 76.2 / 19.6 = 3.89 < 200; .$$

$$F_e = \frac{\pi^2 E}{(kL/R)^2} = \frac{\pi^2 \times 197667}{69.4^2} = 405.1 \text{MPa};$$

$$\lambda_c = \sqrt{\frac{f_y}{f_e}} = \sqrt{\frac{250.9}{405.1}} = 0.787 < 1.5; \quad F_n = (0.658^{\lambda_c}) \bullet f_y = 193.6 \text{MPa}.$$

Check the effective width of the webs:

$$F_{cr} = k \frac{\pi^2 E}{12(1-\mu^2)} \left(\frac{t}{w}\right)^2 = 4 \times \frac{\pi^2 \times 197667}{12 \times (1-0.3^2)} \times \left(\frac{1}{78.5}\right)^2 = 116 \text{MPa}.$$

$$\lambda = \sqrt{\frac{f_n}{F_{cr}}} = \sqrt{\frac{193.6}{116}} = 1.292 > 0.673; \quad \rho = \frac{(1-0.22/1.292)}{1.292} = 0.642;$$

$$b = \rho w = 0.642 \times 85.56 = 54.9 \text{mm};$$

Check the effective width of the flanges:

$$S = 1.28 \sqrt{\frac{E}{f}} = 1.28 \sqrt{\frac{197667}{193.6}} = 40.9; \quad w/t = 31.9 > 0.328S = 13.4;$$

$$I_a = 399 \times 1.09^4 \times \left[ \frac{31.9}{40.9} - 0.328 \right]^3 = 52 \text{ mm}^4 < 1.09^4 \left[ 115 \times \frac{31.9}{40.9} + 5 \right] = 133.7;$$

$$n = \left[ 0.582 - \frac{31.9}{4 \times 40.9} \right] = 0.387 > \frac{1}{3};$$

$$I_s = \frac{1.09 \times 6.23^3}{12} = 22.0 \text{ mm}^4; \quad R_I = \frac{I_s}{I_a} = \frac{22.0}{52} = 0.423;$$

$$D/w = 9.5/34.76 = 0.273 > 0.25 \text{ and } < 0.8$$

$$k = \left( 4.82 - \frac{5 \times 9.5}{34.76} \right) (0.423)^{0.387} + 0.43 = 2.91 < 4;$$

$$F_{cr} = k \frac{\pi^2 E}{12(1-\mu^2)} \left( \frac{t}{w} \right)^2 = 2.91 \times \frac{\pi^2 \times 197667}{12 \times (1-0.3^2)} \times \left( \frac{1}{31.9} \right)^2 = 510.9 \text{ MPa}.$$

$$\lambda = \sqrt{\frac{f_n}{F_{cr}}} = \sqrt{\frac{193.6}{510.9}} = 0.615 < 0.673; \quad b = w = 34.76 \text{ mm};$$

Check the effective width of the lips:

$$F_{cr} = k \frac{\pi^2 E}{12(1-\mu^2)} \left( \frac{t}{w} \right)^2 = 0.43 \times \frac{\pi^2 \times 197667}{12 \times (1-0.3^2)} \times \left( \frac{1}{5.72} \right)^2 = 2348 \text{ MPa}.$$

$$\lambda = \sqrt{\frac{f_n}{F_{cr}}} = \sqrt{\frac{193.6}{2348}} = 0.287 < 0.673; \quad ds' = w = 6.23 \text{ mm}.$$

$$ds = 0.423 \times 6.23 = 2.64 \text{ mm}.$$

$$A_e = 2 \times [201.3 - (85.56 - 54.9) \times 1.09 - 2 \times (6.23 - 2.64) \times 1.09] = 320.1 \text{ mm}^2;$$

$$P_n = A_e \times F_n = 320.1 \times 193.6 / 1000 = 62.0 \text{ kN}.$$

### Wall studs with perforation:

The requirement of Clause D4(a)-(1) ~ (5) are all satisfied in this case.

Check the effective width of the webs:

$$w = (92.1 - 36) / 2 - 3 \times 1.09 = 24.78 \text{ mm}$$

$$F_{cr} = k \frac{\pi^2 E}{12(1 - \mu^2)} \left(\frac{t}{w}\right)^2 = 0.43 \times \frac{\pi^2 \times 197667}{12 \times (1 - 0.3^2)} \times (1.09 / 24.78)^2 = 148.6 \text{ MPa.}$$

$$\lambda = \sqrt{\frac{f_n}{F_{cr}}} = \sqrt{\frac{193.6}{148.6}} = 1.141 > 0.673; \quad \rho = \frac{(1 - 0.22 / 1.141)}{1.141} = 0.707;$$

$$b = \rho w = 0.707 \times 24.78 = 17.5 \text{ mm};$$

Check the effective width of the flanges:

Same as previous calculation,  $b = 34.76 \text{ mm}$ .

Check the effective width of the lips:

Same as previous calculation,  $d_s = 2.64 \text{ mm}$ .

$$A_e = 2 \times [201.3 - (85.56 - 2 \times 17.5) \times 1.09 - 2 \times (6.23 - 2.64) \times 1.09] = 276.7 \text{ mm}^2;$$

$$P_n = A_e \times F_n = 276.7 \times 193.6 / 1000 = 53.6 \text{ kN}.$$

In this thesis, no gravity load was applied to the wall, so the axial load on the chord studs was produced solely by the sheathing connections. The shear flow along the screw lines on the chord studs caused axial forces to increase in a triangular fashion, with the maximum force at the bottom of the end studs and zero at the top (Figure A-V.3). The distance from the edge of the bottom hole in the web of the stud to the lower end of the chord measured 837 mm. Assuming that the chord stud will fail when the force at the

hole location reaches 53.6 kN, it can be hypothesised that the maximum load at the bottom of the studs would be 81.6 kN (Figure A-V.3) under this lateral loading scenario.

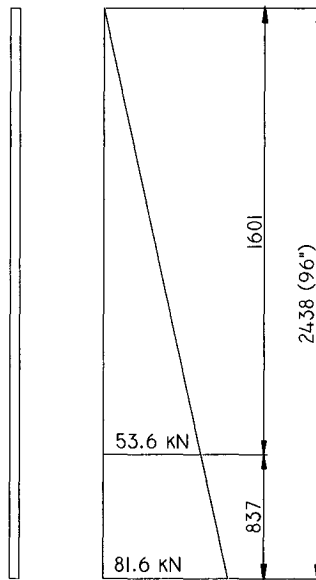


Figure A-V.3 Axial Force Diagram of an End Stud

**Tension capacity of the end studs:**

For sections with holes:

$$T_{studs} = A_n \times f_y = (402.6 - 2 \times 1.09 \times 36) \times 250.9 / 1000 = 81.3kN .$$

For full sections:

$$T_{studs} = A_g \times f_y = 402.6 \times 250.9 / 1000 = 101kN$$

2) Capacity of a hold-down: (The value is from the manufacturer’s website)

$$T_{hd} = 129kN.$$

3) Capacity of the stud connections for studs at panel joints:

(The shear value for single screw is from the manufacturer's website)

$$V = 9 \times 2 \times 1206 \times 4.44822 / 1000 = 96.6 \text{ kN}.$$

Conclusion:

Failure of a chord stud will occur when either the bottom of the stud reaches the full capacity (without holes) 62 kN, or when the force at the bottom hole location reaches 53.6 kN (corresponding force at the bottom end of the stud is 81.6 kN). Given this, it would be assumed that the bottom of the stud will always fail first. However, the bottom of the stud was reinforced by the hold-down connector, and hence the chord's true capacity, although difficult to determine, is certainly higher than 62.0 kN. In this case it is plausible that the force at the chord stud end could reach 81.6 kN, assuming a triangular axial force distribution, and then failure could take place at the first hole location. The information discussed in this section needs to be verified by further detailed research.

In summary, the capacity of the chord stud using the all steel method is 53.6 kN if a constant axial force exists. However, gravity loads were not applied in the tests contained in the thesis, hence the triangular axial force diagram was assumed to represent the compression force in the chord stud. Therefore, the nominal compression capacity of the chord stud, excluding the effect of the hold-downs, was assumed to be 62.0 kN. In practical design, resistance factors must be incorporated into the determination of the factored resistance. Additionally, gravity loads would create a more critical situation for the chord studs because of the higher axial load.

The lateral resistance of a shear wall due to the failure of the back-to-back chord studs, hold-down connections or stud connections is calculated as follows:

For 2 feet walls:

$$S_{y,wall} = 62.0 \times \left( \frac{2 \times 12 \times 25.4 - 170}{2438.4} \right) = 11.2 kN$$

For 4 feet walls:

$$S_{y,wall} = 62.0 \times \left( \frac{4 \times 12 \times 25.4 - 170}{2438.4} \right) = 26.7 kN$$

For 8 feet walls:

$$S_{y,wall} = 62.0 \times \left( \frac{8 \times 12 \times 25.4 - 170}{2438.4} \right) = 57.7 kN$$

**APPENDIX VI**

**COMPARISONS OF TEST RESULTS**

**AND PREDICTION FROM ANALYTICAL MODELS**

**I. MONOTONIC TESTS**

**(1) EEEP\_12.5**

Table A-VI.1  
Comparisons between Test Results and Prediction from Easley's Model

ID	Test Sy (kN)	Predictor (kN)	Ratio	Test Δ <sub>y</sub> (mm)	Predictor (mm)	Ratio
2x8 CSP 6"/12" M	5.02	3.36	1.495	18.9	5.20	3.628
2x8 CSP 4"/12" M	7.49	5.23	1.432	28.9	6.68	4.322
2x8 OSB 6"/12" M	6.12	4.19	1.463	16.9	4.76	3.559
2x8 OSB 4"/12" M	9.13	6.52	1.400	15.9	5.84	2.732
4x8 CSP 6"/12" M	13.6	7.23	1.877	13.0	3.90	3.328
4x8 CSP 4"/12" M	17.3	10.9	1.591	19.0	5.21	3.647
4x8 CSP 3"/12" M	26.2	14.5	1.807	19.7	6.49	3.038
4x8 OSB 6"/12" M	14.3	9.02	1.590	8.09	3.26	2.481
4x8 OSB 4"/12" M	21.1	13.6	1.557	10.2	4.17	2.451
4x8 OSB 3"/12" M	25.4	18.1	1.402	13.3	5.06	2.625
8x8 CSP 6"/12" M	29.1	14.5	2.011	11.6	3.90	2.963
8x8 CSP 4"/12" M	42.6	21.8	1.957	16.8	5.21	3.227
8x8 CSP 3"/12" M	52.7	29.0	1.816	19.1	6.49	2.944
Average			1.646			3.150
Standard Deviation			0.210			0.521
COV			0.128			0.166

Table A-VI.2

Comparisons between Test Results and Prediction from Kallsner & Lam's Elastic Model

ID	Test $S_y$ (kN)	Prediction (kN)	Ratio	Test $\Delta_c$ (mm)	Prediction (mm)	Ratio
2x8 CSP 6"/12" M	5.02	4.62	1.086	18.9	7.58	2.492
2x8 CSP 4"/12" M	7.49	6.90	1.084	28.9	9.24	3.126
2x8 OSB 6"/12" M	6.12	5.76	1.063	16.9	7.01	2.416
2x8 OSB 4"/12" M	9.13	8.61	1.060	15.9	8.17	1.952
4x8 CSP 6"/12" M	13.6	9.31	1.457	13.0	5.58	2.329
4x8 CSP 4"/12" M	17.3	13.9	1.249	19.0	7.19	2.642
4x8 CSP 3"/12" M	26.2	18.4	1.423	19.7	8.81	2.240
4x8 OSB 6"/12" M	14.3	11.6	1.235	8.09	4.81	1.682
4x8 OSB 4"/12" M	21.1	17.3	1.223	10.2	5.93	1.724
4x8 OSB 3"/12" M	25.4	23.0	1.104	13.3	7.05	1.885
8x8 CSP 6"/12" M	29.1	18.6	1.561	11.6	5.58	2.073
8x8 CSP 4"/12" M	42.6	27.7	1.537	16.8	7.19	2.338
8x8 CSP 3"/12" M	52.7	36.8	1.430	19.1	8.81	2.171
Average			1.270			2.236
Standard Deviation			0.181			0.380
COV			0.143			0.170

Table A-VI.3

Comparisons between Test Results and Prediction from Kallsner & Lam's Lower Plastic Model

ID	Test $S_y$ (kN)	Prediction (kN)	Ratio
2x8 CSP 6"/12" M	5.02	4.77	1.052
2x8 CSP 4"/12" M	7.49	7.15	1.047
2x8 OSB 6"/12" M	6.12	5.95	1.030
2x8 OSB 4"/12" M	9.13	8.92	1.023
4x8 CSP 6"/12" M	13.6	9.54	1.423
4x8 CSP 4"/12" M	17.3	14.3	1.211
4x8 CSP 3"/12" M	26.2	19.1	1.374
4x8 OSB 6"/12" M	14.3	11.9	1.206
4x8 OSB 4"/12" M	21.1	17.8	1.185
4x8 OSB 3"/12" M	25.4	23.8	1.066
8x8 CSP 6"/12" M	29.1	19.1	1.525
8x8 CSP 4"/12" M	42.6	28.6	1.489
8x8 CSP 3"/12" M	52.7	38.1	1.381
Average			1.232
Standard Deviation			0.178
COV			0.145

**Table A-VI.4**  
**Comparisons between Test Results and Prediction**  
**from Kallsner & Lam's Upper Plastic Model**

ID	Test Sy (kN)	Prediction (kN)	Ratio
2x8 CSP 6"/12" M	5.02	5.06	0.991
2x8 CSP 4"/12" M	7.49	7.58	0.987
2x8 OSB 6"/12" M	6.12	6.32	0.969
2x8 OSB 4"/12" M	9.13	9.46	0.965
4x8 CSP 6"/12" M	13.6	11.14	1.218
4x8 CSP 4"/12" M	17.3	16.5	1.050
4x8 CSP 3"/12" M	26.2	21.8	1.199
4x8 OSB 6"/12" M	14.3	13.9	1.032
4x8 OSB 4"/12" M	21.1	20.6	1.027
4x8 OSB 3"/12" M*	25.4	26.7	0.950
8x8 CSP 6"/12" M	29.1	22.3	1.305
8x8 CSP 4"/12" M	42.6	33.0	1.291
8x8 CSP 3"/12" M	52.7	43.7	1.205
Average			1.091
Standard Deviation			0.126
COV			0.116

Note: \* means the failure is controlled by the stud capacity.

**Table A-VI.5**  
**Comparisons between Test Results and Prediction from McCutcheon's Model**

ID	Test Sy (kN)	Prediction (kN)	Ratio	Test Δ <sub>u</sub> (mm)	Prediction (mm)	Ratio
2x8 CSP 6"/12" M	5.02	4.92	1.019	18.9	7.74	2.439
2x8 CSP 4"/12" M	7.49	7.34	1.019	28.9	9.50	3.039
2x8 OSB 6"/12" M	6.12	6.14	0.998	16.9	7.10	2.385
2x8 OSB 4"/12" M	9.13	9.16	0.997	15.9	8.33	1.915
4x8 CSP 6"/12" M	13.6	9.42	1.441	13.0	5.61	2.315
4x8 CSP 4"/12" M	17.3	14.1	1.228	19.0	7.27	2.612
4x8 CSP 3"/12" M	26.2	18.8	1.395	19.7	8.94	2.207
4x8 OSB 6"/12" M	14.3	11.8	1.221	8.09	4.83	1.674
4x8 OSB 4"/12" M	21.1	17.6	1.202	10.2	5.99	1.708
4x8 OSB 3"/12" M	25.4	23.4	1.082	13.3	7.15	1.860
8x8 CSP 6"/12" M	29.1	18.8	1.543	11.6	5.61	2.061
8x8 CSP 4"/12" M	42.6	28.2	1.511	16.8	7.27	2.311
8x8 CSP 3"/12" M	52.7	37.6	1.402	19.1	8.94	2.139
Average			1.235			2.205
Standard Deviation			0.196			0.365
COV			0.158			0.165

(2) Max. Load\_12.5&ke

Table A-VI.6  
Comparisons between Test Results and Prediction from Easley's Model

ID	Test $S_y$ (kN)	Prediction (kN)	Ratio	Test $S_y$ (mm)	Prediction (mm)	Ratio
2x8 CSP 6"/12" M	5.02	3.87	1.295	18.9	6.01	3.143
2x8 CSP 4"/12" M	7.49	6.03	1.241	28.9	7.71	3.744
2x8 OSB 6"/12" M	6.12	4.94	1.240	16.9	5.61	3.017
2x8 OSB 4"/12" M	9.13	7.69	1.187	15.9	6.88	2.316
4x8 CSP 6"/12" M	13.6	8.35	1.626	13.0	4.50	2.883
4x8 CSP 4"/12" M	17.3	12.6	1.378	19.0	6.01	3.160
4x8 CSP 3"/12" M	26.2	16.7	1.565	19.7	7.50	2.632
4x8 OSB 6"/12" M	14.3	10.6	1.348	8.09	3.85	2.103
4x8 OSB 4"/12" M	21.1	16.0	1.320	10.2	4.92	2.078
4x8 OSB 3"/12" M	25.4	21.3	1.189	13.3	5.97	2.225
8x8 CSP 6"/12" M	29.1	16.7	1.742	11.6	4.50	2.567
8x8 CSP 4"/12" M	42.6	25.1	1.695	16.8	6.01	2.795
8x8 CSP 3"/12" M	52.7	33.5	1.573	19.1	7.50	2.550
Average			1.415			2.709
Standard Deviation			0.190			0.464
COV			0.134			0.171

Table A-VI.7

Comparisons between Test Results and Prediction from Kallsner & Lam's Elastic Model

ID	Test Sy (kN)	Prediction (kN)	Ratio	Test $\epsilon_c$ (mm)	Prediction (mm)	Ratio
2x8 CSP 6"/12" M	5.02	5.33	0.941	18.9	8.75	2.158
2x8 CSP 4"/12" M	7.49	7.97	0.939	28.9	10.67	2.708
2x8 OSB 6"/12" M	6.12	6.80	0.901	16.9	8.27	2.048
2x8 OSB 4"/12" M	9.13	10.16	0.899	15.9	9.63	1.655
4x8 CSP 6"/12" M	13.6	10.75	1.262	13.0	6.44	2.018
4x8 CSP 4"/12" M	17.3	16.0	1.082	19.0	8.30	2.289
4x8 CSP 3"/12" M	26.2	21.3	1.233	19.7	10.17	1.940
4x8 OSB 6"/12" M	14.3	13.7	1.047	8.09	5.67	1.426
4x8 OSB 4"/12" M	21.1	20.4	1.037	10.2	7.00	1.462
4x8 OSB 3"/12" M*	25.4	26.7	0.950	13.3	8.32	1.598
8x8 CSP 6"/12" M	29.1	21.5	1.352	11.6	6.44	1.796
8x8 CSP 4"/12" M	42.6	32.0	1.331	16.8	8.30	2.025
8x8 CSP 3"/12" M	52.7	42.5	1.239	19.1	10.17	1.880
Average			1.093			1.923
Standard Deviation			0.162			0.339
COV			0.148			0.176

Table A-VI.8

Comparisons between Test Results and Prediction from Kallsner & Lam's Lower Plastic Model

ID	Test Sy (kN)	Prediction (kN)	Ratio
2x8 CSP 6"/12" M	5.02	5.50	0.912
2x8 CSP 4"/12" M	7.49	8.26	0.907
2x8 OSB 6"/12" M	6.12	7.02	0.873
2x8 OSB 4"/12" M	9.13	10.52	0.867
4x8 CSP 6"/12" M	13.6	11.01	1.233
4x8 CSP 4"/12" M	17.3	16.5	1.049
4x8 CSP 3"/12" M	26.2	22.0	1.190
4x8 OSB 6"/12" M	14.3	14.0	1.022
4x8 OSB 4"/12" M	21.1	21.0	1.005
4x8 OSB 3"/12" M*	25.4	26.7	0.950
8x8 CSP 6"/12" M	29.1	22.0	1.321
8x8 CSP 4"/12" M	42.6	33.0	1.290
8x8 CSP 3"/12" M	52.7	44.0	1.196
Average			1.063
Standard Deviation			0.157
COV			0.148

Table A-VI.9  
Comparisons between Test Results and Prediction  
from Kallsner & Lam's Upper Plastic Model

ID	Test S <sub>y</sub> (kN)	Prediction (kN)	Ratio
2x8 CSP 6"/12" M	5.02	5.85	0.858
2x8 CSP 4"/12" M	7.49	8.75	0.855
2x8 OSB 6"/12" M	6.12	7.45	0.822
2x8 OSB 4"/12" M	9.13	11.16	0.818
4x8 CSP 6"/12" M	13.6	12.86	1.055
4x8 CSP 4"/12" M	17.3	19.0	0.909
4x8 CSP 3"/12" M	26.2	25.2	1.039
4x8 OSB 6"/12" M	14.3	16.4	0.875
4x8 OSB 4"/12" M	21.1	24.3	0.871
4x8 OSB 3"/12" M*	25.4	26.7	0.950
8x8 CSP 6"/12" M	29.1	25.7	1.130
8x8 CSP 4"/12" M	42.6	38.1	1.118
8x8 CSP 3"/12" M	52.7	50.4	1.044
Average			0.950
Standard Deviation			0.109
COV			0.114

Table A-VI.10  
Comparisons between Test Results and Prediction from McCutcheon's Model

ID	Test S <sub>y</sub> (kN)	Prediction (kN)	Ratio	Test S <sub>y</sub> (kN)	Prediction (kN)	Ratio
2x8 CSP 6"/12" M	5.02	5.68	0.883	18.9	8.94	2.113
2x8 CSP 4"/12" M	7.49	8.48	0.883	28.9	10.97	2.633
2x8 OSB 6"/12" M	6.12	7.24	0.846	16.9	8.38	2.022
2x8 OSB 4"/12" M	9.13	10.81	0.845	15.9	9.82	1.623
4x8 CSP 6"/12" M	13.6	10.88	1.248	13.0	6.48	2.005
4x8 CSP 4"/12" M	17.3	16.3	1.064	19.0	8.40	2.263
4x8 CSP 3"/12" M	26.2	21.7	1.208	19.7	10.32	1.912
4x8 OSB 6"/12" M	14.3	13.9	1.035	8.09	5.70	1.419
4x8 OSB 4"/12" M	21.1	20.7	1.019	10.2	7.06	1.448
4x8 OSB 3"/12" M*	25.4	26.7	0.950	13.3	8.26	1.609
8x8 CSP 6"/12" M	29.1	21.8	1.337	11.6	6.48	1.785
8x8 CSP 4"/12" M	42.6	32.6	1.309	16.8	8.40	2.002
8x8 CSP 3"/12" M	52.7	43.4	1.214	19.1	10.32	1.853
Average			1.065			1.899
Standard Deviation			0.173			0.324
COV			0.162			0.171

(3) Max. Load\_12.5&ks

Table A-VI.11  
Comparisons between Test Results and Prediction from Easley's Model

ID	Test (kN)	Prediction (kN)	Ratio	Test (mm)	Prediction (mm)	Ratio
2x8 CSP 6"/12" M	5.02	3.87	1.295	18.9	39.1	0.483
2x8 CSP 4"/12" M	7.49	6.03	1.241	28.9	42.2	0.685
2x8 OSB 6"/12" M	6.12	4.94	1.240	16.9	27.8	0.609
2x8 OSB 4"/12" M	9.13	7.69	1.187	15.9	30.0	0.531
4x8 CSP 6"/12" M	13.6	8.35	1.626	13.0	20.4	0.637
4x8 CSP 4"/12" M	17.3	12.6	1.378	19.0	22.0	0.864
4x8 CSP 3"/12" M	26.2	16.7	1.565	19.7	23.5	0.840
4x8 OSB 6"/12" M	14.3	10.6	1.348	8.09	14.5	0.557
4x8 OSB 4"/12" M	21.1	16.0	1.320	10.2	15.7	0.653
4x8 OSB 3"/12" M	25.4	21.3	1.189	13.3	16.7	0.796
8x8 CSP 6"/12" M	29.1	16.7	1.742	11.6	20.4	0.567
8x8 CSP 4"/12" M	42.6	25.1	1.695	16.8	22.0	0.764
8x8 CSP 3"/12" M	52.7	33.5	1.573	19.1	23.5	0.814
Average			1.415			0.677
Standard Deviation			0.190			0.122
COV			0.134			0.181

Table A-VI.12

Comparisons between Test Results and Prediction from Kallsner & Lam's Elastic Model

ID	Test Sy (kN)	Prediction (kN)	Ratio	Test Sy (kN)	Prediction (kN)	Ratio
2x8 CSP 6"/12" M	5.02	5.33	0.941	18.9	59.2	0.319
2x8 CSP 4"/12" M	7.49	7.97	0.939	28.9	61.1	0.473
2x8 OSB 6"/12" M	6.12	6.80	0.901	16.9	42.1	0.402
2x8 OSB 4"/12" M	9.13	10.2	0.899	15.9	43.5	0.366
4x8 CSP 6"/12" M	13.6	10.8	1.262	13.0	33.5	0.388
4x8 CSP 4"/12" M	17.3	16.0	1.082	19.0	35.3	0.538
4x8 CSP 3"/12" M	26.2	21.3	1.233	19.7	37.2	0.531
4x8 OSB 6"/12" M	14.3	13.7	1.047	8.09	23.8	0.339
4x8 OSB 4"/12" M	21.1	20.4	1.037	10.2	25.1	0.407
4x8 OSB 3"/12" M*	25.4	26.7	0.950	13.3	26.4	0.503
8x8 CSP 6"/12" M	29.1	21.5	1.352	11.6	33.5	0.345
8x8 CSP 4"/12" M	42.6	32.0	1.331	16.8	35.3	0.476
8x8 CSP 3"/12" M	52.7	42.5	1.239	19.1	37.2	0.514
Average			1.093			0.431
Standard Deviation			0.162			0.075
COV			0.148			0.174

Table A-VI.13

Comparisons between Test Results and Prediction from Kallsner & Lam's Lower Plastic Model

ID	Test Sy (kN)	Prediction (kN)	Ratio
2x8 CSP 6"/12" M	5.02	5.50	0.912
2x8 CSP 4"/12" M	7.49	8.26	0.907
2x8 OSB 6"/12" M	6.12	7.02	0.873
2x8 OSB 4"/12" M	9.13	10.5	0.867
4x8 CSP 6"/12" M	13.6	11.0	1.233
4x8 CSP 4"/12" M	17.3	16.5	1.049
4x8 CSP 3"/12" M	26.2	22.0	1.190
4x8 OSB 6"/12" M	14.3	14.0	1.022
4x8 OSB 4"/12" M	21.1	21.0	1.005
4x8 OSB 3"/12" M*	25.4	26.7	0.950
8x8 CSP 6"/12" M	29.1	22.0	1.321
8x8 CSP 4"/12" M	42.6	33.0	1.290
8x8 CSP 3"/12" M	52.7	44.0	1.196
Average			1.063
Standard Deviation			0.157
COV			0.148

Table A-VI.14  
Comparisons between Test Results and Prediction  
from Kallsner & Lam's Upper Plastic Model

ID	Test Sv (kN)	Prediction (kN)	Ratio
2x8 CSP 6"/12" M	5.02	5.85	0.858
2x8 CSP 4"/12" M	7.49	8.75	0.855
2x8 OSB 6"/12" M	6.12	7.45	0.822
2x8 OSB 4"/12" M*	9.13	11.2	0.818
4x8 CSP 6"/12" M	13.6	12.9	1.055
4x8 CSP 4"/12" M	17.3	19.0	0.909
4x8 CSP 3"/12" M	26.2	25.2	1.039
4x8 OSB 6"/12" M	14.3	16.4	0.875
4x8 OSB 4"/12" M	21.1	24.3	0.871
4x8 OSB 3"/12" M*	25.4	26.7	0.950
8x8 CSP 6"/12" M	29.1	25.7	1.130
8x8 CSP 4"/12" M	42.6	38.1	1.118
8x8 CSP 3"/12" M	52.7	50.4	1.044
Average			0.950
Standard Deviation			0.109
COV			0.114

Table A-VI.15  
Comparisons between Test Results and Prediction from McCutcheon's Model

ID	Test Sv (kN)	Prediction (kN)	Ratio	Test Sv (kN)	Prediction (kN)	Ratio
2x8 CSP 6"/12" M	5.02	5.68	0.883	18.9	58.7	0.322
2x8 CSP 4"/12" M	7.49	8.48	0.883	28.9	60.8	0.475
2x8 OSB 6"/12" M	6.12	7.24	0.846	16.9	41.8	0.405
2x8 OSB 4"/12" M	9.13	10.8	0.845	15.9	43.2	0.369
4x8 CSP 6"/12" M	13.6	10.9	1.248	13.0	33.5	0.388
4x8 CSP 4"/12" M	17.3	16.3	1.064	19.0	35.4	0.537
4x8 CSP 3"/12" M	26.2	21.7	1.208	19.7	37.3	0.529
4x8 OSB 6"/12" M	14.3	13.9	1.035	8.09	23.8	0.340
4x8 OSB 4"/12" M	21.1	20.7	1.019	10.2	25.2	0.406
4x8 OSB 3"/12" M*	25.4	26.7	0.950	13.3	26.0	0.511
8x8 CSP 6"/12" M	29.1	21.8	1.337	11.6	33.5	0.345
8x8 CSP 4"/12" M	42.6	32.6	1.309	16.8	35.4	0.475
8x8 CSP 3"/12" M	52.7	43.4	1.214	19.1	37.3	0.512
Average			1.065			0.432
Standard Deviation			0.173			0.075
COV			0.162			0.173

(4) EEEP\_25

Table A-VI.16  
Comparisons between Test Results and Prediction from Easley's Model

ID	Test (kN)	Prediction (kN)	Ratio	Test (kN) / Prediction (kN)	Prediction (kN) / Test (kN)	R <sup>2</sup>
2x8 CSP 6"/12" M	5.02	4.19	1.199	18.9	8.48	2.227
2x8 CSP 4"/12" M	7.49	6.52	1.148	28.9	10.41	2.776
2x8 OSB 6"/12" M	6.12	4.62	1.324	16.9	9.65	1.755
2x8 OSB 4"/12" M	9.13	7.20	1.267	15.9	11.03	1.445
4x8 CSP 6"/12" M	13.6	9.02	1.505	13.0	5.82	2.231
4x8 CSP 4"/12" M	17.3	13.6	1.275	19.0	7.46	2.547
4x8 CSP 3"/12" M	26.2	18.1	1.448	19.7	9.06	2.177
4x8 DFP 6"/12" M	16.6	14.4	1.158	15.9	7.00	2.271
4x8 DFP 4"/12" M	25.4	21.6	1.173	20.9	8.45	2.468
4x8 DFP 3"/12" M*	30.1	26.7	1.127	18.9	9.28	2.038
4x8 OSB 6"/12" M	14.3	10.0	1.439	8.09	5.72	1.415
4x8 OSB 4"/12" M	21.1	15.0	1.409	10.2	6.74	1.518
4x8 OSB 3"/12" M	25.4	20.0	1.269	13.3	7.72	1.722
8x8 CSP 6"/12" M	29.1	18.0	1.612	11.6	5.82	1.985
8x8 CSP 4"/12" M	42.6	27.2	1.568	16.8	7.46	2.254
8x8 CSP 3"/12" M	52.7	36.2	1.456	19.1	9.06	2.110
Average			1.336			2.059
Standard Deviation			0.152			0.385
COV			0.114			0.187

Table A-VI.17

Comparisons between Test Results and Prediction from Kallsner &amp; Lam's Elastic Model

ID	Test $S_y$ (kN)	Prediction (kN)	Ratio	Test $\Delta_{top}$ (mm)	Prediction (mm)	Ratio
2x8 CSP 6"/12" M	5.02	5.76	0.871	18.9	12.5	1.513
2x8 CSP 4"/12" M	7.49	8.61	0.869	28.9	14.6	1.984
2x8 OSB 6"/12" M	6.12	6.37	0.962	16.9	14.5	1.172
2x8 OSB 4"/12" M	9.13	9.52	0.959	15.9	15.7	1.013
4x8 CSP 6"/12" M	13.6	11.6	1.168	13.0	8.58	1.514
4x8 CSP 4"/12" M	17.3	17.3	1.001	19.0	10.6	1.794
4x8 CSP 3"/12" M	26.2	23.0	1.141	19.7	12.6	1.565
4x8 DFP 6"/12" M	16.6	18.5	0.899	15.9	10.7	1.481
4x8 DFP 4"/12" M*	25.4	26.7	0.950	20.9	12.3	1.694
4x8 DFP 3"/12" M*	30.1	26.7	1.127	18.9	10.6	1.787
4x8 OSB 6"/12" M	14.3	12.8	1.117	8.09	8.91	0.908
4x8 OSB 4"/12" M	21.1	19.1	1.107	10.2	10.1	1.008
4x8 OSB 3"/12" M	25.4	25.4	0.999	13.3	11.4	1.168
8x8 CSP 6"/12" M	29.1	23.2	1.251	11.6	8.58	1.347
8x8 CSP 4"/12" M	42.6	34.6	1.232	16.8	10.6	1.587
8x8 CSP 3"/12" M	52.7	45.9	1.146	19.1	12.6	1.516
Average			1.050			1.441
Standard Deviation			0.122			0.303
COV			0.116			0.210

Table A-VI.18

Comparisons between Test Results and Prediction from Kallsner &amp; Lam's Lower Plastic Model

ID	Test $S_y$ (kN)	Prediction (kN)	Ratio
2x8 CSP 6"/12" M	5.02	5.95	0.843
2x8 CSP 4"/12" M	7.49	8.92	0.839
2x8 OSB 6"/12" M	6.12	6.57	0.932
2x8 OSB 4"/12" M	9.13	9.86	0.926
4x8 CSP 6"/12" M	13.6	11.9	1.141
4x8 CSP 4"/12" M	17.3	17.8	0.970
4x8 CSP 3"/12" M	26.2	23.8	1.101
4x8 DFP 6"/12" M	16.6	18.9	0.878
4x8 DFP 4"/12" M*	25.4	26.7	0.950
4x8 DFP 3"/12" M*	30.1	26.7	1.127
4x8 OSB 6"/12" M	14.3	13.1	1.091
4x8 OSB 4"/12" M	21.1	19.7	1.072
4x8 OSB 3"/12" M	25.4	26.3	0.965
8x8 CSP 6"/12" M	29.1	23.8	1.222
8x8 CSP 4"/12" M	42.6	35.7	1.194
8x8 CSP 3"/12" M	52.7	47.6	1.107
Average			1.022
Standard Deviation			0.120
COV			0.117

**Table A-VI.19**  
**Comparisons between Test Results and Prediction**  
**from Kallsner & Lam's Upper Plastic Model**

ID	Test (kN)	Prediction (kN)	Ratio
2x8 CSP 6"/12" M	5.02	6.32	0.794
2x8 CSP 4"/12" M	7.49	9.46	0.791
2x8 OSB 6"/12" M	6.12	6.98	0.877
2x8 OSB 4"/12" M	9.13	10.5	0.873
4x8 CSP 6"/12" M	13.6	13.9	0.976
4x8 CSP 4"/12" M	17.3	20.6	0.841
4x8 CSP 3"/12" M*	26.2	26.7	0.981
4x8 DFP 6"/12" M	16.6	22.1	0.751
4x8 DFP 4"/12" M*	25.4	26.7	0.950
4x8 DFP 3"/12" M*	30.1	26.7	1.127
4x8 OSB 6"/12" M	14.3	15.4	0.934
4x8 OSB 4"/12" M	21.1	22.7	0.930
4x8 OSB 3"/12" M*	25.4	26.7	0.950
8x8 CSP 6"/12" M	29.1	27.8	1.046
8x8 CSP 4"/12" M	42.6	41.2	1.035
8x8 CSP 3"/12" M	52.7	54.5	0.966
Average			0.927
Standard Deviation			0.098
COV			0.106

**Table A-VI.20**  
**Comparisons between Test Results and Prediction from McCutcheon's Model**

ID	Test (kN)	Prediction (kN)	Ratio	Test Avg. (mm)	Prediction (mm)	Ratio
2x8 CSP 6"/12" M	5.02	6.14	0.817	18.9	12.6	1.493
2x8 CSP 4"/12" M	7.49	9.16	0.817	28.9	14.8	1.946
2x8 OSB 6"/12" M	6.12	6.78	0.903	16.9	14.5	1.171
2x8 OSB 4"/12" M	9.13	10.1	0.902	15.9	15.8	1.008
4x8 CSP 6"/12" M	13.6	11.8	1.155	13.0	8.6	1.507
4x8 CSP 4"/12" M	17.3	17.6	0.984	19.0	10.7	1.776
4x8 CSP 3"/12" M	26.2	23.4	1.118	19.7	12.8	1.544
4x8 DFP 6"/12" M	16.6	18.7	0.889	15.9	10.8	1.477
4x8 DFP 4"/12" M*	25.4	26.7	0.950	20.9	12.2	1.711
4x8 DFP 3"/12" M*	30.1	26.7	1.127	18.9	10.5	1.805
4x8 OSB 6"/12" M	14.3	13.0	1.105	8.09	8.9	0.906
4x8 OSB 4"/12" M	21.1	19.4	1.088	10.2	10.2	1.002
4x8 OSB 3"/12" M	25.4	25.9	0.980	13.3	11.5	1.157
8x8 CSP 6"/12" M	29.1	23.5	1.237	11.6	8.62	1.341
8x8 CSP 4"/12" M	42.6	35.2	1.211	16.8	10.7	1.571
8x8 CSP 3"/12" M	52.7	46.9	1.124	19.1	12.8	1.497
Average			1.025			1.432
Standard Deviation			0.132			0.300
COV			0.129			0.209

(5) Max. Load<sub>25&ke</sub>

Table A-VI.21  
Comparisons between Test Results and Prediction from Easley's Model

ID	Test (kN)	Prediction (kN)	Ratio	Test (kips)	Prediction (kips)	Ratio
2x8 CSP 6"/12" M	5.02	4.90	1.024	18.9	9.92	1.904
2x8 CSP 4"/12" M	7.49	7.63	0.981	28.9	12.2	2.372
2x8 OSB 6"/12" M	6.12	5.50	1.113	16.9	11.5	1.475
2x8 OSB 4"/12" M	9.13	8.57	1.065	15.9	13.1	1.215
4x8 CSP 6"/12" M	13.6	10.6	1.286	13.0	6.81	1.906
4x8 CSP 4"/12" M	17.3	15.9	1.090	19.0	8.73	2.177
4x8 CSP 3"/12" M	26.2	21.2	1.238	19.7	10.6	1.861
4x8 DFP 6"/12" M	16.6	17.4	0.958	15.9	8.45	1.880
4x8 DFP 4"/12" M	25.4	26.1	0.971	20.9	10.2	2.042
4x8 DFP 3"/12" M*	30.1	26.7	1.127	18.9	9.28	2.038
4x8 OSB 6"/12" M	14.3	11.9	1.210	8.09	6.80	1.189
4x8 OSB 4"/12" M	21.1	17.9	1.184	10.2	8.01	1.276
4x8 OSB 3"/12" M	25.4	23.8	1.066	13.3	9.19	1.447
8x8 CSP 6"/12" M	29.1	21.1	1.378	11.6	6.81	1.697
8x8 CSP 4"/12" M	42.6	31.8	1.340	16.8	8.73	1.926
8x8 CSP 3"/12" M	52.7	42.3	1.244	19.1	10.6	1.803
Average			1.142			1.763
Standard Deviation			0.127			0.339
COV			0.112			0.192

Table A-VI.22

Comparisons between Test Results and Prediction from Kallsner &amp; Lam's Elastic Model

ID	Test $S_y$ (kN)	Prediction (kN)	Ratio	Test $\Delta_{top}$ (mm)	P. $\Delta_{top}$ (mm)	Ratio
2x8 CSP 6"/12" M	5.02	6.74	0.744	18.9	14.6	1.293
2x8 CSP 4"/12" M	7.49	10.1	0.743	28.9	17.0	1.696
2x8 OSB 6"/12" M	6.12	7.58	0.808	16.9	17.2	0.985
2x8 OSB 4"/12" M*	9.13	11.2	0.815	15.9	18.7	0.852
4x8 CSP 6"/12" M	13.6	13.6	0.998	13.0	10.0	1.293
4x8 CSP 4"/12" M	17.3	20.2	0.856	19.0	12.4	1.533
4x8 CSP 3"/12" M*	26.2	26.7	0.981	19.7	14.8	1.337
4x8 DFP 6"/12" M	16.6	22.3	0.744	15.9	13.0	1.225
4x8 DFP 4"/12" M*	25.4	26.7	0.950	20.9	12.3	1.694
4x8 DFP 3"/12" M*	30.1	26.7	1.127	18.9	10.6	1.787
4x8 OSB 6"/12" M	14.3	15.3	0.939	8.09	10.6	0.763
4x8 OSB 4"/12" M	21.1	22.7	0.930	10.2	12.1	0.847
4x8 OSB 3"/12" M*	25.4	26.7	0.950	13.3	12.2	1.094
8x8 CSP 6"/12" M	29.1	27.2	1.069	11.6	10.0	1.151
8x8 CSP 4"/12" M	42.6	40.5	1.053	16.8	12.4	1.356
8x8 CSP 3"/12" M	52.7	53.8	0.980	19.1	14.8	1.296
Average			0.918			1.263
Standard Deviation			0.117			0.301
COV			0.128			0.238

Table A-VI.23

Comparisons between Test Results and Prediction from Kallsner &amp; Lam's Lower Plastic Model

ID	Test $S_y$ (kN)	Prediction (kN)	Ratio
2x8 CSP 6"/12" M	5.02	6.96	0.721
2x8 CSP 4"/12" M	7.49	10.4	0.717
2x8 OSB 6"/12" M	6.12	7.82	0.783
2x8 OSB 4"/12" M*	9.13	11.2	0.815
4x8 CSP 6"/12" M	13.6	13.9	0.975
4x8 CSP 4"/12" M	17.3	20.9	0.829
4x8 CSP 3"/12" M*	26.2	26.7	0.981
4x8 DFP 6"/12" M	16.6	22.9	0.727
4x8 DFP 4"/12" M*	25.4	26.7	0.950
4x8 DFP 3"/12" M*	30.1	26.7	1.127
4x8 OSB 6"/12" M	14.3	15.6	0.917
4x8 OSB 4"/12" M	21.1	23.5	0.901
4x8 OSB 3"/12" M*	25.4	26.7	0.950
8x8 CSP 6"/12" M	29.1	27.8	1.045
8x8 CSP 4"/12" M	42.6	41.8	1.020
8x8 CSP 3"/12" M	52.7	55.7	0.946
Average			0.900
Standard Deviation			0.119
COV			0.133

Table A-VI.24  
Comparisons between Test Results and Prediction  
from Kallsner & Lam's Upper Plastic Model

ID	Test S <sub>y</sub> (kN)	Prediction (kN)	Ratio
2x8 CSP 6"/12" M	5.02	7.39	0.679
2x8 CSP 4"/12" M	7.49	11.1	0.676
2x8 OSB 6"/12" M	6.12	8.31	0.737
2x8 OSB 4"/12" M*	9.13	11.2	0.815
4x8 CSP 6"/12" M	13.6	16.3	0.834
4x8 CSP 4"/12" M	17.3	24.1	0.719
4x8 CSP 3"/12" M*	26.2	26.7	0.981
4x8 DFP 6"/12" M	16.6	26.7	0.622
4x8 DFP 4"/12" M*	25.4	26.7	0.950
4x8 DFP 3"/12" M*	30.1	26.7	1.127
4x8 OSB 6"/12" M	14.3	18.3	0.785
4x8 OSB 4"/12" M*	21.1	26.7	0.792
4x8 OSB 3"/12" M*	25.4	26.7	0.950
8x8 CSP 6"/12" M	29.1	32.5	0.894
8x8 CSP 4"/12" M	42.6	48.2	0.884
8x8 CSP 3"/12" M*	52.7	57.7	0.913
Average			0.835
Standard Deviation			0.129
COV			0.155

Table A-VI.25  
Comparisons between Test Results and Prediction from McCutcheon's Model

ID	Test S <sub>y</sub> (kN)	Prediction (kN)	Ratio	Test S <sub>y</sub> (kN)	Prediction (kN)	Ratio
2x8 CSP 6"/12" M	5.02	7.18	0.698	18.9	14.8	1.276
2x8 CSP 4"/12" M	7.49	10.7	0.698	28.9	17.4	1.663
2x8 OSB 6"/12" M	6.12	8.07	0.759	16.9	17.2	0.984
2x8 OSB 4"/12" M*	9.13	11.2	0.815	15.9	17.7	0.903
4x8 CSP 6"/12" M	13.6	13.8	0.987	13.0	10.1	1.287
4x8 CSP 4"/12" M	17.3	20.6	0.841	19.0	12.5	1.518
4x8 CSP 3"/12" M*	26.2	26.7	0.981	19.7	14.8	1.335
4x8 DFP 6"/12" M	16.6	22.6	0.736	15.9	13.0	1.222
4x8 DFP 4"/12" M*	25.4	26.7	0.950	20.9	12.2	1.711
4x8 DFP 3"/12" M*	30.1	26.7	1.127	18.9	10.5	1.805
4x8 OSB 6"/12" M	14.3	15.5	0.928	8.09	10.6	0.761
4x8 OSB 4"/12" M	21.1	23.1	0.914	10.2	12.1	0.842
4x8 OSB 3"/12" M*	25.4	26.7	0.950	13.3	12.0	1.106
8x8 CSP 6"/12" M	29.1	27.5	1.057	11.6	10.1	1.146
8x8 CSP 4"/12" M	42.6	41.2	1.035	16.8	12.5	1.343
8x8 CSP 3"/12" M	52.7	54.8	0.960	19.1	14.9	1.279
Average			0.902			1.261
Standard Deviation			0.127			0.297
COV			0.140			0.235

(6) Max. Load\_25&ks

Table A-VI.26  
Comparisons between Test Results and Prediction from Easley's Model

Specimen	Test Result (k)	Prediction (k)	Ratio	Test Result (k)	Prediction (k)	Ratio
2x8 CSP 6"/12" M	5.02	4.90	1.024	18.9	52.4	0.360
2x8 CSP 4"/12" M	7.49	7.63	0.981	28.9	56.5	0.511
2x8 OSB 6"/12" M	6.12	5.50	1.113	16.9	58.0	0.292
2x8 OSB 4"/12" M	9.13	8.57	1.065	15.9	61.6	0.259
4x8 CSP 6"/12" M	13.6	10.6	1.286	13.0	27.3	0.476
4x8 CSP 4"/12" M	17.3	15.9	1.090	19.0	29.3	0.649
4x8 CSP 3"/12" M	26.2	21.2	1.238	19.7	31.1	0.633
4x8 DFP 6"/12" M	16.6	17.4	0.958	15.9	34.9	0.456
4x8 DFP 4"/12" M	25.4	26.1	0.971	20.9	36.8	0.567
4x8 DFP 3"/12" M*	30.1	26.7	1.127	18.9	30.0	0.631
4x8 OSB 6"/12" M	14.3	11.9	1.210	8.09	29.2	0.277
4x8 OSB 4"/12" M	21.1	17.9	1.184	10.2	30.5	0.335
4x8 OSB 3"/12" M	25.4	23.8	1.066	13.3	31.7	0.420
8x8 CSP 6"/12" M	29.1	21.1	1.378	11.6	27.3	0.424
8x8 CSP 4"/12" M	42.6	31.8	1.340	16.8	29.3	0.574
8x8 CSP 3"/12" M	52.7	42.3	1.244	19.1	31.1	0.614
Average			1.142			0.467
Standard Deviation			0.127			0.131
COV			0.112			0.281

Table A-VI.27

Comparisons between Test Results and Prediction from Kallsner & Lam's Elastic Model

ID	Test S <sub>y</sub> (kN)	Prediction (kN)	Ratio	Test S <sub>y</sub> (kN)	Prediction (kN)	Ratio
2x8 CSP 6"/12" M	5.02	6.74	0.744	18.9	79.5	0.238
2x8 CSP 4"/12" M	7.49	10.1	0.743	28.9	81.9	0.353
2x8 OSB 6"/12" M	6.12	7.58	0.808	16.9	88.2	0.192
2x8 OSB 4"/12" M*	9.13	11.2	0.815	15.9	89.7	0.178
4x8 CSP 6"/12" M	13.6	13.6	0.998	13.0	44.8	0.290
4x8 CSP 4"/12" M	17.3	20.2	0.856	19.0	47.1	0.403
4x8 CSP 3"/12" M*	26.2	26.7	0.981	19.7	49.5	0.399
4x8 DFP 6"/12" M	16.6	22.3	0.744	15.9	57.9	0.274
4x8 DFP 4"/12" M*	25.4	26.7	0.950	20.9	48.9	0.427
4x8 DFP 3"/12" M*	30.1	26.7	1.127	18.9	38.1	0.496
4x8 OSB 6"/12" M	14.3	15.3	0.939	8.09	48.6	0.166
4x8 OSB 4"/12" M	21.1	22.7	0.930	10.2	50.1	0.204
4x8 OSB 3"/12" M*	25.4	26.7	0.950	13.3	46.2	0.288
8x8 CSP 6"/12" M	29.1	27.2	1.069	11.6	44.8	0.258
8x8 CSP 4"/12" M	42.6	40.5	1.053	16.8	47.1	0.357
8x8 CSP 3"/12" M	52.7	53.8	0.980	19.1	49.5	0.386
Average			0.918			0.307
Standard Deviation			0.117			0.096
COV			0.128			0.313

Table A-VI.28

Comparisons between Test Results and Prediction from Kallsner & Lam's Lower Plastic Model

ID	Test S <sub>y</sub> (kN)	Prediction (kN)	Ratio
2x8 CSP 6"/12" M	5.02	6.96	0.721
2x8 CSP 4"/12" M	7.49	10.4	0.717
2x8 OSB 6"/12" M	6.12	7.82	0.783
2x8 OSB 4"/12" M*	9.13	11.2	0.815
4x8 CSP 6"/12" M	13.6	13.9	0.975
4x8 CSP 4"/12" M	17.3	20.9	0.829
4x8 CSP 3"/12" M*	26.2	26.7	0.981
4x8 DFP 6"/12" M	16.6	22.9	0.727
4x8 DFP 4"/12" M*	25.4	26.7	0.950
4x8 DFP 3"/12" M*	30.1	26.7	1.127
4x8 OSB 6"/12" M	14.3	15.6	0.917
4x8 OSB 4"/12" M	21.1	23.5	0.901
4x8 OSB 3"/12" M*	25.4	26.7	0.950
8x8 CSP 6"/12" M	29.1	27.8	1.045
8x8 CSP 4"/12" M	42.6	41.8	1.020
8x8 CSP 3"/12" M	52.7	55.7	0.946
Average			0.900
Standard Deviation			0.119
COV			0.133

Table A-VI.29  
Comparisons between Test Results and Prediction  
from Kallsner & Lam's Upper Plastic Model

ID	Test Sy (kN)	Prediction (kN)	Ratio
2x8 CSP 6"/12" M	5.02	7.39	0.679
2x8 CSP 4"/12" M	7.49	11.1	0.676
2x8 OSB 6"/12" M	6.12	8.31	0.737
2x8 OSB 4"/12" M*	9.13	11.2	0.815
4x8 CSP 6"/12" M	13.6	16.3	0.834
4x8 CSP 4"/12" M	17.3	24.1	0.719
4x8 CSP 3"/12" M*	26.2	26.7	0.981
4x8 DFP 6"/12" M	16.6	26.7	0.622
4x8 DFP 4"/12" M*	25.4	26.7	0.950
4x8 DFP 3"/12" M*	30.1	26.7	1.127
4x8 OSB 6"/12" M	14.3	18.3	0.785
4x8 OSB 4"/12" M*	21.1	26.7	0.792
4x8 OSB 3"/12" M*	25.4	26.7	0.950
8x8 CSP 6"/12" M	29.1	32.5	0.894
8x8 CSP 4"/12" M	42.6	48.2	0.884
8x8 CSP 3"/12" M*	52.7	57.7	0.913
Average			0.835
Standard Deviation			0.129
COV			0.155

Table A-VI.30  
Comparisons between Test Results and Prediction from McCutcheon's Model

ID	Test Sy (kN)	Prediction (kN)	Ratio	Test $\Delta_{max}$ (mm)	Prediction (mm)	Ratio
2x8 CSP 6"/12" M	5.02	7.18	0.698	18.9	78.8	0.240
2x8 CSP 4"/12" M	7.49	10.7	0.698	28.9	81.4	0.355
2x8 OSB 6"/12" M	6.12	8.07	0.759	16.9	87.2	0.194
2x8 OSB 4"/12" M*	9.13	11.2	0.815	15.9	83.4	0.191
4x8 CSP 6"/12" M	13.6	13.8	0.987	13.0	44.8	0.290
4x8 CSP 4"/12" M	17.3	20.6	0.841	19.0	47.2	0.402
4x8 CSP 3"/12" M*	26.2	26.7	0.981	19.7	49.1	0.402
4x8 DFP 6"/12" M	16.6	22.6	0.736	15.9	57.9	0.275
4x8 DFP 4"/12" M*	25.4	26.7	0.950	20.9	48.1	0.433
4x8 DFP 3"/12" M*	30.1	26.7	1.127	18.9	37.5	0.505
4x8 OSB 6"/12" M	14.3	15.5	0.928	8.09	48.6	0.166
4x8 OSB 4"/12" M	21.1	23.1	0.914	10.2	50.1	0.204
4x8 OSB 3"/12" M*	25.4	26.7	0.950	13.3	45.4	0.293
8x8 CSP 6"/12" M	29.1	27.5	1.057	11.6	44.8	0.258
8x8 CSP 4"/12" M	42.6	41.2	1.035	16.8	47.2	0.356
8x8 CSP 3"/12" M	52.7	54.8	0.960	19.1	49.7	0.385
Average			0.902			0.309
Standard Deviation			0.127			0.096
COV			0.140			0.312

## II. REVERSE CYCLIC TESTS

### (1) EEEP\_25

Table A-VI.31  
Comparisons between Test Results and Prediction from Easley's Model

ID	Test (kN)	Prediction (kN)	Ratio	Test (kip)	Prediction (kip)	Ratio
2x8 CSP 6"/12" C	5.44	4.19	1.299	19.2	14.8	1.302
2x8 CSP 4"/12" C	7.64	6.52	1.171	22.7	17.0	1.339
2x8 OSB 6"/12" C	5.69	4.62	1.230	14.4	11.7	1.235
2x8 OSB 4"/12" C	8.92	7.20	1.238	15.8	13.1	1.204
4x8 CSP 6"/12" C	12.3	9.02	1.359	11.2	8.84	1.269
4x8 CSP 4"/12" C	17.8	13.6	1.307	15.5	10.5	1.481
4x8 CSP 3"/12" C	26.4	18.1	1.458	17.9	12.1	1.480
4x8 DFP 6"/12" C	14.8	14.4	1.033	12.2	10.8	1.129
4x8 DFP 4"/12" C	22.2	21.6	1.026	15.8	12.3	1.293
4x8 DFP 3"/12" C*	29.6	26.7	1.108	17.4	12.9	1.352
4x8 OSB 6"/12" C	12.4	10.0	1.242	7.9	6.70	1.172
4x8 OSB 4"/12" C	19.0	15.0	1.265	8.4	7.72	1.093
4x8 OSB 3"/12" C	25.0	20.0	1.248	9.7	8.70	1.117
8x8 CSP 6"/12" C	28.0	18.0	1.553	13.1	8.84	1.487
8x8 CSP 4"/12" C	41.4	27.2	1.523	16.3	10.5	1.551
8x8 CSP 3"/12" C	56.1	36.2	1.550	17.8	12.1	1.472
Average			1.288			1.311
Standard Deviation			0.162			0.144
COV			0.126			0.110

Table A-VI.32

Comparisons between Test Results and Prediction from Kallsner &amp; Lam's Elastic Model

ID	Test $S_y$ (kN)	Prediction (kN)	Ratio	COV (Test/Min)	Prediction (Min)	Ratio
2x8 CSP 6"/12" C	5.44	5.76	0.943	19.2	22.1	0.871
2x8 CSP 4"/12" C	7.64	8.61	0.887	22.7	24.1	0.940
2x8 OSB 6"/12" C	5.69	6.37	0.893	14.4	17.6	0.822
2x8 OSB 4"/12" C	8.92	9.52	0.937	15.8	18.8	0.841
4x8 CSP 6"/12" C	12.3	11.6	1.055	11.2	13.7	0.818
4x8 CSP 4"/12" C	17.8	17.3	1.027	15.5	15.7	0.988
4x8 CSP 3"/12" C	26.4	23.0	1.148	17.9	17.7	1.009
4x8 DFP 6"/12" C	14.8	18.5	0.802	12.2	17.2	0.709
4x8 DFP 4"/12" C*	22.2	26.7	0.830	15.8	18.6	0.850
4x8 DFP 3"/12" C*	29.6	26.7	1.108	17.4	15.3	1.133
4x8 OSB 6"/12" C	12.4	12.8	0.964	7.9	10.6	0.742
4x8 OSB 4"/12" C	19.0	19.1	0.994	8.4	11.8	0.714
4x8 OSB 3"/12" C	25.0	25.4	0.983	9.7	13.0	0.745
8x8 CSP 6"/12" C	28.0	23.2	1.205	13.1	13.7	0.958
8x8 CSP 4"/12" C	41.4	34.6	1.196	16.3	15.7	1.035
8x8 CSP 3"/12" C	56.1	45.9	1.221	17.8	17.7	1.003
Average			1.012			0.886
Standard Deviation			0.129			0.124
COV			0.127			0.139

Table A-VI.33

Comparisons between Test Results and Prediction from Kallsner &amp; Lam's Lower Plastic Model

ID	Test $S_y$ (kN)	Prediction (kN)	Ratio
2x8 CSP 6"/12" C	5.44	5.95	0.914
2x8 CSP 4"/12" C	7.64	8.92	0.856
2x8 OSB 6"/12" C	5.69	6.57	0.865
2x8 OSB 4"/12" C	8.92	9.86	0.904
4x8 CSP 6"/12" C	12.3	11.9	1.031
4x8 CSP 4"/12" C	17.8	17.8	0.995
4x8 CSP 3"/12" C	26.4	23.8	1.109
4x8 DFP 6"/12" C	14.8	18.9	0.784
4x8 DFP 4"/12" C*	22.2	26.7	0.830
4x8 DFP 3"/12" C*	29.6	26.7	1.108
4x8 OSB 6"/12" C	12.4	13.1	0.941
4x8 OSB 4"/12" C	19.0	19.7	0.963
4x8 OSB 3"/12" C	25.0	26.3	0.949
8x8 CSP 6"/12" C	28.0	23.8	1.177
8x8 CSP 4"/12" C	41.4	35.7	1.159
8x8 CSP 3"/12" C	56.1	47.6	1.179
Average			0.985
Standard Deviation			0.125
COV			0.126

Table A-VI.34  
Comparisons between Test Results and Prediction  
from Kallsner & Lam's Upper Plastic Model

ID	Test Sy (kN)	Prediction (kN)	Ratio
2x8 CSP 6"/12" C	5.44	6.32	0.860
2x8 CSP 4"/12" C	7.64	9.46	0.807
2x8 OSB 6"/12" C	5.69	6.98	0.815
2x8 OSB 4"/12" C	8.92	10.5	0.853
4x8 CSP 6"/12" C	12.3	13.9	0.882
4x8 CSP 4"/12" C	17.8	20.6	0.863
4x8 CSP 3"/12" C*	26.4	26.7	0.988
4x8 DFP 6"/12" C	14.8	22.1	0.671
4x8 DFP 4"/12" C*	22.2	26.7	0.830
4x8 DFP 3"/12" C*	29.6	26.7	1.108
4x8 OSB 6"/12" C	12.4	15.4	0.806
4x8 OSB 4"/12" C	19.0	22.7	0.835
4x8 OSB 3"/12" C*	25.0	26.7	0.935
8x8 CSP 6"/12" C	28.0	27.8	1.008
8x8 CSP 4"/12" C	41.4	41.2	1.005
8x8 CSP 3"/12" C	56.1	54.5	1.029
Average			0.893
Standard Deviation			0.107
COV			0.120

Table A-VI.35  
Comparisons between Test Results and Prediction from McCutcheon's Model

ID	Test Sy (kN)	Prediction (kN)	Ratio	Test S <sub>y</sub> (mm)	Prediction (mm)	Ratio
2x8 CSP 6"/12" C	5.44	6.14	0.885	19.2	22.1	0.869
2x8 CSP 4"/12" C	7.64	9.16	0.834	22.7	24.3	0.934
2x8 OSB 6"/12" C	5.69	6.78	0.838	14.4	17.5	0.823
2x8 OSB 4"/12" C	8.92	10.1	0.881	15.8	18.9	0.839
4x8 CSP 6"/12" C	12.3	11.8	1.043	11.2	13.8	0.816
4x8 CSP 4"/12" C	17.8	17.6	1.009	15.5	15.8	0.982
4x8 CSP 3"/12" C	26.4	23.4	1.126	17.9	17.9	1.000
4x8 DFP 6"/12" C	14.8	18.7	0.793	12.2	17.2	0.708
4x8 DFP 4"/12" C*	22.2	26.7	0.830	15.8	18.4	0.861
4x8 DFP 3"/12" C*	29.6	26.7	1.108	17.4	15.1	1.148
4x8 OSB 6"/12" C	12.4	13.0	0.953	7.9	10.6	0.741
4x8 OSB 4"/12" C	19.0	19.4	0.977	8.4	11.9	0.711
4x8 OSB 3"/12" C	25.0	25.9	0.964	9.7	13.1	0.739
8x8 CSP 6"/12" C	28.0	23.5	1.192	13.1	13.8	0.956
8x8 CSP 4"/12" C	41.4	35.2	1.176	16.3	15.8	1.028
8x8 CSP 3"/12" C	56.1	46.9	1.197	17.8	17.9	0.994
Average			0.988			0.884
Standard Deviation			0.135			0.124
COV			0.136			0.140

(2) Max. Load\_25&ke

Table A-VI.36  
Comparisons between Test Results and Prediction from Easley's Model

ID	Test (kN)	Prediction (kN)	Ratio	Test (kN)	Prediction (kN)	Ratio
2x8 CSP 6"/12" C	5.44	4.90	1.110	19.2	17.3	1.113
2x8 CSP 4"/12" C	7.64	7.63	1.001	22.7	19.8	1.144
2x8 OSB 6"/12" C	5.69	5.50	1.033	14.4	13.9	1.038
2x8 OSB 4"/12" C	8.92	8.57	1.040	15.8	15.6	1.012
4x8 CSP 6"/12" C	12.3	10.6	1.162	11.2	10.3	1.085
4x8 CSP 4"/12" C	17.8	15.9	1.117	15.5	12.3	1.266
4x8 CSP 3"/12" C	26.4	21.2	1.246	17.9	14.2	1.265
4x8 DFP 6"/12" C	14.8	17.4	0.855	12.2	13.0	0.934
4x8 DFP 4"/12" C	22.2	26.1	0.849	15.8	14.8	1.070
4x8 DFP 3"/12" C*	29.6	26.7	1.108	17.4	12.9	1.352
4x8 OSB 6"/12" C	12.4	11.9	1.043	7.9	8.0	0.985
4x8 OSB 4"/12" C	19.0	17.9	1.063	8.4	9.2	0.918
4x8 OSB 3"/12" C	25.0	23.8	1.049	9.7	10.4	0.939
8x8 CSP 6"/12" C	28.0	21.1	1.327	13.1	10.3	1.270
8x8 CSP 4"/12" C	41.4	31.8	1.302	16.3	12.3	1.325
8x8 CSP 3"/12" C	56.1	42.3	1.325	17.8	14.2	1.258
Average			1.102			1.123
Standard Deviation			0.141			0.143
COV			0.128			0.128

Table A-VI.37

## Comparisons between Test Results and Prediction from Kallsner &amp; Lam's Elastic Model

ID	Test (kN)	Prediction (kN)	Ratio	Test (kN)	Prediction (kN)	Ratio
2x8 CSP 6"/12" C	5.44	6.74	0.806	19.2	25.8	0.744
2x8 CSP 4"/12" C	7.64	10.1	0.758	22.7	28.3	0.803
2x8 OSB 6"/12" C	5.69	7.58	0.751	14.4	20.9	0.691
2x8 OSB 4"/12" C*	8.92	11.2	0.796	15.8	22.4	0.707
4x8 CSP 6"/12" C	12.3	13.6	0.902	11.2	16.1	0.699
4x8 CSP 4"/12" C	17.8	20.2	0.878	15.5	18.4	0.845
4x8 CSP 3"/12" C*	26.4	26.7	0.988	17.9	20.8	0.862
4x8 DFP 6"/12" C	14.8	22.3	0.664	12.2	20.7	0.587
4x8 DFP 4"/12" C*	22.2	26.7	0.830	15.8	18.6	0.850
4x8 DFP 3"/12" C*	29.6	26.7	1.108	17.4	15.3	1.133
4x8 OSB 6"/12" C	12.4	15.3	0.810	7.9	12.6	0.624
4x8 OSB 4"/12" C	19.0	22.7	0.835	8.4	14.0	0.600
4x8 OSB 3"/12" C*	25.0	26.7	0.935	9.7	13.9	0.698
8x8 CSP 6"/12" C	28.0	27.2	1.030	13.1	16.1	0.819
8x8 CSP 4"/12" C	41.4	40.5	1.022	16.3	18.4	0.884
8x8 CSP 3"/12" C	56.1	53.8	1.043	17.8	20.8	0.858
Average			0.885			0.775
Standard Deviation			0.122			0.133
COV			0.137			0.171

Table A-VI.38

## Comparisons between Test Results and Prediction from Kallsner &amp; Lam's Lower Plastic Model

ID	Test (kN)	Prediction (kN)	Ratio
2x8 CSP 6"/12" C	5.44	6.96	0.781
2x8 CSP 4"/12" C	7.64	10.4	0.731
2x8 OSB 6"/12" C	5.69	7.82	0.727
2x8 OSB 4"/12" C*	8.92	11.2	0.796
4x8 CSP 6"/12" C	12.3	13.9	0.881
4x8 CSP 4"/12" C	17.8	20.9	0.850
4x8 CSP 3"/12" C*	26.4	26.7	0.988
4x8 DFP 6"/12" C	14.8	22.9	0.649
4x8 DFP 4"/12" C*	22.2	26.7	0.830
4x8 DFP 3"/12" C*	29.6	26.7	1.108
4x8 OSB 6"/12" C	12.4	15.6	0.791
4x8 OSB 4"/12" C	19.0	23.5	0.809
4x8 OSB 3"/12" C*	25.0	26.7	0.935
8x8 CSP 6"/12" C	28.0	27.8	1.006
8x8 CSP 4"/12" C	41.4	41.8	0.991
8x8 CSP 3"/12" C	56.1	55.7	1.007
Average			0.868
Standard Deviation			0.123
COV			0.141

Table A-VI.39  
Comparisons between Test Results and Prediction  
from Kallsner & Lam's Upper Plastic Model

ID	Test Sv (kN)	Prediction (kN)	Ratio
2x8 CSP 6"/12" C	5.44	7.39	0.735
2x8 CSP 4"/12" C	7.64	11.1	0.690
2x8 OSB 6"/12" C	5.69	8.31	0.685
2x8 OSB 4"/12" C*	8.92	11.2	0.796
4x8 CSP 6"/12" C	12.3	16.3	0.754
4x8 CSP 4"/12" C	17.8	24.1	0.737
4x8 CSP 3"/12" C*	26.4	26.7	0.988
4x8 DFP 6"/12" C	14.8	26.7	0.555
4x8 DFP 4"/12" C*	22.2	26.7	0.830
4x8 DFP 3"/12" C*	29.6	26.7	1.108
4x8 OSB 6"/12" C	12.4	18.3	0.677
4x8 OSB 4"/12" C*	19.0	26.7	0.711
4x8 OSB 3"/12" C*	25.0	26.7	0.935
8x8 CSP 6"/12" C	28.0	32.5	0.861
8x8 CSP 4"/12" C	41.4	48.2	0.859
8x8 CSP 3"/12" C*	56.1	57.7	0.972
Average			0.806
Standard Deviation			0.138
COV			0.171

Table A-VI.40  
Comparisons between Test Results and Prediction from McCutcheon's Model

ID	Test Sv (kN)	Prediction (kN)	Ratio	Test Sv (mm)	Prediction (mm)	Ratio
2x8 CSP 6"/12" C	5.44	7.18	0.757	19.2	25.9	0.743
2x8 CSP 4"/12" C	7.64	10.7	0.712	22.7	28.4	0.798
2x8 OSB 6"/12" C	5.69	8.07	0.705	14.4	20.9	0.692
2x8 OSB 4"/12" C*	8.92	11.2	0.796	15.8	21.1	0.751
4x8 CSP 6"/12" C	12.3	13.8	0.892	11.2	16.1	0.698
4x8 CSP 4"/12" C	17.8	20.6	0.863	15.5	18.5	0.839
4x8 CSP 3"/12" C*	26.4	26.7	0.988	17.9	20.7	0.864
4x8 DFP 6"/12" C	14.8	22.6	0.656	12.2	20.8	0.586
4x8 DFP 4"/12" C*	22.2	26.7	0.830	15.8	18.4	0.861
4x8 DFP 3"/12" C*	29.6	26.7	1.108	17.4	15.1	1.148
4x8 OSB 6"/12" C	12.4	15.5	0.801	7.9	12.6	0.623
4x8 OSB 4"/12" C	19.0	23.1	0.821	8.4	14.1	0.597
4x8 OSB 3"/12" C*	25.0	26.7	0.935	9.7	13.8	0.706
8x8 CSP 6"/12" C	28.0	27.5	1.018	13.1	16.1	0.817
8x8 CSP 4"/12" C	41.4	41.2	1.005	16.3	18.5	0.879
8x8 CSP 3"/12" C	56.1	54.8	1.023	17.8	20.9	0.850
Average			0.869			0.778
Standard Deviation			0.128			0.134
COV			0.148			0.172

(3) Max. Load\_25&ks

Table A-VI.41  
Comparisons between Test Results and Prediction from Easley's Model

ID	Test (kN)	Prediction (kN)	Ratio	Test (kips)	Prediction (kips)	Ratio
2x8 CSP 6"/12" C	5.44	4.90	1.110	19.2	52.4	0.367
2x8 CSP 4"/12" C	7.64	7.63	1.001	22.7	56.5	0.402
2x8 OSB 6"/12" C	5.69	5.50	1.033	14.4	49.3	0.293
2x8 OSB 4"/12" C	8.92	8.57	1.040	15.8	52.5	0.302
4x8 CSP 6"/12" C	12.3	10.6	1.162	11.2	27.3	0.412
4x8 CSP 4"/12" C	17.8	15.9	1.117	15.5	29.3	0.531
4x8 CSP 3"/12" C	26.4	21.2	1.246	17.9	31.1	0.575
4x8 DFP 6"/12" C	14.8	17.4	0.855	12.2	28.7	0.424
4x8 DFP 4"/12" C	22.2	26.1	0.849	15.8	30.6	0.518
4x8 DFP 3"/12" C*	29.6	26.7	1.108	17.4	25.1	0.692
4x8 OSB 6"/12" C	12.4	11.9	1.043	7.9	25.0	0.314
4x8 OSB 4"/12" C	19.0	17.9	1.063	8.4	26.3	0.321
4x8 OSB 3"/12" C	25.0	23.8	1.049	9.7	27.4	0.354
8x8 CSP 6"/12" C	28.0	21.1	1.327	13.1	27.3	0.482
8x8 CSP 4"/12" C	41.4	31.8	1.302	16.3	29.3	0.556
8x8 CSP 3"/12" C	56.1	42.3	1.325	17.8	31.1	0.572
Average			1.102			0.445
Standard Deviation			0.141			0.116
COV			0.128			0.260

Table A-VI.42

Comparisons between Test Results and Prediction from Kallsner &amp; Lam's Elastic Model

ID	Test $S_y$ (kN)	Prediction (kN)	Ratio	Test $\Delta_y$ (mm)	Prediction (mm)	Ratio
2x8 CSP 6"/12" C	5.44	6.74	0.806	19.2	79.5	0.242
2x8 CSP 4"/12" C	7.64	10.1	0.758	22.7	81.9	0.277
2x8 OSB 6"/12" C	5.69	7.58	0.751	14.4	74.8	0.193
2x8 OSB 4"/12" C*	8.92	11.2	0.796	15.8	76.4	0.207
4x8 CSP 6"/12" C	12.3	13.6	0.902	11.2	44.8	0.250
4x8 CSP 4"/12" C	17.8	20.2	0.878	15.5	47.1	0.330
4x8 CSP 3"/12" C*	26.4	26.7	0.988	17.9	49.5	0.362
4x8 DFP 6"/12" C	14.8	22.3	0.664	12.2	47.4	0.256
4x8 DFP 4"/12" C*	22.2	26.7	0.830	15.8	40.4	0.393
4x8 DFP 3"/12" C*	29.6	26.7	1.108	17.4	31.7	0.549
4x8 OSB 6"/12" C	12.4	15.3	0.810	7.9	41.5	0.189
4x8 OSB 4"/12" C	19.0	22.7	0.835	8.4	42.9	0.196
4x8 OSB 3"/12" C*	25.0	26.7	0.935	9.7	39.8	0.244
8x8 CSP 6"/12" C	28.0	27.2	1.030	13.1	44.8	0.293
8x8 CSP 4"/12" C	41.4	40.5	1.022	16.3	47.1	0.345
8x8 CSP 3"/12" C	56.1	53.8	1.043	17.8	49.5	0.360
Average			0.885			0.293
Standard Deviation			0.122			0.092
COV			0.137			0.313

Table A-VI.43

Comparisons between Test Results and Prediction from Kallsner &amp; Lam's Lower Plastic Model

ID	Test $S_y$ (kN)	Prediction (kN)	Ratio
2x8 CSP 6"/12" C	5.44	6.96	0.781
2x8 CSP 4"/12" C	7.64	10.4	0.731
2x8 OSB 6"/12" C	5.69	7.82	0.727
2x8 OSB 4"/12" C*	8.92	11.2	0.796
4x8 CSP 6"/12" C	12.3	13.9	0.881
4x8 CSP 4"/12" C	17.8	20.9	0.850
4x8 CSP 3"/12" C*	26.4	26.7	0.988
4x8 DFP 6"/12" C	14.8	22.9	0.649
4x8 DFP 4"/12" C*	22.2	26.7	0.830
4x8 DFP 3"/12" C*	29.6	26.7	1.108
4x8 OSB 6"/12" C	12.4	15.6	0.791
4x8 OSB 4"/12" C	19.0	23.5	0.809
4x8 OSB 3"/12" C*	25.0	26.7	0.935
8x8 CSP 6"/12" C	28.0	27.8	1.006
8x8 CSP 4"/12" C	41.4	41.8	0.991
8x8 CSP 3"/12" C	56.1	55.7	1.007
Average			0.868
Standard Deviation			0.123
COV			0.141

Table A-VI.44  
Comparisons between Test Results and Prediction  
from Kallsner & Lam's Upper Plastic Model

ID	Test Sy (kN)	Prediction (kN)	Ratio
2x8 CSP 6"/12" C	5.44	7.39	0.735
2x8 CSP 4"/12" C	7.64	11.1	0.690
2x8 OSB 6"/12" C	5.69	8.31	0.685
2x8 OSB 4"/12" C*	8.92	11.2	0.796
4x8 CSP 6"/12" C	12.3	16.3	0.754
4x8 CSP 4"/12" C	17.8	24.1	0.737
4x8 CSP 3"/12" C*	26.4	26.7	0.988
4x8 DFP 6"/12" C	14.8	26.7	0.555
4x8 DFP 4"/12" C*	22.2	26.7	0.830
4x8 DFP 3"/12" C*	29.6	26.7	1.108
4x8 OSB 6"/12" C	12.4	18.3	0.677
4x8 OSB 4"/12" C*	19.0	26.7	0.711
4x8 OSB 3"/12" C*	25.0	26.7	0.935
8x8 CSP 6"/12" C	28.0	32.5	0.861
8x8 CSP 4"/12" C	41.4	48.2	0.859
8x8 CSP 3"/12" C	56.1	57.7	0.972
Average			0.806
Standard Deviation			0.138
COV			0.171

Table A-VI.45  
Comparisons between Test Results and Prediction from McCutcheon's Model

ID	Test Sy (kN)	Prediction (kN)	Ratio	Test Sy (kN)	Prediction (kN)	Ratio
2x8 CSP 6"/12" C	5.44	7.18	0.757	19.2	78.8	0.244
2x8 CSP 4"/12" C	7.64	10.7	0.712	22.7	81.4	0.279
2x8 OSB 6"/12" C	5.69	8.07	0.705	14.4	74.1	0.195
2x8 OSB 4"/12" C*	8.92	11.2	0.796	15.8	71.0	0.223
4x8 CSP 6"/12" C	12.3	13.8	0.892	11.2	44.8	0.251
4x8 CSP 4"/12" C	17.8	20.6	0.863	15.5	47.2	0.329
4x8 CSP 3"/12" C*	26.4	26.7	0.988	17.9	49.1	0.365
4x8 DFP 6"/12" C	14.8	22.6	0.656	12.2	47.4	0.257
4x8 DFP 4"/12" C*	22.2	26.7	0.830	15.8	39.7	0.399
4x8 DFP 3"/12" C*	29.6	26.7	1.108	17.4	31.2	0.558
4x8 OSB 6"/12" C	12.4	15.5	0.801	7.9	41.5	0.189
4x8 OSB 4"/12" C	19.0	23.1	0.821	8.4	43.0	0.196
4x8 OSB 3"/12" C*	25.0	26.7	0.935	9.7	39.2	0.248
8x8 CSP 6"/12" C	28.0	27.5	1.018	13.1	44.8	0.293
8x8 CSP 4"/12" C	41.4	41.2	1.005	16.3	47.2	0.345
8x8 CSP 3"/12" C	56.1	54.8	1.023	17.8	49.7	0.358
Average			0.869			0.295
Standard Deviation			0.128			0.093
COV			0.148			0.313

**APPENDIX VII**  
**GRAPHS OF COMPARISONS BETWEEN TEST RESULTS**  
**AND PREDICTION FROM ANALYTICAL MODELS**

**I. MONOTONIC TESTS**

**(1) EEEP\_12.5**

Note: In the following graphs, T represents the values from tests and P represents the predicted values using analytical models.

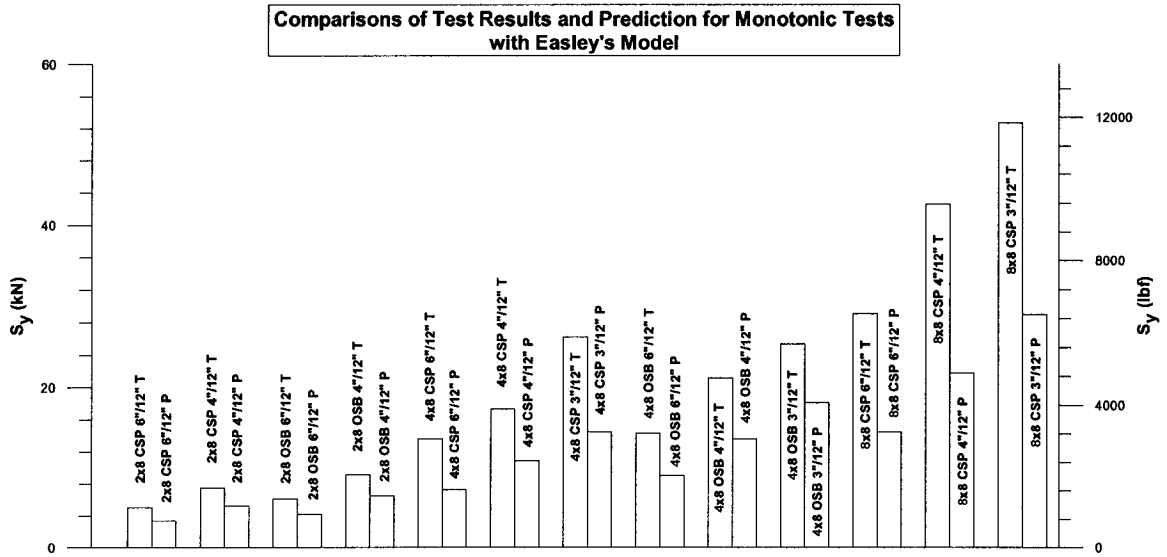


Figure A-VII.1

Comparisons between Test Results and Prediction from Easley's Model

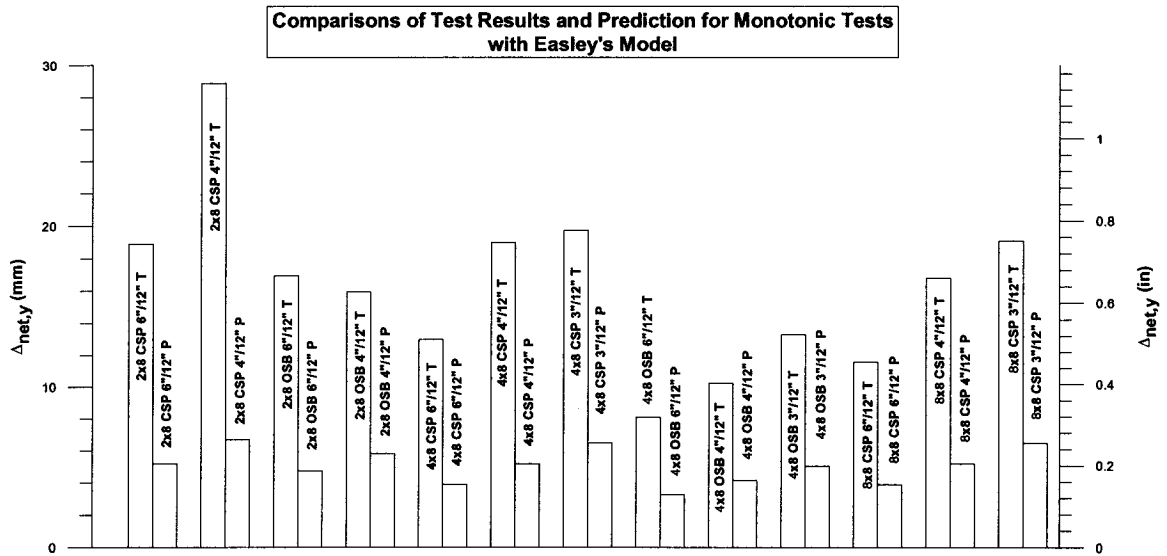


Figure A-VII.2

Comparisons between Test Results and Prediction from Easley's Model

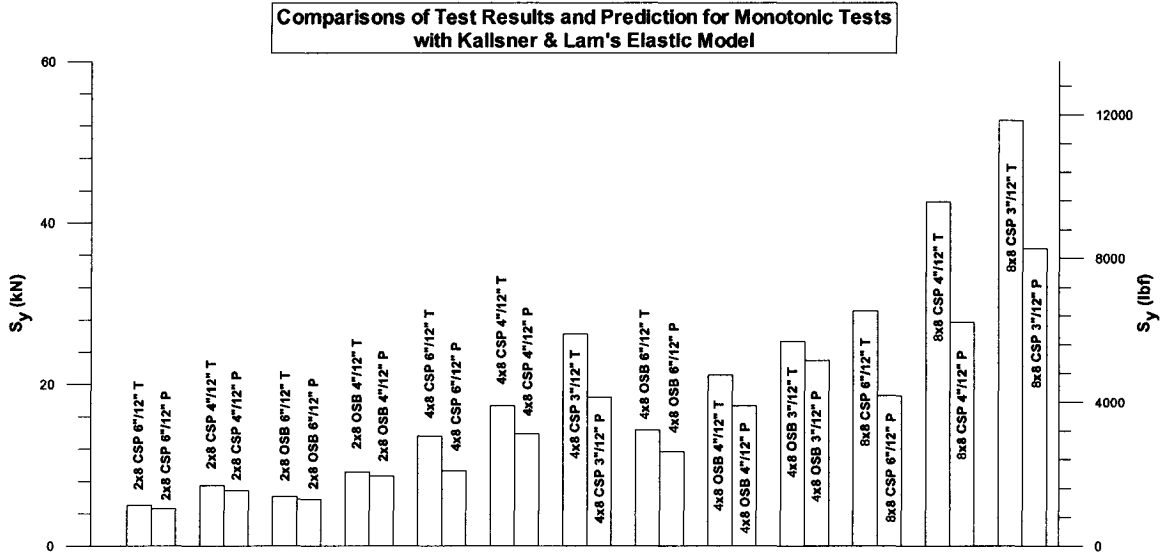


Figure A-VII.3

Comparisons between Test Results and Prediction from Kallsner & Lam's Elastic Model

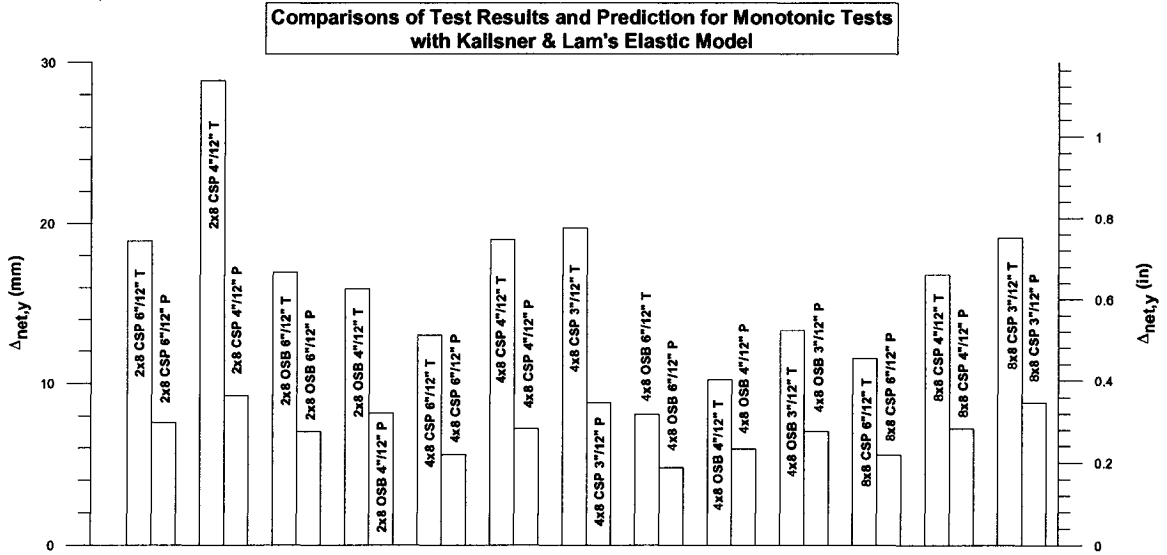


Figure A-VII.4

Comparisons between Test Results and Prediction from Kallsner & Lam's Elastic Model

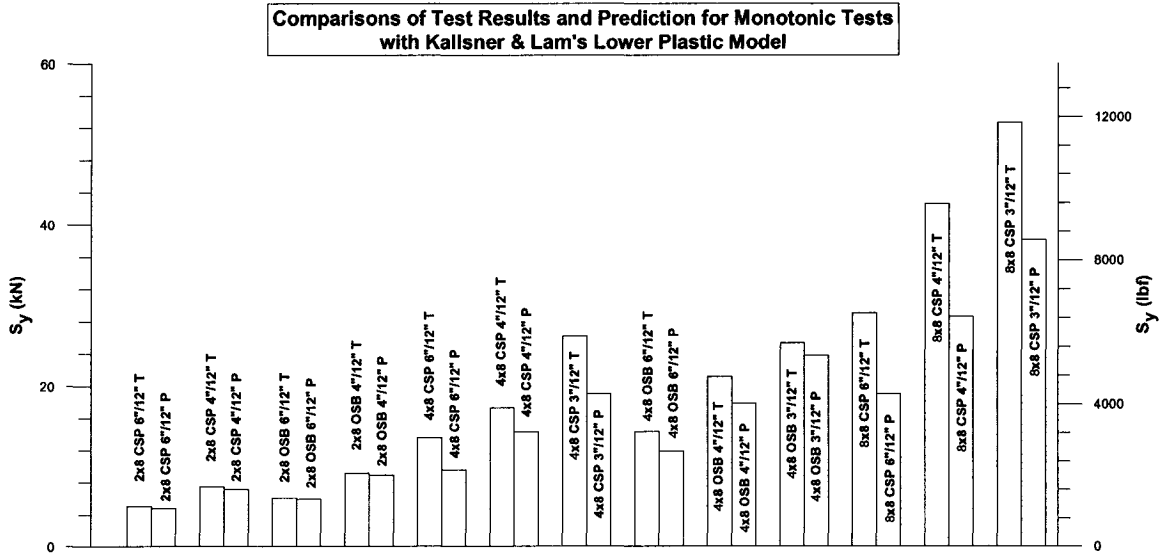


Figure A-VII.5

Comparisons between Test Results and Prediction from Kallsner & Lam's Lower Plastic Model

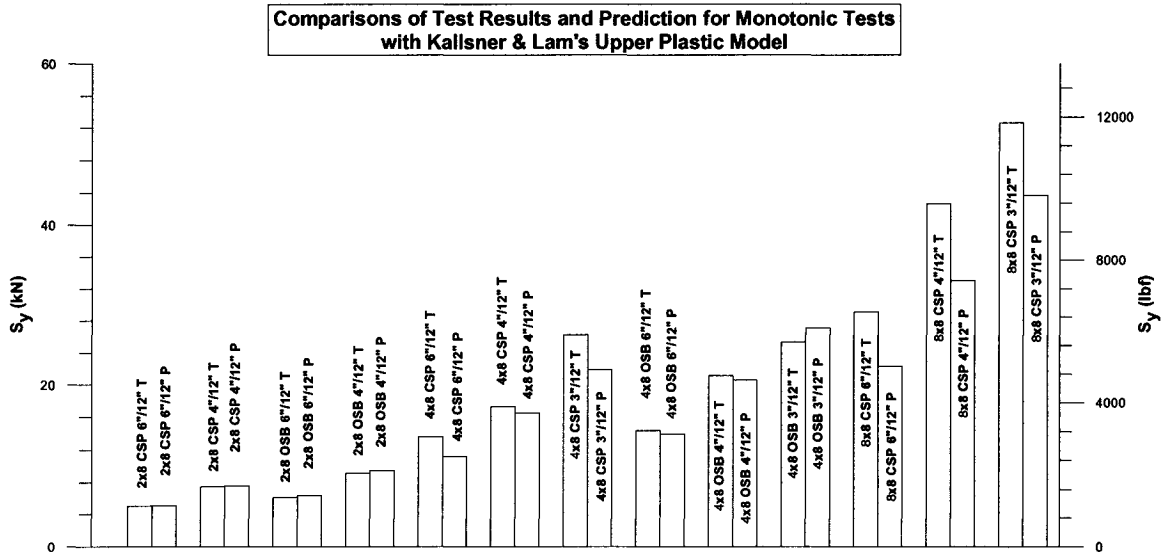


Figure A-VII.6

Comparisons between Test Results and Prediction from Kallsner & Lam's Upper Plastic Model

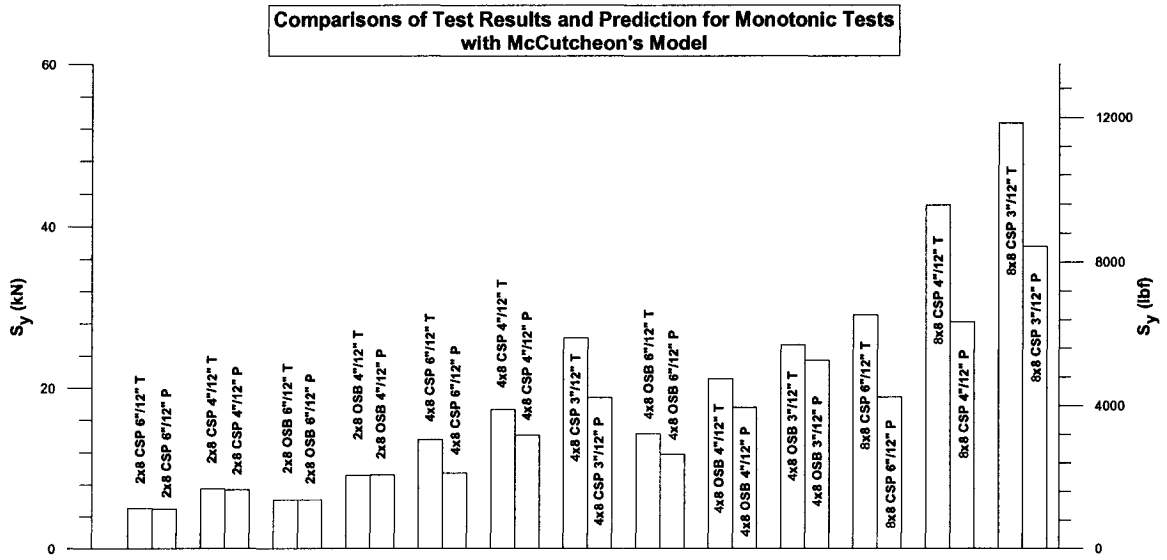


Figure A-VII.7

Comparisons between Test Results and Prediction from McCutcheon's Model

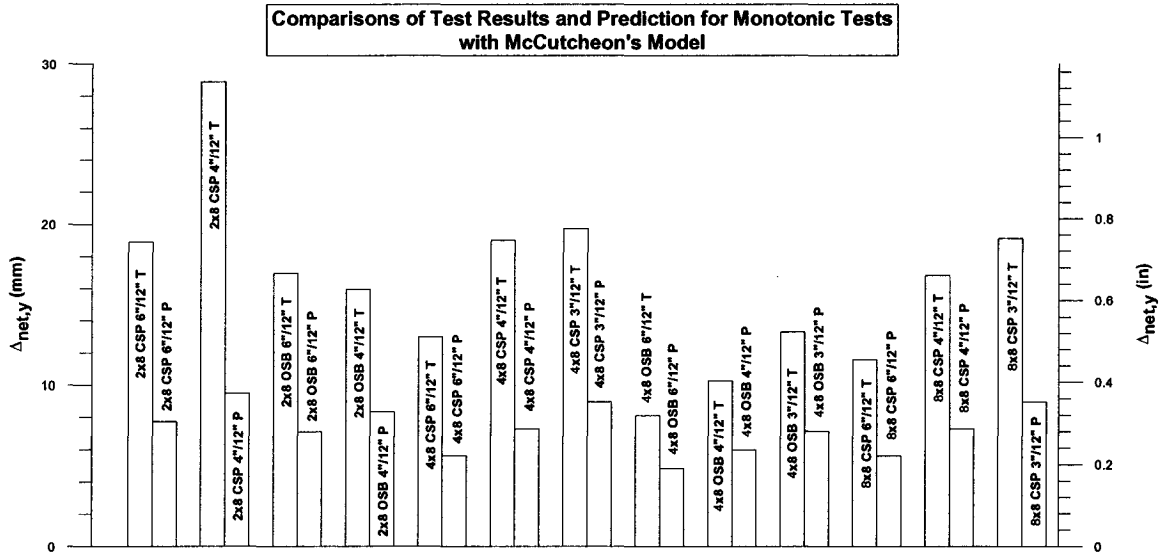


Figure A-VII.8

Comparisons between Test Results and Prediction from McCutcheon's Model

(2) Max. Load\_12.5&k

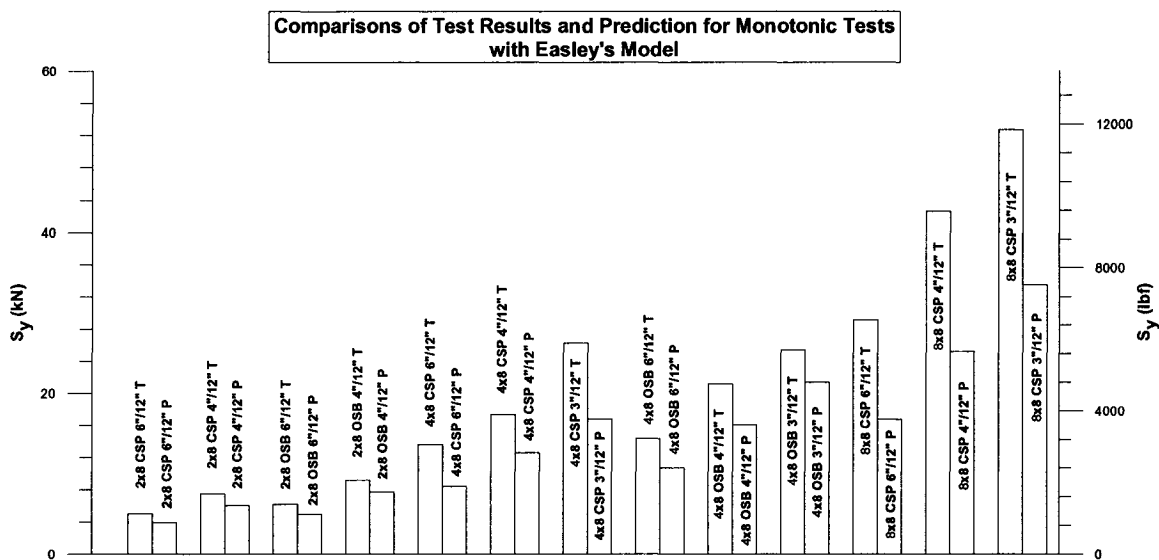


Figure A-VII.9

Comparisons between Test Results and Prediction from Easley's Model

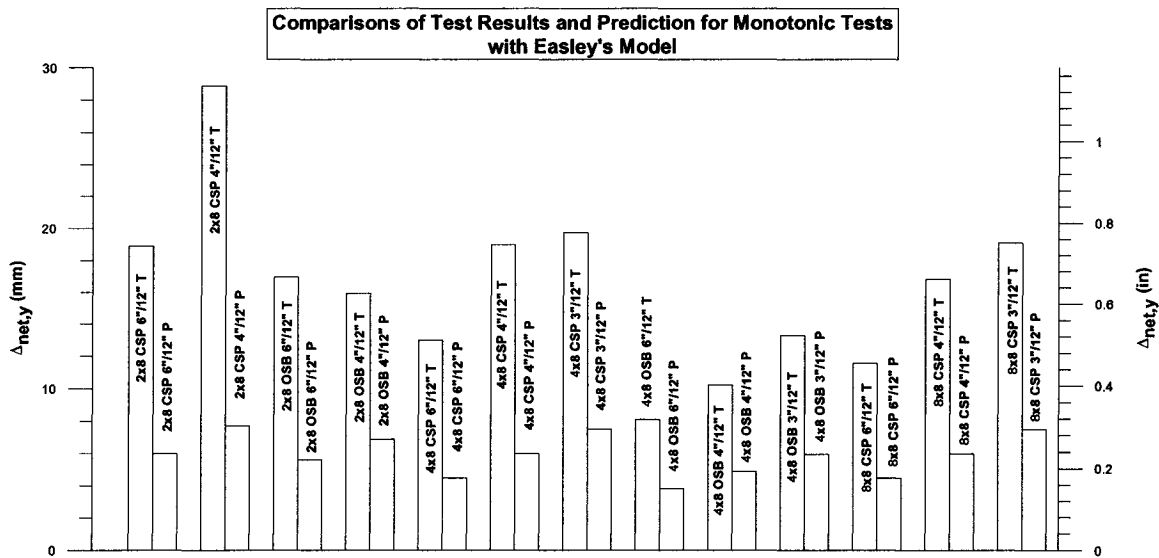


Figure A-VII.10

Comparisons between Test Results and Prediction from Easley's Model

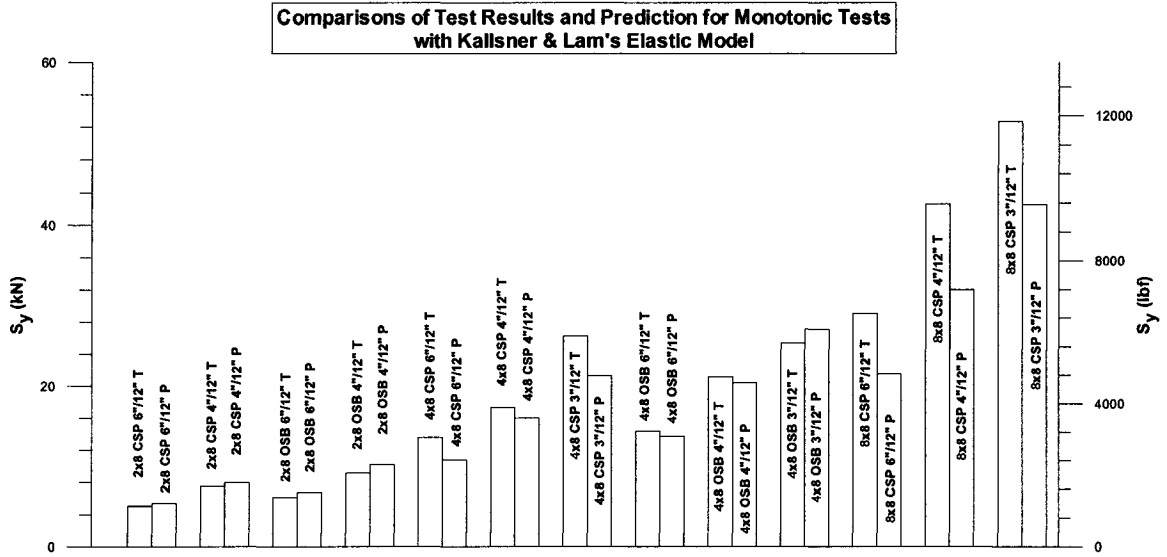


Figure A-VII.11

Comparisons between Test Results and Prediction from Kallsner & Lam's Elastic Model

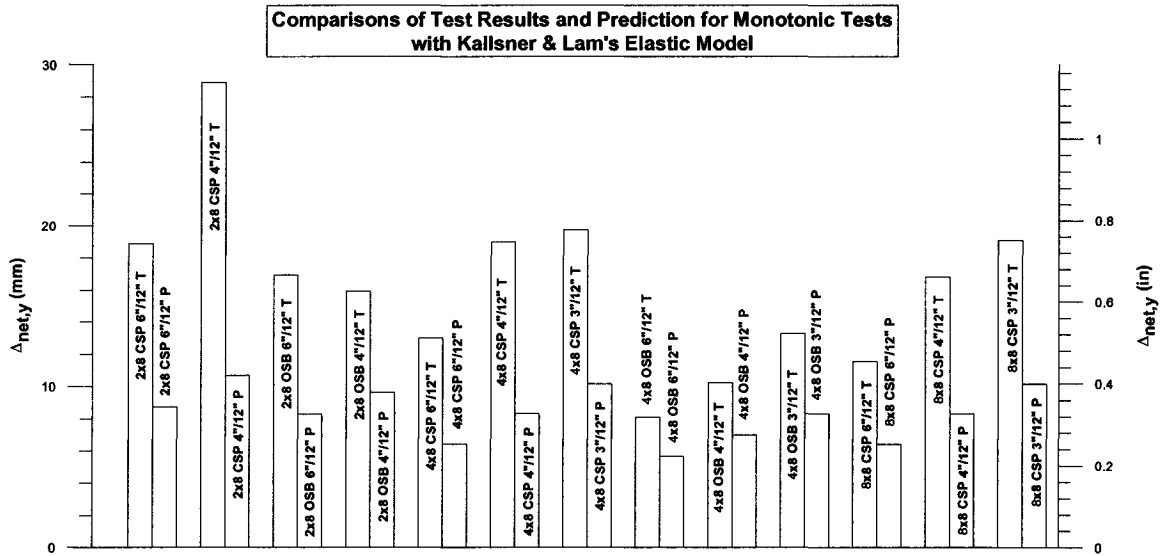


Figure A-VII.12

Comparisons between Test Results and Prediction from Kallsner & Lam's Elastic Model

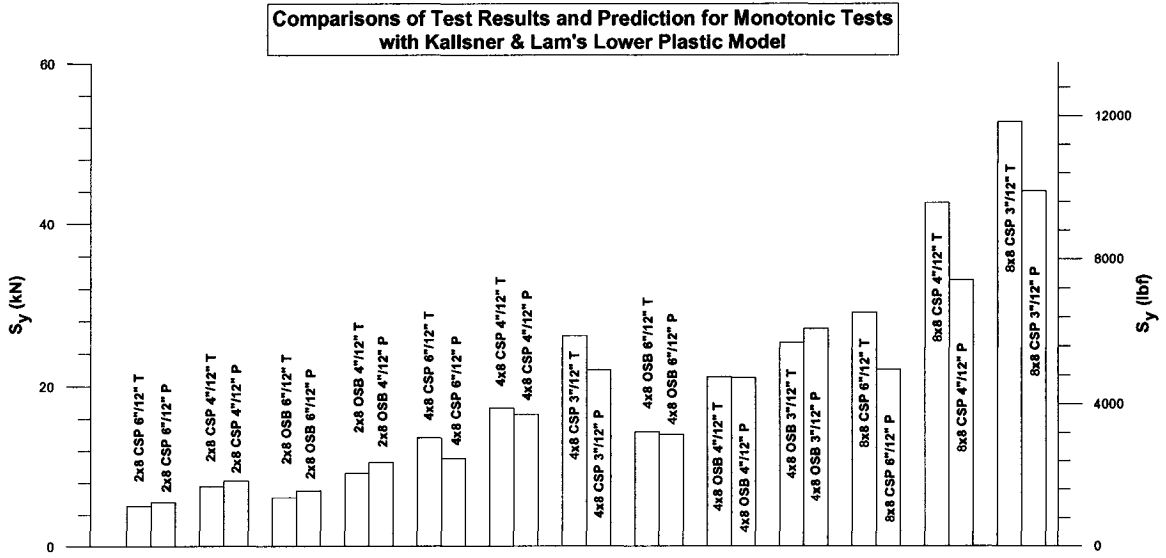


Figure A-VII.13

Comparisons between Test Results and Prediction from Kallsner & Lam's Lower Plastic Model

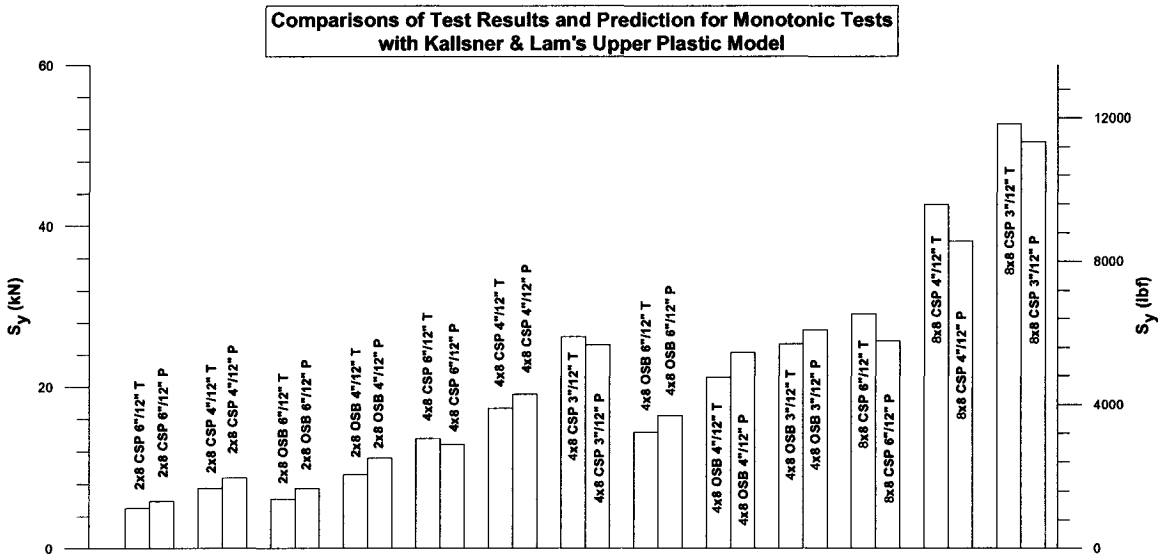


Figure A-VII.14

Comparisons between Test Results and Prediction from Kallsner & Lam's Upper Plastic Model

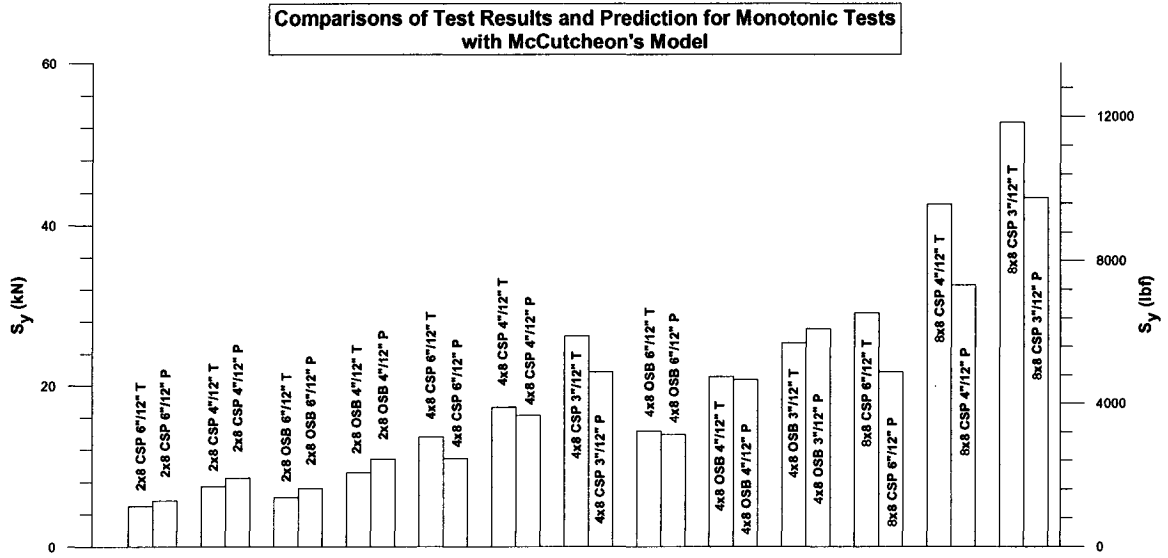


Figure A-VII.15

Comparisons between Test Results and Prediction from McCutcheon's Model

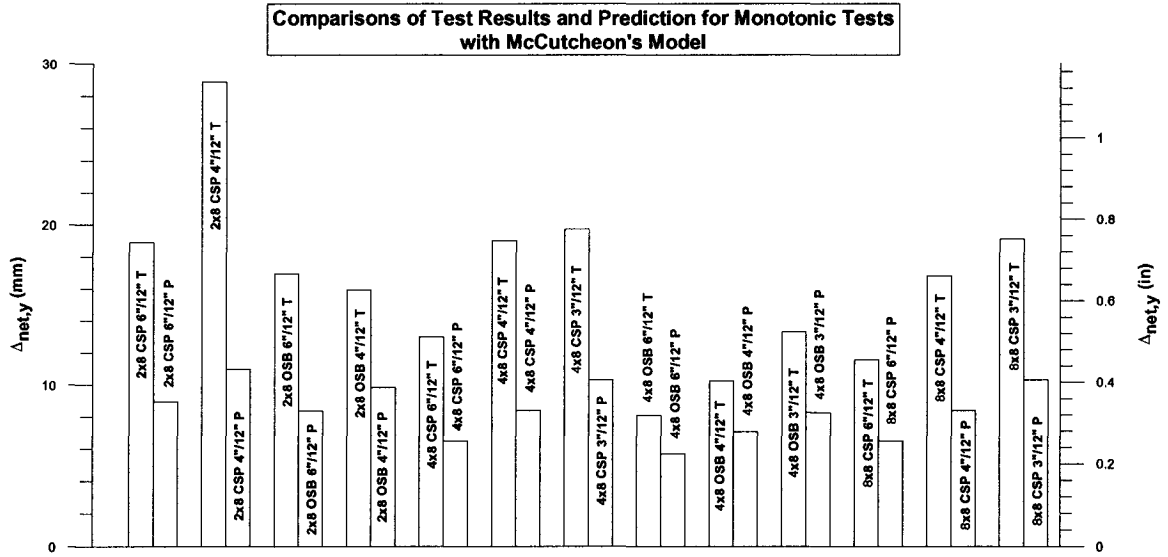


Figure A-VII.16

Comparisons between Test Results and Prediction from McCutcheon's Model

### (3) Max. Load\_12.5&ks

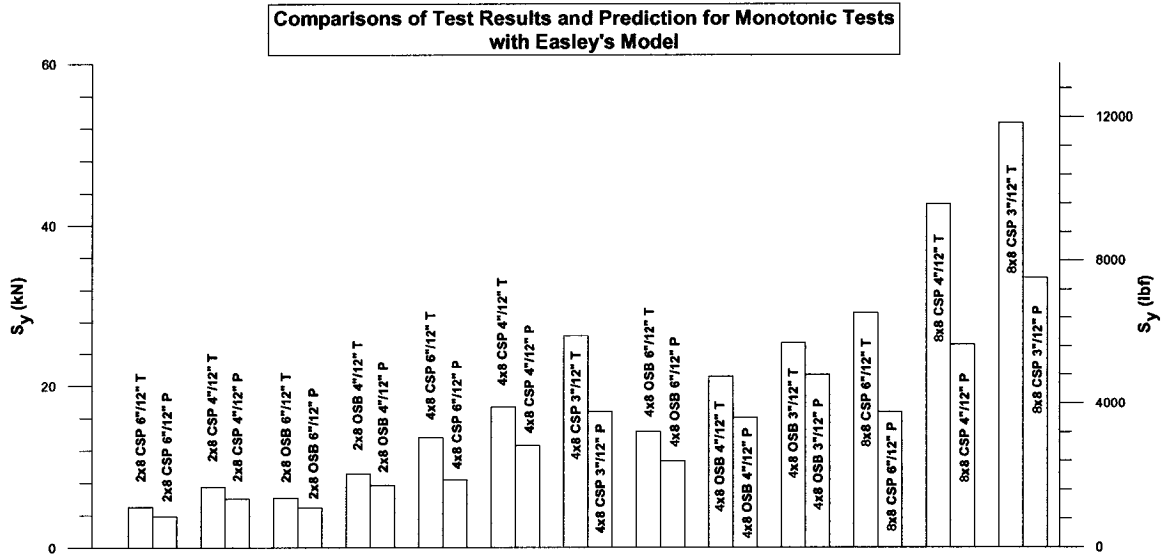


Figure A-VII.17

Comparisons between Test Results and Prediction from Easley's Model

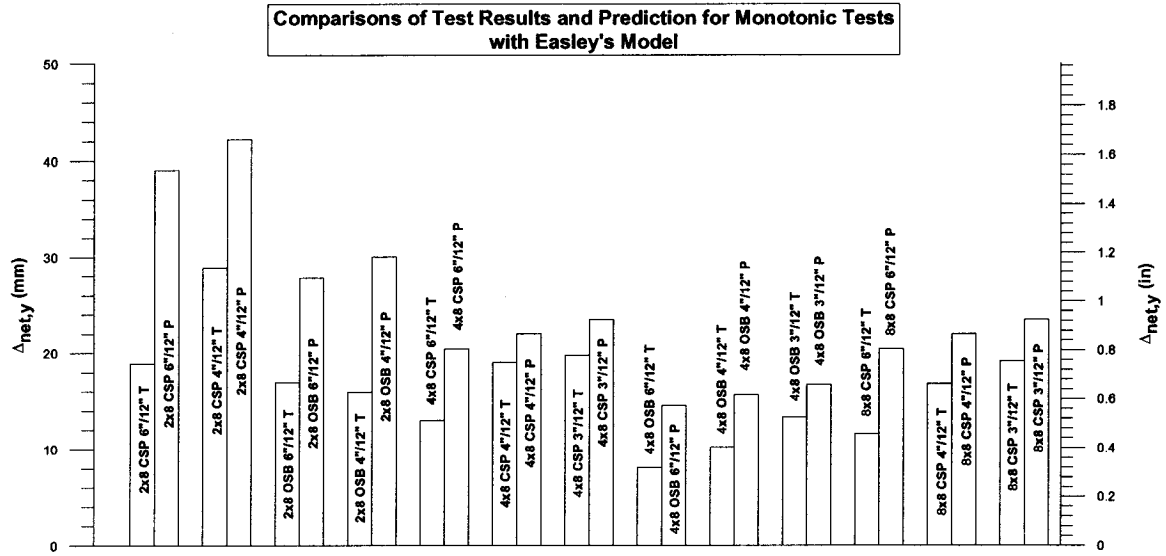


Figure A-VII.18

Comparisons between Test Results and Prediction from Easley's Model

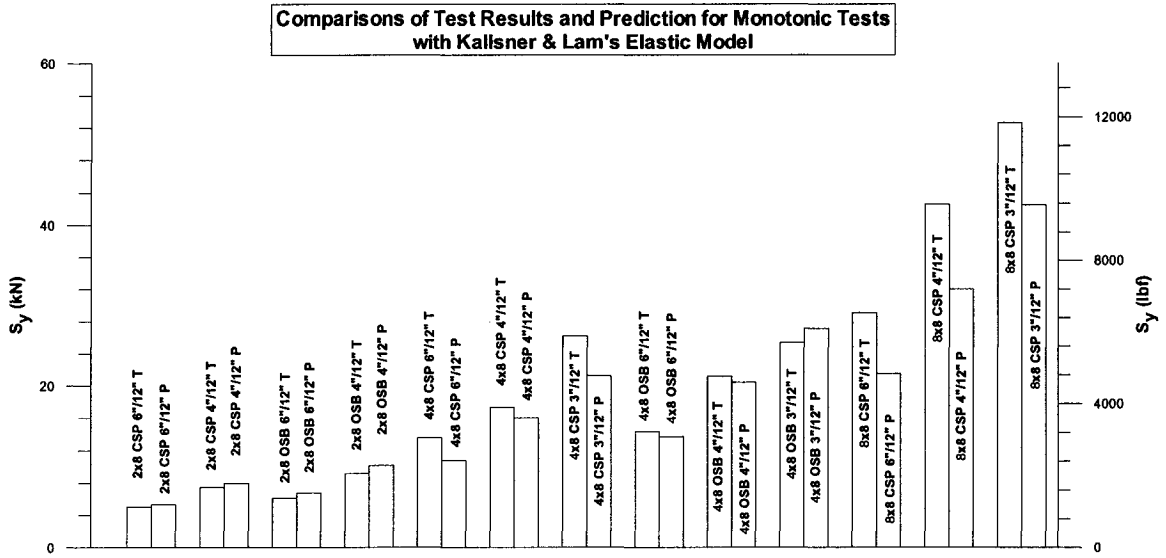


Figure A-VII.19

Comparisons between Test Results and Prediction from Kallsner & Lam's Elastic Model

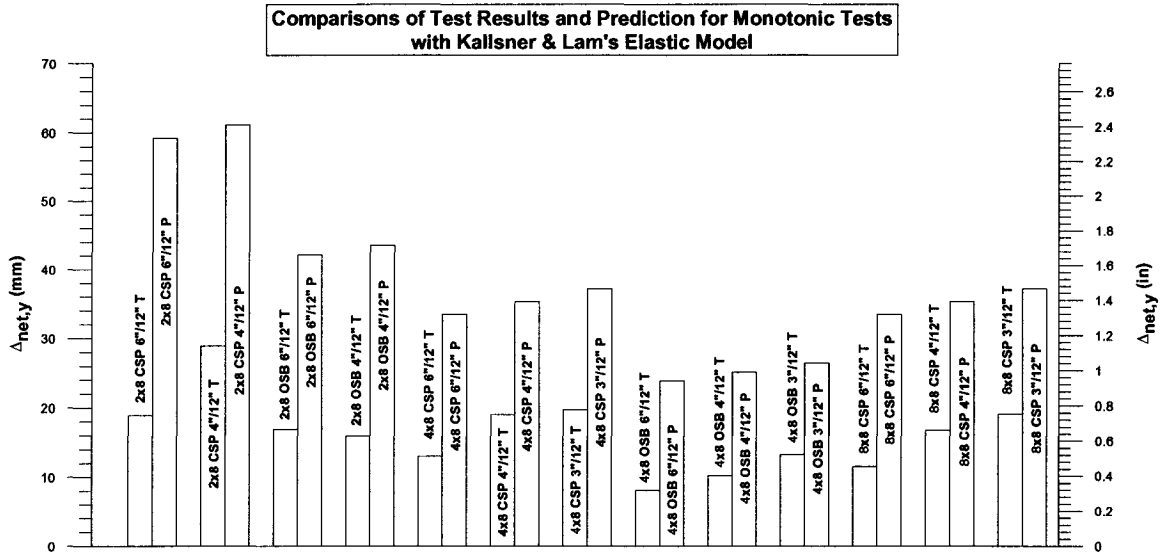


Figure A-VII.20

Comparisons between Test Results and Prediction from Kallsner & Lam's Elastic Model

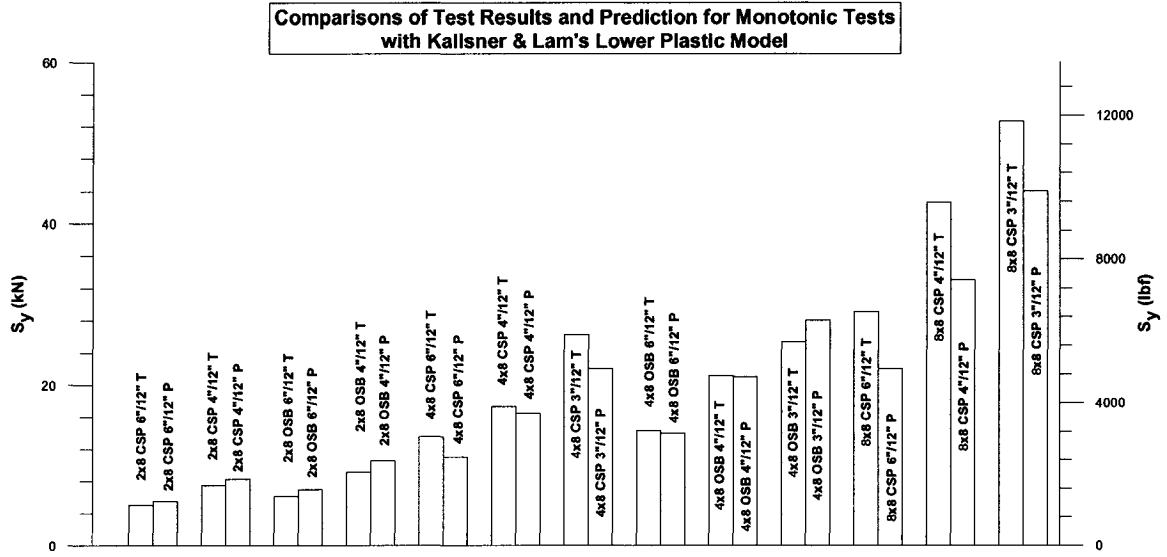


Figure A-VII.21

Comparisons between Test Results and Prediction from Kallsner & Lam's Lower Plastic Model

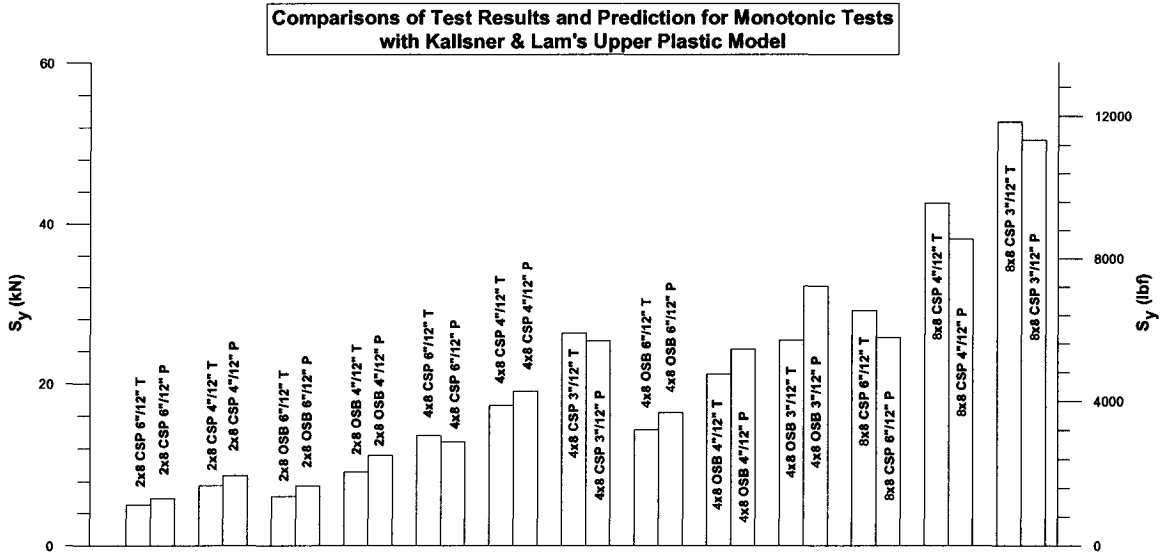


Figure A-VII.22

Comparisons between Test Results and Prediction from Kallsner & Lam's Upper Plastic Model

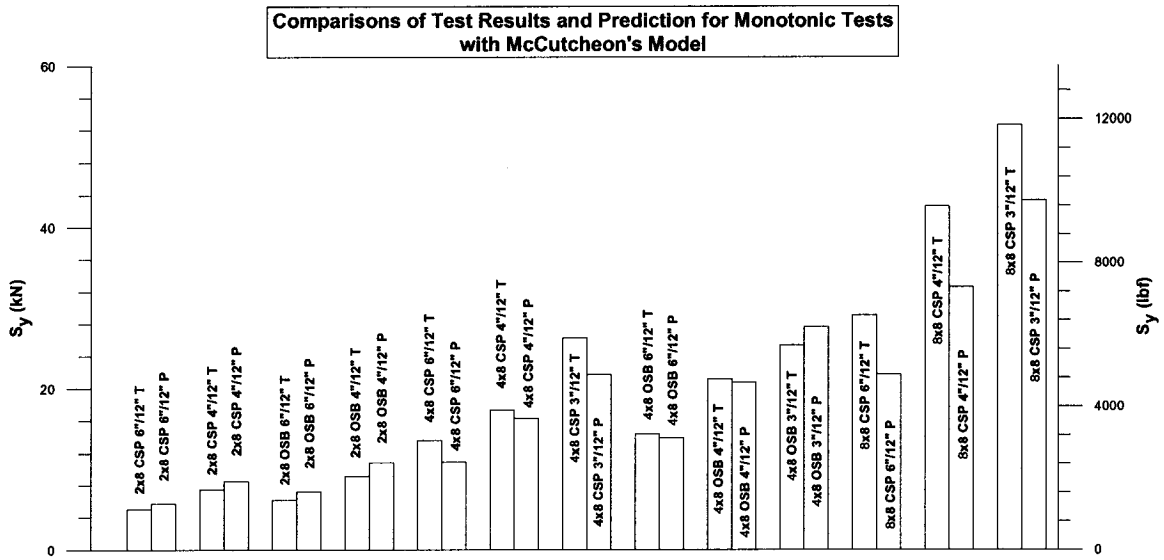


Figure A-VII.23

Comparisons between Test Results and Prediction from McCutcheon's Model

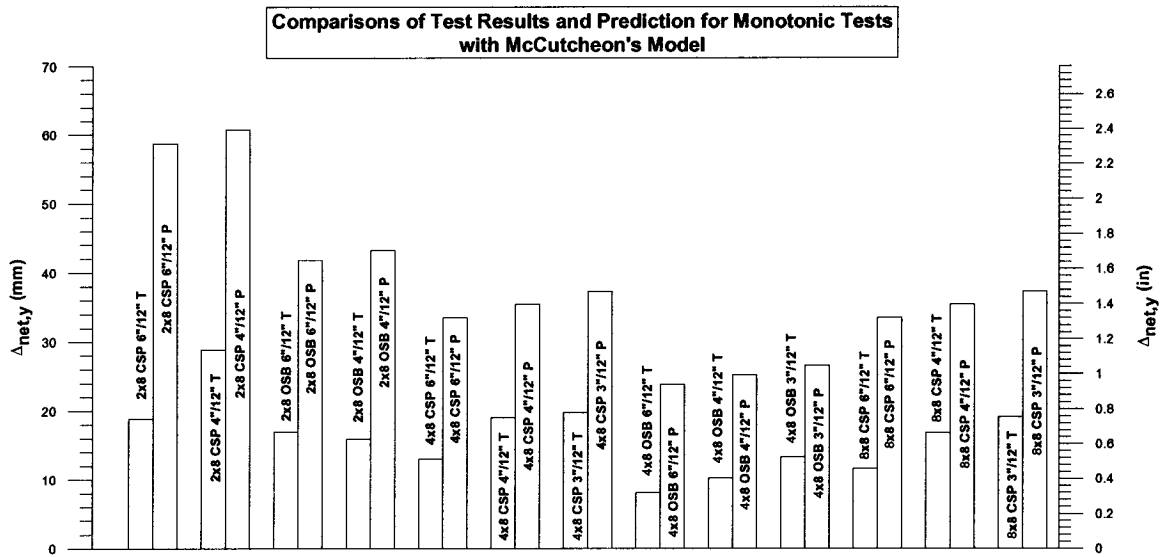


Figure A-VII.24

Comparisons between Test Results and Prediction from McCutcheon's Model

(4) EEEP\_25

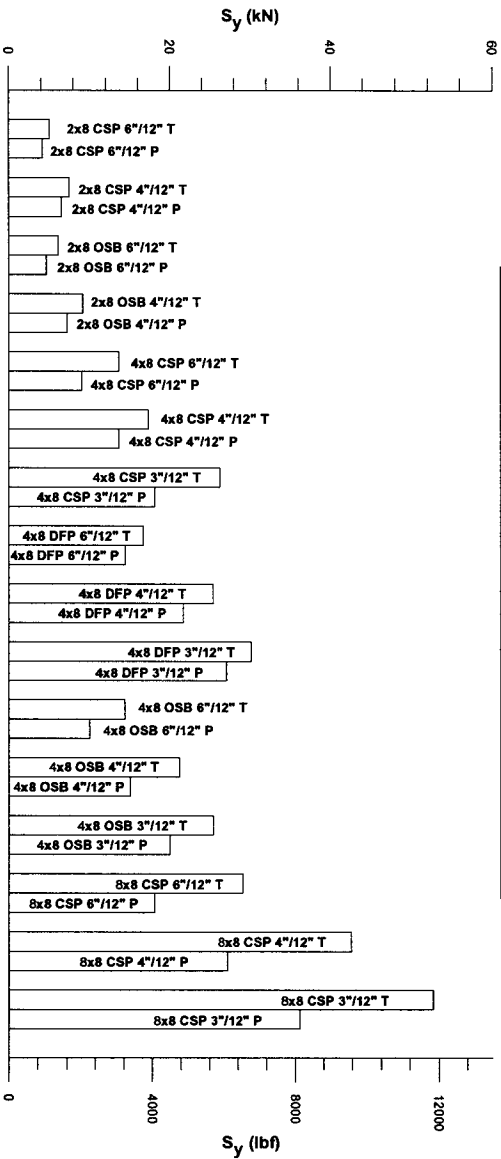


Figure A-VII.25

Comparisons between Test Results and Prediction from Easley's Model

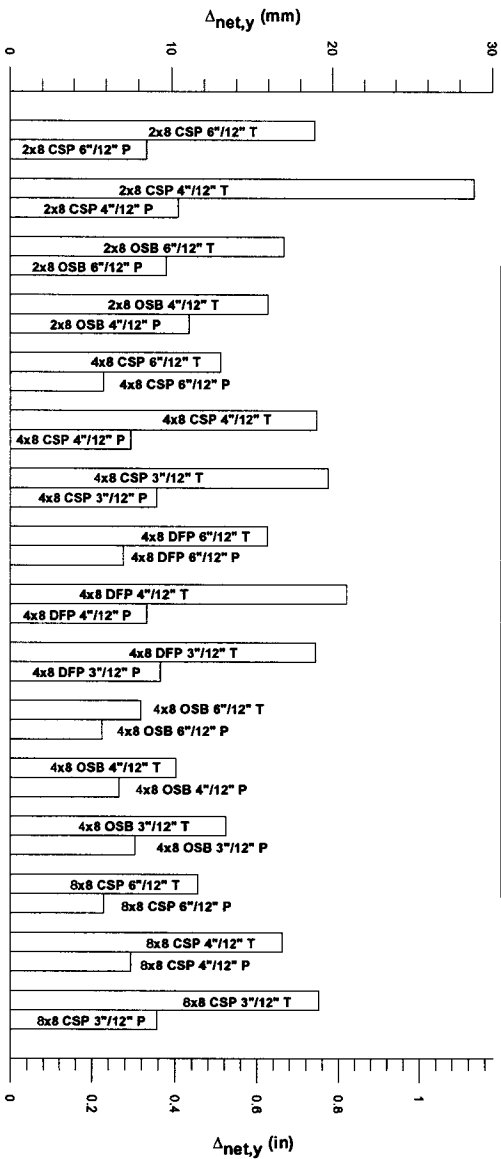


Figure A-VII.26

Comparisons between Test Results and Prediction from Easley's Model

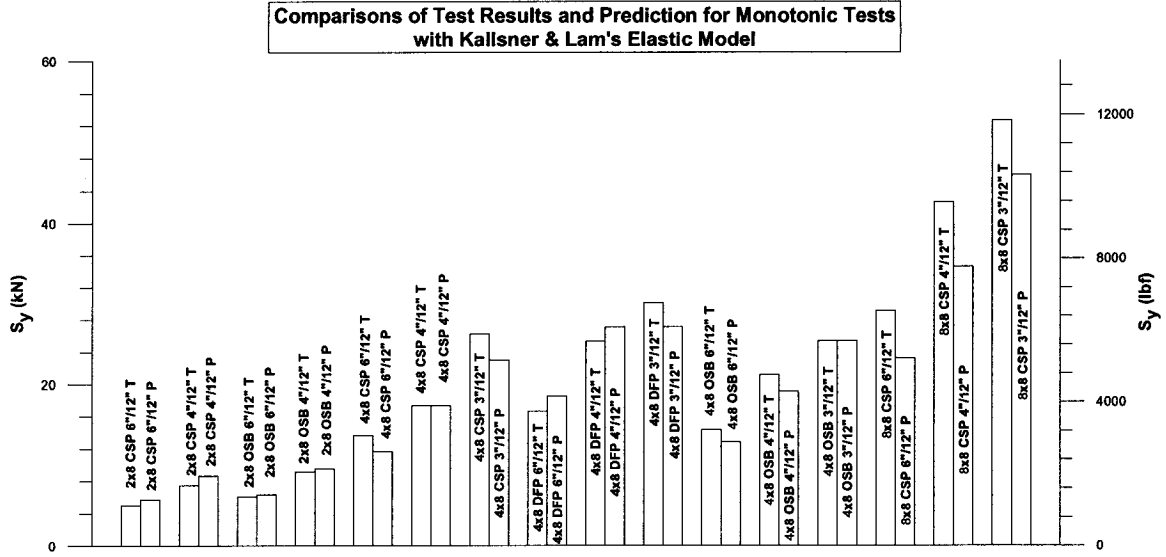


Figure A-VII.27

Comparisons between Test Results and Prediction from Kallsner & Lam's Elastic Model

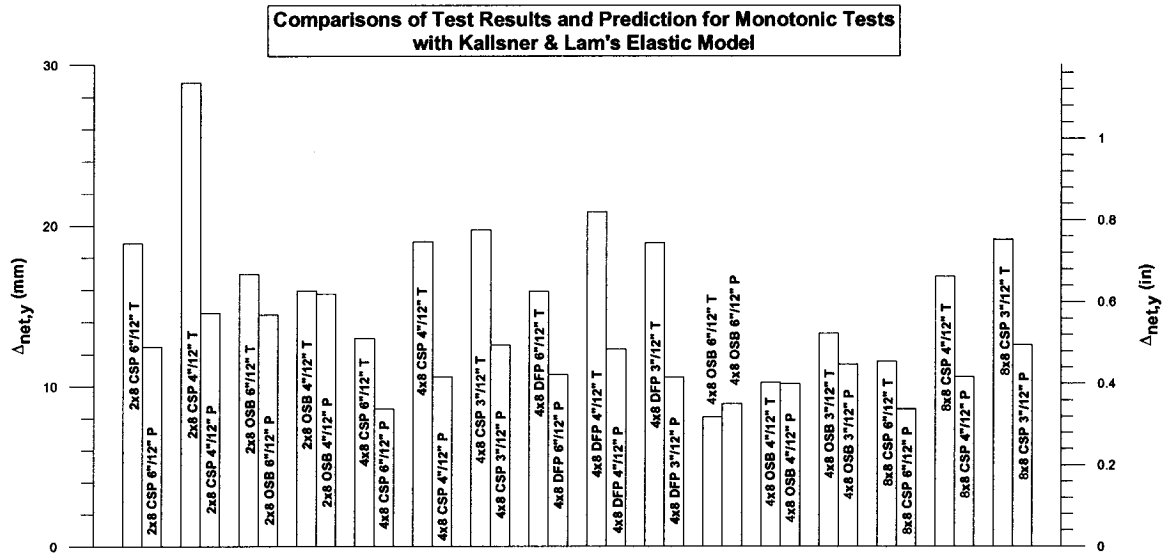


Figure A-VII.28

Comparisons between Test Results and Prediction from Kallsner & Lam's Elastic Model

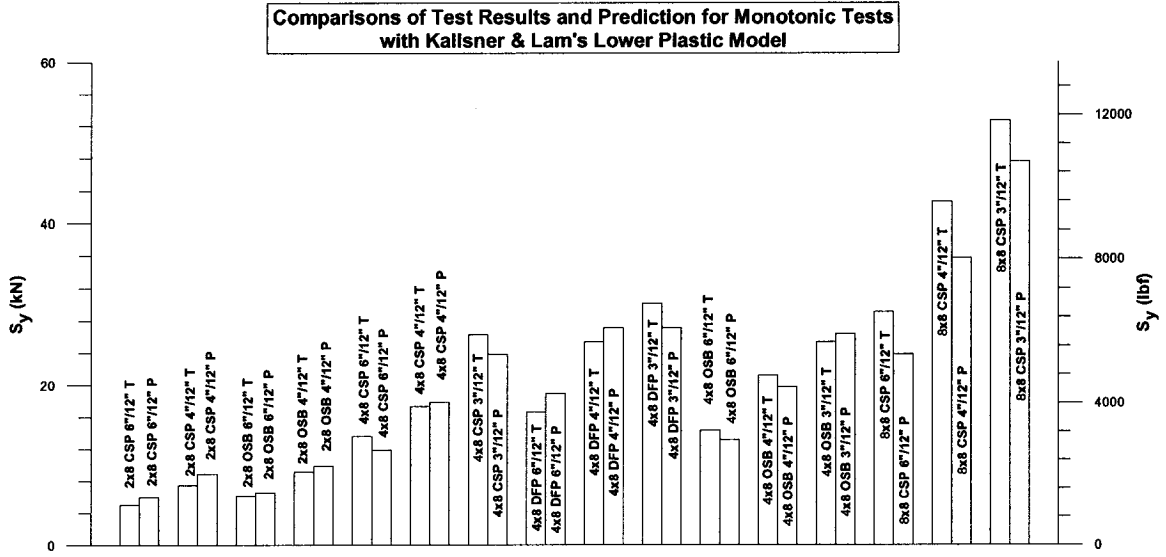


Figure A-VII.29

Comparisons between Test Results and Prediction from Kallsner & Lam's Lower Plastic Model

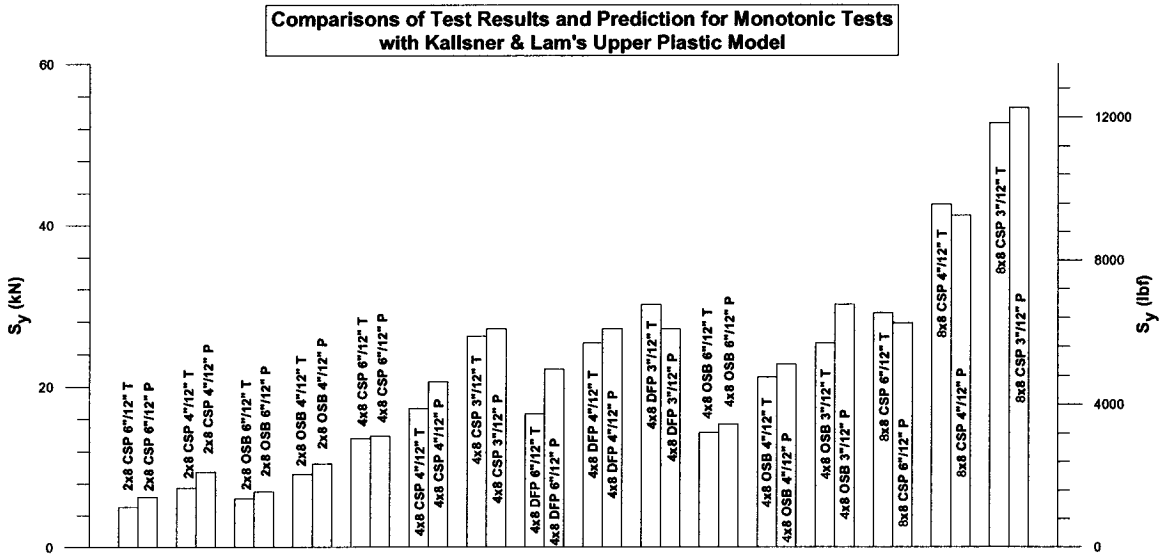


Figure A-VII.30

Comparisons between Test Results and Prediction from Kallsner & Lam's Upper Plastic Model

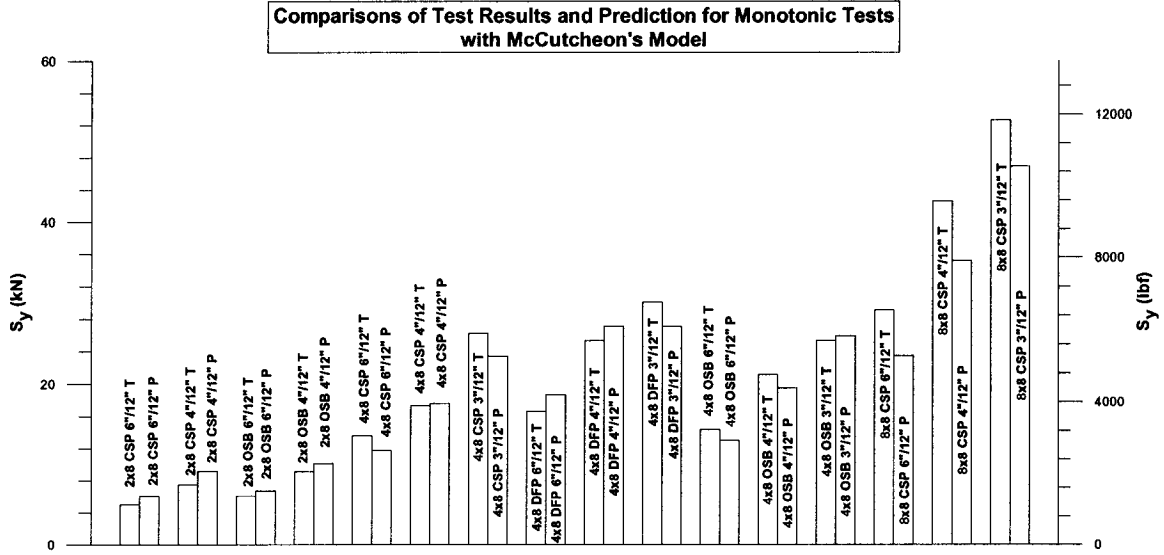


Figure A-VII.31

Comparisons between Test Results and Prediction from McCutcheon's Model

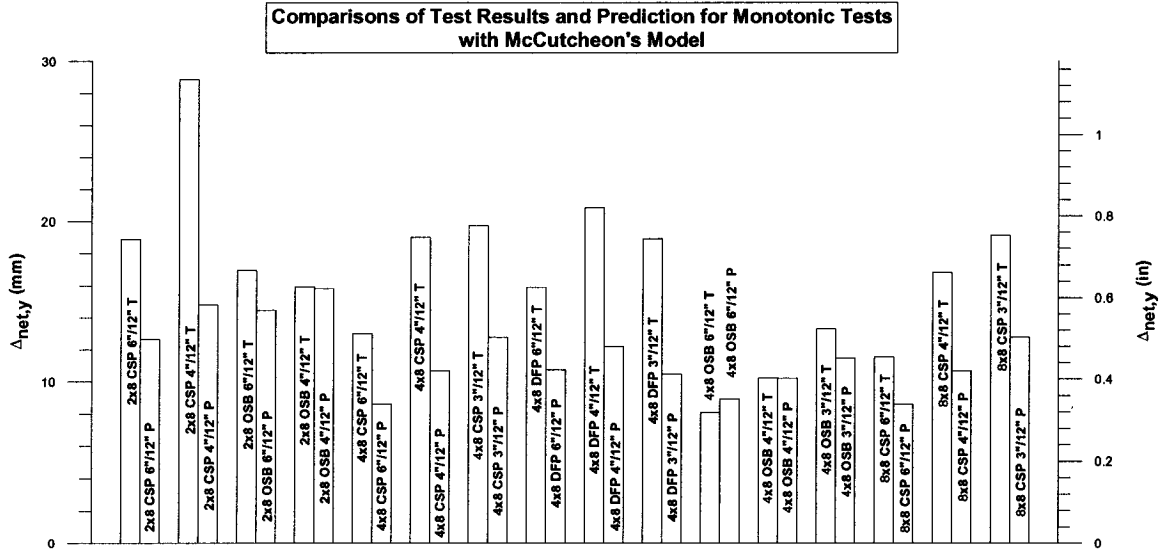


Figure A-VII.32

Comparisons between Test Results and Prediction from McCutcheon's Model

(5) Max. Load\_25&ke

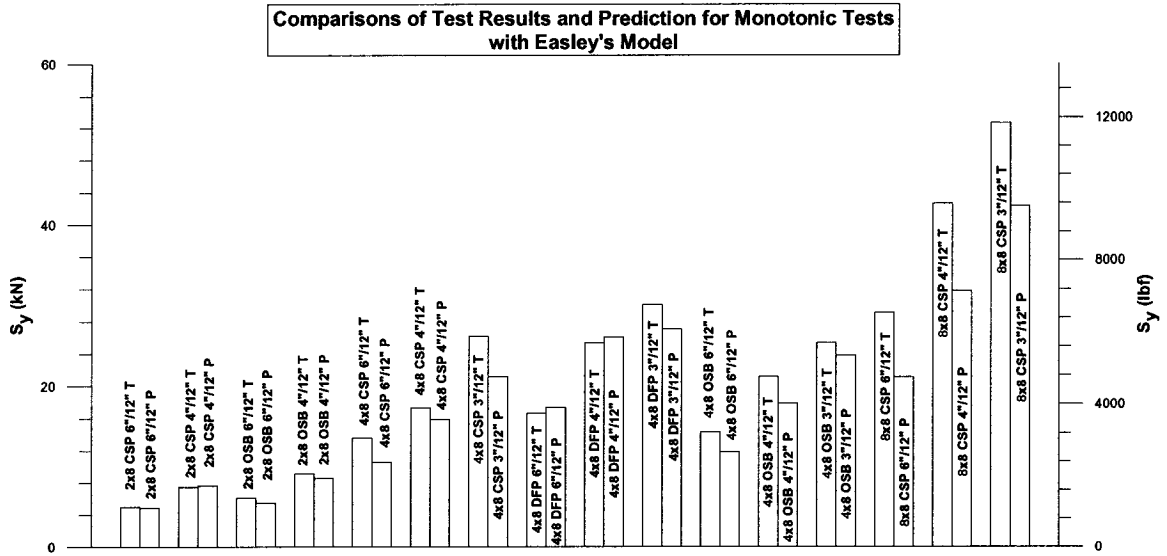


Figure A-VII.33

Comparisons between Test Results and Prediction from Easley's Model

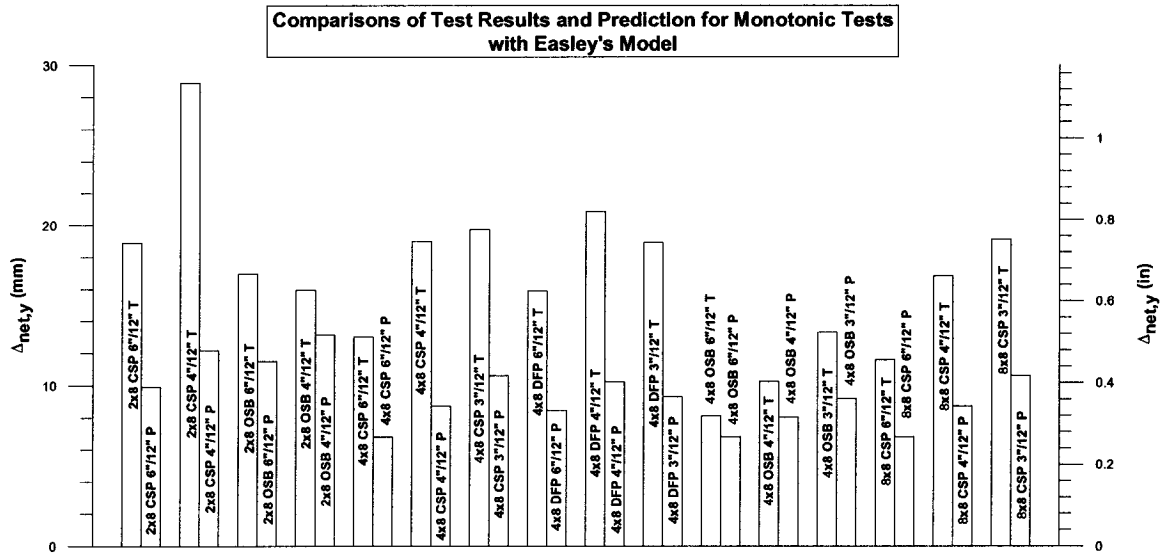


Figure A-VII.34

Comparisons between Test Results and Prediction from Easley's Model

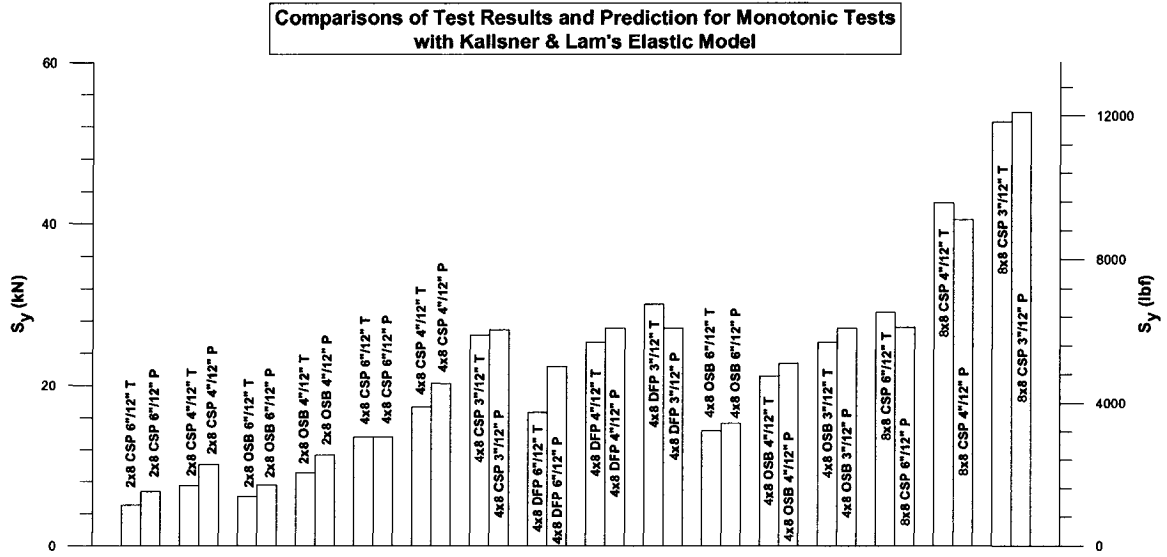


Figure A-VII.35

Comparisons between Test Results and Prediction from Kallsner & Lam's Elastic Model

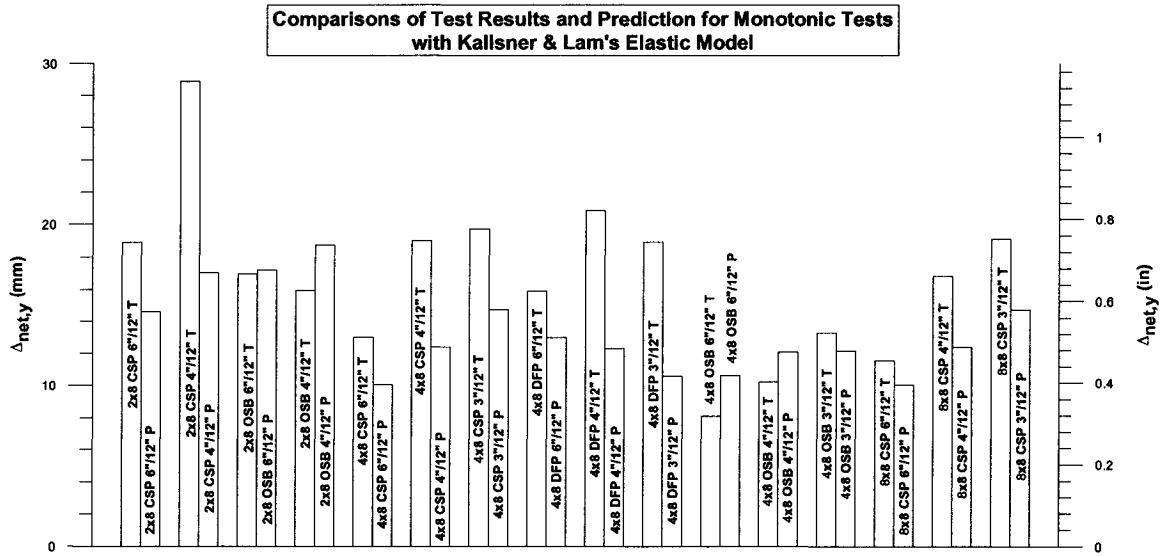


Figure A-VII.36

Comparisons between Test Results and Prediction from Kallsner & Lam's Elastic Model

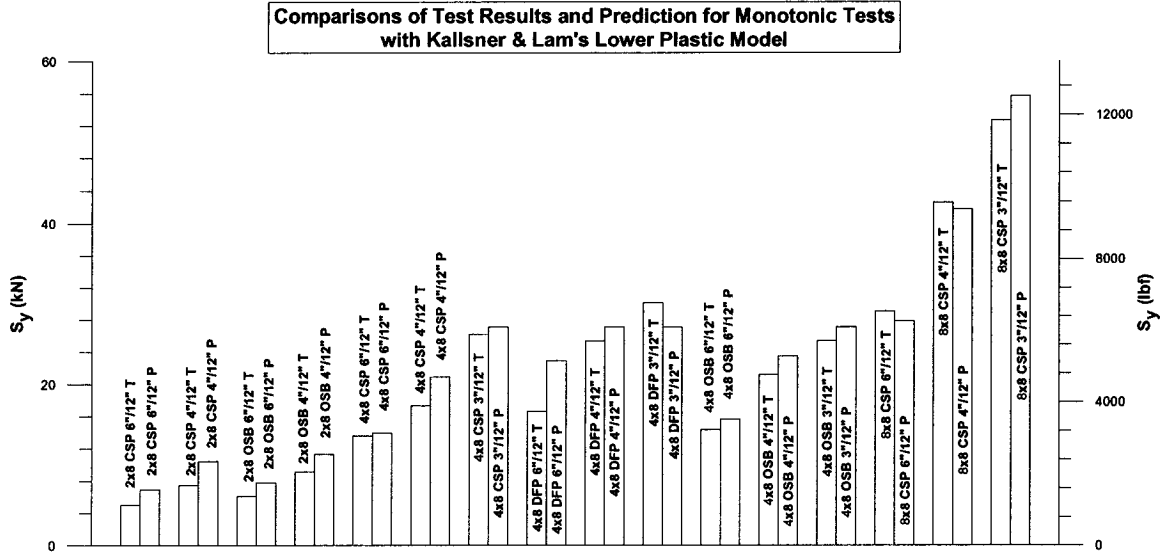


Figure A-VII.37

Comparisons between Test Results and Prediction from Kallsner & Lam's Lower Plastic Model

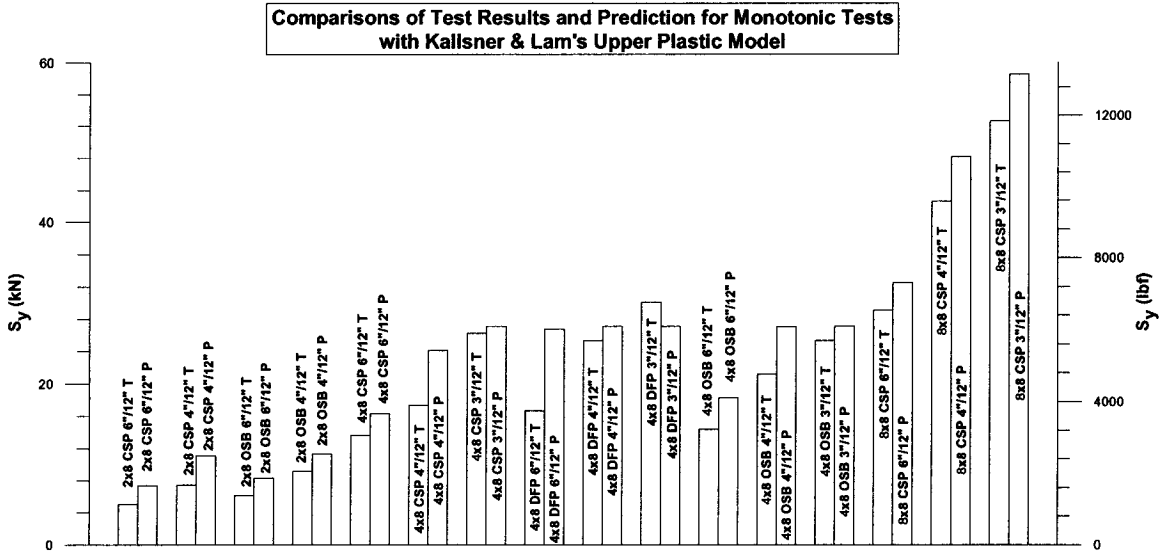


Figure A-VII.38

Comparisons between Test Results and Prediction from Kallsner & Lam's Upper Plastic Model

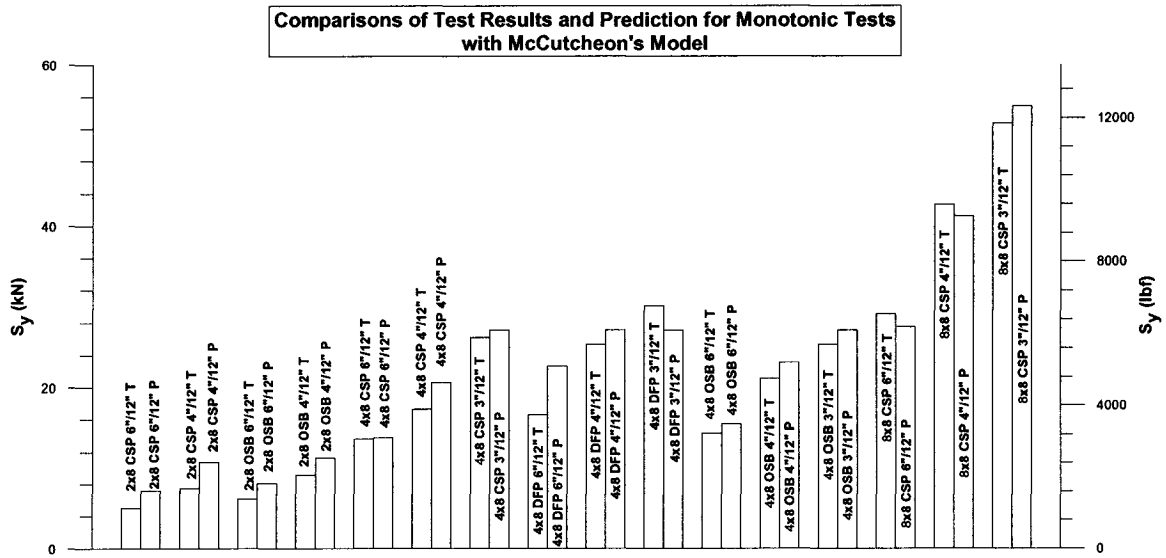


Figure A-VII.39

Comparisons between Test Results and Prediction from McCutcheon's Model

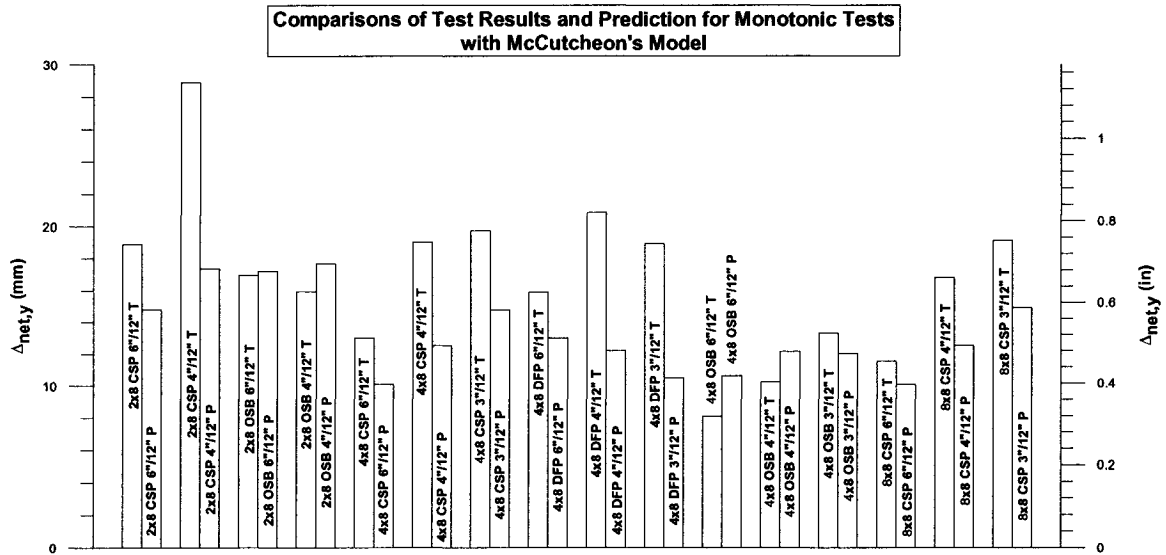


Figure A-VII.40

Comparisons between Test Results and Prediction from McCutcheon's Model

(6) Max. Load\_25&ks

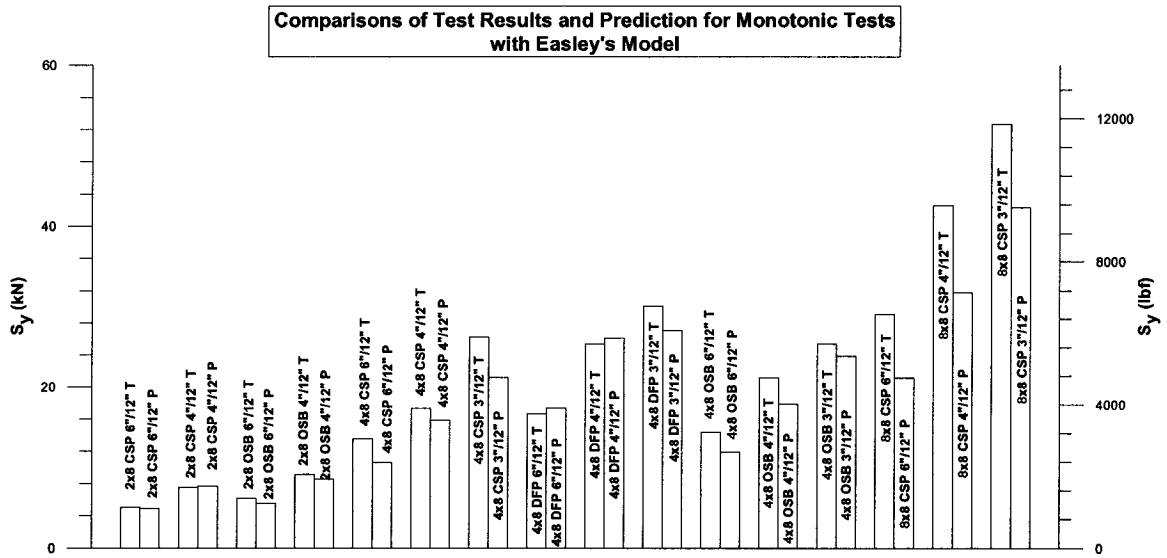


Figure A-VII.41

Comparisons between Test Results and Prediction from Easley's Model

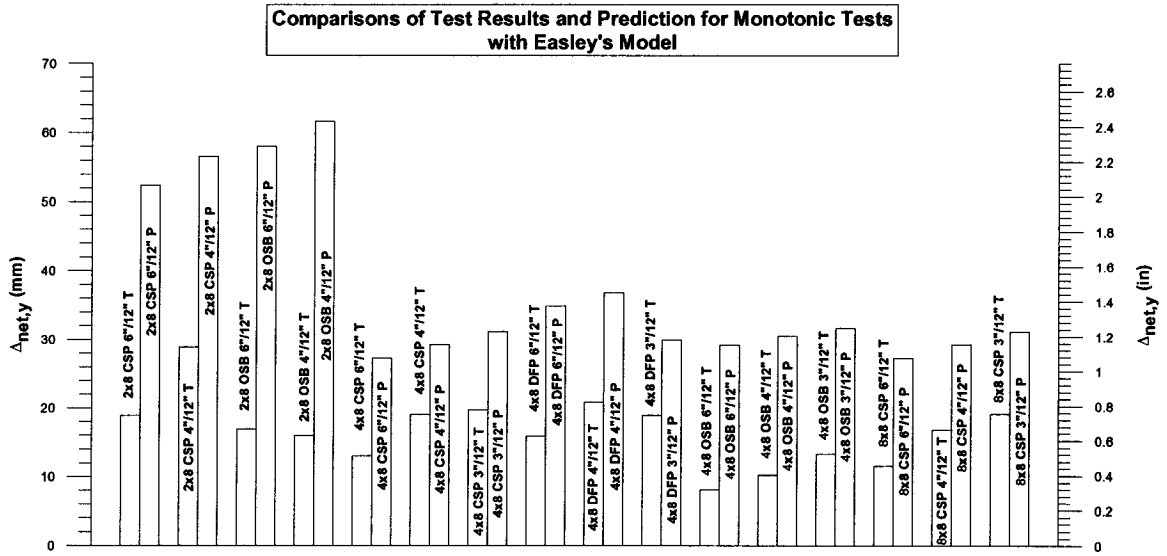


Figure A-VII.42

Comparisons between Test Results and Prediction from Easley's Model

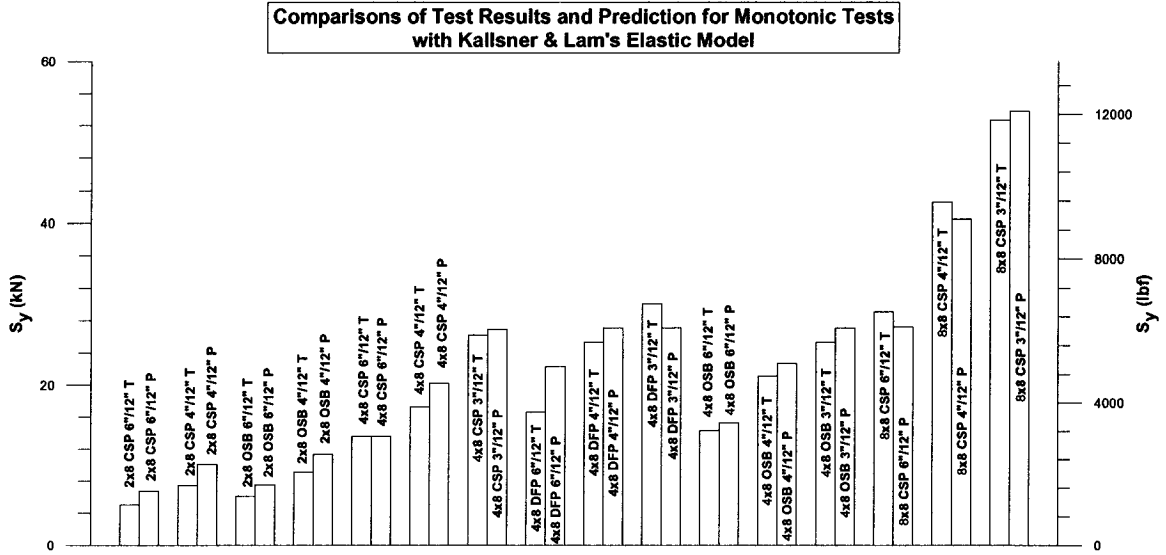


Figure A-VII.43

Comparisons between Test Results and Prediction from Kallsner & Lam's Elastic Model

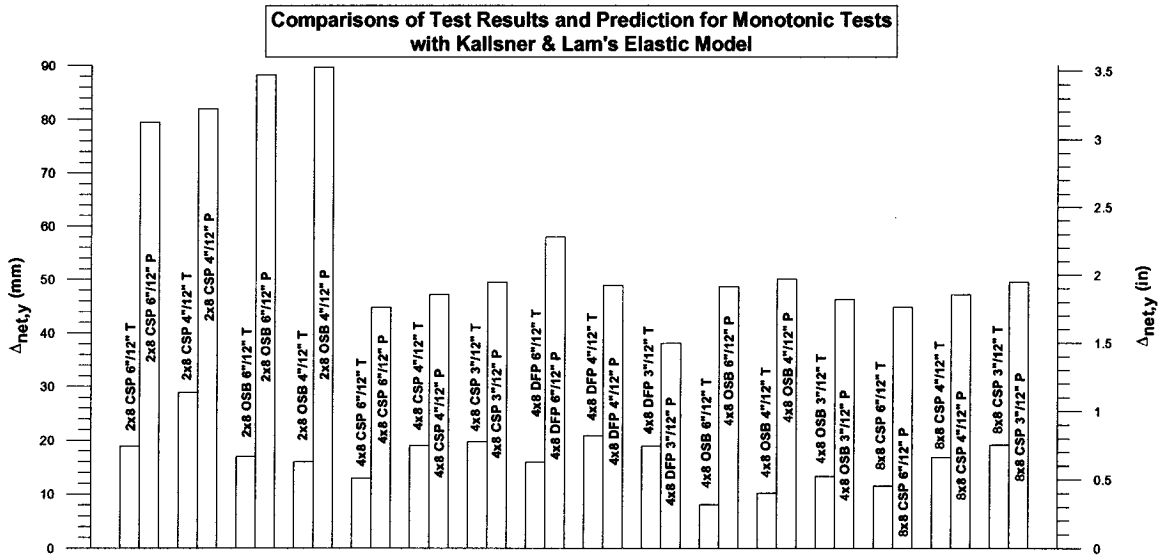


Figure A-VII.44

Comparisons between Test Results and Prediction from Kallsner & Lam's Elastic Model

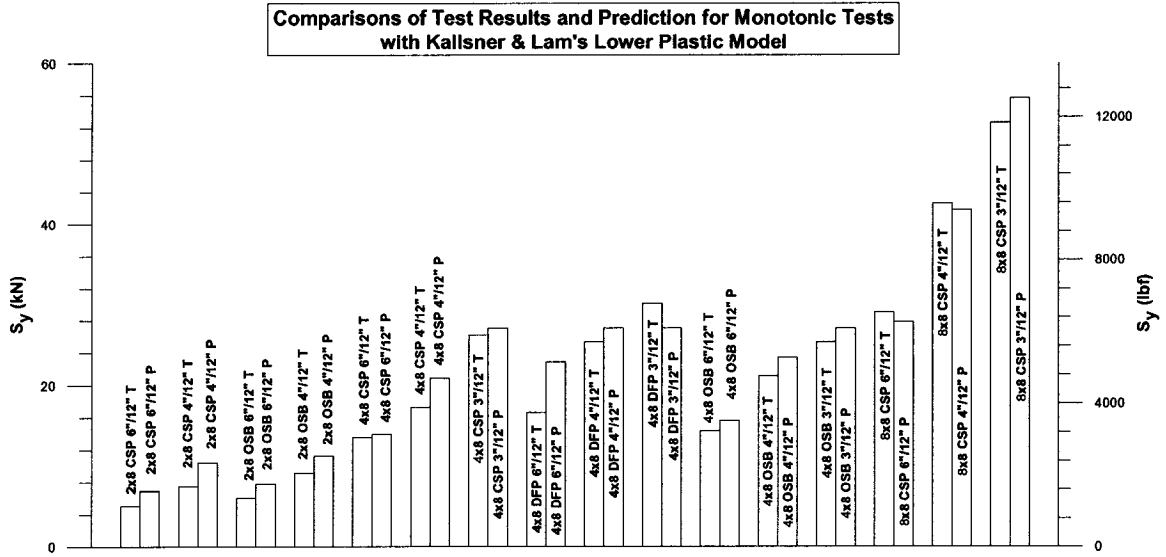


Figure A-VII.45

Comparisons between Test Results and Prediction from Kallsner & Lam's Lower Plastic Model

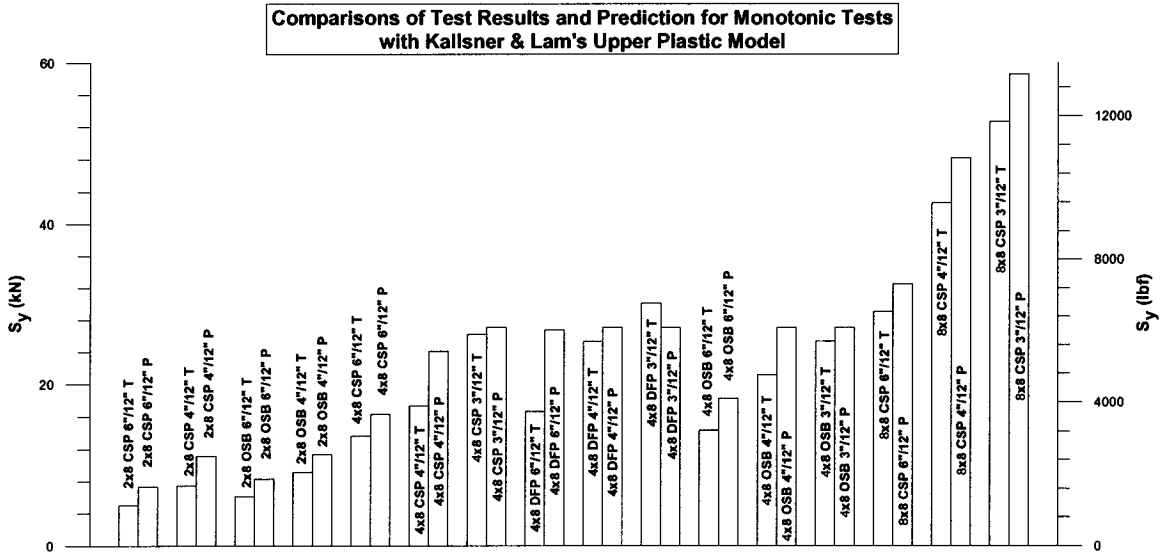


Figure A-VII.46

Comparisons between Test Results and Prediction from Kallsner & Lam's Upper Plastic Model

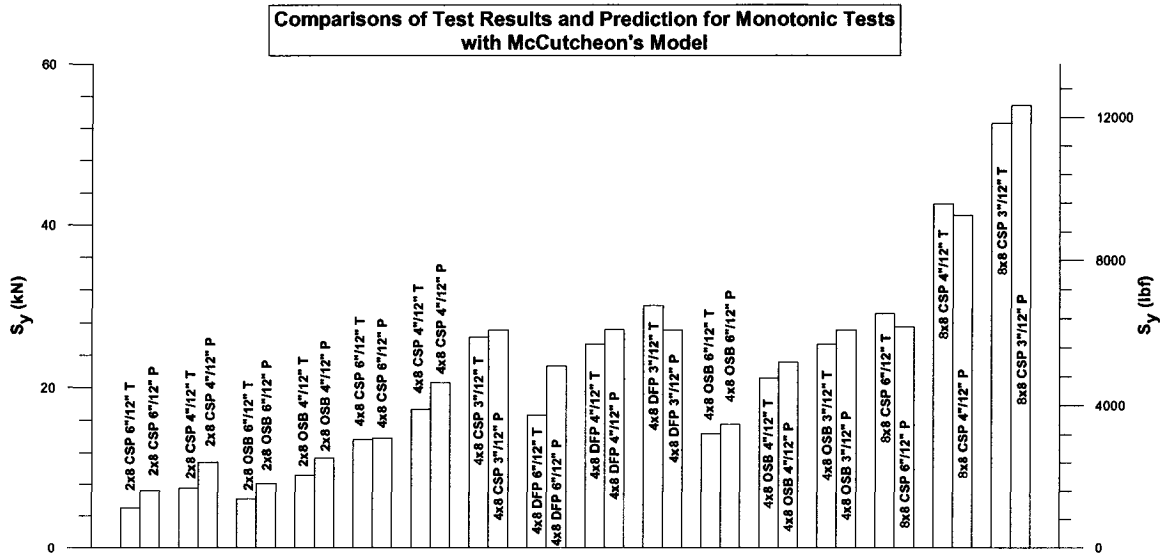


Figure A-VII.47

Comparisons between Test Results and Prediction from McCutcheon's Model

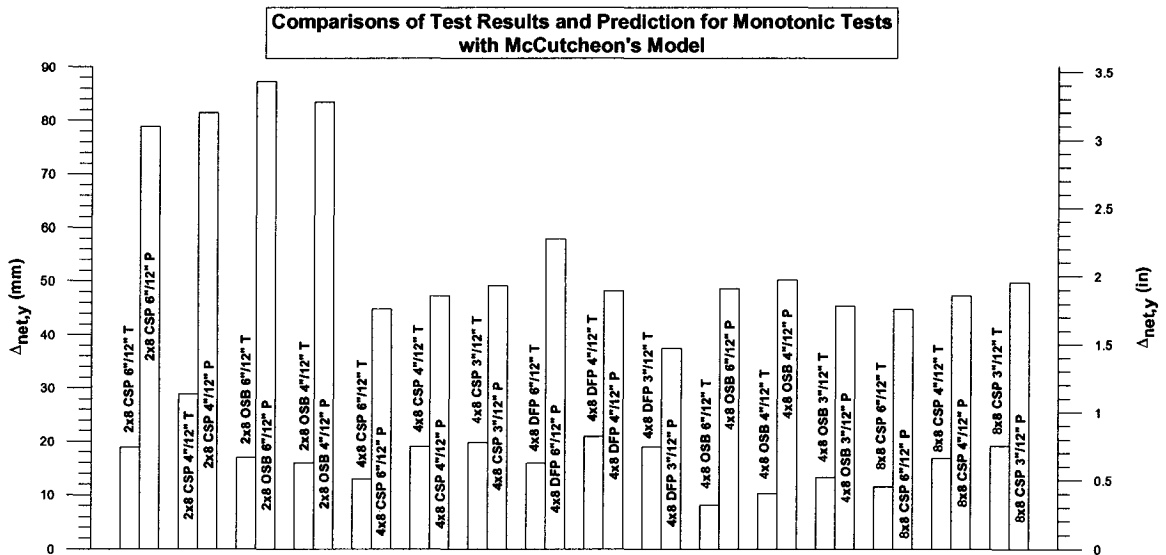


Figure A-VII.48

Comparisons between Test Results and Prediction from McCutcheon's Model

## II. REVERSE CYCLIC TESTS

### (1) EEEP\_25

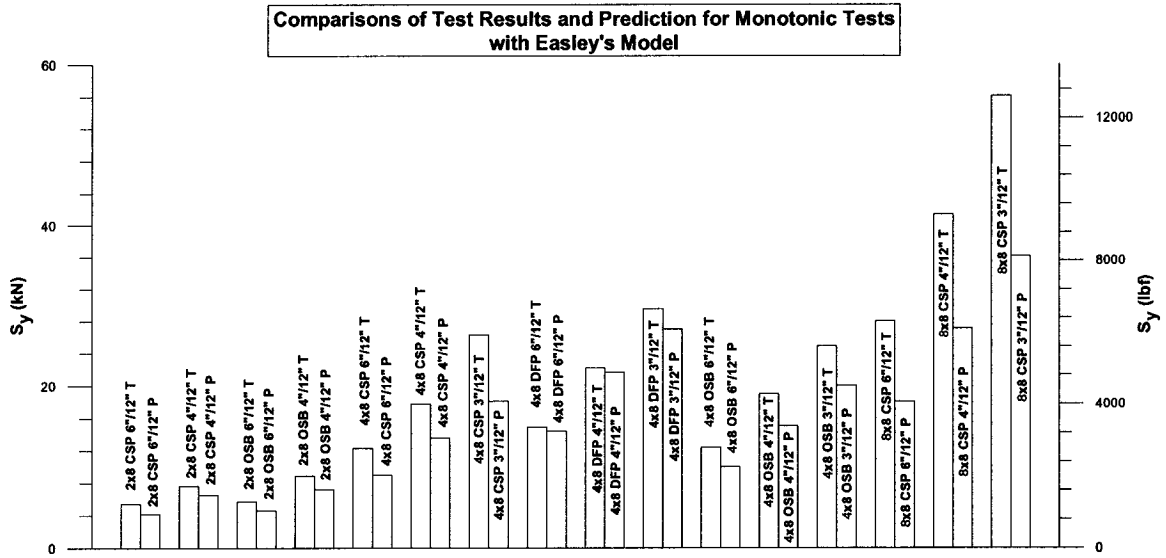


Figure A-VII.49

Comparisons between Test Results and Prediction from Easley's Model

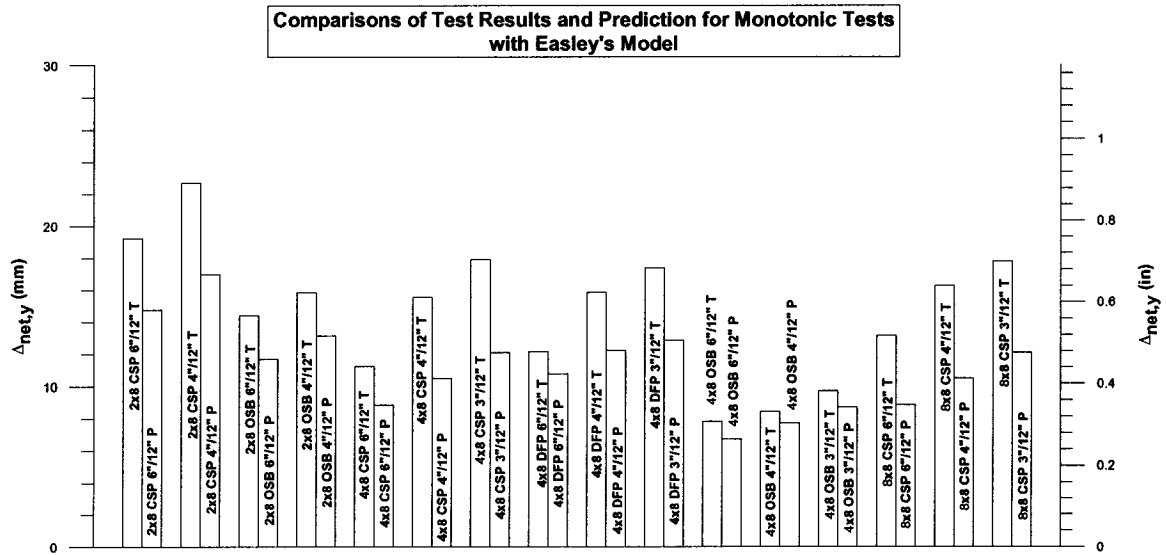


Figure A-VII.50

Comparisons between Test Results and Prediction from Easley's Model

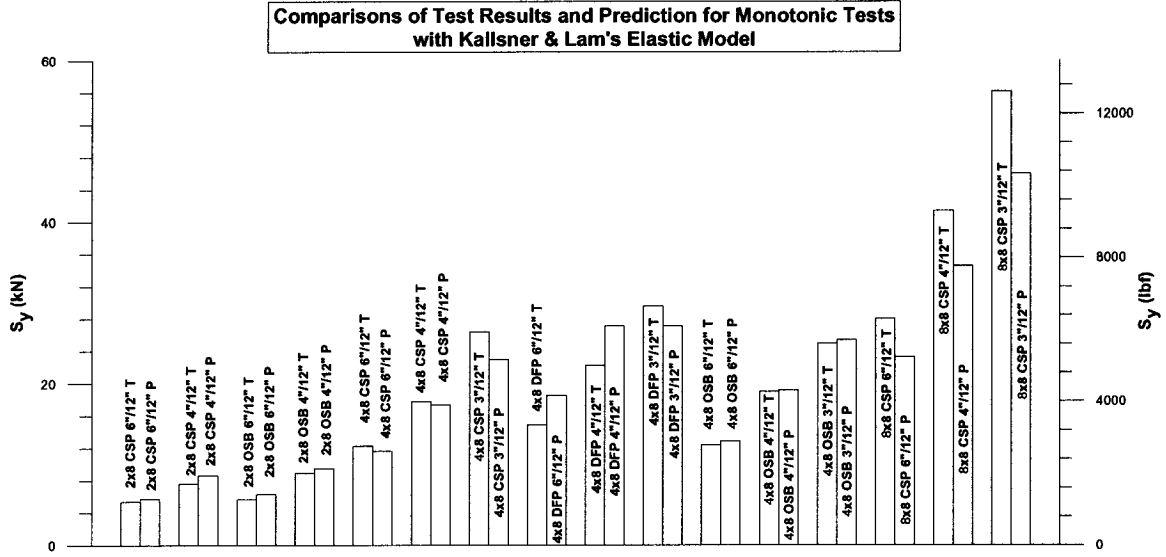


Figure A-VII.51

Comparisons between Test Results and Prediction from Kallsner & Lam's Elastic Model

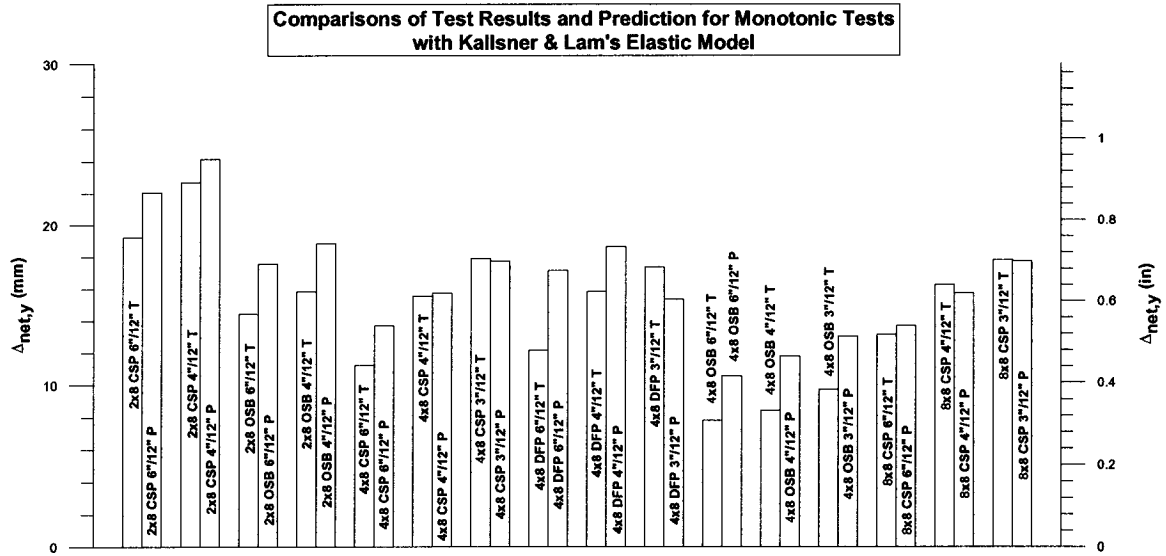


Figure A-VII.52

Comparisons between Test Results and Prediction from Kallsner & Lam's Elastic Model

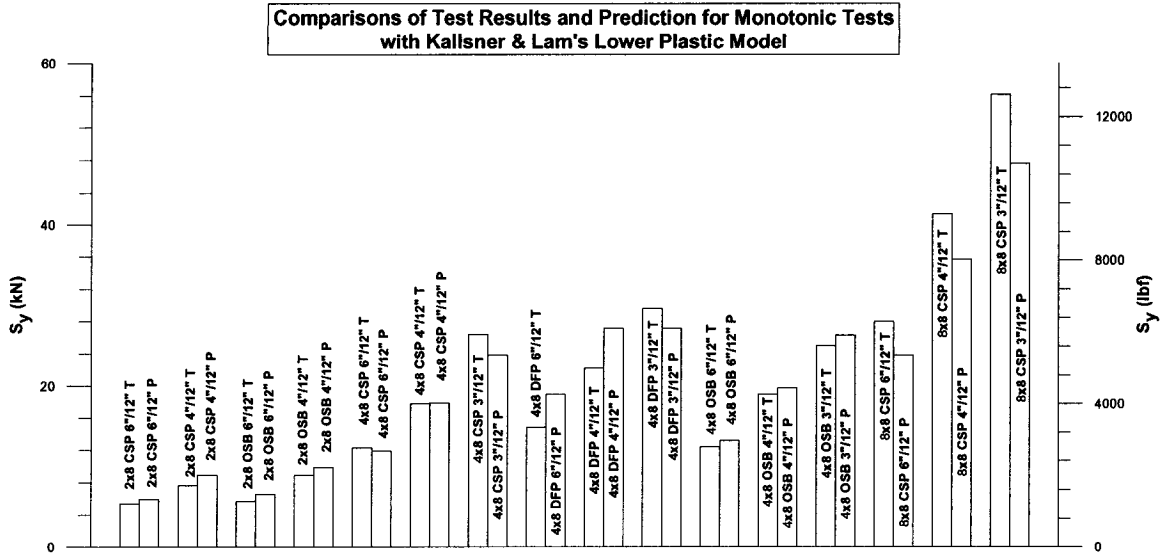


Figure A-VII.53

Comparisons between Test Results and Prediction from Kallsner & Lam's Lower Plastic Model

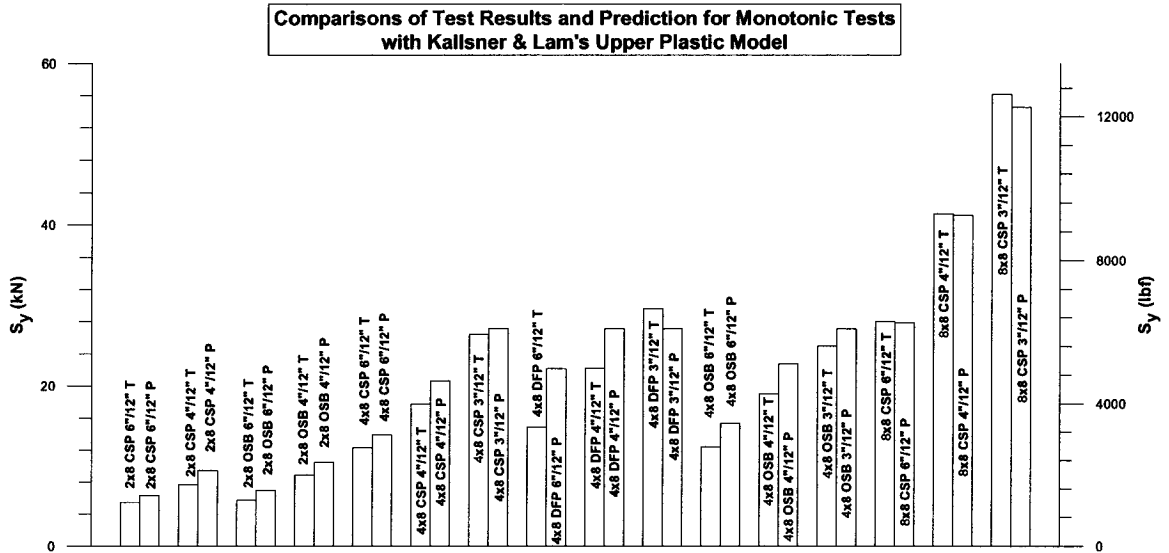


Figure A-VII.54

Comparisons between Test Results and Prediction from Kallsner & Lam's Upper Plastic Model

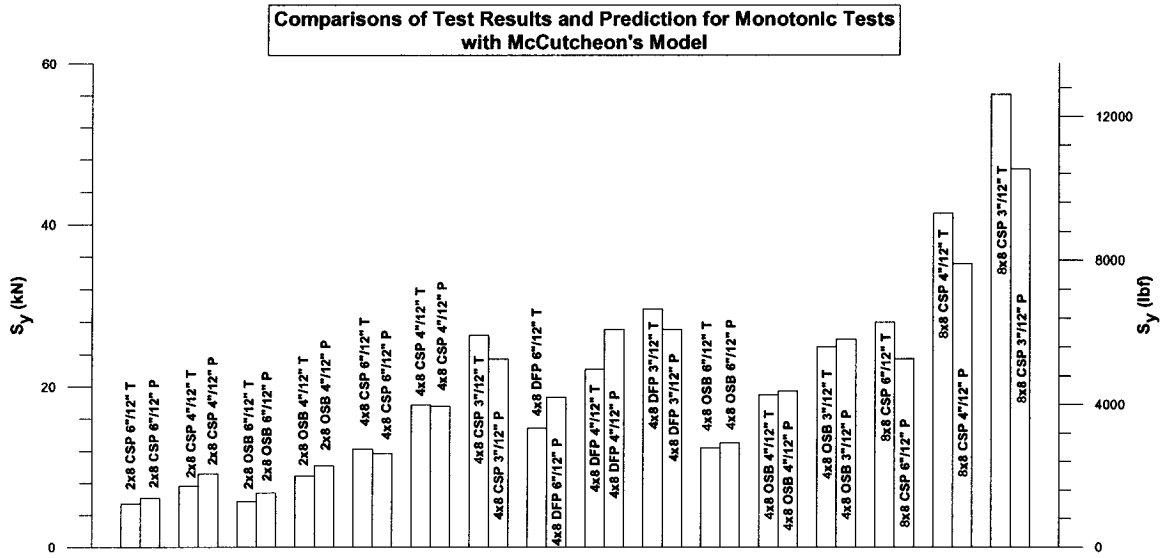


Figure A-VII.55

Comparisons between Test Results and Prediction from McCutcheon's Model

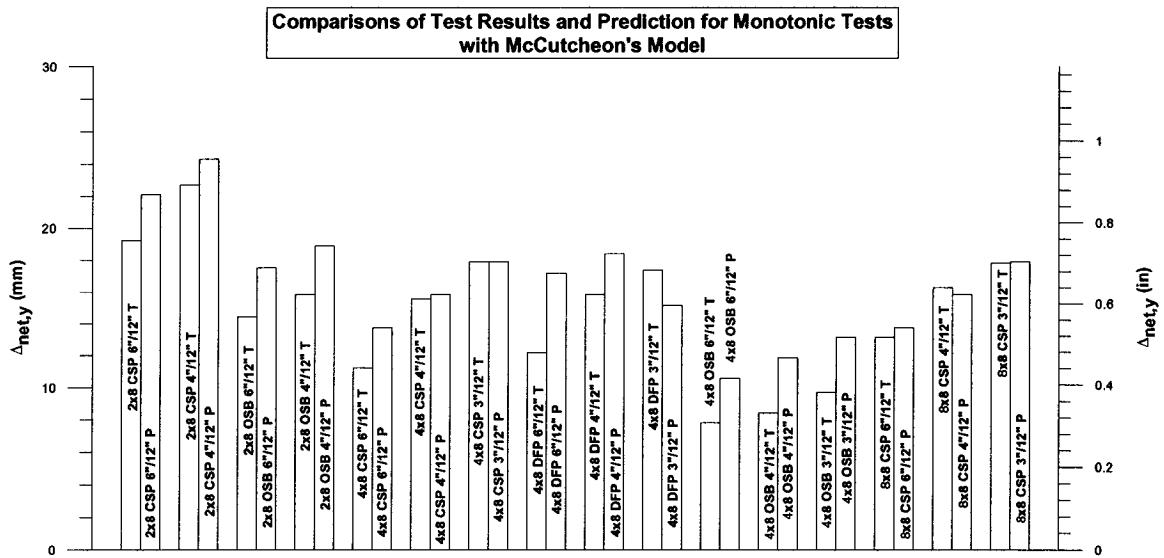


Figure A-VII.56

Comparisons between Test Results and Prediction from McCutcheon's Model

(2) Max. Load\_25&ke

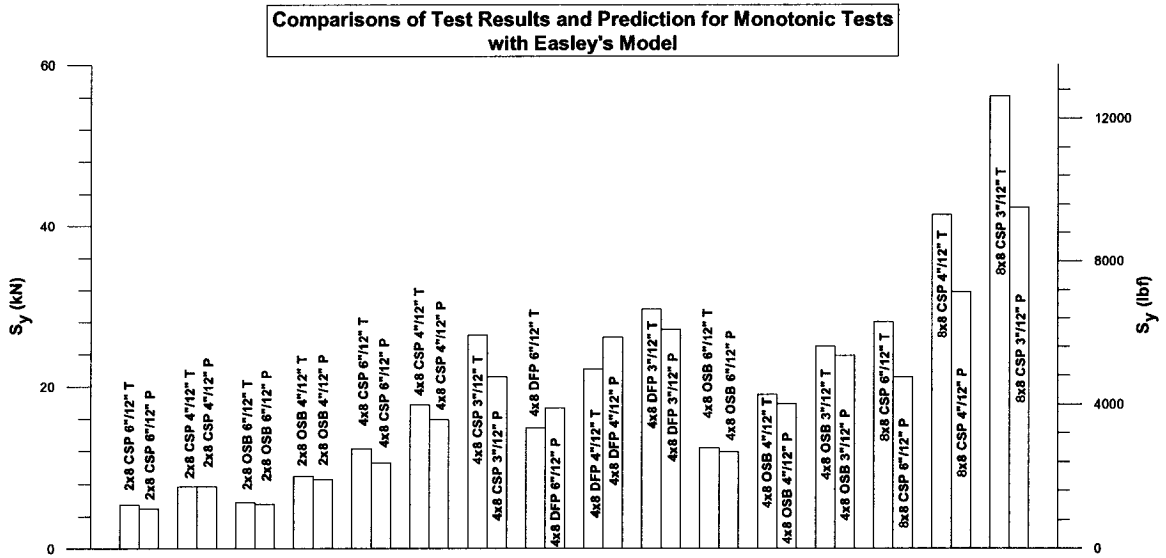


Figure A-VII.57

Comparisons between Test Results and Prediction from Easley's Model

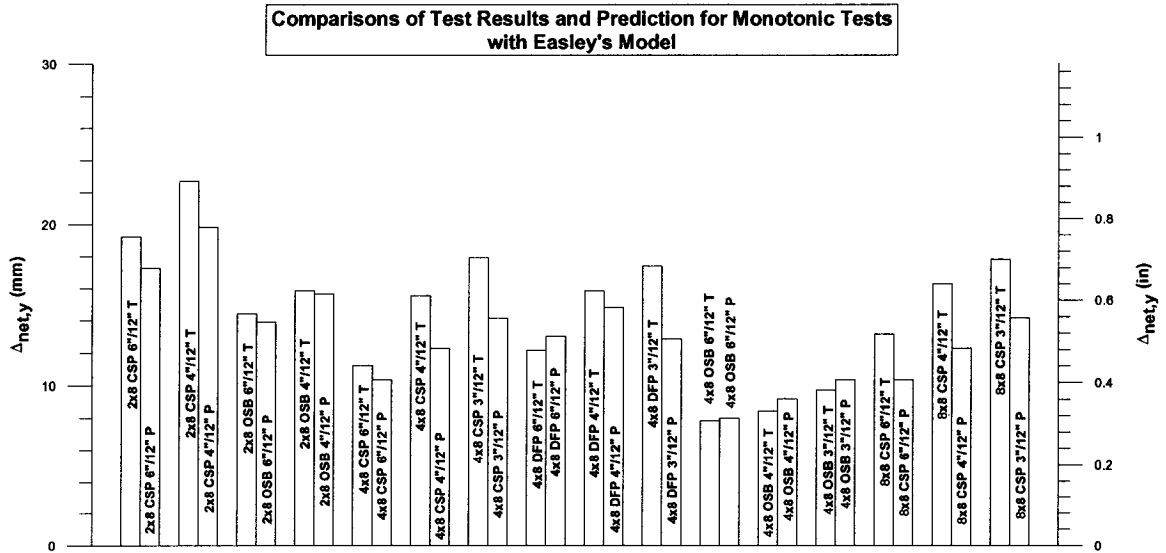


Figure A-VII.58

Comparisons between Test Results and Prediction from Easley's Model

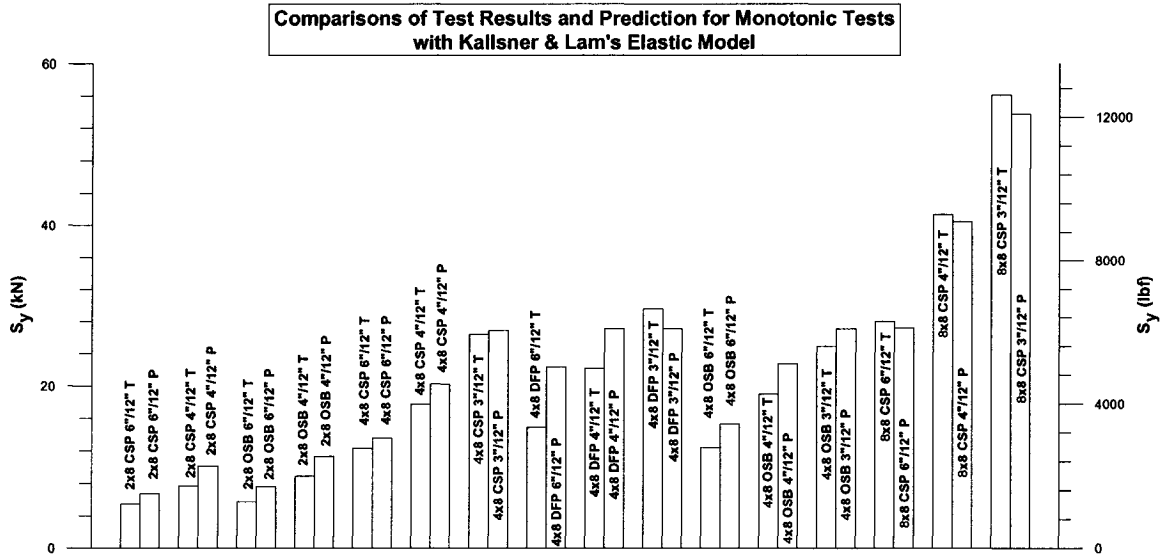


Figure A-VII.59

Comparisons between Test Results and Prediction from Kallsner & Lam's Elastic Model

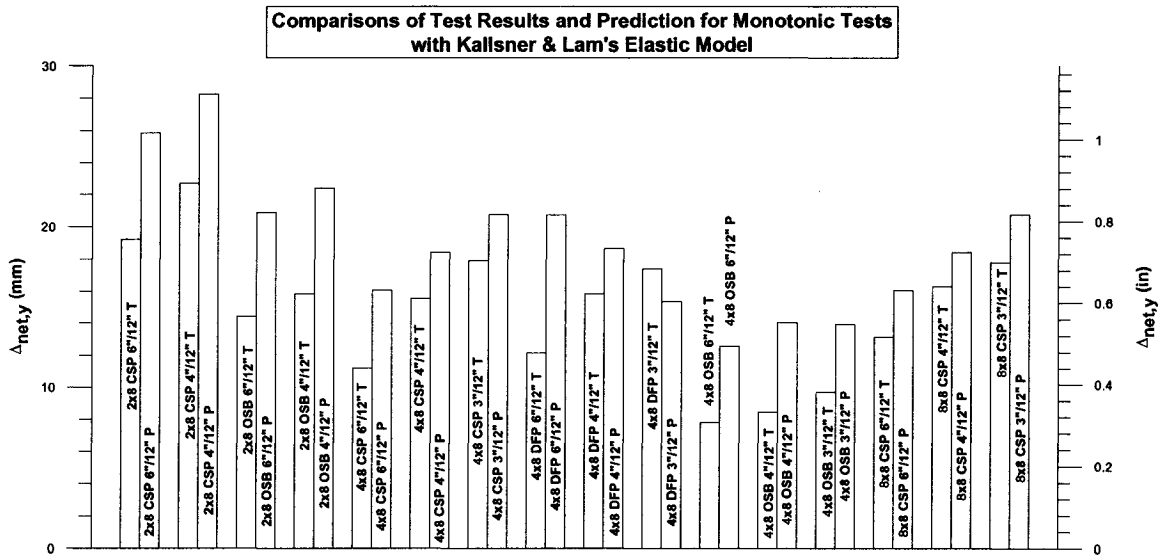


Figure A-VII.60

Comparisons between Test Results and Prediction from Kallsner & Lam's Elastic Model

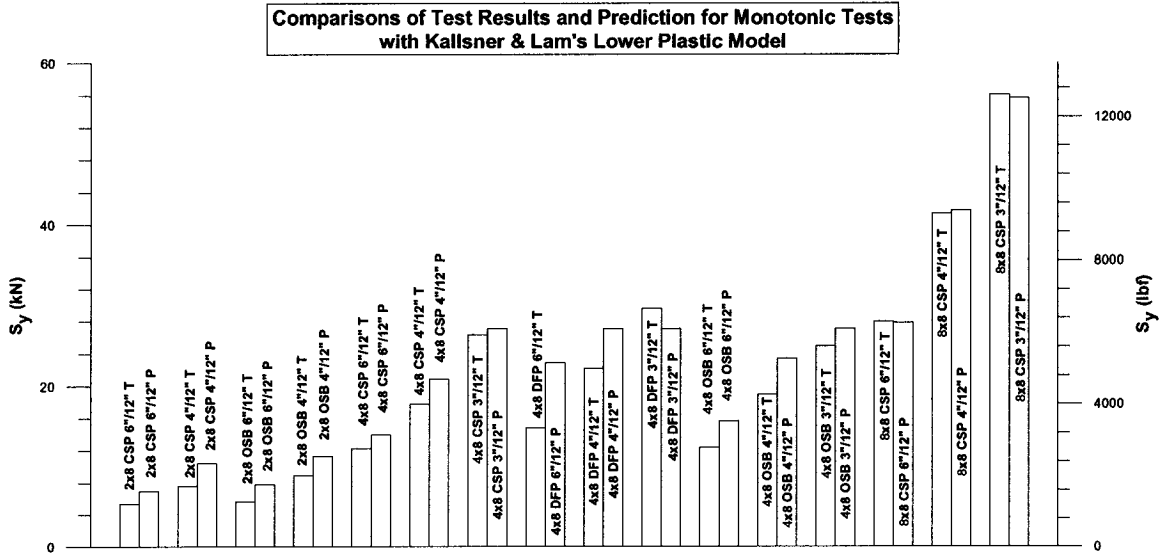


Figure A-VII.61

Comparisons between Test Results and Prediction from Kallsner & Lam's Lower Plastic Model

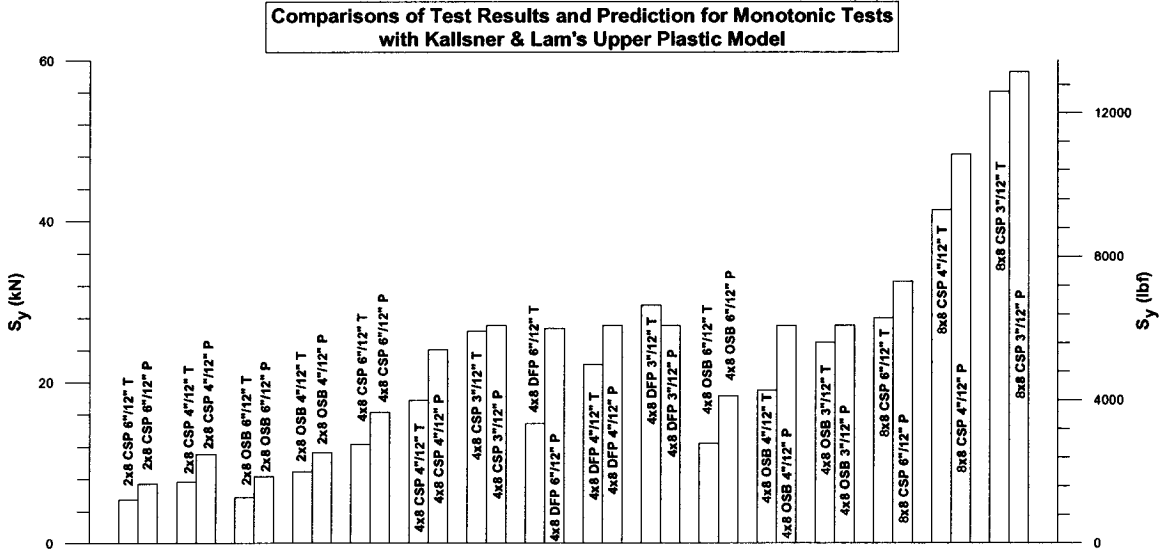


Figure A-VII.62

Comparisons between Test Results and Prediction from Kallsner & Lam's Upper Plastic Model

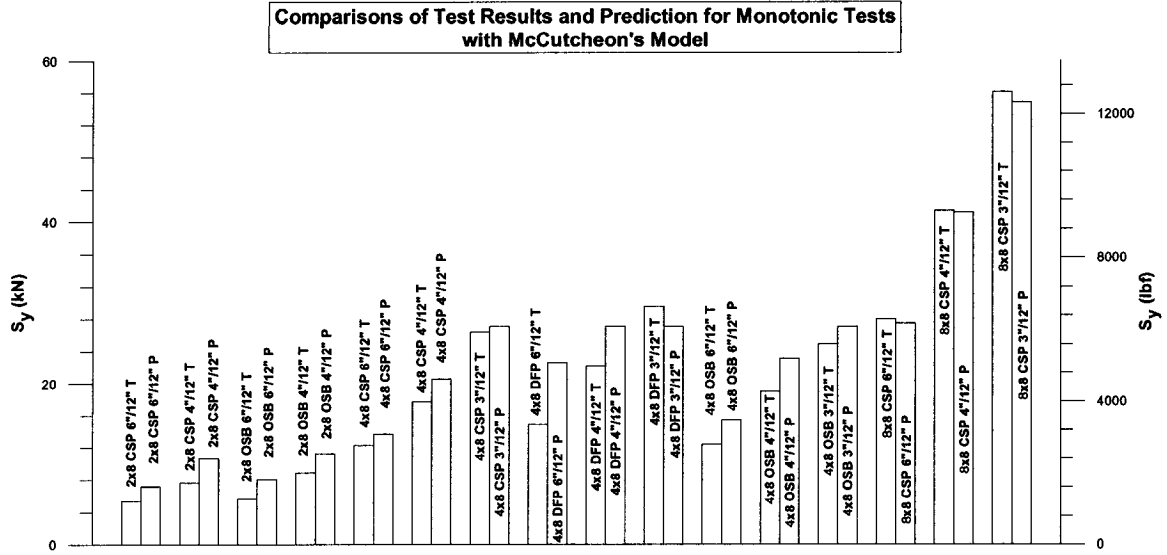


Figure A-VII.63

Comparisons between Test Results and Prediction from McCutcheon's Model

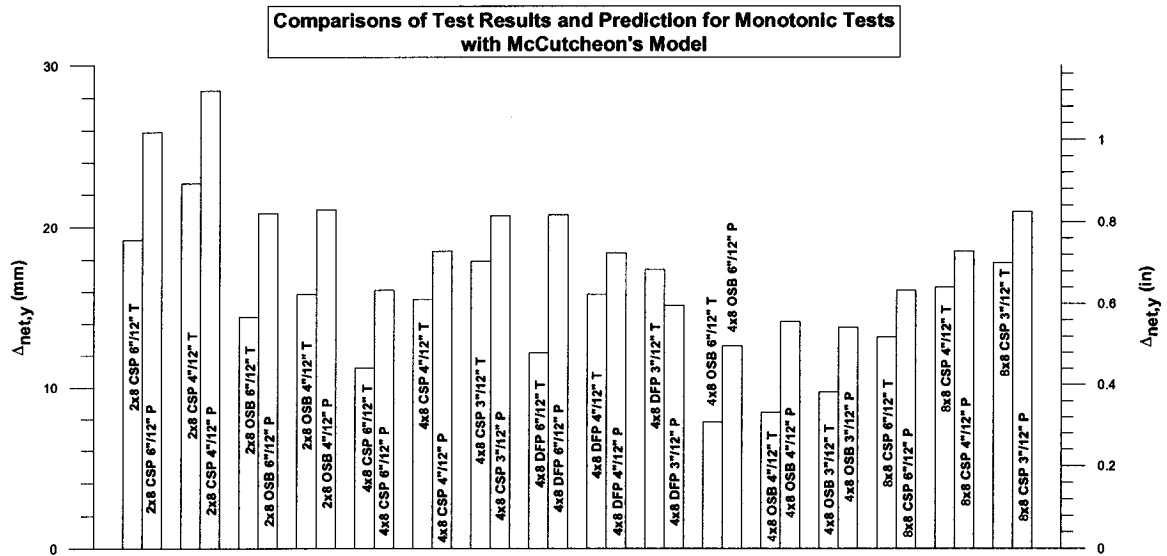


Figure A-VII.64

Comparisons between Test Results and Prediction from McCutcheon's Model

### (3) Max. Load\_25&ks

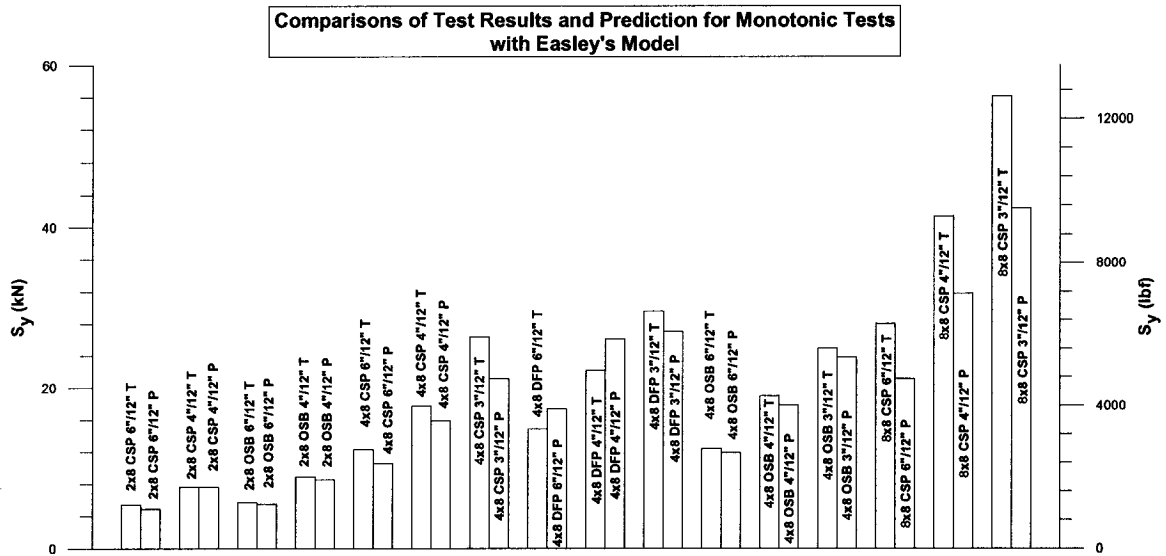


Figure A-VII.65

Comparisons between Test Results and Prediction from Easley's Model

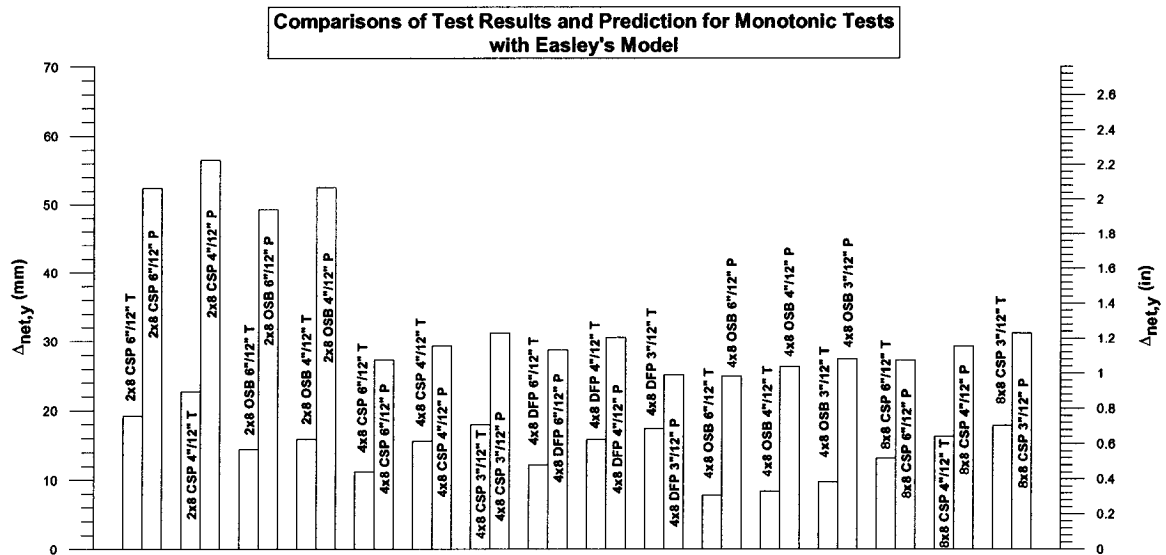


Figure A-VII.66

Comparisons between Test Results and Prediction from Easley's Model

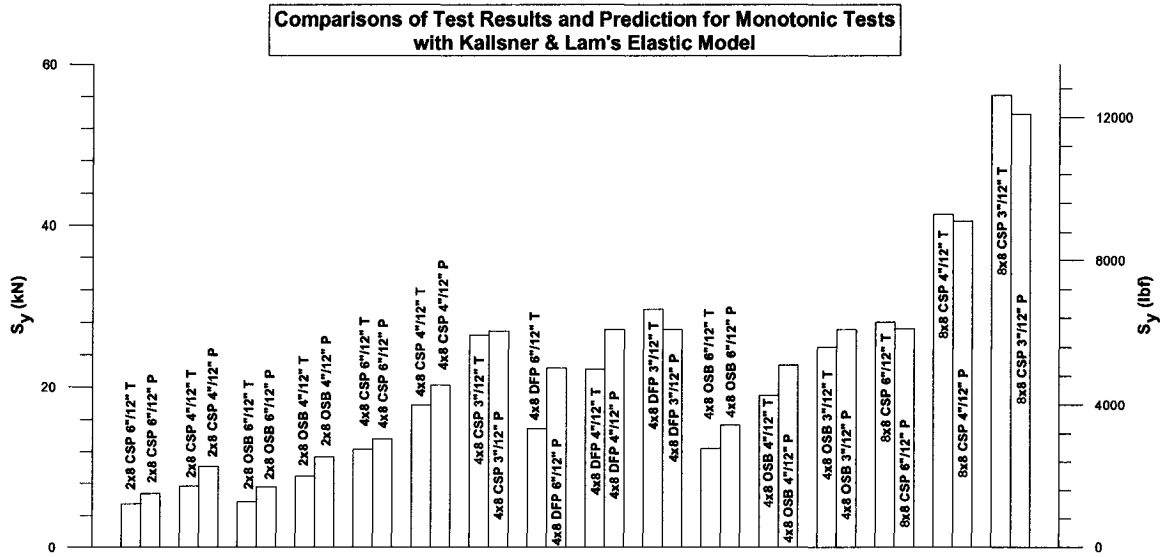


Figure A-VII.67

Comparisons between Test Results and Prediction from Kallsner & Lam's Elastic Model

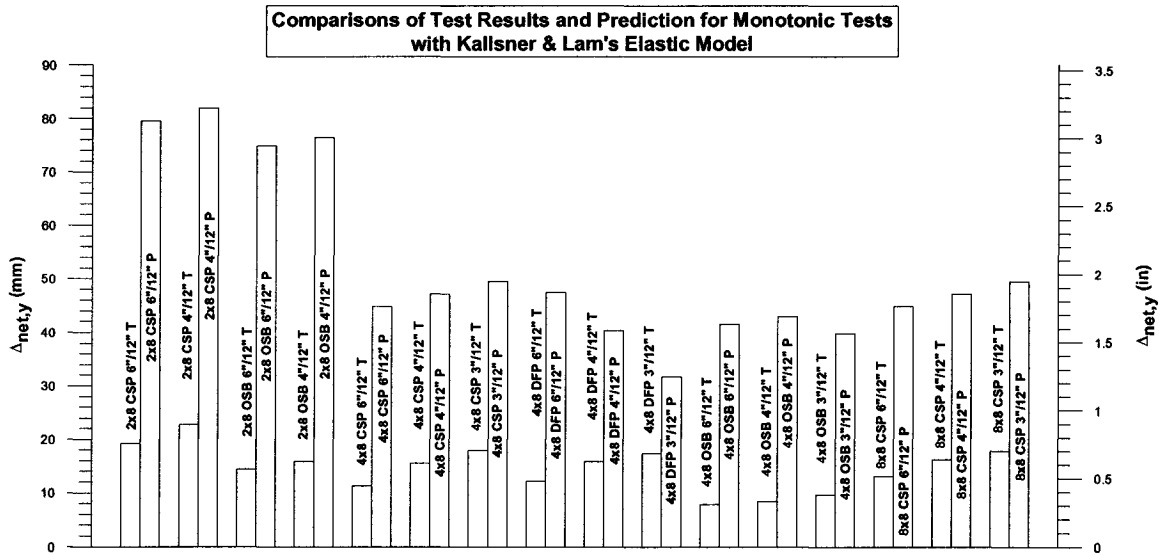


Figure A-VII.68

Comparisons between Test Results and Prediction from Kallsner & Lam's Elastic Model

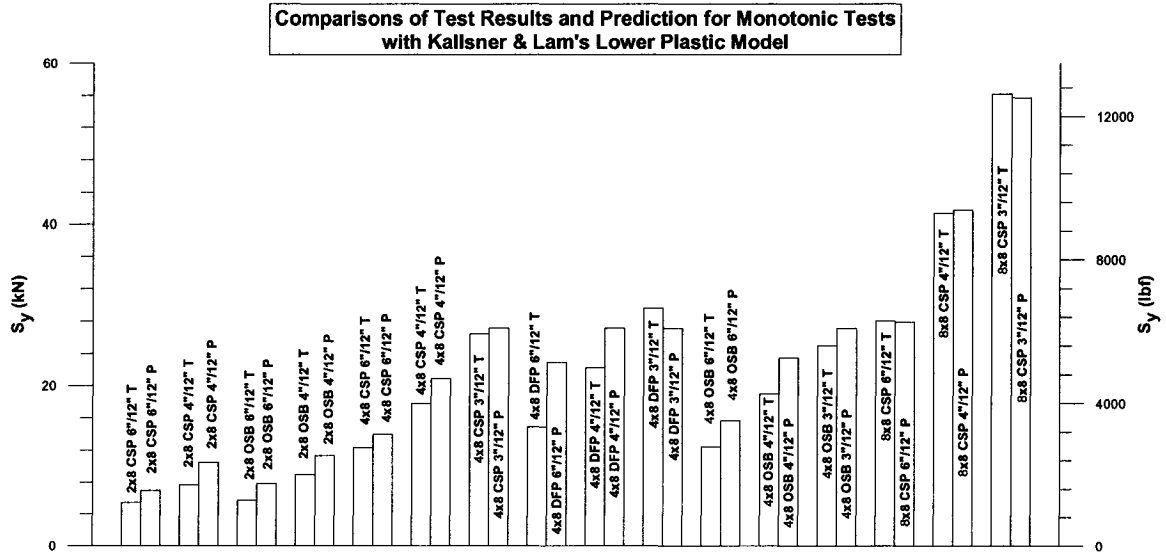


Figure A-VII.69

Comparisons between Test Results and Prediction from Kallsner & Lam's Lower Plastic Model

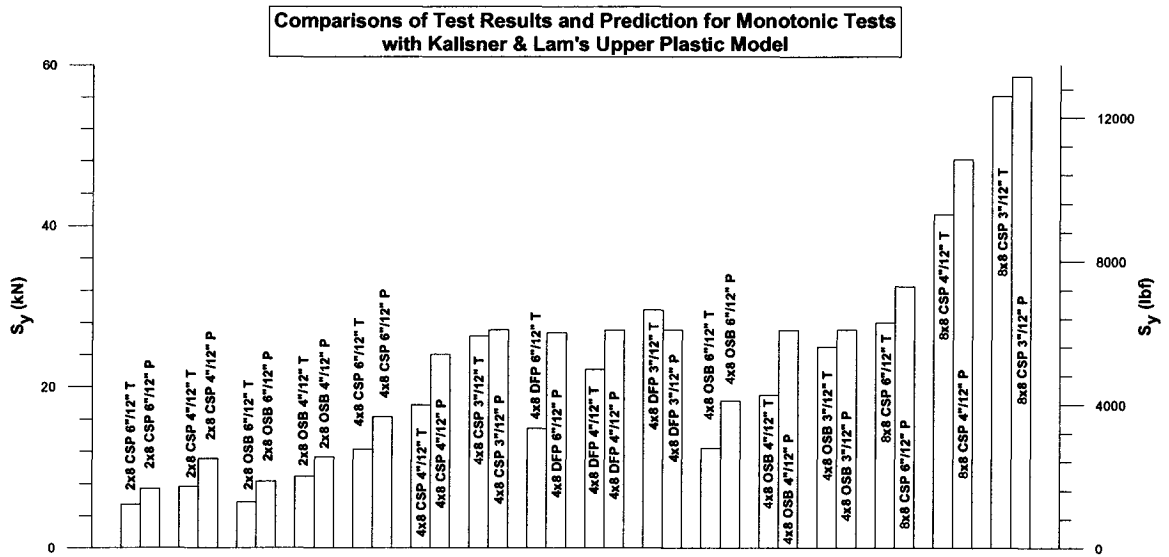


Figure A-VII.70

Comparisons between Test Results and Prediction from Kallsner & Lam's Upper Plastic Model

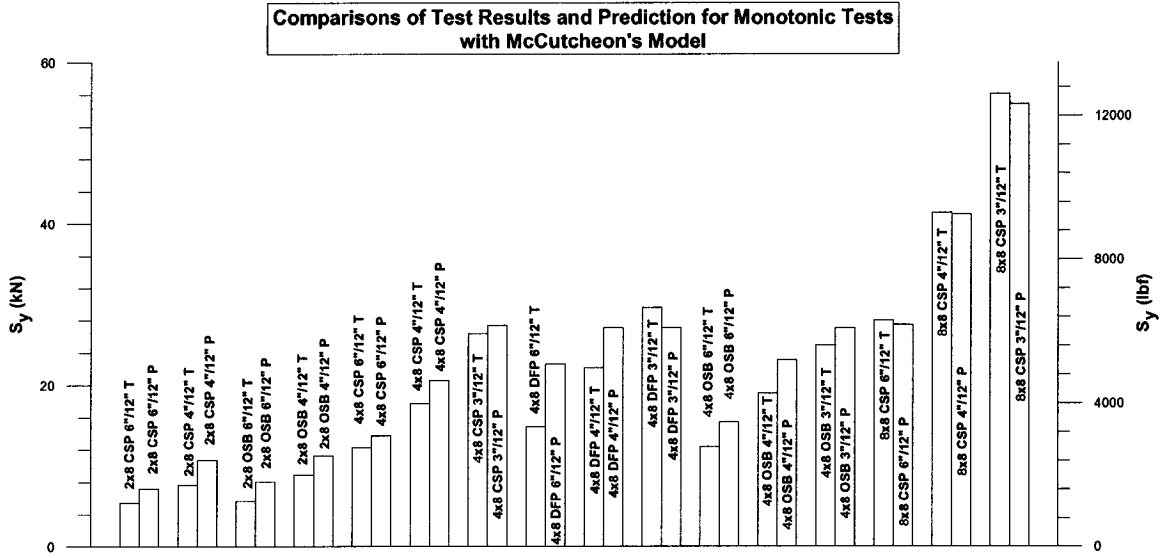


Figure A-VII.71

Comparisons between Test Results and Prediction from McCutcheon's Model

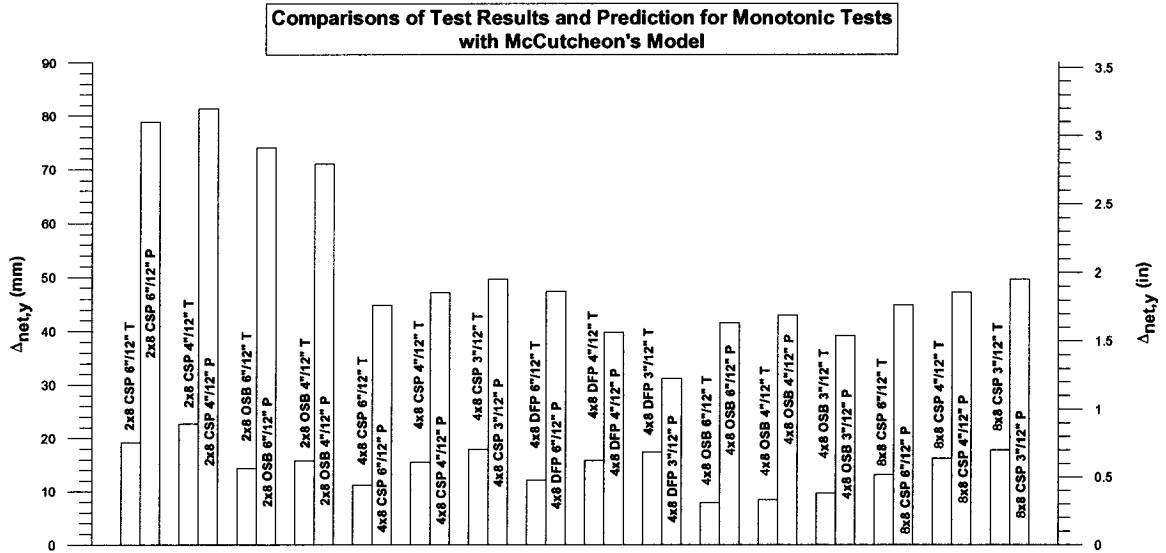


Figure A-VII.72

Comparisons between Test Results and Prediction from McCutcheon's Model

## APPENDIX VIII RELATIVE ROTATION BETWEEN SHEATHING AND FRAMING

Table VIII.1: Relative Rotation for 2x8 Walls in Monotonic Tests

	SPECIMEN	NORTH CHORD ROTATION (°)	SOUTH CHORD ROTATION (°)	BOTTOM TRACK ROTATION (°)	NORTH PANEL BOTTOM ROTATION (°)	NORTH PANEL TOP ROTATION (°)	SOUTH PANEL BOTTOM ROTATION (°)	SOUTH PANEL TOP ROTATION (°)	AVERAGE CHORD ROTATION (°)	AVERAGE NORTH PANEL ROTATION (°)	AVERAGE SOUTH PANEL ROTATION (°)	RELATIVE ROTATION TO TRACKS (°)	RELATIVE ROTATION TO CHORDS (°)
	2x8 CSP 6"/12"M-A	15A	2.787	2.595	0.249	2.602	2.013		2.691	2.307		2.307	0.384
	2x8 CSP 6"/12"M-B	15B	2.728	2.565	0.189	2.613	2.044		2.646	2.329		2.329	0.318
	2x8 CSP 6"/12"M-C	15C	2.804	2.828	0.054	2.704	1.900		2.716	2.302		2.302	0.414
	<b>AVERAGE</b>		<b>2.773</b>	<b>2.596</b>	<b>0.164</b>	<b>2.640</b>	<b>1.986</b>		<b>2.684</b>	<b>2.313</b>		<b>2.313</b>	<b>0.372</b>
	2x8 CSP 4"/12"M-A	17A	3.309	3.133	0.600	3.258	2.001		3.221	2.630		2.630	0.591
	2x8 CSP 4"/12"M-B	17B	3.176	2.999	0.367	3.002	1.871		3.087	2.436		2.436	0.651
	2x8 CSP 4"/12"M-C	17C	2.997	2.829	0.459	2.719	1.637		2.913	2.178		2.178	0.735
	<b>AVERAGE</b>		<b>3.161</b>	<b>2.987</b>	<b>0.475</b>	<b>2.993</b>	<b>1.836</b>		<b>3.074</b>	<b>2.415</b>		<b>2.415</b>	<b>0.659</b>
	2x8 OSB 6"/12"M-A	19A	2.228	2.126	0.293	2.092	1.474		2.177	1.783		1.783	0.394
	2x8 OSB 6"/12"M-B	19B	2.305	2.197	0.325	2.302	1.714		2.251	2.008		2.008	0.243
	2x8 OSB 6"/12"M-C	19C	2.149	2.050	0.228	2.107	1.654		2.100	1.880		1.880	0.220
	<b>AVERAGE</b>		<b>2.228</b>	<b>2.124</b>	<b>0.282</b>	<b>2.187</b>	<b>1.614</b>		<b>2.176</b>	<b>1.890</b>		<b>1.890</b>	<b>0.286</b>
	2x8 OSB 4"/12"M-A	27A	2.451	2.314	0.436	2.218	1.605		2.382	1.911		1.911	0.471
	2x8 OSB 4"/12"M-B	27B	3.009	2.799	1.039	2.085	1.341		2.904	1.703		1.703	1.201
	2x8 OSB 4"/12"M-C	27C	2.127	2.033	0.191	2.020	1.582		2.080	1.801		1.801	0.280
	<b>AVERAGE</b>		<b>2.529</b>	<b>2.382</b>	<b>0.555</b>	<b>2.101</b>	<b>1.509</b>		<b>2.456</b>	<b>1.805</b>		<b>1.805</b>	<b>0.651</b>

Table VIII.2: Relative Rotation for 8x8 Walls in Monotonic Tests

	SPECIMEN	NORTH CHORD ROTATION (°)	SOUTH CHORD ROTATION (°)	BOTTOM TRACK ROTATION (°)	NORTH PANEL BOTTOM ROTATION (°)	NORTH PANEL TOP ROTATION (°)	SOUTH PANEL BOTTOM ROTATION (°)	SOUTH PANEL TOP ROTATION (°)	AVERAGE CHORD ROTATION (°)	AVERAGE NORTH PANEL ROTATION (°)	AVERAGE SOUTH PANEL ROTATION (°)	RELATIVE ROTATION TO TRACKS (°)	RELATIVE ROTATION (°)
	8x8 CSP 6"/12"M-A	29A	1.338	1.261	0.042	0.882	0.786	0.851	1.300	0.834	0.834	0.834	0.465
	8x8 CSP 6"/12"M-B	29B	1.293	1.200	0.037	0.828	0.748	0.818	1.247	0.788	0.808	0.798	0.449
	8x8 CSP 6"/12"M-C	29C	1.324	1.234	0.054	0.886	0.821	0.824	1.279	0.854	0.814	0.834	0.446
	<b>AVERAGE</b>		<b>1.319</b>	<b>1.232</b>	<b>0.044</b>	<b>0.865</b>	<b>0.785</b>	<b>0.831</b>	<b>1.275</b>	<b>0.825</b>	<b>0.819</b>	<b>0.822</b>	<b>0.453</b>
	8x8 CSP 4"/12"M-A	31A	1.544	1.454	0.077	0.977	0.792	0.877	1.499	0.884	0.833	0.859	0.640
	8x8 CSP 4"/12"M-B	31B	1.563	1.461	0.084	0.977	0.778	0.954	1.512	0.877	0.910	0.894	0.618
	8x8 CSP 4"/12"M-C	31C	1.547	1.449	0.058	0.925	0.728	0.914	1.498	0.826	0.864	0.845	0.653
	<b>AVERAGE</b>		<b>1.551</b>	<b>1.455</b>	<b>0.073</b>	<b>0.960</b>	<b>0.786</b>	<b>0.915</b>	<b>1.503</b>	<b>0.863</b>	<b>0.869</b>	<b>0.866</b>	<b>0.637</b>
	8x8 CSP 3"/12"M-A	33A	1.717	1.560	0.069	0.995	0.774	0.855	1.638	0.884	0.842	0.863	0.775
	8x8 CSP 3"/12"M-B	33B	1.763	1.643	0.109	1.076	0.746	0.868	1.703	0.911	0.844	0.878	0.826
	8x8 CSP 3"/12"M-C	33C	1.737	1.633	0.111	0.995	0.744	0.852	1.685	0.869	0.815	0.842	0.842
	<b>AVERAGE</b>		<b>1.739</b>	<b>1.612</b>	<b>0.096</b>	<b>1.022</b>	<b>0.755</b>	<b>0.858</b>	<b>1.675</b>	<b>0.888</b>	<b>0.834</b>	<b>0.861</b>	<b>0.814</b>

Table VIII.3: Relative Rotation for 4x8 Walls in Monotonic Tests

	SPECIMEN	NORTH CHORD ROTATION (°)	SOUTH CHORD ROTATION (°)	BOTTOM TRACK ROTATION (°)	NORTH PANEL BOTTOM ROTATION (°)	NORTH PANEL TOP ROTATION (°)	SOUTH PANEL BOTTOM ROTATION (°)	SOUTH PANEL TOP ROTATION (°)	AVERAGE CHORD ROTATION (°)	AVERAGE NORTH PANEL ROTATION (°)	AVERAGE SOUTH PANEL ROTATION (°)	RELATIVE ROTATION TO TRACKS (°)	RELATIVE ROTATION (°)
4x8 CSP 4'/12"M-A	1A	1.730	1.627	0.141	1.194	0.846			1.678	1.020		1.020	0.659
4x8 CSP 4'/12"M-B	1B	1.731	1.641	0.215	1.120	0.766			1.686	0.943		0.943	0.743
4x8 CSP 4'/12"M-C	1C	1.609	1.517	0.135	1.047	0.801			1.563	0.924		0.924	0.639
	<b>AVERAGE</b>	<b>1.690</b>	<b>1.595</b>	<b>0.164</b>	<b>1.120</b>	<b>0.804</b>			<b>1.642</b>	<b>0.962</b>		<b>0.962</b>	<b>0.680</b>
4x8 DFP 4'/12"M-A	5A	1.677	1.590	0.115	1.127	0.806			1.633	0.967		0.967	0.667
4x8 DFP 4'/12"M-B	5B	1.709	1.589	0.214	0.851	0.380			1.649	0.615		0.615	1.034
4x8 DFP 4'/12"M-C	5C	1.695	1.604	0.130	1.076	0.725			1.649	0.901		0.901	0.748
4x8 DFP 4'/12"M-D	5D	1.664	1.538	0.131	1.079	0.753			1.601	0.916		0.916	0.685
	<b>AVERAGE</b>	<b>1.686</b>	<b>1.580</b>	<b>0.147</b>	<b>1.033</b>	<b>0.666</b>			<b>1.633</b>	<b>0.850</b>		<b>0.850</b>	<b>0.783</b>
4x8 CSP 6'/12"M-A	7A	1.380	1.305	0.060	0.904	0.771			1.342	0.838		0.838	0.505
4x8 CSP 6'/12"M-B	7B	1.267	1.190	0.103	0.928	0.706			1.228	0.817		0.817	0.411
4x8 CSP 6'/12"M-C	7C	1.414	1.326	0.083	0.997	0.753			1.370	0.875		0.875	0.495
	<b>AVERAGE</b>	<b>1.354</b>	<b>1.273</b>	<b>0.082</b>	<b>0.943</b>	<b>0.743</b>			<b>1.314</b>	<b>0.843</b>		<b>0.843</b>	<b>0.470</b>
4x8 CSP 3'/12"M-A	9A	1.958	1.836	0.304	1.179	0.752			1.897	0.965		0.965	0.932
4x8 CSP 3'/12"M-B	9B	1.857	1.708	0.338	1.101	0.699			1.783	0.900		0.900	0.882
4x8 CSP 3'/12"M-C	9C	1.767	1.658	0.238	1.012	0.645			1.713	0.829		0.829	0.884
	<b>AVERAGE</b>	<b>1.861</b>	<b>1.734</b>	<b>0.293</b>	<b>1.097</b>	<b>0.699</b>			<b>1.798</b>	<b>0.898</b>		<b>0.898</b>	<b>0.899</b>
4x8 DFP 6'/12"M-A	11A	1.561	1.475	0.117	1.070	0.845			1.518	0.958		0.958	0.561
4x8 DFP 6'/12"M-B	11B	1.532	1.447	0.108	1.027	0.827			1.490	0.927		0.927	0.563
4x8 DFP 6'/12"M-C	11C	1.346	1.266	0.087	0.902	0.692			1.306	0.797		0.797	0.510
	<b>AVERAGE</b>	<b>1.480</b>	<b>1.396</b>	<b>0.104</b>	<b>1.000</b>	<b>0.788</b>			<b>1.438</b>	<b>0.894</b>		<b>0.894</b>	<b>0.544</b>
4x8 DFP 3'/12"M-A	13A	1.715	1.601	0.270	1.092	0.533			1.658	0.813		0.813	0.846
4x8 DFP 3'/12"M-B	13B	1.760	1.627	0.233	1.048	0.550			1.694	0.799		0.799	0.895
4x8 DFP 3'/12"M-C	13C	1.847	1.699	0.302	1.195	0.489			1.773	0.842		0.842	0.931
	<b>AVERAGE</b>	<b>1.774</b>	<b>1.642</b>	<b>0.268</b>	<b>1.111</b>	<b>0.524</b>			<b>1.708</b>	<b>0.818</b>		<b>0.818</b>	<b>0.891</b>
4x8 OSB 6'/12"M-A	21A	1.077	1.009	0.092	0.707	0.552			1.043	0.629		0.629	0.414
4x8 OSB 6'/12"M-B	21B	1.107	1.040	0.101	0.776	0.554			1.073	0.665		0.665	0.409
4x8 OSB 6'/12"M-C	21C	1.179	1.116	0.074	0.869	0.706			1.147	0.788		0.788	0.360
	<b>AVERAGE</b>	<b>1.121</b>	<b>1.055</b>	<b>0.089</b>	<b>0.784</b>	<b>0.604</b>			<b>1.088</b>	<b>0.694</b>		<b>0.694</b>	<b>0.394</b>
4x8 OSB 4'/12"M-A	23A	1.136	1.058	0.160	0.782	0.509			1.097	0.645		0.645	0.452
4x8 OSB 4'/12"M-B	23B	1.187	1.105	0.137	0.756	0.521			1.146	0.639		0.639	0.507
4x8 OSB 4'/12"M-C	23C	1.136	1.061	0.140	0.784	0.538			1.099	0.661		0.661	0.438
	<b>AVERAGE</b>	<b>1.153</b>	<b>1.075</b>	<b>0.146</b>	<b>0.774</b>	<b>0.523</b>			<b>1.114</b>	<b>0.648</b>		<b>0.648</b>	<b>0.466</b>
4x8 OSB 3'/12"M-A	25A	0.021	1.144	0.251	0.881	0.433			0.582	0.657		0.657	-0.074
4x8 OSB 3'/12"M-B	25B	1.314	1.202	0.226	0.752	0.263			1.258	0.507		0.507	0.751
4x8 OSB 3'/12"M-C	25C	1.275	1.178	0.189	0.924	0.458			1.226	0.691		0.691	0.535
	<b>AVERAGE</b>	<b>0.870</b>	<b>1.174</b>	<b>0.222</b>	<b>0.852</b>	<b>0.384</b>			<b>1.022</b>	<b>0.618</b>		<b>0.618</b>	<b>0.404</b>

Table VIII.4: Relative Rotation for 2x8 Walls in Reversed Cyclic Tests

	SPECIMEN	NORTH CHORD ROTATION (°)	SOUTH CHORD ROTATION (°)	BOTTOM TRACK ROTATION (°)	NORTH PANEL BOTTOM ROTATION (°)	NORTH PANEL TOP ROTATION (°)	SOUTH PANEL BOTTOM ROTATION (°)	SOUTH PANEL TOP ROTATION (°)	AVERAGE CHORD ROTATION (°)	AVERAGE NORTH PANEL ROTATION (°)	AVERAGE SOUTH PANEL ROTATION (°)	RELATIVE ROTATION TO TRACKS (°)	RELATIVE ROTATION TO CHORDS (°)
2x8 CSP 6"/12"C-A	16A	1.771	1.654	0.086	1.589	1.495			1.713	1.542		1.542	0.171
	AVERAGE	-1.762	-1.661	-0.194	-1.566	-1.185			-1.711	-1.375		-1.375	-0.336
2x8 CSP 6"/12"C-B	16B	1.767	1.658	0.140	1.577	1.340			1.712	1.459		1.459	0.253
	AVERAGE	-1.941	-1.843	-0.414	-1.641	-1.288			-1.892	-1.465		-1.465	-0.427
2x8 CSP 6"/12"C-C	16C	2.668	2.498	0.144	2.494	2.071			2.583	2.283		2.283	0.300
	AVERAGE	2.304	2.171	0.279	2.068	1.680			2.237	1.874		1.874	0.364
2x8 CSP 6"/12"C-C	18C	-1.963	-1.869	-0.582	-1.063	-0.641			-1.916	-0.852		-0.852	-1.064
	AVERAGE	2.679	2.479	0.433	1.821	1.034			2.579	1.428		1.428	1.151
	AVERAGE(A,B,C)	2.321	2.174	0.508	1.442	0.838			2.248	1.140		1.140	1.108
2x8 CSP 4"/12"C-A	18A	2.131	2.001	0.309	1.696	1.286			2.066	1.491		1.491	0.575
	AVERAGE	2.848	2.588	0.205	2.298	1.849			2.718	2.074		2.074	0.644
	AVERAGE	-2.795	-2.650	-0.920	-2.570	-1.564			-2.722	-2.067		-2.067	-0.655
2x8 CSP 4"/12"C-B	18B	2.821	2.619	0.563	2.434	1.707			2.720	2.070		2.070	0.650
	AVERAGE	-2.177	-2.056	-0.367	-1.369	-0.768			-2.117	-1.068		-1.068	-1.048
2x8 CSP 4"/12"C-C	18C	2.744	2.530	0.463	2.115	1.154			2.637	1.634		1.634	1.003
	AVERAGE	2.460	2.293	0.415	1.742	0.961			2.377	1.351		1.351	1.026
2x8 CSP 4"/12"C-C	18C	-2.197	-2.082	-0.395	-1.948	-1.367			-2.140	-1.658		-1.658	-0.482
	AVERAGE	2.700	2.530	0.280	2.351	1.865			2.615	2.108		2.108	0.507
	AVERAGE(A,B,C)	2.449	2.306	0.337	2.150	1.616			2.377	1.883		1.883	0.495
2x8 OSB 6"/12"C-A	20A	2.577	2.406	0.438	2.108	1.428			2.492	1.768		1.768	0.723
	AVERAGE	-1.669	-1.568	-0.332	-1.558	-1.158			-1.619	-1.358		-1.358	-0.261
	AVERAGE	2.364	2.215	0.152	2.150	1.948			2.289	2.049		2.049	0.241
2x8 OSB 6"/12"C-B	20B	2.016	1.892	0.242	1.854	1.553			1.954	1.703		1.703	0.251
	AVERAGE	-1.649	-1.550	-0.264	-1.479	-0.980			-1.600	-1.230		-1.230	-0.370
	AVERAGE	2.348	2.189	0.161	2.012	1.772			2.269	1.892		1.892	0.377
2x8 OSB 6"/12"C-C	20C	1.999	1.870	0.213	1.746	1.376			1.934	1.561		1.561	0.374
	AVERAGE	-1.173	-1.099	-0.293	-1.065	-0.774			-1.136	-0.919		-0.919	-0.217
	AVERAGE	1.620	1.499	0.090	1.549	1.356			1.560	1.453		1.453	0.107
	AVERAGE(A,B,C)	1.397	1.299	0.191	1.307	1.065			1.348	1.186		1.186	0.162
2x8 OSB 4"/12"C-A	28A	1.804	1.687	0.215	1.636	1.331			1.745	1.483		1.483	0.262
	AVERAGE	-1.655	-1.558	-0.156	-1.470	-1.142			-1.607	-1.306		-1.306	-0.300
	AVERAGE	2.417	2.261	0.473	2.138	1.672			2.339	1.905		1.905	0.434
2x8 OSB 4"/12"C-B	28B	2.036	1.910	0.315	1.804	1.407			1.973	1.606		1.606	0.367
	AVERAGE	2.361	2.208	0.221	2.206	1.774			2.285	1.990		1.990	0.294
	AVERAGE	-2.458	-2.368	-0.322	-2.315	-1.743			-2.413	-2.029		-2.029	-0.384
2x8 OSB 4"/12"C-C	28C	2.409	2.288	0.271	2.261	1.758			2.349	2.010		2.010	0.339
	AVERAGE	2.360	2.209	0.335	2.088	1.656			2.284	1.872		1.872	0.412
	AVERAGE	-2.408	-2.301	-0.261	-2.297	-1.703			-2.354	-2.000		-2.000	-0.355
	AVERAGE(A,B,C)	2.384	2.255	0.298	2.193	1.679			2.319	1.936		1.936	0.383
	AVERAGE(A,B,C)	2.276	2.151	0.295	2.086	1.615			2.214	1.850		1.850	0.363

Table VIII.5: Relative Rotation for 8x8 Walls in Reversed Cyclic Tests

	SPECIMEN	NORTH CHORD ROTATION (°)	SOUTH CHORD ROTATION (°)	BOTTOM TRACK ROTATION (°)	NORTH PANEL BOTTOM ROTATION (°)	NORTH PANEL TOP ROTATION (°)	SOUTH PANEL BOTTOM ROTATION (°)	SOUTH PANEL TOP ROTATION (°)	AVERAGE CHORD ROTATION (°)	AVERAGE NORTH PANEL ROTATION (°)	AVERAGE SOUTH PANEL ROTATION (°)	RELATIVE ROTATION TO TRACKS (°)	RELATIVE ROTATION (°)
8x8 CSP 8'/12"C-A	30A	-1.022	-0.973	-0.059	-0.678	-0.601	-0.736	-0.550	-0.998	-0.639	-0.643	-0.641	-0.359
		1.348	1.261	0.053	0.914	0.873	0.913	0.864	1.304	0.894	0.888	0.891	0.411
	AVERAGE	1.185	1.117	0.056	0.796	0.737	0.824	0.707	1.151	0.766	0.766	0.766	0.385
8x8 CSP 6'/12"C-B	30B	-1.017	-0.968	-0.041	-0.649	-0.626	-0.701	-0.565	-0.993	-0.638	-0.633	-0.635	-0.355
		1.381	1.278	0.039	0.933	0.863	0.935	0.926	1.330	0.898	0.930	0.914	0.431
	AVERAGE	1.199	1.123	0.040	0.791	0.745	0.818	0.745	1.181	0.768	0.782	0.775	0.393
8x8 CSP 6'/12"C-C	30C	-1.002	-0.933	-0.046	-0.687	-0.629	-0.668	-0.514	-0.967	-0.658	-0.591	-0.625	-0.310
		1.361	1.300	0.066	0.985	0.892	0.899	0.794	1.331	0.938	0.846	0.892	0.392
	AVERAGE	1.182	1.117	0.056	0.836	0.761	0.784	0.654	1.149	0.798	0.719	0.758	0.351
	AVERAGE(A,B,C)	1.189	1.119	0.051	0.808	0.747	0.809	0.702	1.154	0.778	0.755	0.766	0.376
8x8 CSP 4'/12"C-A	32A	-1.166	-1.094	-0.083	-0.629	-0.631	-0.713	-0.525	-1.130	-0.630	-0.619	-0.624	-0.500
		1.547	1.417	0.144	0.977	0.752	0.934	0.791	1.482	0.864	0.863	0.864	0.618
	AVERAGE	1.356	1.255	0.114	0.803	0.692	0.824	0.658	1.306	0.747	0.741	0.744	0.559
8x8 CSP 4'/12"C-B	32B	-1.162	-1.098	-0.076	-0.663	-0.657	-0.743	-0.559	-1.130	-0.660	-0.651	-0.656	-0.470
		1.602	1.460	0.187	1.001	0.801	0.936	0.788	1.531	0.901	0.862	0.882	0.630
	AVERAGE	1.382	1.279	0.131	0.832	0.729	0.840	0.673	1.331	0.781	0.757	0.769	0.550
8x8 CSP 4'/12"C-C	32C	-1.171	-1.121	-0.106	-0.684	-0.594	-0.754	-0.554	-1.146	-0.639	-0.654	-0.646	-0.507
		1.573	1.438	0.177	1.012	0.758	0.913	0.817	1.505	0.885	0.865	0.875	0.620
	AVERAGE	1.372	1.279	0.142	0.848	0.676	0.833	0.685	1.326	0.762	0.759	0.761	0.564
	AVERAGE(A,B,C)	1.370	1.271	0.129	0.827	0.699	0.832	0.672	1.321	0.763	0.752	0.758	0.557
8x8 CSP 3'/12"C-A	34A	-1.270	-1.194	-0.126	-0.660	-0.535	-0.725	-0.514	-1.232	-0.598	-0.620	-0.609	-0.634
		1.784	1.622	0.202	1.070	0.855	0.905	0.723	1.703	0.962	0.814	0.888	0.741
	AVERAGE	1.527	1.408	0.164	0.865	0.695	0.815	0.618	1.467	0.780	0.717	0.748	0.687
8x8 CSP 3'/12"C-B	34B	-1.279	-1.182	-0.110	-0.642	-0.569	-0.723	-0.500	-1.230	-0.605	-0.612	-0.609	-0.625
		1.768	1.623	0.180	1.072	0.777	0.913	0.810	1.695	0.924	0.862	0.893	0.771
	AVERAGE	1.523	1.402	0.145	0.857	0.673	0.818	0.655	1.463	0.765	0.737	0.751	0.698
8x8 CSP 3'/12"C-C	34C	-1.260	-1.202	-0.099	-0.661	-0.550	-0.765	-0.510	-1.241	-0.606	-0.637	-0.622	-0.635
		1.707	1.597	0.153	0.992	0.809	0.879	0.835	1.652	0.900	0.857	0.879	0.752
	AVERAGE	1.493	1.400	0.126	0.826	0.680	0.822	0.672	1.446	0.753	0.747	0.750	0.694
	AVERAGE(A,B,C)	1.514	1.403	0.145	0.849	0.682	0.818	0.649	1.459	0.766	0.734	0.750	0.693

Table VIII.6: Relative Rotation for 4x8 CSP Walls in Reversed Cyclic Tests

	SPECIMEN	NORTH CHORD ROTATION (°)	SOUTH CHORD ROTATION (°)	BOTTOM TRACK ROTATION (°)	NORTH PANEL BOTTOM ROTATION (°)	NORTH PANEL TOP ROTATION (°)	SOUTH PANEL BOTTOM ROTATION (°)	SOUTH PANEL TOP ROTATION (°)	AVERAGE CHORD ROTATION (°)	AVERAGE NORTH PANEL ROTATION (°)	AVERAGE SOUTH PANEL ROTATION (°)	RELATIVE ROTATION TO TRACKS (°)	RELATIVE ROTATION (°)
4x8 CSP 4"/12°C-A	4A	-1.302	-1.218	-0.168	-0.859	-0.800			-1.280	-0.729		-0.729	-0.531
		1.628	1.506	0.137	1.179	0.894			1.567	1.036		1.036	0.531
	AVERAGE	1.465	1.362	0.152	1.019	0.747			1.413	0.883		0.883	0.531
4x8 CSP 4"/12°C-B	4B	-1.310	-1.196	-0.164	-0.886	-0.540			-1.253	-0.713		-0.713	-0.540
		1.621	1.466	0.177	1.077	0.841			1.543	0.959		0.959	0.584
	AVERAGE	1.466	1.331	0.170	0.982	0.691			1.398	0.836		0.836	0.562
4x8 CSP 4"/12°C-C	4C	-1.305	-1.216	-0.225	-0.864	-0.506			-1.261	-0.685		-0.685	-0.576
		1.684	1.533	0.198	0.976	0.714			1.809	0.845		0.845	0.764
	AVERAGE	1.495	1.374	0.212	0.920	0.610			1.435	0.765		0.765	0.670
4x8 CSP 6"/12°C-A	8A	-1.042	-0.983	-0.080	-0.717	-0.486			-1.012	-0.602		-0.602	-0.411
		1.426	1.323	0.142	1.001	0.828			1.374	0.914		0.914	0.460
	AVERAGE	1.234	1.153	0.111	0.859	0.657			1.193	0.758		0.758	0.435
4x8 CSP 6"/12°C-B	8B	-1.059	-1.011	-0.101	-0.763	-0.516			-1.035	-0.640		-0.640	-0.395
		1.398	1.310	0.106	0.984	0.855			1.354	0.919		0.919	0.435
	AVERAGE	1.228	1.160	0.103	0.873	0.685			1.194	0.779		0.779	0.415
4x8 CSP 6"/12°C-C	8C	-1.037	-0.972	-0.105	-0.710	-0.523			-1.005	-0.616		-0.616	-0.388
		1.424	1.306	0.122	1.027	0.859			1.365	0.943		0.943	0.422
	AVERAGE	1.231	1.139	0.114	0.868	0.691			1.185	0.780		0.780	0.405
4x8 CSP 3"/12°C-A	10A	-1.276	-1.183	-0.205	-0.806	-0.431			-1.230	-0.619		-0.619	-0.611
		1.705	1.557	0.272	0.964	0.613			1.631	0.789		0.789	0.842
	AVERAGE	1.491	1.370	0.239	0.885	0.522			1.430	0.704		0.704	0.727
4x8 CSP 3"/12°C-B	10B	-1.263	-1.165	-0.156	-0.765	-0.432			-1.214	-0.599		-0.599	-0.616
		1.784	1.602	0.282	1.053	0.708			1.683	0.880		0.880	0.802
	AVERAGE	1.513	1.383	0.219	0.909	0.570			1.448	0.739		0.739	0.709
4x8 CSP 3"/12°C-C	10C	-1.255	-1.170	-0.180	-0.750	-0.337			-1.213	-0.544		-0.544	-0.669
		1.732	1.565	0.355	0.996	0.621			1.649	0.808		0.808	0.841
	AVERAGE	1.494	1.368	0.267	0.873	0.479			1.431	0.676		0.676	0.755
	AVERAGE(A,B,C)	1.499	1.374	0.242	0.889	0.524			1.437	0.706		0.706	0.730

Table VIII.7: Relative Rotation for 4x8 DFP Walls in Reversed Cyclic Tests

	SPECIMEN	NORTH CHORD ROTATION (°)	SOUTH CHORD ROTATION (°)	BOTTOM TRACK ROTATION (°)	NORTH PANEL BOTTOM ROTATION (°)	NORTH PANEL TOP ROTATION (°)	SOUTH PANEL BOTTOM ROTATION (°)	SOUTH PANEL TOP ROTATION (°)	AVERAGE CHORD ROTATION (°)	AVERAGE NORTH PANEL ROTATION (°)	AVERAGE SOUTH PANEL ROTATION (°)	RELATIVE ROTATION TO TRACKS (°)	RELATIVE ROTATION (°)
	4x8 DFP 6"/12"C-A	12A	-1.097	-1.009	-0.088	-0.679	-0.431		-1.053	-0.555		-0.555	-0.498
			1.433	1.288	0.114	0.908	0.654		1.360	0.781		0.781	0.579
		AVERAGE	1.265	1.148	0.101	0.794	0.543		1.206	0.668		0.668	0.538
	4x8 DFP 6"/12"C-B	12B	-1.092	-1.029	-0.086	-0.750	-0.514		-1.060	-0.632		-0.632	-0.428
			1.464	1.356	0.116	1.028	0.880		1.410	0.954		0.954	0.456
		AVERAGE	1.278	1.193	0.101	0.889	0.697		1.235	0.793		0.793	0.442
	4x8 DFP 6"/12"C-C	12C	-1.110	-1.043	-0.095	-0.784	-0.544		-1.076	-0.664		-0.664	-0.412
			1.447	1.344	0.111	1.056	0.812		1.396	0.934		0.934	0.461
		AVERAGE	1.278	1.194	0.103	0.920	0.678		1.236	0.799		0.799	0.437
		AVERAGE(A,B,C)	1.274	1.178	0.102	0.868	0.639		1.226	0.754		0.754	0.472
	4x8 DFP 4"/12"C-A	6A	-1.213	-1.172	-0.122	-0.797	-0.467		-1.192	-0.632		-0.632	-0.560
			1.704	1.527	0.107	1.059	0.834		1.615	0.947		0.947	0.668
		AVERAGE	1.458	1.349	0.114	0.928	0.650		1.404	0.789		0.789	0.614
	4x8 DFP 4"/12"C-B	6B	-1.255	-1.188	-0.125	-0.801	-0.456		-1.221	-0.628		-0.628	-0.593
			1.598	1.478	0.141	0.999	0.695		1.538	0.847		0.847	0.691
		AVERAGE	1.426	1.333	0.133	0.900	0.575		1.380	0.738		0.738	0.642
	4x8 DFP 4"/12"C-C	6C	-1.246	-1.179	-0.168	-0.890	-0.488		-1.213	-0.689		-0.689	-0.524
			1.644	1.516	0.157	1.030	0.747		1.580	0.889		0.889	0.692
		AVERAGE	1.445	1.348	0.162	0.960	0.617		1.396	0.789		0.789	0.608
		AVERAGE(A,B,C)	1.443	1.343	0.136	0.930	0.614		1.393	0.772		0.772	0.621
	4x8 DFP 3"/12"C-A	14A	1.852	1.511	0.218	1.023	0.547		1.581	0.785		0.785	0.796
			-1.706	-1.580	-0.203	-1.136	-0.632		-1.643	-0.884		-0.884	-0.759
		AVERAGE	1.679	1.546	0.210	1.080	0.590		1.612	0.835		0.835	0.778
	4x8 DFP 3"/12"C-B	14B	-1.136	-1.047	-0.192	-0.734	-0.331		-1.092	-0.533		-0.533	-0.559
			1.512	1.388	0.176	0.924	0.470		1.450	0.697		0.697	0.752
		AVERAGE	1.324	1.217	0.184	0.829	0.401		1.271	0.615		0.615	0.656
	4x8 DFP 3"/12"C-C	14C	1.671	1.530	0.235	0.973	0.585		1.601	0.779		0.779	0.822
			-1.709	-1.585	-0.243	-1.103	-0.578		-1.647	-0.841		-0.841	-0.806
		AVERAGE	1.690	1.557	0.239	1.038	0.581		1.624	0.810		0.810	0.814
	4x8 DFP 3"/12"C-D	14C-2	1.607	1.458	0.238	0.905	0.520		1.532	0.712		0.712	0.820
			-1.625	-1.491	-0.237	-1.059	-0.605		-1.558	-0.832		-0.832	-0.726
		AVERAGE	1.616	1.474	0.237	0.982	0.562		1.545	0.772		0.772	0.773
		AVERAGE(A,B,C)	1.577	1.449	0.218	0.982	0.534		1.513	0.758		0.758	0.755

Table VIII.8: Relative Rotation for 4x8 OSB Walls in Reversed Cyclic Tests

	SPECIMEN	NORTH CHORD ROTATION (°)	SOUTH CHORD ROTATION (°)	BOTTOM TRACK ROTATION (°)	NORTH PANEL BOTTOM ROTATION (°)	NORTH PANEL TOP ROTATION (°)	SOUTH PANEL BOTTOM ROTATION (°)	SOUTH PANEL TOP ROTATION (°)	AVERAGE CHORD ROTATION (°)	AVERAGE NORTH PANEL ROTATION (°)	AVERAGE SOUTH PANEL ROTATION (°)	RELATIVE ROTATION TO TRACKS (°)	RELATIVE ROTATION (°)
	4x8 OSB 6"/12"C-A	22A	-0.863	-0.808	-0.127	-0.670	-0.410						
			1.170	1.089	0.095	0.865	0.679						
		AVERAGE	1.016	0.949	0.111	0.768	0.544		1.130	0.772		0.772	0.358
	4x8 OSB 6"/12"C-B	22B	-0.873	-0.817	-0.100	-0.680	-0.480						
			1.157	1.093	0.056	0.863	0.759						
		AVERAGE	1.015	0.965	0.078	0.771	0.609		1.125	0.811		0.811	0.314
	4x8 OSB 6"/12"C-C	22C	-0.866	-0.811	-0.093	-0.701	-0.428						
			1.130	1.066	0.128	0.796	0.652						
		AVERAGE	0.998	0.934	0.111	0.749	0.540		0.966	0.644		0.644	0.321
		AVERAGE(A,B,C)	1.010	0.946	0.100	0.762	0.565		0.978	0.663		0.663	0.314
	4x8 OSB 4"/12"C-A	24A	0.810	0.781	0.050	0.487	0.383						
			-0.811	-0.743	-0.106	-0.542	-0.314						
		AVERAGE	0.811	0.752	0.078	0.515	0.348		-0.777	-0.428		-0.428	-0.349
	4x8 OSB 4"/12"C-B	24B	-0.845	-0.784	-0.102	-0.681	-0.374						
			1.228	1.151	0.105	0.892	0.646						
		AVERAGE	1.036	0.968	0.103	0.776	0.510		1.190	0.769		0.769	0.421
	4x8 OSB 4"/12"C-C	24C	-0.825	-0.786	-0.098	-0.591	-0.362						
			1.051	0.972	0.094	0.714	0.582						
		AVERAGE	0.938	0.869	0.096	0.652	0.472		-0.796	-0.476		-0.476	-0.319
		AVERAGE(A,B,C)	0.928	0.863	0.092	0.648	0.443		1.012	0.648		0.648	0.364
	4x8 OSB 3"/12"C-A	26A	-0.865	-0.796	-0.181	-0.656	-0.217						
			1.207	1.115	0.210	0.821	0.463						
		AVERAGE	1.036	0.955	0.196	0.738	0.340		-0.830	-0.437		-0.437	-0.394
	4x8 OSB 3"/12"C-B	26B	0.861	0.795	0.102	0.532	0.252						
			-0.877	-0.802	-0.231	-0.717	-0.201						
		AVERAGE	0.869	0.788	0.167	0.624	0.226		0.828	0.392		0.392	0.436
	4x8 OSB 3"/12"C-C	26C	1.297	1.199	0.133	0.939	0.623						
			-1.278	-1.181	-0.184	-0.918	-0.592						
		AVERAGE	1.287	1.190	0.159	0.928	0.607		1.248	0.781		0.781	0.467
		AVERAGE(A,B,C)	1.064	0.981	0.174	0.764	0.391		-1.229	-0.755		-0.755	-0.475
									1.239	0.768		0.768	0.471
									1.023	0.577		0.577	0.445